

Elucidating the Role of GRASPs in and Out of the Golgi Apparatus

by

Erpan Ahat

A dissertation submitted in partial fulfillment
of the requirements for the degree of
Doctor of Philosophy
(Molecular, Cellular and Developmental Biology)
in the University of Michigan
2021

Doctoral Committee:

Professor Yanzhuang Wang, Chair
Professor Yuqing Eugene Chen
Professor Cunming Duan
Professor Ursula Jakob

Erpan Ahat

erpan@umich.edu

ORCID iD: 0000-0002-4057-9120

© Erpan Ahat 2021

Dedication

This dissertation is dedicated to my grandmother.

Acknowledgements

Numerous people helped me along the way to complete this thesis. I would like to express my deepest gratitude to my mentors, colleagues, friends, and my family. First, I would like to thank my PhD advisor, Dr. Yanzhuang Wang, whose continuous patient guidance and examples by action made me a better person, a better scientist, and a better thinker. I still vividly remember the day he interviewed me for the PhD program. It was one of the longest interviews I have ever done, and I felt I did bad because I was not able to answer some of his super detail-oriented questions. Eventually, it worked out and I came to join MCDB and joined Wang lab. Even though sometimes it was hard as it should be, overall, I had great experience working with and learning from Dr. Wang during my PhD in his research program. His strong organization skills, sharp questions and attention to details have been super helpful in my growth in his lab.

I also would like to thank my thesis committee members, Dr. Ursula Jakob, Dr. Eugene Chen, and Dr. Cunming Duan. I am grateful for their insightful suggestions and kind support to my research projects.

This thesis work would not have been possible without the help from former and current Wang lab members. Two senior postdocs, Dr. Xiaoyan Zhang and Dr. Michael Bekier, were instrumental in my progress, growth, and success in Wang Lab. Both were great role models in their own ways. Xiaoyan's attention to details, art in her techniques and her kindness to help others whenever she can, touched and influenced me tremendously. Michael is sharp, critical, and always knew how to get to the essence of a question. Being in the lab with them every day

was a great learning experience for me. Dr. Jie Li is another postdoc in the lab that shared the most overlap with me during my PhD, and she has been very helpful during my PhD. We worked together in cowriting two review articles which was a great pleasure. Two former PhD students, Dr. Leibin Wang and Dr. Stephen Ireland, were my seniors and they were kind, supportive and always provided me with good resources. Stephen and I spent late Friday nights in the lab together sometimes over a beer and that was always fun. I wish them both good luck.

In my senior years, new lab members joined our lab. Dr. Sarah Bui and Dr. Jianchao Zhang are the newest Wang lab postdocs. They are smart and diligent. Especially during the shift work schedules due to COVID, I got to know them a lot better, and we became good friends. Sarah was instrumental in shifting the lab dynamic and she brought in different kind of vibe that everyone really enjoyed. I am happy that they joined Wang lab and I wish nothing but success to their careers.

Outside of the lab, within MCDB, I have had great group of friends that brought fun and happiness into my life as a PhD student. I would like to thank my cohort, my friends outside of my cohort including Ajai, Abhishek, and many others that I can't name one by one. I also would like to thank Diane Durfy, Mary Carr, and Stella Bublitz for their kind support; Gregg Sobocinski for the trainings he provided; Dr. Lyle Simmons and Dr. Ken Cadigan for their guidance and support during my PhD in MCDB.

I also would like to thank my dear Uyghur community in Michigan for their kind guidance, advice in life and fun times during traditional festivals. I know I am going to miss this community when I leave Michigan. Finally, I would like to thank my family. I am grateful to have my best friend, my soulmate, and my wife Muattar in my life. She made huge sacrifices during my PhD, but I have a whole life to make up for that. I am looking forward to the

endeavors we will have. Lastly, I would like to thank my parents, my relatives, and my dear friends back in my hometown. I am missing you every day.

Preface

Chapter 1 is modified and reorganized from Ahat, E., Li, J., & Wang, Y. (2019). **New insights into the Golgi stacking proteins.** *Frontiers in cell and developmental biology*, 7, 131. E.A wrote the first draft of majority of the review, J.L contributed to the GRASP interacting proteins section, and Y.W revised the paper.

Chapter 2 is reprinted from Ahat, E., Xiang, Y., Zhang, X., Bekier, M. E., & Wang, Y. (2019). **GRASP depletion–mediated Golgi destruction decreases cell adhesion and migration via the reduction of $\alpha 5\beta 1$ integrin.** *Molecular biology of the cell*, 30(6), 766-777. E.A., Y.X. and Y.W. designed the experiments; E.A., Y.X. performed most of the experiments; X.Z. performed the radioactive labeling and $\beta 1$ integrin CHX chase experiment; M.B. and E.A. performed the biotinylation assay. E.A., Y.X. and Y.W analyzed the data and wrote the paper.

Chapter 3 is reprinted from Ahat, E.*, Song, Y.*, Xia, K., Reid, W., Li, J., Bui, S., Zhang, F., Linhardt, R.J. and Wang, Y. (2021). **Golgi structural defect impairs glycosaminoglycan synthesis, sulfation, and secretion.** *bioRxiv*. E.A., Y.S., F.Z., R.L. and Y.W. designed the experiments; E.A. prepared the samples and Y.S., K.X. performed labeling and LC-MS experiments. E.A. performed most of the other experiments. W.R. and S.B. performed data search and analysis from the RNA-seq and Proteomics experiments. J.L. and E.A. performed the flow cytometry experiment. E.A., Y.S., R.L. and Y.W. analyzed the data.

E.A. and Y.W. made the figures and wrote the first draft; Y.S. K.X., F.Z. and R.L. edited the manuscript. All authors discussed the results and contributed to the final manuscript. (*, equal contribution)

Chapter 4 is reprinted from Ahat, E., Bui, S., Zhang, J., da Veiga Leprevost, F., Sharkey, L.M., Reid, W., Nesvizhskii, A.I., Paulson, H.L. and Wang, Y. (2021). **GRASP55 regulates mutant huntingtin unconventional secretion and aggregation.** *bioRxiv*. E.A. and Y.W. designed the experiments; E.A. performed most of the experiments. S.B. performed the western blot experiments for p23 level analysis. J.Z. performed the IP experiment to determine p23-GRASP55 interaction. F.V and A.N performed the bioinformatics analysis of the secretome data. W.R performed the signal peptide and secretomeP data search of the secretome. L.S and H.L.P. provided the control and HD mouse brain lysates. E.A. and Y.W. analyzed the data. E.A. and Y.W. made the figures and wrote the first draft; all authors discussed the results and contributed to the final manuscript.

Table of Contents

| | |
|---|-------------|
| Dedication | ii |
| Acknowledgements | iii |
| Preface..... | vi |
| List of Tables | x |
| List of Figures..... | xi |
| Abstract..... | xiii |
| Chapter 1 Introduction to the Golgi Structure and Function | 1 |
| 1.1 GRASP55 and GRASP65 as tools to probe the biological significance of Golgi structure formation | 4 |
| 1.2 New discoveries on GRASP55 and GRASP65 interacting proteins..... | 5 |
| 1.3 GRASP55 regulates autophagosome-lysosome fusion..... | 8 |
| 1.4 GRASP55/65 and unconventional secretion..... | 11 |
| 1.5 Outlook..... | 16 |
| Chapter 2 GRASP Depletion-mediated Golgi Destruction Decreases Cell Adhesion and Migration Via the Reduction of $\alpha 5\beta 1$ Integrin..... | 22 |
| 2.1 GRASP depletion reduces cell adhesion..... | 26 |
| 2.2 GRASP depletion reduces cell migration and invasion | 27 |
| 2.3 Golgi unstacking reduces $\alpha 5\beta 1$ integrin protein level in the cell..... | 29 |
| 2.4 Expression of $\alpha 5\beta 1$ integrin rescues the attachment and migration defects of GRASP knockout cells..... | 32 |
| 2.5 GRASP depletion reduces $\alpha 5\beta 1$ integrin protein synthesis | 33 |
| 2.6 GRASP depletion enhances total protein synthesis and cell growth | 34 |

| | |
|--|------------|
| Chapter 3 Golgi Structural Defect Impairs Glycosaminoglycan Synthesis, Sulfation, and Secretion..... | 63 |
| 3.1 GRASP KO increases GAG synthesis but decreases their secretion. | 67 |
| 3.2 GRASP KO increases HS synthesis but decreases its sulfation and secretion. | 68 |
| 3.3 GRASP KO decreases CS synthesis and secretion. | 69 |
| 3.4 GRASP KO regulates key enzymes in HS and CS synthesis and sulfation..... | 70 |
| Chapter 4 GRASP55 Regulates Mutant Huntingtin Unconventional Secretion and Aggregation | 102 |
| 4.1 GRASP55 is required for unconventional secretion of mutant Htt..... | 106 |
| 4.2 Mutant Htt is selectively secreted through a Golgi-independent pathway..... | 108 |
| 4.3 GFP-Htt-Q74 secretion is enhanced by cellular stress..... | 110 |
| 4.4 GRASP55 level is upregulated by cellular stress and by Htt expression..... | 111 |
| 4.5 GFP-Htt-Q74 secretion is autophagy dependent..... | 113 |
| 4.6 GRASP55 facilitates GFP-Htt-Q74 secretion through promoting autophagosome maturation and stabilizing p23/TMED10..... | 114 |
| 4.7 Inhibition of Htt secretion by 55KO enhances Htt aggregation and toxicity in the cell. .. | 116 |
| 4.8 Secretome analysis of WT and 55KO cells identifies new proteins secreted by GRASP55-dependent unconventional secretion. | 117 |
| Chapter 5 Summary and Future Directions..... | 160 |
| 5.1 Effects of Golgi destruction on cell attachment, migration, and growth | 161 |
| 5.2 Heparan sulfate (HS) and Chondroitin sulfate (CS) synthesis, sulfation and secretion are regulated by GRASPs..... | 163 |
| 5.3 GRASP55 and autophagy regulates mutant huntingtin unconventional secretion and aggregation. | 166 |
| References..... | 170 |

List of Tables

| | |
|--|------------|
| Table 1.1. GRASP interacting proteins and functions | 18 |
| Table 3.1. GRASP KO alters HS and CS synthesis enzymes at both the mRNA and protein levels. | 93 |
| Supplemental Table 3.1. The amount of three kinds of GAG from cell samples..... | 96 |
| Supplemental Table 3.2. The amount of three kinds of GAG from medium samples. | 97 |
| Supplemental Table 3.3. The percentage of each detected HS disaccharide from cell samples. | 98 |
| Supplemental Table 3.4. The percentage of each detected HS disaccharide from medium samples. | 99 |
| Supplemental Table 3.5. The percentage of each detected CS disaccharide from cell samples. | 100 |
| Supplemental Table 3.6. The percentage of each detected CS disaccharide from medium samples. | 101 |
| Supplemental Table 4.1. List of differentially secreted proteins in 55KO vs. WT. | 153 |
| Supplemental Table 4.2. List of selected GO term analysis of WT and 55KO secretome. | 158 |

List of Figures

| | |
|--|------------|
| Figure 1.1. GRASP55 and GRASP65 domain structures and interacting proteins. | 19 |
| Figure 1.2. GRASP55 regulates autophagy and unconventional secretion. | 20 |
| Figure 2.1. GRASP depletion reduces cell attachment..... | 45 |
| Figure 2.2. GRASP depletion reduces cell migration. | 46 |
| Figure 2.3. GRASP expression rescues the cell migration defects in GRASP knockout cells. | 47 |
| Figure 2.4. GRASP depletion reduces cell migration and invasion. | 49 |
| Figure 2.5. GRASP knockout reduces $\alpha 5\beta 1$ integrin protein level. | 51 |
| Figure 2.6. GRASP depletion reduces $\alpha 5$ and $\beta 1$ integrin synthesis but has no effect on their turnover. | 54 |
| Figure 2.7. Depletion of GRASP55 and/or GRASP65 enhances cell growth and total protein synthesis. | 56 |
| Figure 3.1. Golgi structure disruption by GRASP KO increases GAG synthesis but reduces its secretion. | 85 |
| Figure 3.2. GRASP KO increases HS synthesis but reduces its sulfation and secretion..... | 87 |
| Figure 3.3. GRASP KO reduces CS synthesis and secretion. | 89 |
| Figure 3.4. GRASP KO alters the expression level of GAG synthesis and sulfation enzymes. | 91 |
| Figure 4.1. GRASP55 is required for unconventional secretion of mutant huntingtin..... | 133 |
| Figure 4.2. Htt secretion is enhanced by various stress stimuli. | 136 |
| Figure 4.3. GRASP55 expression is upregulated under different stress conditions. | 139 |
| Figure 4.4. Htt secretion is autophagy dependent..... | 141 |
| Figure 4.5. GRASP55 regulates Htt secretion via autophagy and p23. | 144 |

| | |
|--|------------|
| Figure 4.6. Secretome analysis identifies candidate proteins secreted by GRASP55-dependent unconventional secretion. | 146 |
| Supplemental Figure 2.1. GRASP knockout reduces cell attachment. | 57 |
| Supplemental Figure 2.2. GRASP deletion reduces cell migration. | 58 |
| Supplemental Figure 2.3. GRASP expression rescues the decreased cell migration in GRASP-knockout cells. | 59 |
| Supplemental Figure 2.4. Depletion of GRASP55 and/or GRASP65 reduces $\alpha 5$ and $\beta 1$ integrin levels. | 60 |
| Supplemental Figure 2.5. Restoration of $\alpha 5\beta 1$ integrin level rescues the decreased cell migration in GRASP-knockout (KO) cells. | 61 |
| Supplemental Figure 2.6. GRASP knockout does not increase $\alpha 5$ integrin turnover. | 62 |
| Supplemental Figure 3.1. GRASP KO increases HS level at the cell surface and GRASP re-expression rescues CS defects in GRASP KO cells. | 94 |
| Supplemental Figure 4.1. GRASP55 is required for the secretion of a subset of neurotoxic proteins. | 150 |
| Supplemental Figure 4.2. GRASP55 facilitates Htt secretion by stabilizing p23. | 151 |

Abstract

The stacking of flattened cisternae is the basic structure of the Golgi apparatus. In mammalian cells, these stacks are linked into a ribbon-like structure located at the perinuclear region of the cell. It has been previously demonstrated that the two Golgi peripheral membrane proteins, GRASP55 and GRASP65, form *trans*-oligomers to link flattened cisternae into stacks. Depletion of either one of the two GRASP proteins decreases the number and length of the cisternae in each stack, whereas depletion of both GRASPs causes complete unstacking and ribbon unlinking of the Golgi. Functional studies revealed that Golgi destruction by GRASP-depletion accelerates protein trafficking in the Golgi but results in N-glycosylation defects of cell surface proteins and mis-sorting lysosome enzymes.

However, whether these defects affect cellular functions such as cell attachment, migration and growth was unclear. In the **first** part of my thesis (Chapter 2), we disrupted the Golgi stacks by GRASP55/65 knockdown/knockout and determined the subsequent impact on multiple cellular activities. We found that this decreases cell attachment, migration, and invasion mainly due to the reduction of $\alpha 5\beta 1$ integrin levels. Our results showed that GRASP depletion decreases $\alpha 5\beta 1$ integrin via reducing its synthesis but not due to accelerated degradation. We also found that GRASP depletion accelerates cell growth, which may be attributed to the increased overall protein synthesis and accelerated protein trafficking.

The Golgi is well-known for its unique stacked structure, but why stack formation is important for Golgi function is a long-standing question in cell biology. To study the significance of Golgi stack formation in glycosaminoglycan (GAGs) synthesis, in Chapter 3 of my thesis, we determined the effect of Golgi unstacking on the synthesis, sulfation, and secretion of heparan sulfate (HS) and chondroitin sulfate (CS), two major types of GAGs synthesized in the Golgi. We found that GRASP depletion increases HS synthesis while decreasing CS synthesis in cells, alters HS and CS sulfation, and reduces both HS and CS secretion. We identified EXTL3, GalNacT1, and PAPSS2, key enzymes in HS and CS synthesis and sulfation pathways, whose level changes cause the alterations in GAG synthesis and sulfation.

In addition to its roles in Golgi structure formation, GRASP55 has recently been shown to regulate autophagy and unconventional secretion via translocation to other membrane structures upon stress conditions. Although the function of GRASP55 in autophagy and unconventional secretion seems to be interconnected, the mechanism of GRASP55-dependent unconventional secretion is poorly understood. In the **third** part of my thesis (Chapter 4), we determined the role of GRASP55 in unconventional secretion of cytosolic neurotoxic proteins using polyQ-Htt as a marker. We discovered that polyQ-Htt is unconventionally secreted via a GRASP55-dependent pathway, which regulates its aggregation and toxicity. GRASP55 regulates the secretion of Htt via two mechanisms: 1) facilitation of autophagosome-lysosome fusion by functioning as a tether between LC3 on autophagosomes and LAMP2 on lysosomes; 2) interacting with and stabilization of p23/TMED10, an ER-Golgi intermediate compartment (ERGIC) protein that functions as a channel for cytoplasmic cargoes translocation into ERGIC lumen. To further elucidate the role of GRASP55 in unconventional secretion, we performed

secretome analysis to systematically analyze GRASP55-dependent conventional and unconventional cargoes and identified new bona fide unconventional pathway cargoes such as TAGLN1, PAICS, and PRDX1. Our research sheds light on the understanding of the unconventional protein secretory pathway and progression of Huntington's disease.

Chapter 1 Introduction to the Golgi Structure and Function

Abstract

The Golgi stacking proteins, GRASP55 and GRASP65, are best known for their roles in Golgi structure formation. These peripheral Golgi proteins form *trans*-oligomers that hold the flat cisternal membranes into stacks. Depletion of both GRASP proteins in cells disrupts the Golgi stack structure, increases protein trafficking, but impairs accurate glycosylation and sorting. In addition to Golgi structure formation, GRASPs, in particular GRASP55, have recently drawn attention in their roles in autophagy and unconventional secretion. In autophagy, GRASP55 senses the energy level by O-GlcNAcylation, which regulates GRASP55 translocation from the Golgi to the autophagosome-lysosome interface, where it interacts with LC3 and LAMP2 to facilitate autophagosome-lysosome fusion. This newly discovered function of GRASP55 in autophagy may help explain its role in the stress-induced, autophagosome-dependent unconventional secretion. In this review, we summarize the emerging functions of the GRASP proteins, focusing on their roles in autophagy, unconventional secretion, as well as on novel GRASP-interacting proteins.

Introduction

The Golgi apparatus is an essential membrane-bound organelle in the cell that functions as a “post station” in the secretory pathway (Klute et al., 2011). In mammalian cells, Golgi membranes are organized as stacks of multiple flat cisternae, which are further linked into a ribbon-like structure located in the perinuclear region (Klumperman, 2011). The Golgi functions as a protein modification and sorting center in the secretory pathway, with different modification enzymes residing in different sub-compartments, including cis-Golgi network (CGN), cis-, medial-, and trans-cisternae, and trans-Golgi network (TGN) (Goldfischer, 1982). The Golgi receives newly synthesized proteins and lipids from the endoplasmic reticulum (ER), sequentially modifies and dispatches them to distinct destinations by protein sorting at the TGN (Brandizzi and Barlowe, 2013, Marsh and Howell, 2002).

The highly ordered Golgi stack structure, which is the functional unit of the Golgi, is believed to facilitate sequential protein modification and processing in mammals. Using *in vitro* assays mimicking Golgi disassembly and reassembly that occur during the cell cycle, two Golgi peripheral membrane proteins, GRASP65 and GRASP55 (Golgi ReAssembly and Stacking Protein), were identified as Golgi stacking factors (Barr et al., 1997, Shorter et al., 1999, Wang et al., 2003). Both GRASPs were further characterized and confirmed to control Golgi stacking and ribbon linking *in vivo* (Xiang and Wang, 2010, Puthenveedu et al., 2006, Feinstein and Linstedt, 2008, Wang et al., 2003). GRASP65 is mainly targeted to cis-Golgi, whereas GRASP55 localizes to medial- and trans-cisternae. GRASP65 and GRASP55 have similar domain

structures. The conserved GRASP domain at the N-terminus contains a membrane anchor and can form dimers and trans-oligomers. The more divergent serine proline-rich (SPR) domain at the C-terminus contains multiple phosphorylation sites, whose phosphorylation inhibits GRASP oligomerization in mitosis (Wang et al., 2005, Vielemeyer et al., 2009, Tang et al., 2012) and perhaps also in stress and pathological conditions (Figure 1.1; Figure 1.2A) (Joshi and Wang, 2015, Joshi et al., 2014, Joshi et al., 2015). In coordination with GRASPs, GRASPs interacting proteins, including the GRASP65 binding partner GM130 and GRASP55 binding protein Golgin-45, may also be involved in Golgi structure formation (Lee et al., 2014).

Since depletion or inhibition of GRASP55 and GRASP65 impairs Golgi structure formation, these proteins have been recently used as tools to disrupt the Golgi structure and thereby determine the functional consequence of Golgi structural disruption. In addition, a number of novel GRASP-interacting proteins have been identified and GRASPs have been linked to autophagy, unconventional secretion, and other cellular activities, such as cell adhesion, migration, and growth. In this review, we attempt to summarize these new discoveries on GRASP functions and discuss the potential links between these new findings.

1.1 GRASP55 and GRASP65 as tools to probe the biological significance of Golgi structure formation

The role of GRASPs in Golgi stack formation and the impact of GRASP depletion or inhibition on Golgi functions have been explored using a number of experimental approaches. Inhibition of GRASP65 by microinjecting inhibitory antibodies, knocking down (KD) GRASPs by siRNA, or knocking out (KO) GRASPs by CRISPR/Cas9, all significantly impair Golgi stack formation (Wang et al., 2003, Tang et al., 2010, Bekier et al., 2017). Research from the Rothman and Wang labs demonstrated that depletion of GRASPs, which results in Golgi fragmentation, increases the trafficking of selected cargo molecules, including vesicular stomatitis virus G-protein (VSVG), $\alpha 5$ integrin and CD8 (Wang et al., 2008, Xiang et al., 2013, Lee et al., 2014). A plausible explanation for this result is that Golgi unstacking increases the membrane surface for vesicle formation and thus accelerates protein trafficking (Wang et al., 2008, Zhang and Wang, 2015b, Ahat et al., 2019b, Bekier et al., 2017). Need to mention, in contrast to the results described above, D'Angelo et al. reported that GRASP55/65 bind the C-terminal hydrophobic tail of specific transmembrane proteins such as CD8, and this interaction is required for CD8 trafficking through the Golgi stack (D'Angelo et al., 2009). These controversial results could be caused by the different constructs used in the studies; the first two labs used full length CD8 (or a fusion protein with full length CD8), while the last one used a VSVG-CD8 α (C-terminal tail) chimera. Other factors, such as the knockdown efficiency, may also be involved. Considering that there is currently no other way to disrupt Golgi stacking other than manipulating GRASPs, this subject requires further investigation.

Glycomic analysis by mass spectrometry showed that GRASP depletion, especially GRASP55 single depletion or GRASP55/65 double-depletion, results in a reduction in the overall glycan abundance, complexity, and glycoprotein composition at the plasma membrane. Interestingly, GRASP depletion-mediated Golgi unstacking also causes mis-sorting of lysosome enzymes such as cathepsin D (Xiang et al., 2013, Zhang et al., 2015). Therefore, it has been proposed that cisternal stacking impedes the intra-Golgi trafficking speed by reducing the accessibility of coat proteins to Golgi membranes, which ensures accurate glycosylation and sorting (Huang and Wang, 2017, Zhang and Wang, 2015b, Zhang and Wang, 2016). Recently, GRASP55 and GRASP65 single knockout mice have been reported, with only limited defects in Golgi structure and function (Veenendaal et al., 2014, Chiritoiu et al., 2019). One possibility is that the knockout effect of one GRASP may be compensated by the redundancy of the other GRASP protein. It has been demonstrated that when one GRASP is depleted in cells, the level of the other GRASP protein may increase to compensate for the knockout effect (Bekier et al., 2017). GRASP55 and GRASP65 double knockout mice have not been reported so far.

1.2 New discoveries on GRASP55 and GRASP65 interacting proteins

Recently, some new discoveries have been made on the known interacting partners of GRASPs. Golgin-45 is one of the earliest identified GRASP55-binding proteins, which is involved in vesicle tethering and Golgi structure regulation (Short et al., 2001, Lee et al., 2014).

The structural basis of GRASP55 interaction with Golgin-45 has recently been revealed. The last C-terminal residues of Golgin-45, QGELIAL, insert into the canonical PDZ-peptide binding pocket in the PDZ1 domain of GRASP55, while the upstream residues of the C-terminal sequence of Golgin-45, TRYENITFNCCNHC, interacts with both PDZ domains by inserting into the cleft between them. Furthermore, the C-terminus of Golgin-45 also binds the PDZ2 domains of the two neighboring GRASP55 molecules, which enhances GRASP55 oligomerization. This is thought to play an important role in Golgi stacking. The third interaction site between Golgin-45 and GRASP55 is a unique zinc finger-like structure formed between Cys393/Cys396 of Golgin-45 and His18 (β 1)/Cys103 (β 2) of GRASP55 (Zhao et al., 2017). Similar to the Golgin-45 and GRASP55 interaction, GM130 interacts with GRASP65 via its C-terminal KITVI sequence that binds PDZ1, and via the IPFFY sequence that interacts with both PDZ domains by inserting into the hydrophobic cleft between them. But unlike the Golgin-45 and GRASP55 interaction, GRASP65 undergoes conformational change on PDZ domain upon GM130 interaction but does not form a zinc-finger structure on GM130-GRASP65 interaction (Hu et al., 2015, Zhao et al., 2017).

In the past several years, a number of new GRASP binding proteins have been identified (Figure 1.1; Table 1.1). Two interacting proteins have recently been discovered for GRASP65, the actin elongation factor Mena (mammalian enabled homologue) and the Hsc70 (heat shock cognate 71 kDa protein) co-chaperone DjA1 (DnaJ homolog subfamily A member 1). Mena is recruited to the Golgi membranes by GRASP65 to facilitate actin polymerization and GRASP65

oligomerization, and thus functions as a bridging protein in Golgi ribbon linking (Tang et al., 2016). DjA1 binds to GRASP65 and promotes GRASP65 oligomerization in a Hsc70-independent manner (Li et al., 2019c).

Most recently, several novel GRASP55 binding partners have been identified that are related to the newly discovered function of GRASP55 in autophagy. GRASP55 not only facilitates autophagosome-lysosome fusion via the interactions with LC3 on autophagosomes and LAMP2 on lysosomes (Zhang et al., 2018, Zhang and Wang, 2018b, Zhang and Wang, 2018a), but also directly binds Beclin-1 (BECN1) and UVRAG to facilitate the assembly and membrane association of the phosphatidylinositol 3-kinase (PtdIns3K, or PI3K) complex (Zhang et al., 2019b), and therefore plays an important role in autophagosome maturation during both glucose depletion and amino acid starvation. Moreover, GRASP55 binds cystic fibrosis transmembrane conductance regulator (CFTR) and transforming growth factor beta 1 (TGF β 1) to facilitate their unconventional secretion (Gee et al., 2011, Nüchel et al., 2018). These new findings reveal novel roles for GRASPs in cellular activities outside of the Golgi. While some of these findings have been recently reviewed elsewhere (Li et al., 2019a), several key advances are discussed below in detail.

1.3 GRASP55 regulates autophagosome-lysosome fusion

How the Golgi copes with different stresses and whether there is a Golgi stress sensor have not been systematically studied. In an effort to explore how the Golgi responds to energy deprivation, a number of Golgi proteins were examined for O-GlcNAcylation, a cytosolic glycosylation that serves as an energy sensor to regulate cellular pathways (Zhang et al., 2018). In this study, Zhang et al. discovered that GRASP55, but not other Golgi matrix proteins examined, including GRASP65, GM130 and Golgin-45, is O-GlcNAcylated under growth condition. Upon glucose starvation, GRASP55 is de-O-GlcNAcylated and forms puncta outside of the Golgi area. Since glucose starvation induces autophagy, the function of GRASP55 in autophagy was then tested. Indeed, depletion of GRASP55, but not GRASP65, increased the number of autophagosomes but decreased the autophagic flux, indicating a defect in autophagosome-lysosome fusion.

How does a Golgi protein like GRASP55 regulate autophagy? The study by Zhang et al. (Zhang et al., 2018) revealed that GRASP55 de-O-GlcNAcylation upon glucose deprivation allows some of the GRASP55 molecules to colocalize with autophagosomes. GRASP55 targeting to autophagosomes is regulated by O-GlcNAcylation, as it is enhanced by mutating the O-GlcNAcylation sites on GRASP55 as well as by glucose starvation which reduces GRASP55 O-GlcNAcylation. Further biochemical studies demonstrate that GRASP55 interacts with LC3-II on autophagosomes, and this interaction is enhanced by GRASP55 de-O-GlcNAcylation. In addition, GRASP55 also interacts with LAMP2 on lysosomes. These together suggest a

possibility that GRASP55 may function as a bridging protein to facilitate LC3-LAMP2 interaction as well as autophagosome-lysosome fusion. Indeed, this possibility was subsequently confirmed using *in vivo* and *in vitro* approaches (Figure 1.2B) (Zhang et al., 2018). In cells, GRASP55 depletion reduces LC3 and LAMP2 colocalization as well as autophagosome-lysosome fusion. *In vitro*, GRASP55 facilitates autophagosome-lysosome fusion in an *in vitro* fusion assay. Furthermore, the addition of recombinant GRASP55 enhances LC3 and LAMP2 co-immunoprecipitation from cell lysates (Zhang et al., 2018). Thus, like in Golgi stacking, GRASP55 oligomers serve as membrane tethers to facilitate autophagosome-lysosome fusion.

The role of GRASP55 in autophagosome-lysosome fusion is not limited to glucose starvation, but also in amino acid starvation. Upon amino acid starvation, GRASP55 not only physically interacts with LC3 and LAMP2, but also regulates the formation of the PI3K UVRAG complex that is known to facilitate autophagosome-lysosome fusion (Zhang et al., 2019b). Here, GRASP55 directly interacts with Beclin-1, induces the UVRAG PI3K complex formation and increases its membrane association. These reports identified GRASP55 as a specific energy and nutrient sensor on the Golgi to regulate autophagy.

Since GRASP55 still appears on autophagosomes in the presence of the protein synthesis inhibitor cycloheximide, it is speculated that GRASP55 is targeted to autophagosomes from an existing pool upon autophagy induction (Zhang et al., 2018). One remaining interesting question concerns how GRASP55 is targeted to autophagosomes. GRASP55 is unlikely translocated to

the autophagosomes with the entire Golgi as cargo for autophagic degradation, since no other Golgi markers are found in the newly formed autophagosomes and GRASP55 is localized on the outer membrane of autophagosomes instead of the lumen (Zhang et al., 2019b, Zhang et al., 2018). One possibility is through vesicular transport, similar to the transmembrane protein Atg9 that is normally enriched in the Golgi and is translocated to autophagosomes upon autophagy induction. However, unlike Atg9, GRASP55 does not have a transmembrane domain, and how the translocation occurs selectively on de-O-GlcNAcylated GRASP55 remains unknown. Alternatively, it is possible that a small pool of GRASP55 constantly shuttles between the Golgi, cytosol, and autophagosomes; and the equilibrium is regulated by GRASP55 O-GlcNAcylation. Nevertheless, how GRASP55 is targeted to autophagosomes under stress conditions requires further investigation.

While the discovery of GRASP55 as a membrane tether in autophagosome-lysosome fusion is exciting, it is unknown how GRASP55 interplays with other known tethering proteins, in particular Rab7 and the HOPS complex, as well as the STX17-SNAP29-VAMP7/8 SNARE complex that mediates the fusion (Jager et al., 2004, Itakura et al., 2012, Jiang et al., 2014). It is possible that these proteins function sequentially during autophagosome-lysosome fusion. Alternatively, GRASP55 may function as an independent mechanism in autophagosome-lysosome fusion.

1.4 GRASP55/65 and unconventional secretion

It was long believed that only proteins with canonical ER signal peptides at the N-terminus can be secreted out of the cell. Since the discovery of the Golgi-independent unconventional secretion of the cytokine interleukin 1 beta (IL-1 β) (Muesch et al., 1990), more proteins without ER signal sequences (leaderless proteins) and some integral membrane proteins have been reported to be transported or secreted in a Golgi-independent manner (Kinseth et al., 2007, Schotman et al., 2008, Gee et al., 2011). Collectively, the non-canonical Golgi-independent secretion is referred to as unconventional protein secretion (UPS). Interestingly, although UPS itself is Golgi-independent, it requires two important Golgi proteins, GRASP55 and GRASP65, in mammalian cells and their homologues in other model organisms. Whether unconventional secretion is a by-product of loss of Golgi functions, or vice-versa, has not been ruled out due to the lack of molecular tools to manipulate Golgi structure and function without affecting GRASPs. In a previous review (Rabouille, 2017), unconventional secretion is generally classified into four categories, type I is direct translocation of cargo molecules across the plasma membrane via pore formation, type II is unconventional secretion through ATP-binding cassette (ABC) transporters, type III is vesicle-mediated secretion of cytosolic proteins, and type IV is the Golgi bypassing transportation of integral membrane proteins. GRASPs and their homologues have been reported to play a role in type III and type IV UPS, which is the focus of this review in terms of unconventional secretion.

GRASPs and unconventional trafficking of integral membrane proteins

CFTR

The Phe508 deletion from CFTR results in the inhibition of its trafficking to the plasma membrane and ER-associated degradation. It has been shown that GRASP55 and GRASP65 are required for the unconventional secretion of both WT and DeltaF508 CFTR when ER-to-Golgi trafficking is inhibited by expressing a dominant negative Sar1 or Arf1, or by inhibiting vesicle fusion via overexpression of syntaxin 5 (Gee et al., 2011). GRASP55 is phosphorylated at Ser441 during certain ER stresses, monomerized and located near the ER to regulate unconventional secretion of CFTR, which requires CFTR-GRASP55 interaction (Figure 1.2C) (Kim et al., 2016, Gee et al., 2018). Similar to GRASP55, GRASP65 overexpression rescued the secretion defect of mutant CFTR, although GRASP65 was not extensively tested in the same studies.

One contradiction in these reports is that overexpression of the GRASP55-G2A mutant inhibits CFTR secretion, whereas expression of N-terminally tagged GRASP55, which has been shown to abolish its membrane targeting similar to the GRASP-G2A mutant, increases CFTR secretion (Gee et al., 2011, Kim et al., 2016, Heinrich et al., 2014). Considering that GRASP55 regulates CFTR secretion by direct binding, GRASP55 may serve as a cytosolic chaperone to regulate CFTR sequestration by autophagosomes or by multivesicular bodies (MVBs) (Noh et al., 2018). Here, GRASP55 phosphorylation and re-localization in response to ER stress is necessary for CFTR secretion. A recent report showed that GRASP55 regulates the IRE1 ER unfolded protein response (UPR) pathway (Chiritoiu et al., 2019). It is unclear why the

medial/trans-Golgi protein GRASP55, but not the *cis*-Golgi protein GRASP65, is the main player in regulating this activity as GRASP65 is localized on the Golgi compartments closer to the ER.

Integrin

dGRASP, the *Drosophila* homologue of GRASP, regulates the Golgi bypassing, noncanonical trafficking of the alpha subunit of integrin during *Drosophila* wing development (Schotman et al., 2008). Unlike normal situations in which dGRASP is localized on the Golgi, during wing development, dGRASP localizes near the plasma membrane to regulate noncanonical secretion of alpha-integrin. It was proposed that dGRASP regulates integrin secretion via facilitating the fusion of integrin-containing vesicles with the plasma membrane (Schotman et al., 2008). Alternatively, GRASP depletion may cause mis-sorting of an unknown, plasma membrane destined vesicle fusion protein (i.e. SNARE), which subsequently affects the noncanonical secretion of integrin. Unlike CFTR, it is unclear if dGRASP binding is required for integrin secretion. Considering that GRASP55 translocates to the ER in CFTR secretion while dGRASP translocates to near the plasma membrane area in integrin secretion, GRASP may regulate the secretion of these two transmembrane cargoes through different mechanisms.

GRASP55 and endosome/autophagosome-dependent unconventional secretion of cytosolic proteins

IL-1 β

IL-1 β , the major cytosolic regulator of inflammation, was one of the first identified cargoes of UPS (Muesch et al., 1990). IL-1 β and another cytokine, TGF β 1, are secreted via a non-canonical secretory pathway distinct from the conventional ER-Golgi pathway (Nüchel et al., 2018). IL-1 β is exported either through vesicle mediated secretion or via Gasdermin-D-mediated pore formation at the plasma membrane (Kayagaki et al., 2015). More recently, it was revealed that IL-1 β is first restrained in the intermembrane space of autophagosomes and then secreted by the fusion of autophagosomes with the plasma membrane (Figure 1.2D). This fusion process is mediated by SNAREs including Sec22b on autophagosomes, syntaxin 3 and syntaxin 4 on the plasma membrane, and SNAP-23 and SNAP-29 from the cytosol (Dupont et al., 2011, Kimura et al., 2017). Most recently, a question was raised on whether autophagy is indeed involved in IL-1 β secretion (Chiritoiu et al., 2019).

Interestingly, depletion of GRASP55 or GRASP65 reduces IL-1 β secretion (Zhang et al., 2015) (Figure 1.2D). GRASP55 may regulate the secretion of IL-1 β through its role in autophagy or by modulating the IRE α /XBP-1 UPR pathway (Dupont et al., 2011, Zhang and Wang, 2018b, Chiritoiu et al., 2019, van Ziel et al., 2019). Considering the function of GRASP55 in autophagosome-lysosome fusion, it is reasonable to speculate that GRASP55 may also be involved in autophagosome-plasma membrane fusion in this scenario.

AcbA/Acb1

GRASP65 and GRASP55 were originally identified in mammalian cells to regulate Golgi stacking and ribbon linking. Kinseth et al. (Kinseth et al., 2007) provided the first evidence that GRASP regulates unconventional secretion in *Dictyostelium*. This unexpected finding came from the observation that knockout of GrpA, the GRASP homolog in *Dictyostelium*, results in a secretion defect of AcbA, a protein that is processed in the extracellular environment to produce the spore differentiation factor-2 (SDF 2) (Kinseth et al., 2007, Levi and Glick, 2007). Later, it was reported that Acb1, the budding yeast homologue of ACBP, is also unconventionally secreted, which depends on Grh1 (the GRASP homologue in the budding yeast), core Atg genes, ESCRT machinery and SNAREs, but is independent of COPII coated vesicles (Figure 1.2D) (Manjithaya et al., 2010, Duran et al., 2010).

Although GRASP is required for Acb1 secretion, it is not clear at which step GRASP is involved. It seems that the vesicles carrying Acb1 are distinct from autophagosomes because GFP-Grh1 colocalizes with neither the autophagosome marker Atg8 nor the phagophore marker Ape1 (Bruns et al., 2011). Instead, a novel membrane-bound compartment called CUPS (compartment for unconventional protein secretion) is required for Acb1 secretion. However, the formation and identity of this membrane structure are largely unknown (Ye, 2018).

1.5 Outlook

It is clear that GRASP65 and GRASP55 have both Golgi-dependent and Golgi-independent functions. On the Golgi, GRASP trans-oligomers are the primary machineries for Golgi stack formation. The recent finding of reduced cell adhesion and migration under GRASP depletion strengthens the essential role of Golgi stacking in protein trafficking, modification, and signaling.

Under certain stress conditions or at certain stages of development, GRASPs also function outside of the Golgi, likely as membrane tethers as within the Golgi stacks. The findings are interesting, but several outstanding questions remain. For example, how is GRASP55 targeted to different locations outside of the Golgi? Do GRASPs function as tethers in the regulation of unconventional secretion? The recent findings of GRASP55 in autophagy may help address these questions. Furthermore, the role of GRASPs in unconventional secretion has been confirmed in a variety of systems, but not all types of unconventional secretion require GRASPs. For example, unconventional secretion of a misfolding-associated protein secretion (MAPS) cargo GFP1-10 and a cilia transmembrane protein Peripherin/rds is reported to be GRASP-independent (Lee et al., 2016, Tian et al., 2014). This indicates a heterogeneity of unconventional secretion and the specificity of GRASPs in the regulation of unconventional secretion of certain substrates. Future studies by comparing different cargo molecules may help understand the exact roles of GRASPs in unconventional secretion.

GRASP proteins play important roles in unconventional secretion, but the underlying mechanism remains largely unknown. Both unconventional secretion of certain cargoes and autophagy are augmented under stress conditions. The newly uncovered roles of GRASP55 as an energy sensor in the Golgi and a membrane tether in autophagy indicate that it may serve as a stress sensor and an effector in stress response; and these roles may be linked to unconventional secretion of certain cargo molecules. GRASP55 may coordinate Golgi-dependent and Golgi-independent trafficking pathways in the cell under different conditions. In addition to autophagy, the emerging role of GRASP55 in the regulation of ER stress and UPR indicates that GRASP55 may affect unconventional secretion through UPR (Chiritoiu et al., 2019, van Ziel et al., 2019). Systematic studies on Golgi response to different stress stimuli and identification of novel GRASP interacting proteins under normal and stress conditions may shed light on the mechanism of GRASP55 and GRASP65 in Golgi-dependent and Golgi-independent functions.

Table 1.1. GRASP interacting proteins and functions

| Names | Golgi Localization | Interaction Proteins | Functions |
|---------------------|-------------------------------|--|--|
| GRASP55/ GORASP2 | <i>medial/trans</i> | <ul style="list-style-type: none"> - Golgin-45 (Short et al., 2001, Zhao et al., 2017) - p24 (Barr et al., 2001) - TGF-α (Kuo et al., 2000), CD8a and Frizzled 4 (D'Angelo et al., 2009) - LC3, LAMP2 (Zhang et al., 2018), Beclin-1, UVRAG (Zhang et al., 2019b) - CFTR (Gee et al., 2011), TGFβ1 (Nüchel et al., 2018) - JAM (Cartier-Michaud et al., 2017) | <p>Golgi stacking (Shorter et al., 1999, Xiang and Wang, 2010, Bekier et al., 2017, Short et al., 2001, Zhao et al., 2017)</p> <p>p24 cargo receptor retention (Barr et al., 2001)</p> <p>Transport of specific cargo (Kuo et al., 2000, D'Angelo et al., 2009)</p> <p>Autophagosome-lysosome fusion (Zhang et al., 2018, Zhang and Wang, 2018b, Zhang and Wang, 2018a)</p> <p>Unconventional secretion (Gee et al., 2011, Nüchel et al., 2018, Rabouille, 2017)</p> <p>Spermatogenesis (Cartier-Michaud et al., 2017)</p> |
| GRASP65/ GORASP1 | <i>cis</i> | <ul style="list-style-type: none"> - GM130 (Barr et al., 1998), DjA1(Li et al., 2019c) - Mena (Tang et al., 2016) - p24 (Barr et al., 2001) - CD8a, Frizzled 4 (D'Angelo et al., 2009) - Bcl-X_L (Cheng et al., 2010), caspase-3 (Lane et al., 2002) | <p>Golgi stacking (Barr et al., 1997, Xiang and Wang, 2010, Bekier et al., 2017, Li et al., 2019c)</p> <p>Golgi ribbon formation (Tang et al., 2016)</p> <p>p24 cargo receptor retention (Barr et al., 2001)</p> <p>Transport of specific cargo (D'Angelo et al., 2009)</p> <p>Apoptosis (Lane et al., 2002, Cheng et al., 2010)</p> |

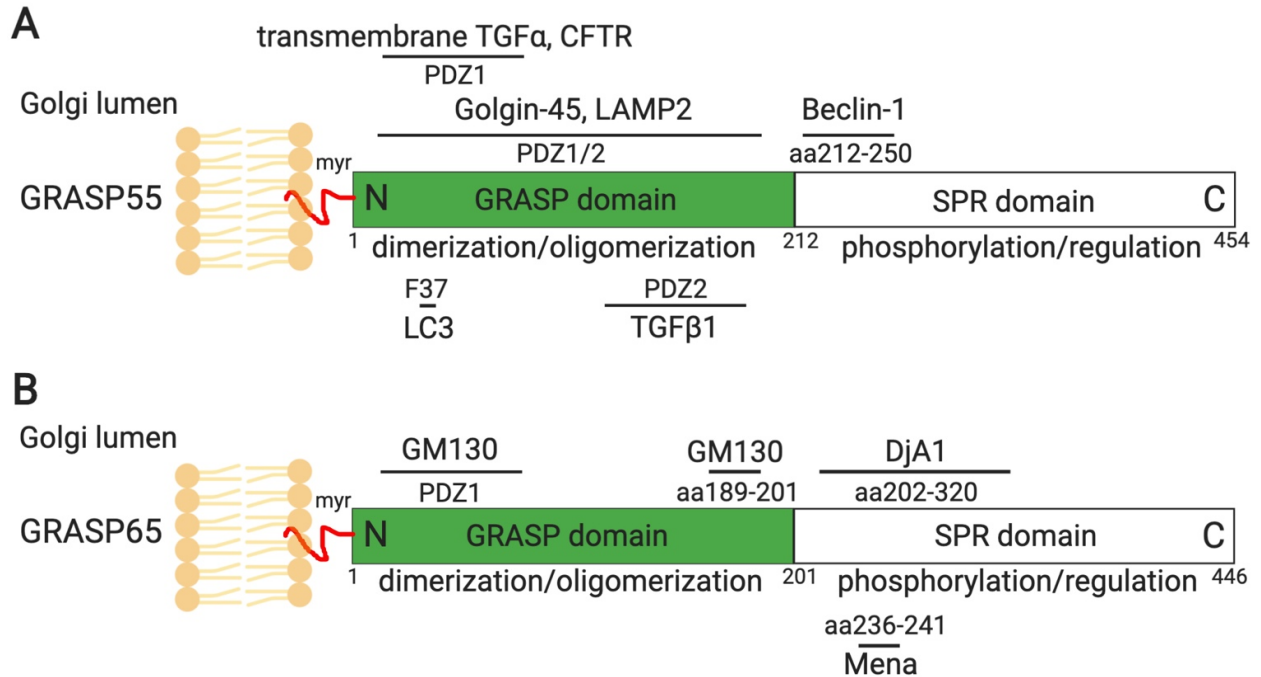


Figure 1.1. GRASP55 and GRASP65 domain structures and interacting proteins.

GRASP55 and GRASP65 are peripheral membrane proteins that are attached to the Golgi membranes via myristoylation (myr). Both GRASPs share similar domain structures, with a conserved GRASP domain at the N-terminus consisted of PDZ1 and PDZ2 subdomains, and a C-terminal serine/proline-rich (SPR) domain. The GRASP domain forms dimers and *trans*-oligomers that tether adjacent membranes. The SPR domain contains multiple phosphorylation sites whose phosphorylation in mitosis impairs GRASP oligomerization and leads to Golgi fragmentation (Wang et al., 2003, Wang et al., 2005, Tang et al., 2012). GRASP55 and GRASP65 interacts with Golgin-45 and GM130, respectively, which are essential for their roles in Golgi structure formation and function (Short et al., 2001, Barr et al., 1997). GRASP55 also regulates autophagy by interacting with Beclin-1, LC3 and LAMP2, and controls CFTR, TGF α

(pro form) and TGF β 1 secretion (Zhang et al., 2019b, Zhang et al., 2018, Gee et al., 2011, Kuo et al., 2000, Nüchel et al., 2018). GRASP65 interacts with Mena and Dja1, which are essential for Golgi structure formation (Tang et al., 2016, Li et al., 2019c). More GRASP-interacting proteins can be found on Table 1.1, only those with known binding sites on GRASPs are shown here. Indicated sites are based on rat GRASP sequences.

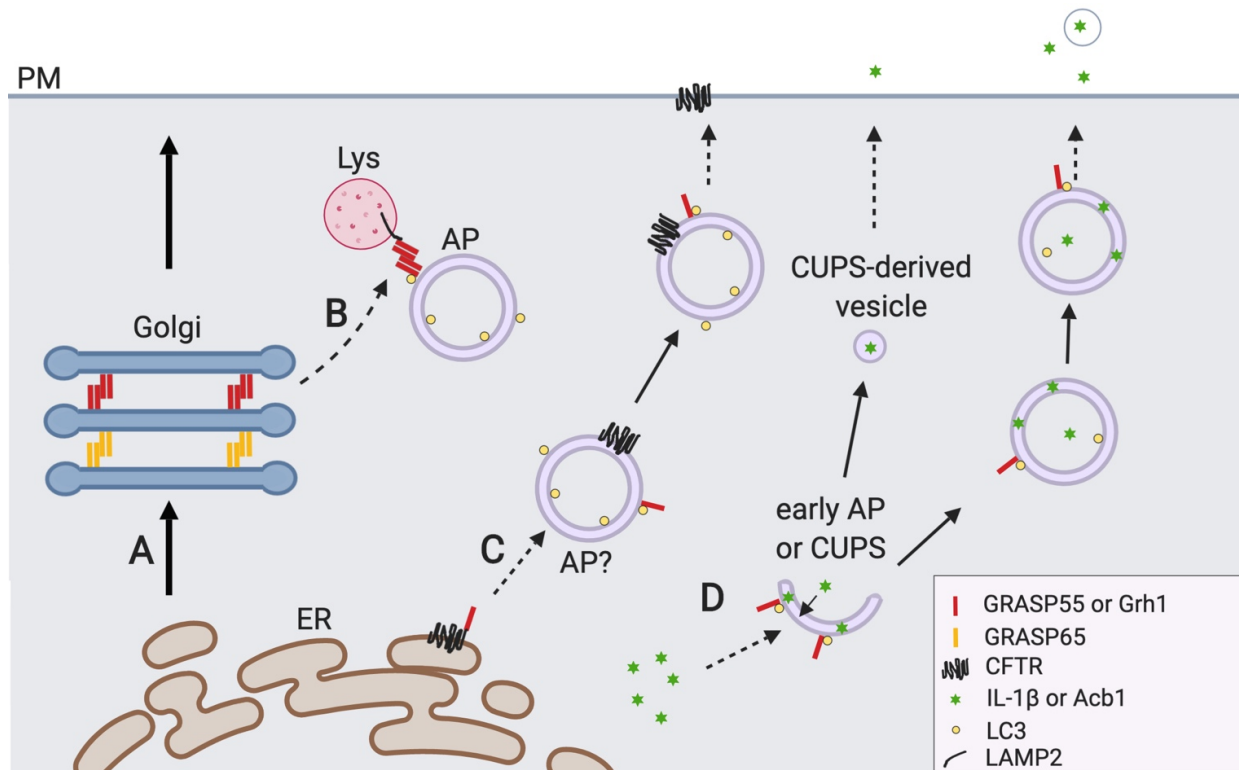


Figure 1.2. GRASP55 regulates autophagy and unconventional secretion.

(A) The conventional ER-Golgi-plasma membrane (PM) secretory pathway. (B) GRASP55 facilitates autophagosome (AP)-lysosome (Lys) fusion. Upon glucose starvation or amino acid starvation, GRASP55 is translocated to the AP-Lys interface to promote autolysosome formation

by bridging LC3 and LAMP2 and by facilitating the UVRAG PI3K complex formation (not shown) (Zhang et al., 2019b, Zhang et al., 2018). Undigested contents in the autolysosomes and lysosomes may be secreted by lysosome exocytosis (not shown) (Reddy et al., 2001, Samie and Xu, 2014). **(C)** GRASP55 is required for CFTR trafficking that bypasses the Golgi. Mutant CFTR is transported to the PM in a Golgi-independent manner under ER stress and inhibition of the conventional secretory pathway. During this process phosphorylated and monomerized GRASP55 binds CFTR at the ER membrane and regulates its sequestration (Kim et al., 2016). So far no evidence has been provided that CFTR is indeed localized on the outer membrane of AP, and how CFTR is translocated from ER to AP remains elusive. GRASP55 may also regulate this pathway by facilitating direct fusion of CFTR containing APs with PM or Lys via *trans*-oligomer formation (not reported). **(D)** GRASP55 is involved in unconventional secretion of leaderless cytosolic proteins (i.e. Acb1, IL-1 β). IL-1 β could be secreted via secretory autophagosomes which is GRASP55 dependent (Zhang et al., 2015). The function of GRASP55 here is unclear but GRASP55 may serve as an ER stress sensor or unfolded protein response (UPR) regulator in this process (Chiritoiu et al., 2019). Yeast protein Acb1 secretion requires the formation of a new type of Grh1-positive membrane compartment called CUPS (compartment for unconventional protein secretion) whose identity is largely unknown (Bruns et al., 2011). CUPS derived vesicles (sacculles) fuse with plasma membrane and releases Acb1 to outside of the cell (Curwin et al., 2016).

Chapter 2 GRASP Depletion-mediated Golgi Destruction Decreases Cell Adhesion and Migration Via the Reduction of $\alpha 5\beta 1$ Integrin

Abstract

The Golgi apparatus is a membrane-bound organelle that serves as the center for trafficking and processing of proteins and lipids. To perform these functions, the Golgi forms a multi-layer stacked structure held by GRASP55 and GRASP65 *trans*-oligomers and perhaps their binding partners. Depletion of GRASP proteins disrupts Golgi stack formation and impairs critical functions of the Golgi, such as accurate protein glycosylation and sorting. However, how Golgi destruction affects other cellular activities is so far unknown. Here we report that depletion of GRASP proteins reduces cell attachment and migration. Interestingly, GRASP depletion reduces the protein level of $\alpha 5\beta 1$ integrin, the major cell adhesion molecules at the surface of HeLa and MDA-MB-231 cells, due to decreased integrin protein synthesis. GRASP depletion also increases cell growth and total protein synthesis. These new findings will enrich our understanding on the role of the Golgi in cell physiology and provide potential target for treating protein trafficking disorders.

Introduction

The Golgi Apparatus is an essential cellular membrane organelle at the center of the secretory pathway (Klute et al., 2011). Its basic structure is a stack of flat, closely arranged cisternae. Each mammalian cell contains about 100 Golgi stacks, which often line up and laterally link to form a ribbon localized in the perinuclear region (Rambourg et al., 1987, Klumperman, 2011). The primary function of the Golgi is to process membrane and secretory proteins. Cargo proteins synthesized at the endoplasmic reticulum (ER) are transferred by COPII vesicles to the *cis*-Golgi (Brandizzi and Barlowe, 2013). While travelling across the Golgi stack, they undergo posttranslational modifications, including glycosylation, phosphorylation, and proteolysis (Goldfischer, 1982). In the *trans*-Golgi network (TGN), proteins are sorted for delivery to proper destinations, such as endosomes, lysosomes, the plasma membrane, or outside of the cell by constitutive or regulated secretion (Marsh and Howell, 2002). Proteins derived from one third of the human genes travel through the secretory pathway (Pfeffer, 2013), and proper functioning of the Golgi is required for a variety of cellular activities and homeostasis.

The exact mechanism of Golgi stack formation is not fully understood, but the two Golgi ReAssembly and Stacking Proteins (GRASPs), GRASP55 and GRASP65, are so far the only identified Golgi stacking proteins (Barr et al., 1997, Shorter et al., 1999, Zhang and Wang, 2015a, Xiang and Wang, 2010). GRASP55 and GRASP65, localize at *medial-trans*- and *cis*-Golgi, respectively, form *trans*-oligomers through the N-terminal GRASP domain to hold the cisternae together into stacks (Wang et al., 2005) and link Golgi stacks into a ribbon (Puthenveedu et al., 2006). The C-terminal Serine-Proline Rich (SPR) domains of GRASP55 and GRASP65 are more divergent, but both are phosphorylated in mitosis to dissociate the protein

trans-oligomers and disassemble the Golgi structure. In telophase, Golgi tubules and vesicles are divided equally between daughter cells, where they are reassembled into stacks and ribbons upon dephosphorylation of GRASP proteins (Tang et al., 2012, Vielemeyer et al., 2009). Therefore, GRASPs are essential proteins for maintaining an intact and dynamic Golgi structure (Zhang and Wang, 2015a, Zhang and Wang, 2016). In addition to GRASPs, GRASP-interacting proteins such as GM130 and Golgin 45 may also facilitate Golgi stack formation (Lee et al., 2014).

The discovery of the GRASP proteins provides us with a molecular tool to control Golgi stacking and thus to probe the functional significance of Golgi structure formation. We have inhibited Golgi stacking by microinjecting GRASP65 antibodies (Wang et al., 2003, Wang et al., 2008), by depleting both GRASPs in cells via knockdown (Tang et al., 2010, Xiang and Wang, 2010), or by GRASP knockout (Bekier et al., 2017). These caused accelerated trafficking of several marker proteins, including CD8, Vesicular stomatitis virus G-protein (VSVG), cathepsin D, and integrins (Wang et al., 2008, Xiang et al., 2013, Bekier et al., 2017). Furthermore, GRASP depletion significantly decreased both global N-linked glycosylation and glycan complexity and changed the glycolipid composition at the cell surface (Bekier et al., 2017, Xiang et al., 2013). A plausible explanation is that stacking reduces the accessibility of coat proteins to Golgi membranes, which decreases the rate of vesicle budding and transport but ensures accurate glycosylation and sorting. The Golgi harbors various glycosyltransferases and glycosidases in different sub-compartments, but unlike the ER that contains a high concentration of folding chaperones that retain improperly modified cargos (Helenius and Aebi, 2001, Pearse and Hebert, 2010, Hebert and Molinari, 2007), the Golgi lacks a rigorous system to control the fidelity of its biosynthetic processes. An ordered structure and a controlled cargo flow through the Golgi are

likely required to carry out precise, sequential modifications as cargo proteins pass between cisternae (Zhang and Wang, 2015a, Huang and Wang, 2017). In addition, GRASP depletion also caused mis-sorting of the lysosomal enzyme cathepsin D to the extracellular space (Xiang et al., 2013), suggesting that stacking may ensure that sorting occurs only when cargo molecules reach the TGN. These findings demonstrate that Golgi stack formation is fundamentally important for Golgi function (Zhang and Wang, 2016).

Proper glycosylation and sorting of proteins in the Golgi are required for many cell activities, such as cell attachment, migration, proliferation, and embryonic development (Ono and Hakomori, 2004, Hang et al., 2017, Janik et al., 2010, Zheng et al., 1994). In addition, Golgi structural defects have been linked to human diseases, including Alzheimer's (Aridor and Balch, 1999, Joshi et al., 2014, Evin, 2015), Huntington's (Hilditch-Maguire et al., 2000), Parkinson's (Mizuno et al., 2001), autoimmune diseases (Bizzaro et al., 1999, Fritzler et al., 1984), cancer (Yoshimura et al., 1996, Roberts et al., 1998, Krishnan et al., 2005, Diaz-Corrales et al., 2004, Dennis et al., 1999), viral infections (Ng et al., 2003), and congenital disorders of glycosylation and Wiskott-Aldrich syndrome (Durand and Seta, 2000, Freeze and Ng, 2011). However, the causal relationship between Golgi defects and disease pathogenesis remains largely unexplored. Therefore, it is crucial to understand how Golgi structure disruption affects essential cellular activities and physiology such as cell attachment, migration, and growth.

Cell attachment depends on a set of cell adhesion proteins called integrins; $\alpha 5 \beta 1$ integrin is the main form of integrin complex in HeLa and MDA-MB-231 cells (Yu et al., 2011, Feng Jia, 2016, Mierke et al., 2011). As highly glycosylated transmembrane proteins, $\alpha 5$ and $\beta 1$ integrins

are processed by the Golgi and transported to the plasma membrane for their proper functions. When transported through the TGN, $\alpha 5$ integrin undergoes post-translational cleavage for activation, where pro-integrin $\alpha 5$ (~170 kDa) is cleaved by proprotein convertases (PCs) into heavy (~130 kDa) and light (~19 kDa) chains that are linked by a disulfide bond (Paule et al., 2012). Since GRASP depletion accelerates $\alpha 5$ integrin trafficking and processing (Xiang et al., 2013), it is reasonable to expect that it may also affect $\alpha 5$ and $\beta 1$ integrin glycosylation and sorting as well as cell attachment.

In this study, we found that Golgi destruction by GRASP depletion reduces $\alpha 5\beta 1$ integrin protein level, which results in compromised cell activities such as decreased cell adhesion and migration. Using radioactive labeling and pulse chase assays, we showed that decreased protein level of $\alpha 5\beta 1$ integrin is due to reduced protein synthesis rather than accelerated protein degradation. Surprisingly, Golgi unstacking accelerated overall protein synthesis and cell proliferation. Our study revealed a direct link between Golgi structure, function, and cellular activities.

Results

2.1 GRASP depletion reduces cell adhesion

The proper glycosylation and localization of cell surface proteins are important for cell adhesion and migration. When examined under a phase contrast microscope, we observed that, in comparison with cells transfected with control or GRASP55 small interfering RNA (siRNA), HeLa cells depleted of GRASP65 or both GRASPs spread less well on the dish, and they also formed clusters and appeared to be more round (Figure 2.1, C & D vs. A & B; Figure 2.1E). To

further assess the effect of GRASP depletion on cell adhesion, we detached the cells using EDTA and placed the cells on fibronectin-coated plates. After incubation with serum-free medium at 37°C for 30 min, the attached cells were counted. Compared to the control, in which 55±4% of cells were attached to the dish, only 38±1% of GRASP55-depleted cells and 31±3% of GRASP65-depleted cells bound to the dish (Figure 2.1F). When both GRASP55 and GRASP65 were depleted, the percentage of attached cells was further reduced to 22±4% (Figure 2.1F). This effect was rescued by the exogenous expression of GFP-tagged GRASP65 or GRASP55, but not GFP alone (Figure 2.1 G-H). Similar results were obtained in HeLa cells in which GRASPs were knocked out by CRISPR/Cas9-mediated genome editing (Supplemental Figure 2.1) (Bekier et al., 2017). These results demonstrate that Golgi unstacking reduces cell adhesion.

2.2 GRASP depletion reduces cell migration and invasion

To determine the effect of Golgi unstacking on cell migration, we first used a well-established wound-healing assay using the human breast cancer cell line MDA-MB-231 (Liang et al., 2007). Both GRASP55 and GRASP65 could be readily depleted by siRNA treatment in this cell line (Figure 2.2A). Seventy-two hours after siRNA transfection, fully confluent MDA-MB-231 cells were starved in serum-free medium for 24 h. A scratch was made in the confluent layer using a 200- μ l pipette tip, and the cells were cultured in complete growth medium for another 20 h to allow the cells to migrate into the wounded region. When examined under a microscope, cells that had been transfected with control siRNA almost completely covered the wound area, while GRASP-depleted cells only covered a portion of the wound region (Figure 2.2B). Control siRNA-treated cells migrated approximately 39±1 μ m per hour, while cells depleted of GRASP55, GRASP65, or both, migrated at 33±1, 25±2, and 19±2 μ m per hour,

respectively, which were significantly slower than the control cells (Figure 2.2C). Same wound healing assay was done with GRASP-knockout HeLa cells, and consistent results were obtained (Figure 2.3; Supplemental Figure 2.2). Cells deleted of GRASP55, GRASP65, or both, migrated at 22 ± 2 , 16 ± 2 , and 15 ± 2 μm per hour, respectively, significantly slower than the 32 ± 3 μm per hour of wild type cells (Supplemental Figure 2.2). This defect was rescued by the expression of GFP-tagged GRASP65 or GRASP55, but not GFP alone (Figure 2.3A-C). Interestingly, the level of the cell adhesion molecule $\alpha 5$ integrin appeared to be lower in GRASP knockout cells, which was rescued by the expression of GRASP55-GFP and GRASP65-GFP in the corresponding knockout cells (Figure 2.3C, lanes 6 & 7 vs. 4 & 5).

To confirm the result that GRASP depletion reduces cell migration by a different approach, we performed a transwell assay using wild type and GRASP knockout HeLa cells (Isaji et al., 2006). In this assay, the same number of cells were seeded in the inserts with serum free medium, and full growth medium with serum was added in the lower chamber as chemoattractant. After 20 h incubation, cells on the lower side of the membrane were fixed, stained with crystal violet, and imaged. The results showed that the migration rate was significantly reduced by the knockout of GRASP55 or GRASP65, while double deletion of both GRASPs had a more severe effect (Figure 2.4A-C). In the control, 184 ± 3 cells migrated to the lower side of the membrane per field of view, while GRASP55, GRASP65, and double knockout cells had 94 ± 15 , 100 ± 15 , and 59 ± 28 cells migrate to the bottom side, respectively (Figure 2.4C). Exogenous expression of GFP-tagged GRASP65 or GRASP55 rescued the migration defect in GRASP knockout cells (Figure 2.4D; Supplemental Figure 2.3). Based on the results from the

wound healing and transwell assays, we conclude that GRASP depletion results in decreased cell migration and invasion.

2.3 Golgi unstacking reduces $\alpha 5\beta 1$ integrin protein level in the cell

The fact that Golgi unstacking reduces cell adhesion and migration (Figures 1.1-4) suggests that it may affect cell adhesion molecules such as integrin, as shown in Figure 2.3C. Therefore, we examined the effects of GRASP deletion on the protein level of several integrins that are known to be expressed in HeLa cells, including $\alpha 1$, $\alpha 2$, $\alpha 3$, $\alpha 5$, αV , $\alpha 6$, $\beta 1$, $\beta 3$, and $\beta 5$ (Liu et al., 2009, Ratcliffe et al., 2016, Scheffer et al., 2013, Wan et al., 2014, Bergman et al., 1995), by Western blot. As shown in Figure 2.5A, $\alpha 1$, αV , and $\alpha 6$ levels did not change in GRASP knockout cells compared to that in wild type HeLa. $\alpha 3$ integrin was reduced only in GRASP65 KO cells, while $\beta 3$ level was slightly reduced only in GRASP55 KO cells. Consistent with the results shown in Figure 2.3C, both $\alpha 5$ and $\beta 1$ integrins were robustly reduced in GRASP single or double knockout cells, suggesting that Golgi unstacking reduces cell adhesion through decreasing the $\alpha 5\beta 1$ integrin level.

Integrins are heterodimers consisting of α and β subunits, both of which are type I transmembrane proteins with a small cytosolic tail and a large extracellular domain. The best-characterized integrin complex in HeLa cells is the $\alpha 5\beta 1$ integrin (Hang et al., 2017, Feng Jia, 2016, Yu et al., 2011), which mediates cell adhesion by binding to fibronectin, and this requires proper N-glycosylation of $\alpha 5\beta 1$ integrin (Isaji et al., 2006, Guo et al., 2002). Given the reduced binding of GRASP-depleted cells to fibronectin-coated plates (Figure 2.1; Supplemental Figure 2.1), we further examined the effects of GRASP depletion on the protein level of $\alpha 5$ integrin

using two antibodies that recognize N- or C-terminus of the protein, or the heavy (~130 kDa) or light (~19 kDa) chain of the mature protein, respectively (Figure 2.5B). Depletion of GRASP proteins by siRNA, or knockout of GRASPs by CRISPR/cas9, both significantly reduced $\alpha 5\beta 1$ integrin protein levels (Figure 2.5C-D; Supplemental Figure 2.4, A and B), whereas the protein level of other cell surface proteins, such as transferrin receptor (TfR) and insulin-like growth factor-1 receptor (IGF-R) did not change (Figure 2.5F; Supplemental Figure 2.4A-B). In contrast to GRASP depletion, disruption of the Golgi structure by nocodazole (Noc) or Brefeldin A (BFA) treatment had no effect on the protein level of $\alpha 5\beta 1$ integrin (Supplemental Figure 2.4C). In addition, disruption of the Golgi ribbon by Golgin 84 depletion had no effect on integrin level (Supplemental Figure 2.6 in (Xiang et al., 2013)). These results indicate a unique role of Golgi stacking rather than ribbon linking in regulating integrin-mediated cell adhesion and migration.

Through the use of both N- and C-terminal antibodies, we confirmed that $\alpha 5$ integrin heavy chain, light chain, and full length proteins were equally decreased in GRASP-knockout HeLa cells (Figure 2.5B-D). In addition, we analyzed the samples under both reducing and non-reducing conditions. Under non-reducing condition, both heavy and light chains are held together by a disulfide bond to form mature $\alpha 5$ integrin; while under reducing condition, the heavy and light chains of $\alpha 5$ integrin are unlinked when the disulfide bond is disrupted by dithiothreitol (DTT). As shown in Figure 2.5E, both mature $\alpha 5$ integrin and its individual components were equally reduced by GRASP knockout.

As a cell surface receptor, mature $\alpha 5\beta 1$ integrin is mainly localized at the plasma membrane and is dynamically internalized and recycled. Given that only those molecules at the

surface are functional in cell adhesion, we performed a cell surface biotinylation and streptavidin pulldown assay. The results showed that the cell surface level of $\alpha 5\beta 1$ integrin was robustly reduced in GRASP-knockout cells compared with that in control cells (Figure 2.5F). Another plasma membrane protein, TfR, was unaffected by GRASP knockout and was also pulled down, while the cytosolic protein actin was not detected in the pulldown. As an internal control, only the glycosylated upper band of $\beta 1$ integrin was isolated (Figure 2.5F). These results demonstrate that GRASP deletion reduces $\alpha 5\beta 1$ integrin level at the cell surface, which subsequently decreases cell adhesion.

$\alpha 5$ integrin is synthesized by the ER and transported through the Golgi to the plasma membrane. In the TGN, it is cleaved by proprotein convertases (PCs) to become mature. To determine whether GRASP deletion reduces $\alpha 5$ integrin level by inducing ER-associated protein degradation (ERAD) or by affecting its maturation, we blocked newly synthesized $\alpha 5$ integrin in the ER by BFA treatment for 2 h and released it for indicated times in the presence of cycloheximide (CHX) and MG132 or monensin. MG132 inhibits ERAD, while monensin blocks the trafficking of $\alpha 5$ integrin from the Golgi stack to TGN and thus inhibits $\alpha 5$ integrin cleavage. In this experiment, we determined the level of the full-length uncleaved form of $\alpha 5$ integrin on reducing gels. As GRASP KO cells have lower integrin levels, we exposed those gels longer and so all cell lines had a similar signal at 0 time point to start with, and the reduction of the protein was assessed over time. As shown in Figure 2.5G, the decrease of full-length $\alpha 5$ integrin in GRASP-knockout cells was faster than in wild type cells. The reduction of full-length $\alpha 5$ integrin could be explained by two reasons. One is by ERAD; this possibility was ruled out, since the $\alpha 5$ integrin level was not rescued by MG132 (Figure 2.5G, lane 5 vs. 4). The other possibility is that

$\alpha 5$ integrin is cleaved by PCs in the TGN to mature; this explanation was supported by the inhibition of the reduction by monensin (Figure 2.5G, lane 6 vs. 4). These results demonstrate that GRASP KO does not cause ERAD of $\alpha 5$ integrin; rather, it accelerates integrin trafficking and maturation, which is consistent with our previous observation in GRASP depleted cells (Xiang et al., 2013).

2.4 Expression of $\alpha 5\beta 1$ integrin rescues the attachment and migration defects of GRASP knockout cells

So far, we have confirmed that GRASP depletion reduces $\alpha 5\beta 1$ integrin level (Figure 2.5) and decreases cell attachment and migration (Figures 2.1-2.4). Re-expression of GRASP in the related GRASP knockout cells not only restored $\alpha 5\beta 1$ integrin level (Figure 2.3C) but also the defects in cell attachment (Figure 2.1G-H; Supplemental Figure 2.1) and migration (Figures 2.3 and 2.4; Supplemental Figures 2.1 and 2.3). To determine whether the reduction of $\alpha 5\beta 1$ integrin is the main reason for the decreased cell attachment and migration in GRASP depleted cells, we exogenously expressed $\alpha 5$ integrin-GFP, which is known to restore the protein level of both $\alpha 5$ and $\beta 1$ integrins (Isaji et al., 2009, Isaji et al., 2006). As expected, expression of $\alpha 5$ -GFP, but not GFP alone, increased the protein levels of both $\alpha 5$ and $\beta 1$ integrins in GRASP single and double knockout cells to comparable levels in wild type cells (Figure 2.5H). Significantly, restoration of $\alpha 5\beta 1$ integrin level in GRASP knockout cells largely rescued the reduced cell adhesion (Figure 2.5I) and migration (Supplemental Figure 2.5) phenotype. These results demonstrate that GRASP depletion decreases cell adhesion and migration via the reduction of $\alpha 5\beta 1$ integrin.

2.5 GRASP depletion reduces $\alpha 5\beta 1$ integrin protein synthesis

To determine whether the reduction of $\alpha 5\beta 1$ integrin level is due to decreased protein synthesis or increased degradation, we assessed integrin synthesis by measuring the incorporation of ^{35}S -labeled methionine and cysteine. Cells transfected with control or GRASP siRNAs were incubated in a medium containing ^{35}S -labeled methionine and cysteine for 1 h, and $\alpha 5$ and $\beta 1$ integrins were immunoprecipitated and analyzed by SDS-PAGE and autoradiography. The newly synthesized $\alpha 5$ and $\beta 1$ integrin existed as single bands of 135 kDa and 110 kDa, respectively (Figure 2.6A), corresponding to their immature ER forms. Notably, the amount of the $\alpha 5$ and $\beta 1$ integrin was reduced by approximately 50% following GRASP depletion (Figure 2.6B), consistent with the observation that the $\alpha 5$ and $\beta 1$ integrin protein levels were reduced in GRASP knockout cells in a steady state (Figure 2.5A-E).

To test the possibility that GRASP depletion may also affect the stability of $\alpha 5\beta 1$ integrin, we blocked protein synthesis by cycloheximide (CHX) treatment and assessed the $\alpha 5\beta 1$ integrin level over time. These proteins are stable, with no significant reduction within 36 h of CHX treatment and were not affected by GRASP knockdown (Figure 2.6C) or knockout (Supplemental Figure 2.6). These results are consistent with previous reports that integrins are stable proteins in the cell (Lobert et al., 2010, Bottcher et al., 2012). To further confirm these results by an alternative approach, we performed the same metabolic labeling and pulse chase assay as described above. HeLa cells transfected with control or GRASP siRNAs were incubated in a medium containing ^{35}S -labeled methionine and cysteine for 1 h, chased for 12 h, 24 h, or 48 h, and lysed. $\alpha 5$ and $\beta 1$ integrin were immunoprecipitated and analyzed by nonreducing SDS-PAGE and autoradiography. We found that within 48 h, the degradation rate of both $\alpha 5$ and $\beta 1$

integrin was not significantly affected by GRASP depletion (Figure 2.6D-F). Therefore, we conclude that GRASP depletion reduces the synthesis of $\alpha 5\beta 1$ integrin but does not affect their stability.

2.6 GRASP depletion enhances total protein synthesis and cell growth

To determine how GRASP depletion-mediated Golgi destruction affects cell growth, we examined the growth rate of GRASP-depleted cells using an established crystal violet assay (Tang et al., 2010). Cells were transfected with indicated control or GRASP siRNAs and seeded into 24-well plates 24 h after transfection. After incubation for 24 h, the number of cells was assessed for 6 successive days. As shown in Figure 2.7A, the increase in the cell number was significantly higher in cells treated with GRASP siRNAs compared with those treated with control siRNA.

We then determined the total amount of protein synthesis occurring in these cells. Cells treated with control or GRASP siRNAs were labeled using ^{35}S -labeled methionine and cysteine for 1 h and lysed in detergent. Equal amounts of total protein were then precipitated by trichloroacetic acid (TCA), and the total amount of radioactivity incorporated was measured using a scintillation counter. As shown in Figure 2.7B, compared to control siRNA-treated cells, the total protein synthesis increased when GRASPs were depleted. This result is consistent with the observation that Golgi unstacking increases cell growth, suggesting a link between protein synthesis, trafficking, post-translational modification, and cell growth.

Discussion

In this study, we found that disruption of the Golgi structure by GRASP knockdown or knockout impacted multiple cell activities, including decreased cell attachment, migration, and invasion, which could be explained by the decreased level of $\alpha 5\beta 1$ integrin. We also found that GRASP depletion increased cell growth, which may be attributed to the increased overall protein synthesis and accelerated protein trafficking. Based on the literature, this is the first systematic study that links Golgi structure formation and function with cellular activities, including cell attachment, migration, and growth. It is reasonable to speculate that Golgi fragmentation found in diseases may cause global defects in protein trafficking, glycosylation and secretion that impact essential cell activities. Thus, studying the cellular activities under Golgi destruction and discovering the factors that drive these changes will help us understand their pathogenesis. In the long term, molecular tools may be developed to restore normal Golgi structure and function under disease conditions and thus to delay disease development.

Using GRASP knockdown and knockout cells, we demonstrated that disrupting the Golgi stacks reduced cell adhesion and migration. As integrins are key proteins in these cellular activities, we determined the protein level of 9 integrins that are known to be expressed in HeLa cells. Among these integrin subunits, $\alpha 5$ and $\beta 1$, the major and best characterized integrins in HeLa cells, exhibited the most dramatic reduction in GRASP knockout cells, while other integrins did not change or only modestly decreased. This demonstrates that different integrins are regulated differently in their expression, as previously described (Judware and Culp, 1997, Palomino et al., 2005). We then used two different antibodies and different gel systems to further characterize $\alpha 5\beta 1$ integrin in GRASP knockout cells. We found that both mature integrins and the individual components in the complex were all reduced by GRASP depletion. More

importantly, restoration of the $\alpha 5\beta 1$ integrin level in GRASP knockout cells rescued the reduced cell adhesion and migration phenotype. These results indicate that the reduced cell adhesion and migration after GRASP depletion is mostly attributed to the reduced $\alpha 5\beta 1$ integrin expression.

Our results are consistent with previous reports that a higher expression level of $\alpha 5$ integrin or increased trafficking to the plasma membrane increases cell attachment and migration (Breuksch et al., 2017, Wan et al., 2014). Given that the Golgi plays a critical role in protein glycosylation and sorting (Huang and Wang, 2017, Zhang and Wang, 2016) and that proper glycosylation of $\alpha 5\beta 1$ integrin is important for its function and activation (Gu and Taniguchi, 2004, Guo et al., 2002, Hang et al., 2017, Zheng et al., 1994), we expected that Golgi structural defects might affect integrin glycosylation, trafficking, and degradation. There are two possible reasons for the reduced $\alpha 5\beta 1$ integrin level in GRASP-depleted cells: one is by increased degradation, the other is via decreased synthesis. Given that protein glycosylation has been thought to be a key mechanism to help protein folding and maintain protein stability (Live et al., 1996, Shental-Bechor and Levy, 2008, Lee et al., 2015, Sola and Griebenow, 2009), we originally expected that GRASP depletion might affect integrin stability. However, the results demonstrated that GRASP depletion did not trigger integrin degradation by ERAD or its turnover; instead, it reduced $\alpha 5\beta 1$ integrin synthesis, although the underlying mechanism remains unknown. In addition, GRASP depletion also accelerated $\alpha 5$ integrin trafficking and maturation, which is consistent with our previous finding (Xiang et al., 2013).

In contrast to the reduced integrin synthesis, total protein synthesis was increased by GRASP depletion, while some other proteins at the cell surface, such as IGFR and TfR, were

unaffected. The observation of increased protein synthesis in this study could also be attributed to the increased demand of the cells for more proteins with increased trafficking and cell growth. It has been demonstrated that at the onset of mitosis, phosphorylation of GRASPs and golgins by mitotic kinases results in Golgi disassembly, which is required for cell cycle progression (Jesch et al., 2001, Sutterlin et al., 2002, Duran et al., 2008, Xiang and Wang, 2010, Guizzunti and Seemann, 2016), and GRASP depletion accelerates cell cycle progression (Tang et al., 2010). It is conceivable that cells with unstacked Golgi grow faster, as protein synthesis and cargo transport are enhanced. Some signaling pathways may be selectively activated or inhibited to control the synthesis of different proteins. Exploiting the underlying mechanism will be a future direction of this study.

In summary, we found that disrupting the Golgi structure by GRASP knockdown or knockout results in decreased cell adhesion and migration due to decreased synthesis of $\alpha 5\beta 1$ integrin. These cells grow faster, possibly because of accelerated protein trafficking and increased overall protein synthesis.

Materials and methods

Reagents, plasmids, and antibodies

All reagents were purchased from Sigma-Aldrich, Roche, Calbiochem, and Fisher unless otherwise stated. Most of the cDNA constructs used in this paper were described previously: pEGFP-N1-GRASP55 (wild type), pEGFP-N1-GRASP65 (wild type), and pEGFP-N1 (Zhang et al., 2018, Xiang and Wang, 2010). pEGFP-N1- $\alpha 5$ integrin (wild type) cDNA construct was a kind gift from Dr. Jianguo Gu. Antibodies: antibodies used in this study include monoclonal

antibodies against β -actin (Proteintech Group, Cat# 66009-1-Ig), GFP (Protein tech, Cat# 66002-1-Ig), α 1 integrin (Santa Cruz, Cat# SC-271034), α 2 integrin (Santa Cruz, Cat# SC-74466), α 3 integrin (Santa Cruz, Cat# SC-374242), α 5 integrin (DSHB, Cat# BIIG2), α 6 integrin (Santa Cruz, Cat# SC-19622), α V integrin (Santa Cruz, Cat# SC-376156), β 1 integrin (DSHB, Cat# P5D2), β 3 integrin (Santa Cruz, Cat# SC-46655), β 5 integrin (Santa Cruz, Cat# SC-398214), and transferrin receptor (Invitrogen, Cat# 13-6800), and α -tubulin (DSHB, Cat# AA4.3); polyclonal antibodies against human GRASP55 (Proteintech Group, Inc., Cat# 10598-1-AP), IGF-R β (Santa Cruz, Cat# sc-713), α 5 integrin C-terminus (Millipore, Cat# AB1928), α 5 integrin N-terminus (Cell signaling, Cat# 4705), β 1 integrin C-terminus (Abcam, Cat# EP1041Y), β 1 integrin C-terminus (Cell Signaling, Cat# 4706), and human GRASP65 (Gift from Dr. Joachim Seemann, University of Texas Southwestern Medical Center).

Cell culture, transfection and treatment

For cell culture, HeLa and MDA-MB-231 cells were grown in DMEM (Invitrogen) containing 10% super calf serum (Gemini, Cat# 100-510) and glutamine at 37°C in a 5% CO₂ incubator. To knock down GRASP55 and/or GRASP65, HeLa cells were plated at 40% confluency in six-well plates, 3 μ l of a 50 μ M siRNA stock was added to 250 μ l of Opti-MEM. In a separate tube, 5 μ l of transfectamine RNAiMAX (Invitrogen) was mixed with 250 μ l of Opti-MEM and incubated for 5 min at room temperature. The two mixtures were combined and incubated at room temperature for 20 min, then added to the cells in 2 ml DMEM containing 10% super calf serum. siRNAs for human GRASP55 (AACTGTCGAGAAGTGATTATT) and GRASP65 (CCTGAAGGCACTACTGAAAGCCAAT) (Xiang and Wang, 2010, Xiang et al., 2013) were purchased from Ambion and Invitrogen, respectively. Control non-specific siRNAs

were purchased from Ambion. GRASP-knockout cell lines were described previously (Bekier et al., 2017).

To express exogenous GRASP proteins, HeLa cells of ~60% confluency were transfected with indicated GRASP constructs (Xiang and Wang, 2010, Tang et al., 2010). For a 10 cm plate, 10 µg of pEGFP-N1-GRASP65 (wild type) construct or 15 µg of pEGFP-N1-GRASP55 (wild type) construct was mixed with 30 µl polyethylenimine (PEI) and 1 ml serum free medium for 15 min at room temperature and then added to the cells in 9 ml DMEM containing 10% super calf serum. For control treatment, 10 µg of pEGFP-N1 construct was mixed with 30 µl PEI and 1 ml serum free medium for 15 min and then added to the cells in 9 ml DMEM containing 10% super calf serum.

To restore $\alpha 5\beta 1$ integrin level in GRASP knockout cells, cells of ~60% confluency in a 6 cm plate were transfected with 8 µg $\alpha 5$ -GFP cDNA construct by Lipofectamine 2000 (Invitrogen, Cat# 11668019) following the manufacture's instruction, and pEGFP-N1 was used as control. In three independent experiments, the transfection rate of $\alpha 5$ -GFP in GRASP55, GRASP65, and double knockout cells was 66±1%, 67±3% and 71±1%, respectively. This was tested at 72 h post transfection, a time point used for the cell adhesion and migration assays.

For drug treatment, 5 µg/ml BFA, 500 ng/ml nocodazole, 100 µg/ml CHX, 50 µM MG132 or 2 µM monensin was directly applied to the medium alone or in combination for indicated times. Cells were lysed and analyzed by Western blotting.

Cell attachment assay

For cell attachment, a total of 3×10^5 control (ctrl) or GRASP siRNA-treated cells were seeded on fibronectin-coated plates and incubated in serum-free medium for 30 min. Twelve-well plates were coated with fibronectin from human plasma (Sigma, F0895) at a concentration of 1 $\mu\text{g/ml}$ in Tris-buffered saline (pH 7.5) at 4°C for 16 h and blocked with 2% bovine serum albumin (BSA) for 30 min. HeLa cells transfected with indicated siRNAs, or GRASP knockout HeLa cells with or without GRASP or integrin rescue, were detached using 20 mM EDTA in Phosphate-buffered saline (PBS), pelleted, and re-suspended in serum-free DMEM. The cells were seeded on the plate (3×10^5 cell per well, three wells for each condition) and cultured in serum-free DMEM at 37°C for 30 min. Cells were then gently washed four times with PBS, and the attached cells were treated by 20 mM EDTA, collected by centrifugation, resuspended in 200 μl growth medium, and counted using hemocytometer. Attachment was presented as the percentage of attached cells out of the total number of cells.

Wound-healing assay

The wound-healing assay used here was performed using the protocol described by Jun-Lin Guan and colleagues (Liang et al., 2007). MDA-MB-231 or HeLa cells were transfected with the indicated plasmids; and 48 hours after transfection, the cells were re-plated in 12-well plates at 80% confluence in complete growth medium. Twenty-four hours later, after the cells became confluent and formed a monolayer, the medium was replaced with serum-free DMEM. Twenty-four hours afterwards, the cell monolayer was scraped in a straight line to create a “scratch” with a 200- μl pipette tip. The cells were washed once with DMEM, and images were taken using an inverted bright field microscope with a 4x lens and an IMAGING ERTIGA 1300R camera. The

cells were then allowed to grow in complete growth medium for 20 h, and images of the same area were taken. Images were analyzed with NIH Image J software or Wimasis, 2016.

WimScratch: Wound Healing Assay Image Analysis Solution. Release 4.0. Available from: <https://www.wimasis.com/en/products/9/WimScratch> (Jameson et al., 2013).

Transwell assay

HeLa cells were detached with 20 mM EDTA and re-suspended in serum free DMEM. Cells were seeded in transwell inserts (BD BioCoat control 8.0- μ m-pore-size inserts, Cat# 0877121) at the concentration of 5×10^4 in 250 μ l serum free DMEM. In the lower chamber, 750 μ l full growth medium was added as chemoattractant. After incubation at 37°C for 20 h, cells on the upper side were gently removed by scraping with a cotton swab. The membranes in the inserts were fixed with 4% paraformaldehyde (PFA) for 30 min, stained with 0.5% crystal violet for 1 h, and cells that had migrated to the lower side were visualized under a Leica MZ FLIII stereomicroscope. Images were analyzed with NIH Image J software.

Cell growth rate

HeLa cells transfected with indicated siRNAs were trypsinized 24 hours after transfection. Cells (1×10^4) were plated in 24-well plates and incubated in complete growth medium. One day later, the cell number was measured every 24 h for 6 days using crystal violet staining, as described previously (Feinstein and Linstedt, 2007). Briefly, cells were washed with PBS, fixed in 4% paraformaldehyde for 30 min, stained with 0.5% crystal violet (in 30% methanol) for 15 min, and extensively washed with H₂O. The crystal violet was extracted using 1

ml of 10% acetic acid for 5 min, and the optical density (OD) was measured at 590 nm. The cell number at different times was normalized to the cell number from the first measurement (Day 0).

Radioactive labeling and immunoprecipitation

This method was previously described (Xiang et al., 2013). Briefly, HeLa cells grown in 60 mm dishes were incubated in methionine/cysteine-free DMEM (Invitrogen) for 1 h and labeled with 1 ml of medium containing 250 $\mu\text{Ci/ml}$ TRANS ^{35}S -LABEL [^{35}S] (MP BIOMEDICALS, Cat# 15100614) for 1 h. After washing with PBS, cells were collected either immediately on ice or after incubation in 4 ml complete growth medium containing 2 mM L-cysteine and L-methionine for the indicated time periods. Cells were lysed in 0.8 ml lysis buffer (PBS containing 1 mM CaCl_2 , 0.5 mM MgCl_2 , 1% Triton X-100, protease inhibitor cocktail, and 1 μM pepstatin A) and centrifugation at 14,000 rpm for 15 min. The protein concentration of the supernatant was measured using a Bio-Rad protein assay (Bio-Rad Laboratories, Cat# 5000006). The cell lysates (2 mg) were immunoprecipitated with 50 ng of the $\alpha 5$ integrin antibody BIIG2 and 60 ng of the $\beta 1$ integrin antibody P5D2 overnight at 4°C. The antibodies were precipitated with 30 μl protein G beads (Roche Diagnostics GmbH, Germany) at 4°C for 2 h. The beads were washed five times with lysis buffer, and the immunisolated materials were eluted by boiling for 5 min in nonreducing SDS sample buffer. Integrins were resolved using 6.5% non-reducing SDS-PAGE followed by autoradiography.

To determine the total protein synthesis, 40 μl of the cell lysate was precipitated with 10 μl of 100% (w/v) trichloroacetic acid (TCA) at 4°C for 10 min. The protein pellets were washed with acetone, dissolved in 0.2 M NaOH, neutralized with 0.2 M HCl, and mixed with scintiverse

BD cocktail (Fisher Scientific, Cat# B14001). The incorporation of radioactivity was analyzed using scintillation counting and normalized based on the total protein amount.

Cell surface biotinylation

All procedures were performed on ice or at 4°C. Cells grown in 15 cm plates were incubated on ice for 20 min, washed three times with PBS, treated with 6 ml 0.5 mg/ml NHS-SS-biotin (Fisher, Cat# P121331) in PBS for 20 min, and quenched by 100 mM Glycine/PBS for 10 min. After three times wash with PBS, cells were lysed in RIPA buffer (20 mM Tris-HCl, pH 8.0, 150 mM NaCl, 1% Triton X-100, 0.1% SDS, 0.1% sodium deoxycholate, 1 mM EDTA, and 0.5% Sodium orthovanadate, 0.1% Sodium Fluoride, and 1x protease inhibitor Cocktail (Bimake, Cat# B14001)). Cell lysates were adjusted to 5.86 mg/ml in lysis buffer and 3 mg samples were incubated with 50 µl streptavidin-agarose beads (GE Healthcare, Cat# 17-511-01) at 4°C overnight. After washing, beads were boiled in SDS sample buffer with 100 mM DTT and bound proteins were analyzed by SDS-PAGE, transferred to PVDF membranes and blotted with $\alpha 5$ integrin (Cell Signaling, Cat# 4705), $\beta 1$ integrin (Cell Signaling, Cat# 4706), Transferrin receptor (Invitrogen, Cat# 13-6800) and β -actin (Proteintech, Cat# 66009-1-Ig) antibodies.

Quantification and statistics

In all figures, the quantification results are expressed as the mean \pm SEM (standard error of the mean) from three independent experiments, unless otherwise stated. The statistical significance of the results was assessed using a Student's *t*-test. *, $p < 0.05$, **, $p < 0.01$, ***, $p < 0.001$.

Supplemental Information

Supplemental Information includes six supplemental figures. Supplemental Figure 2.1 and 2.2 shows that GRASP KO reduces cell attachment and migration, respectively. Supplemental Figure 2.3 provides evidence that GRASP re-expression rescues cell migration defects in GRASP KO cells. Supplemental Figure 2.4 shows that GRASP KD using siRNA also reduces $\alpha 5\beta 1$ integrin. Supplemental Figure 2.5 demonstrates that re-expression of $\alpha 5\beta 1$ integrin rescues cell migration defects in GRASP KO cells. Supplemental Figure 2.6 is a CHX chase providing evidence that GRASP depletion does not increase $\alpha 5\beta 1$ integrin degradation.

Acknowledgements

We thank Dr. Cunming Duan for IGFR antibodies, Dr. Joachim Seemann for GRASP65 antibodies, Dr. Sai Srinivas Panapakkam Giridharan for transferrin receptor antibodies, Dr. Jianguo Gu for $\alpha 5$ integrin-GFP construct, and members of the Wang lab for stimulating discussions and technical support. This work was supported by the National Institutes of Health (Grant GM112786), MCubed, and the Fast Forward Protein Folding Disease Initiative of the University of Michigan to Y. Wang, and a University of Michigan Rackham Predoctoral fellowship to E. Ahat. All authors discussed the results and contributed to the final manuscript.

Competing Interest

The authors declare that no competing interests exist.

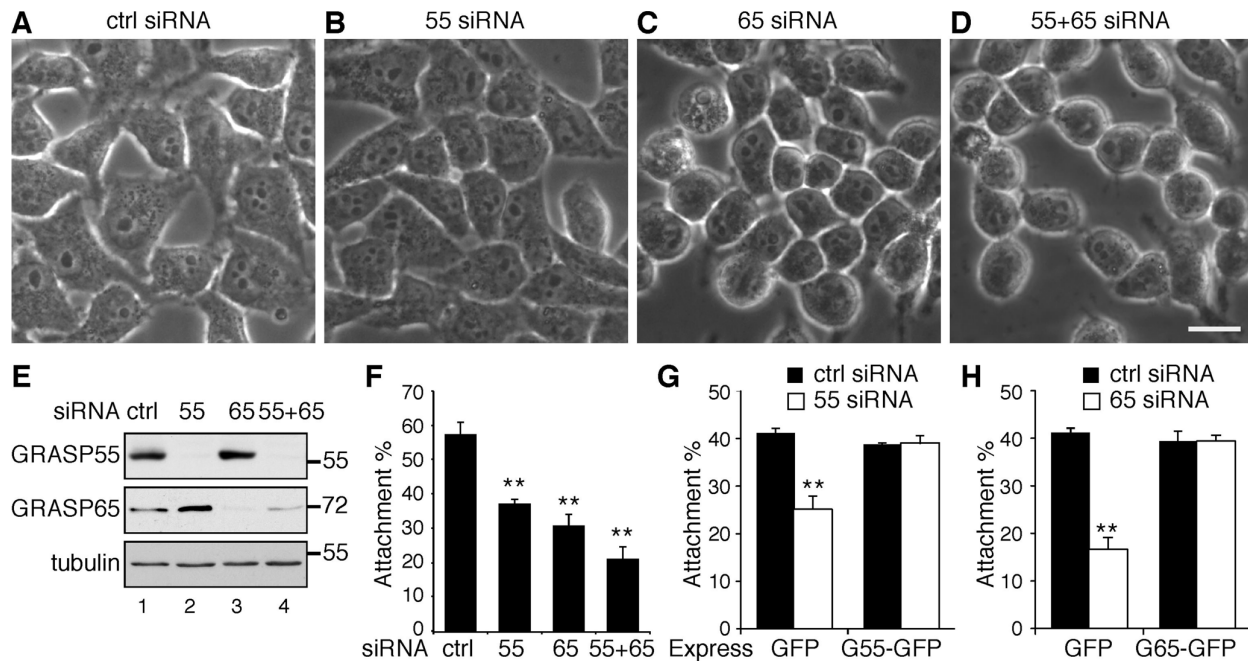


Figure 2.1. GRASP depletion reduces cell attachment.

(A-D) Phase contrast images of HeLa cells transfected with indicated siRNAs. Scale bar, 20 μ m. Note that GRASP-depleted cells are generally more round than control siRNA-treated cells. (E) Western blots of HeLa cells transfected with indicated siRNAs. GRASP55 and GRASP65 were effectively depleted. (F) Cell attachment was reduced by GRASP depletion. A total of 3×10^5 control (ctrl) or GRASP siRNA-treated cells were seeded on fibronectin-coated plates and incubated in serum-free medium for 30 min. After the removal of unbound cells, the number of attached cells was counted. Results were presented as mean \pm SEM, statistical analysis was performed by comparing to control siRNA treated cells by student's *t-test*. *, $p < 0.05$; **, $p < 0.01$; ***, $p < 0.001$. (G) The reduced attachment of GRASP55-depleted cells was rescued by the expression of GRASP55-GFP but not GFP. (H) The reduced attachment of GRASP65-depleted cells was rescued by expressing GRASP65-GFP.

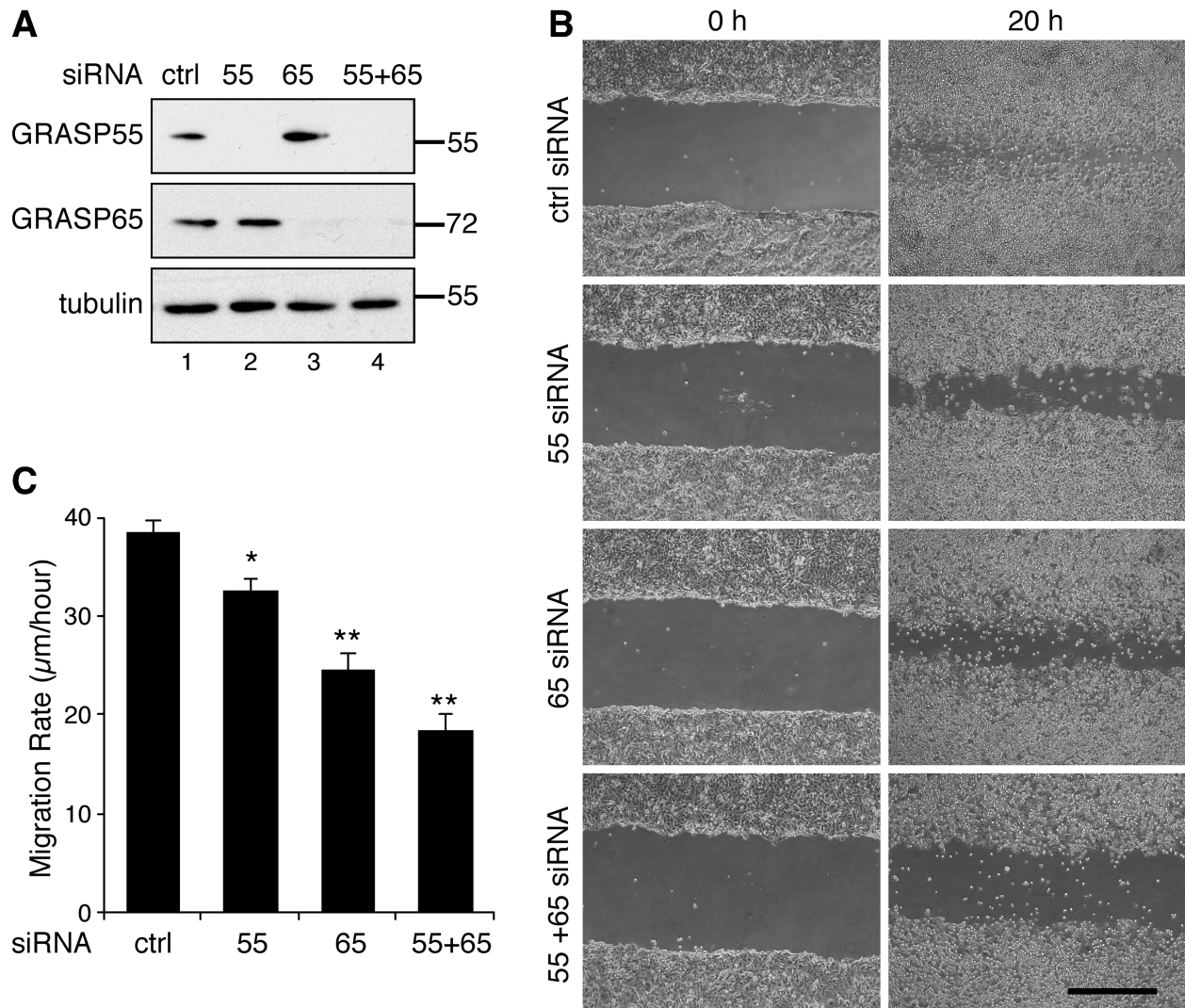


Figure 2.2. GRASP depletion reduces cell migration.

(A) Western blots of MDA-MB-231 cells transfected with indicated siRNAs. GRASP55 and GRASP65 were effectively depleted. (B) GRASP depletion reduces MDA-MB-231 cell migration. Cells transfected with indicated siRNAs were analyzed in a wound-healing assay. Images were taken at 0 h and 20 h after scratching. Scale bar, 500 µm. (C) Quantitation of the migration rate in (B). Statistical analysis was performed by comparing to control siRNA treated cells by student's *t*-test. *, $p < 0.05$; **, $p < 0.01$.

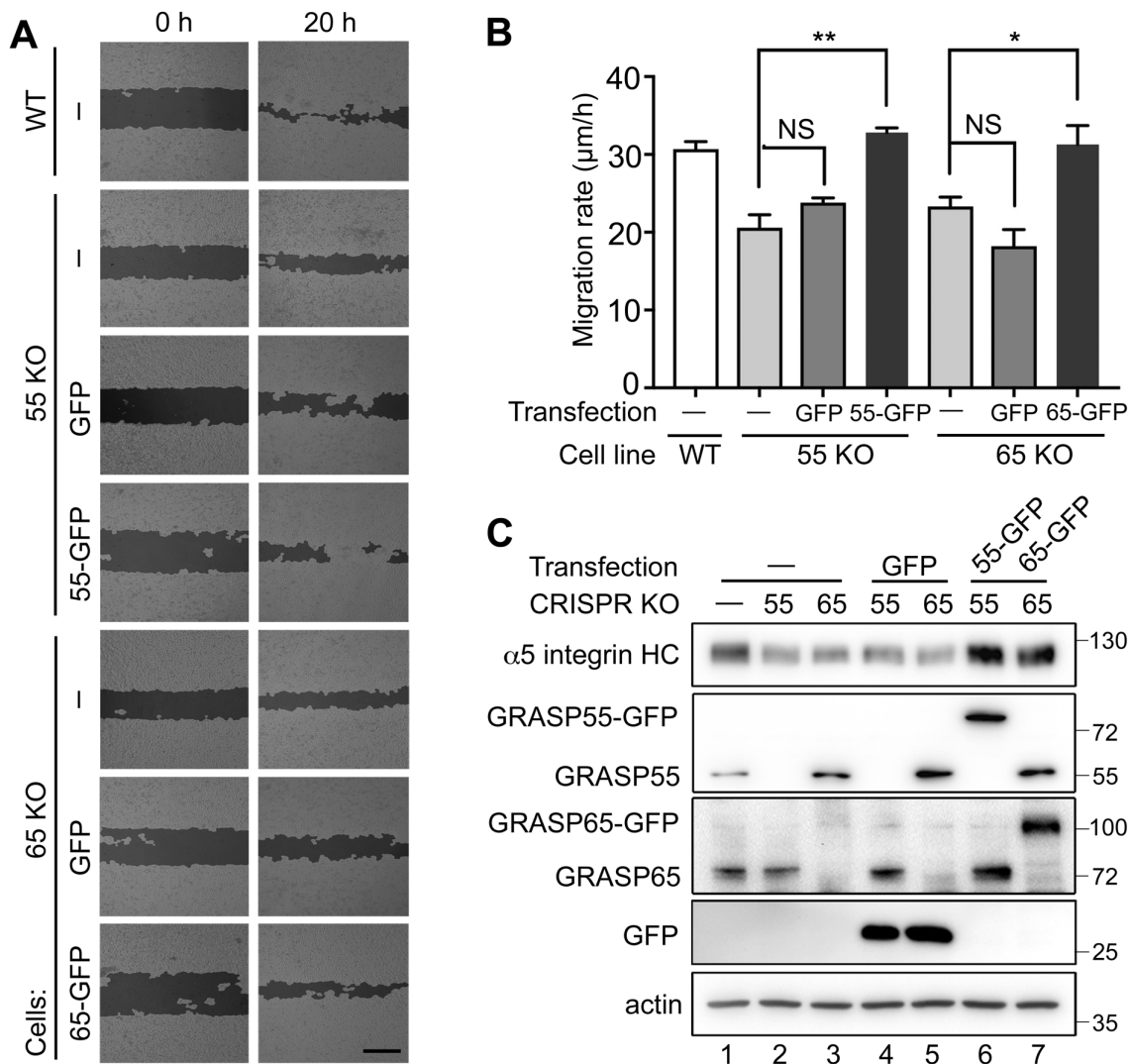


Figure 2.3. GRASP expression rescues the cell migration defects in GRASP knockout cells.

(A) GRASP expression rescues the decreased cell migration in GRASP-knockout (KO) HeLa cells. Cells transfected with indicated constructs were tested in a wound-healing assay and images were processed by Wimasis Image Analysis. Images were taken at 0 h and 20 h after scratching. Scale bar, 500 µm. **(B)** Quantitation of (A). The reduced migration of GRASP55 and GRASP65 KO cells was rescued by expressing GRASP55-GFP and GRASP65-GFP, respectively, but not by GFP alone. Results were presented as mean ± SEM, statistical analysis was performed by comparing to wild type control (ctrl) by student's *t-test*. *, $p < 0.05$; **, $p < 0.01$.

(C) Western blot of HeLa cells transfected with indicated constructs. $\alpha 5$ integrin heavy chain ($\alpha 5$ integrin HC), GRASP55, GRASP65, GFP and actin were blotted. The reduced protein levels of $\alpha 5$ integrin in GRASP55 and GRASP65 KO cells were rescued by expressing GRASP55-GFP or GRASP65-GFP, respectively, but not by GFP alone.

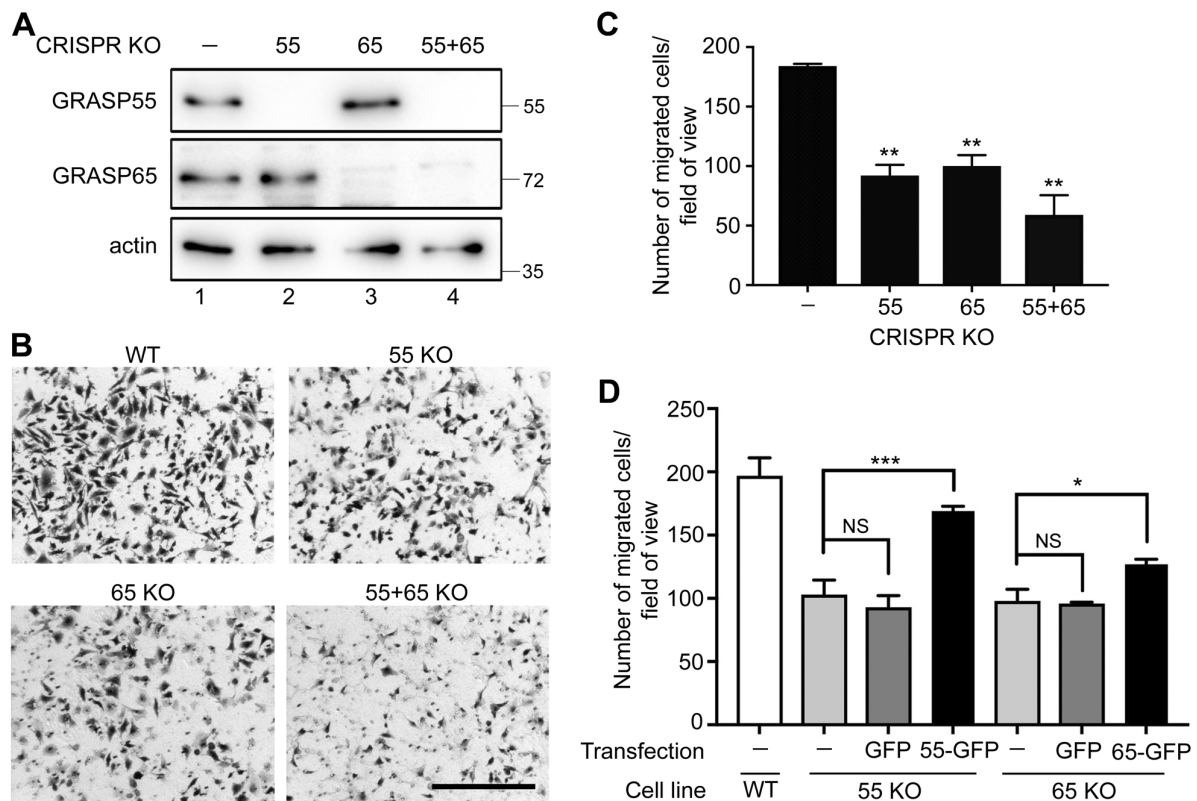


Figure 2.4. GRASP depletion reduces cell migration and invasion.

(A) Western blots of wild type (WT) and GRASP-knockout (KO) HeLa cells for GRASP55, GRASP65 and actin. (B) GRASP deletion reduces cell migration and invasion. Indicated WT and GRASP KO HeLa cells were analyzed in a transwell assay. Images were taken after 20 h migration. Scale bar, 500 μ m. (C) Quantitation of the migration rate in (B). Results were presented as mean \pm SEM, statistical analysis was assessed by comparing to WT cells by student's *t-test*. (D) GRASP expression rescues the decreased cell migration in GRASP KO cells. GRASP55 or GRASP65 KO cells transfected with indicated constructs were analyzed by a transwell assay. Example images are shown in Supplemental Figure 2.3. Note that defects in cell invasion in GRASP55 and GRASP65 KO cells were rescued by the expression of GRASP55-GFP and GRASP65-GFP, respectively, but not by GFP alone. Results were presented as mean \pm

SEM, statistical analysis was assessed by comparing to WT cells (ctrl) by student's *t-test*. *,
p<0.05; **, p<0.01; ***, p<0.001.

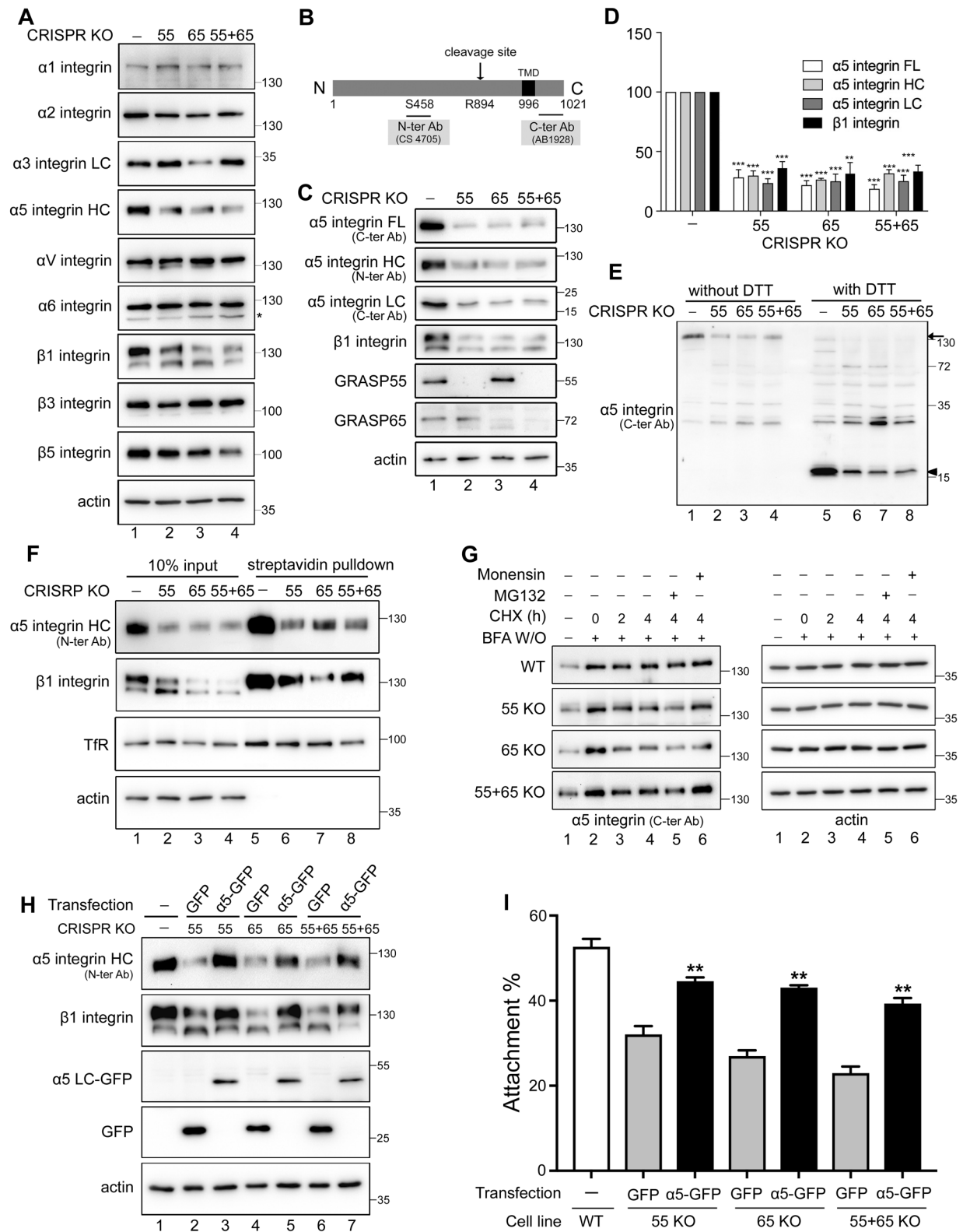


Figure 2.5. GRASP knockout reduces $\alpha 5\beta 1$ integrin protein level.

(A) GRASP knockout (KO) reduces $\alpha 5\beta 1$ level but has only modest effects on other integrins. Western blots of wild type (WT) and GRASP-knockout (KO) HeLa cells for indicated integrins and actin. Note that the protein levels of $\alpha 1$, αV , $\alpha 6$ did not change after GRASP depletion in contrast to the robust reduction of $\alpha 5$ and $\beta 1$ integrins. **(B)** Schematic $\alpha 5$ integrin domain structure and epitopes of indicated antibodies. **(C)** GRASP KO reduces the $\alpha 5\beta 1$ integrin level. The full length (FL), heavy chain (HC) and light chain (LC) of $\alpha 5$ integrin, $\beta 1$ integrin, GRASP55, GRASP65 and actin were blotted. Note the reduced protein level of $\alpha 5$ integrin on all three blots as well as $\beta 1$ integrin compared to that in WT cells. **(D)** Quantitation of (C) normalized with actin. Statistics was assessed by comparing to WT cells. **(E)** Western blot of $\alpha 5$ integrin on non-reducing (without DTT) and reducing gels (with DTT). Arrow and arrowhead indicate full length and light chain, respectively. **(F)** GRASP knockout reduces $\alpha 5\beta 1$ integrin level at the cell surface. GRASP KO cells were surface biotinylated followed by streptavidin pulldown and Western blotting of $\alpha 5$ integrin, $\beta 1$ integrin, Transferrin Receptor (TfR), and actin. Note that only the highly glycosylated forms of integrins were pulled down; this was more clear with $\beta 1$ integrin (upper band). **(G)** GRASP knockout accelerates $\alpha 5$ integrin maturation. WT and GRASP KO HeLa cells were pretreated with brefeldin A (BFA) for 2 h and washed out, released into cycloheximide (CHX) for 0 h, 2 h, 4 h, or 4 h with MG132 or monensin. As GRASP KO cells have lower level of integrin level, we exposed those gels longer and so all cell lines had a similar signal at 0 time point to start with, and the reduction of the protein was assessed over time. **(H)** Western blot of indicated HeLa cells transfected with $\alpha 5$ integrin-GFP or GFP. $\alpha 5$ integrin heavy chain ($\alpha 5$ integrin HC), $\beta 1$ integrin, GFP and actin were blotted. The reduced protein levels of $\alpha 5$ and $\beta 1$ integrins in GRASP KO cells were rescued by expressing $\alpha 5$ integrin-GFP, but not by GFP alone. **(I)** $\alpha 5$ integrin expression rescues the decreased cell attachment of

GRASP KO cells. Cells transfected with indicated constructs were analyzed in an attachment assay as described in Figure 1. Shown are the quantitation results. *, $p < 0.05$; **, $p < 0.01$; ***, $p < 0.001$.

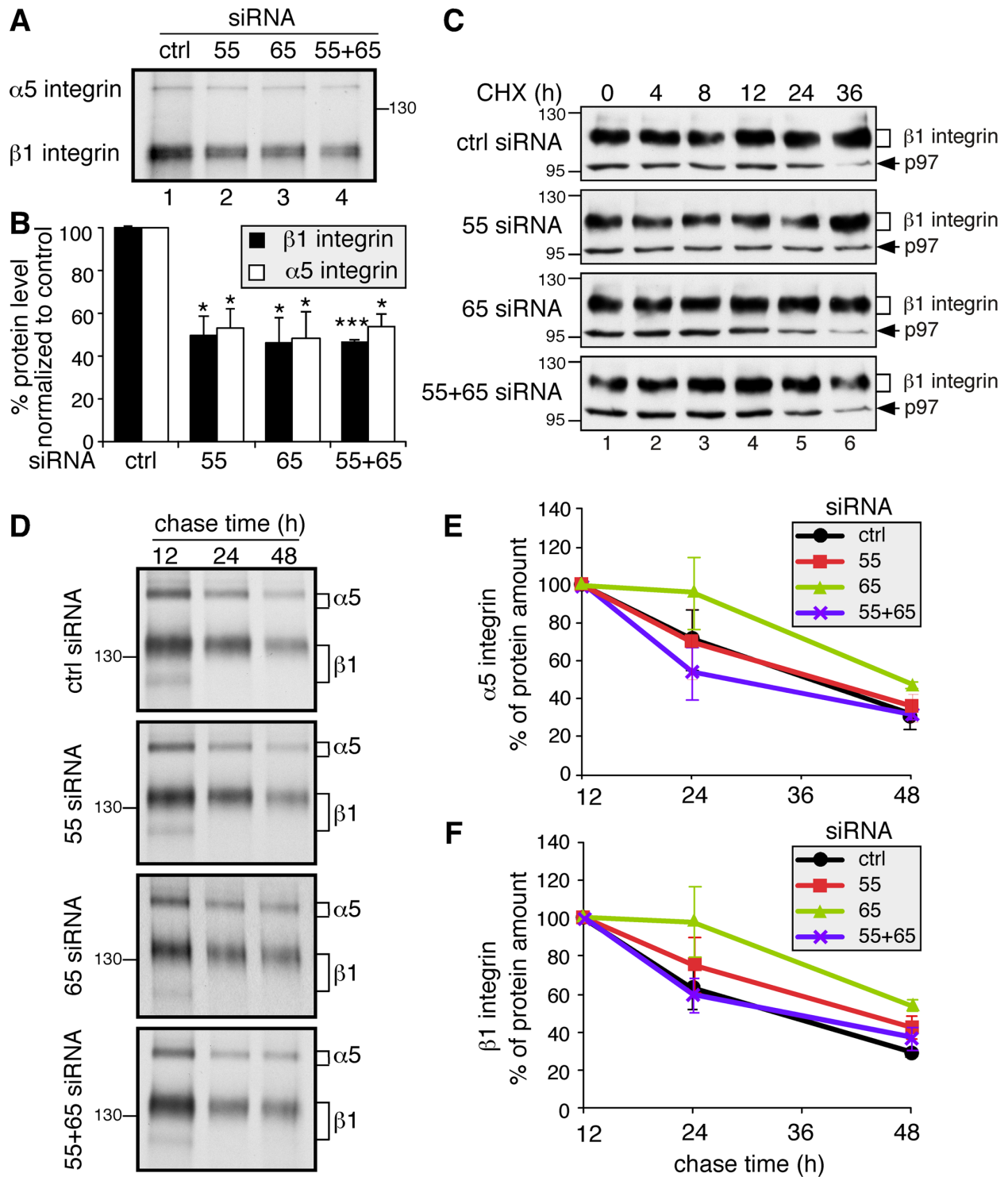


Figure 2.6. GRASP depletion reduces $\alpha 5$ and $\beta 1$ integrin synthesis but has no effect on their turnover.

(A) GRASP depletion reduces protein synthesis of $\alpha 5$ and $\beta 1$ integrin. Equal number of HeLa cells transfected with indicated siRNAs were labeled with TRANS ^{35}S -LABEL [^{35}S] for 1 h. Immunoprecipitated $\alpha 5\beta 1$ integrin was analyzed by gel electrophoresis and autoradiography. The protein synthesis rates of both $\alpha 5$ and $\beta 1$ integrin decreased in GRASP-depleted cells. **(B)** Quantitation of (A). Statistics was assessed by comparing to control siRNA (ctrl) treated cells. *, $p < 0.05$; ***, $p < 0.001$. **(C)** Western blot of GRASP-depleted HeLa cells treated with cycloheximide (CHX) for indicated times. 72 h post transfection with indicated siRNA, cells were treated with 100 μM CHX for 0, 4, 8, 12, 24 and 36 h, lysed and analyzed by Western blot for $\beta 1$ integrin and p97 on the same gel. As GRASP knockdown cells have lower level of integrins, we exposed those gels longer and so all cell lines had a similar signal at 0 time point to start with, and the reduction of the protein was assessed over time. **(D)** GRASP depletion does not increase $\alpha 5$ and $\beta 1$ integrin degradation. HeLa cells transfected with indicated siRNAs were labeled with TRANS ^{35}S -LABEL [^{35}S] for 1 h and chased for 12 h, 24 h and 48 h. Immunoprecipitated $\alpha 5\beta 1$ integrin were analyzed by SDS-PAGE and autoradiography. **(E)** Quantification of $\alpha 5$ integrin in (D). Note that there is no significant difference in the degradation rate of $\alpha 5$ integrin between control siRNA treated and GRASP-depleted cells. **(F)** Quantification of $\beta 1$ integrin in (D). There is no significant difference in the degradation rate of $\beta 1$ integrin between control-siRNA treated and GRASP-depleted cells.

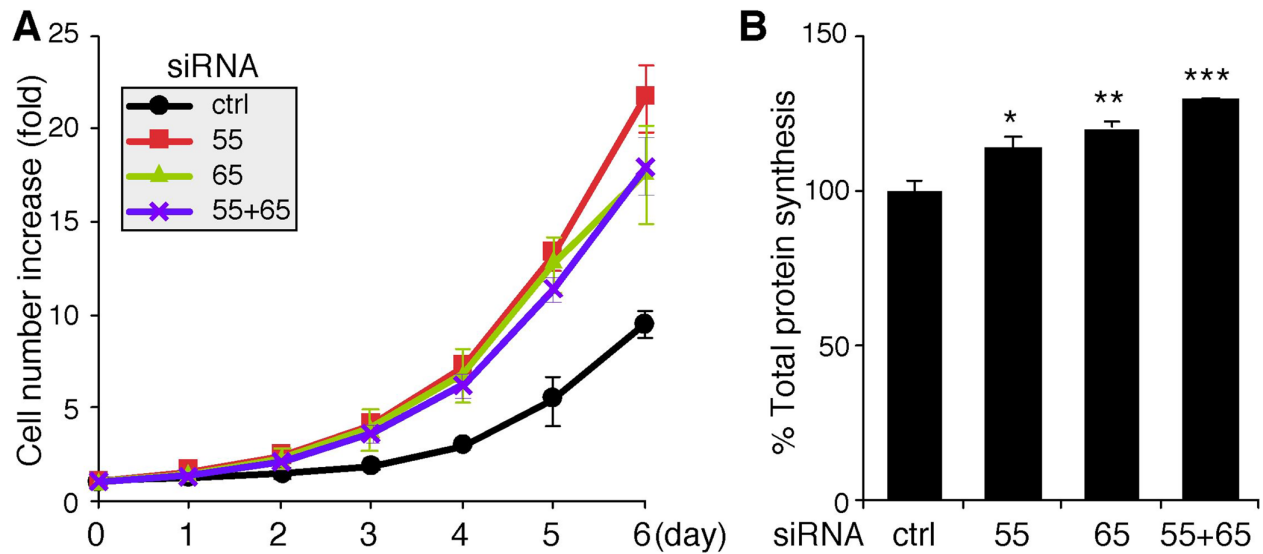
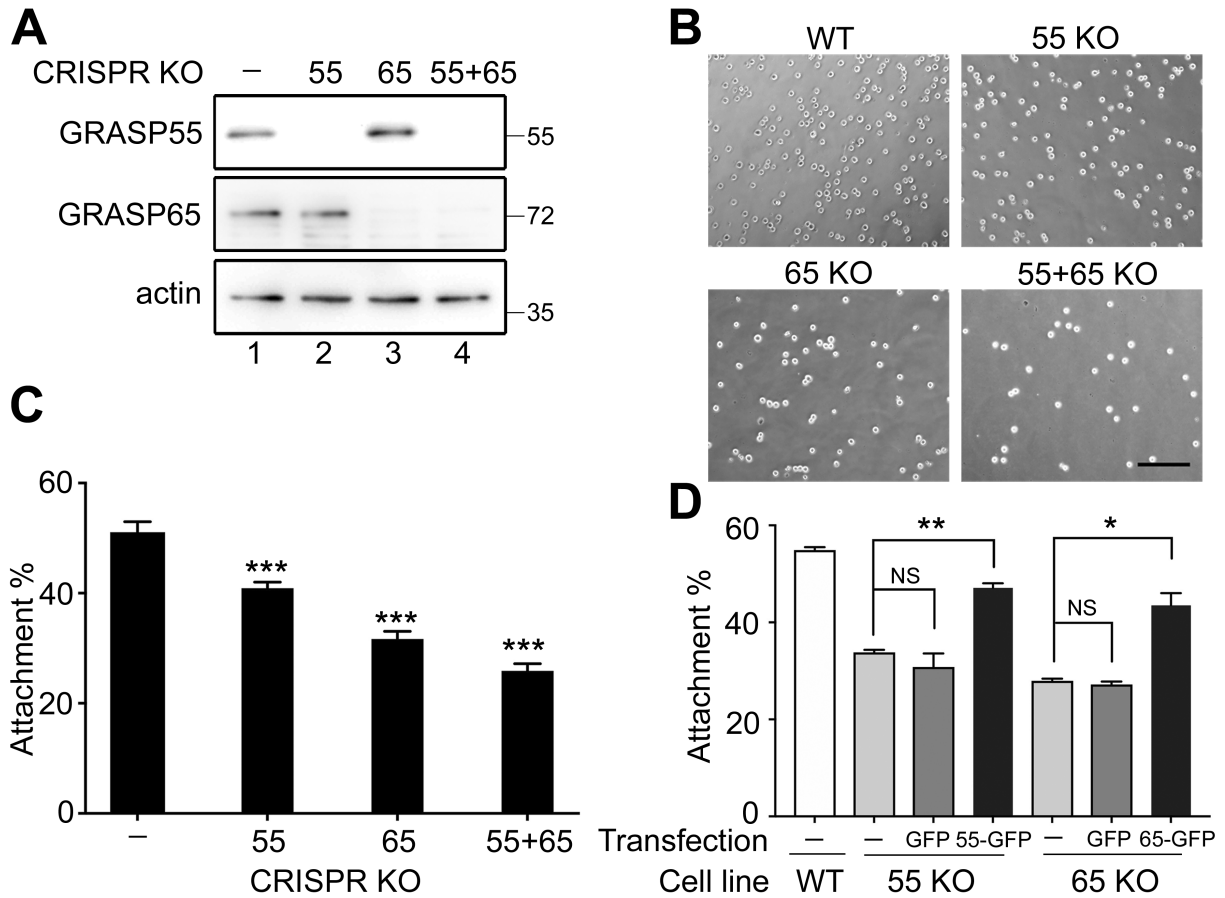


Figure 2.7. Depletion of GRASP55 and/or GRASP65 enhances cell growth and total protein synthesis.

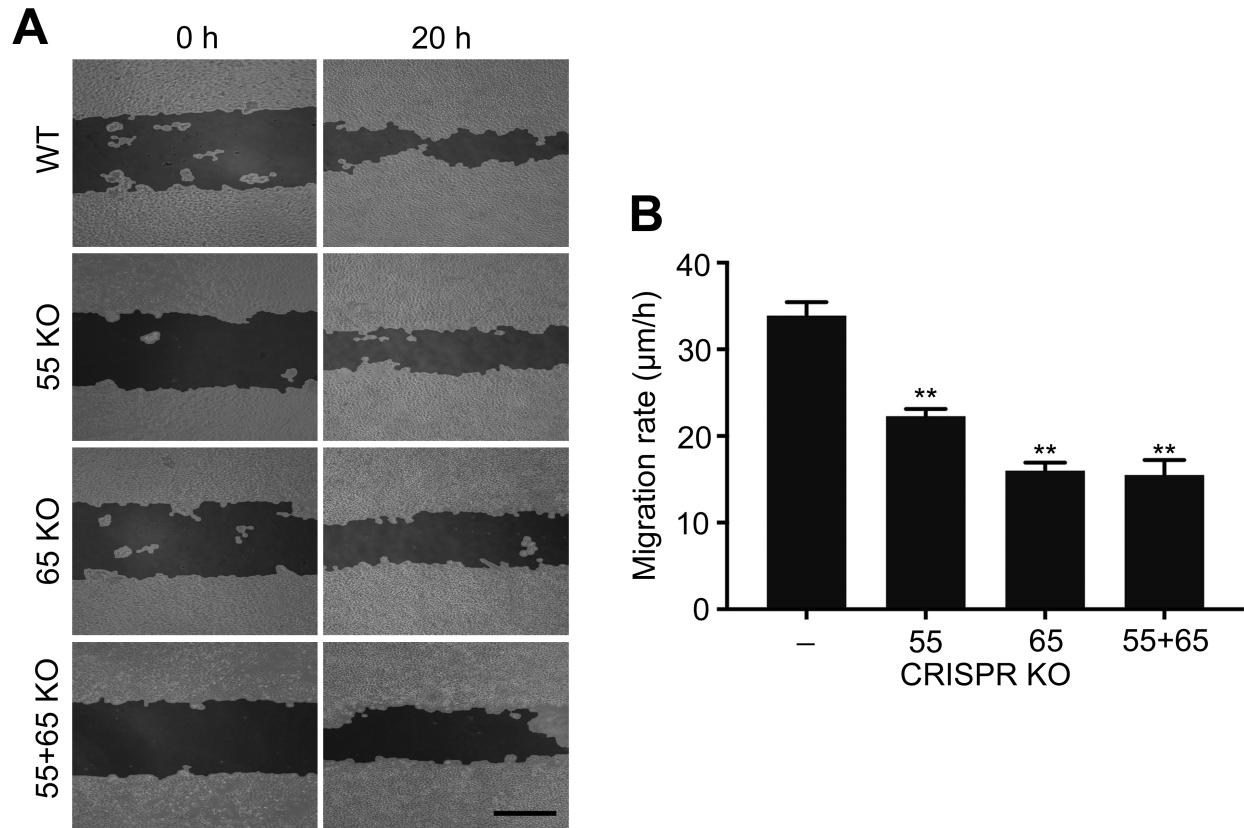
(A) Growth rate of HeLa cells transfected with indicated siRNAs, as measured using crystal violet staining. The measurement began 48 hours after transfection. **(B)** Total protein synthesis is enhanced in GRASP-depleted cells. HeLa cells transfected with indicated siRNAs were labeled with TRANS ^{35}S -LABEL [^{35}S] for 1 h. Equal amounts of total proteins were precipitated with TCA, and [^{35}S]-methionine/cysteine incorporation was assessed by scintillation counting. Statistics was assessed by normalizing and comparing to control siRNA treated cells (ctrl) by student's *t*-test. *, $p < 0.05$; **, $p < 0.01$; ***, $p < 0.001$.



Supplemental Figure 2.1. GRASP knockout reduces cell attachment.

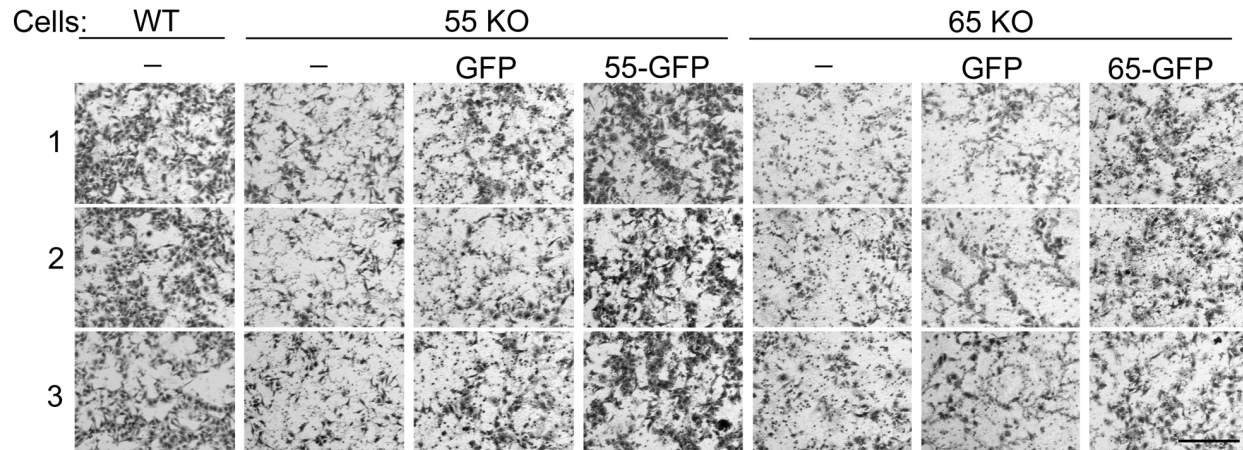
(A) Western blot of wild type (WT) and GRASP55 and/or GRASP65 knockout (KO) HeLa cells.

(B) The attachment of cells was reduced by GRASP KO. A total of 3×10^5 cells were seeded on fibronectin coated plates and incubated in serum-free medium for 30 min. After the removal of unbound cells, the number of attached cells was counted. Scale bar, 500 μ m. (C) Quantitation of cell attachment in (B). Results were presented as mean \pm SEM, statistical analysis was assessed by comparing to control cells (ctrl) by student's *t*-test. (D) GRASP expression rescues the decreased cell attachment of GRASP KO cells. Cells transfected with indicated constructs were analyzed in an attachment assay as in (B). Shown are the quantitation results. Expression of GRASP55-GFP or GRASP65-GFP, but not GFP alone, in the related cells rescued the defects in cell attachment. *, $p < 0.05$; **, $p < 0.01$; ***, $p < 0.001$.



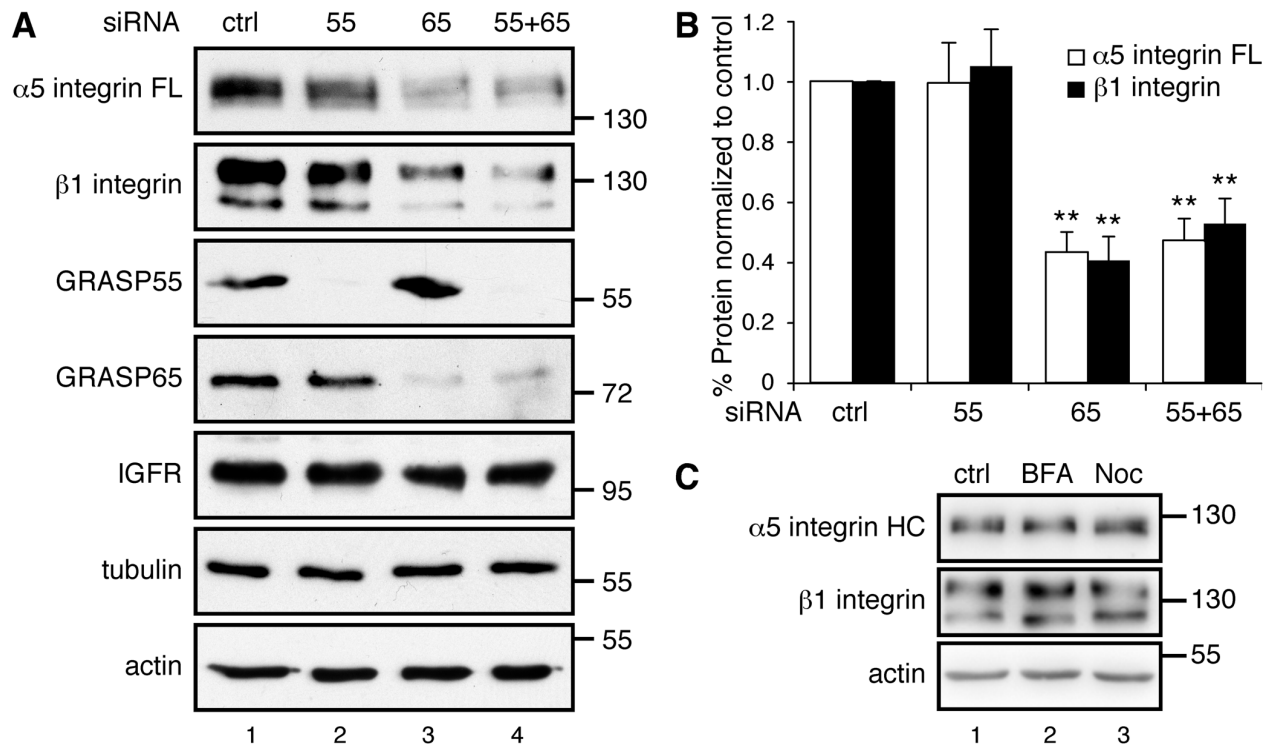
Supplemental Figure 2.2. GRASP deletion reduces cell migration.

(A) GRASP deletion reduces HeLa cells migration. Control or GRASP-knockout (KO) cells were analyzed in a wound-healing assay. Shown images were taken at 0 h and 20 h after scratching. Scale bar, 500 µm. (B) Quantitation of the migration rate in (A). Statistical analysis was assessed by comparing to WT cells by student's *t-test*. *, $p < 0.05$; **, $p < 0.01$.



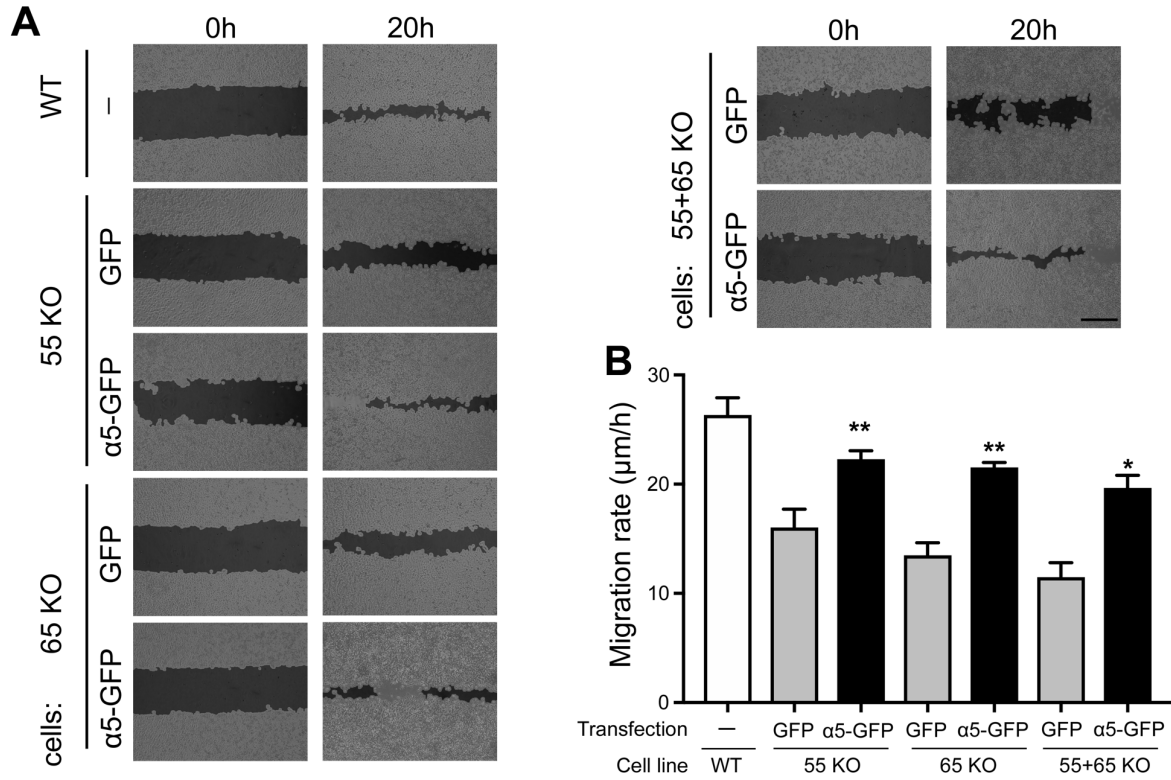
Supplemental Figure 2.3. GRASP expression rescues the decreased cell migration in GRASP-knockout cells.

Wild type (WT) and GRASP KO HeLa cells transfected with the indicated constructs were analyzed by a transwell assay. Shown images were taken after 20 h migration. Cells that had migrated to the lower side were visualized under a Leica MZ FLIII stereomicroscope with 10x lens. Scale bar, 500 μ m. Triplicate images were shown for each treatment, and the quantification results are shown in Figure 2.4D.



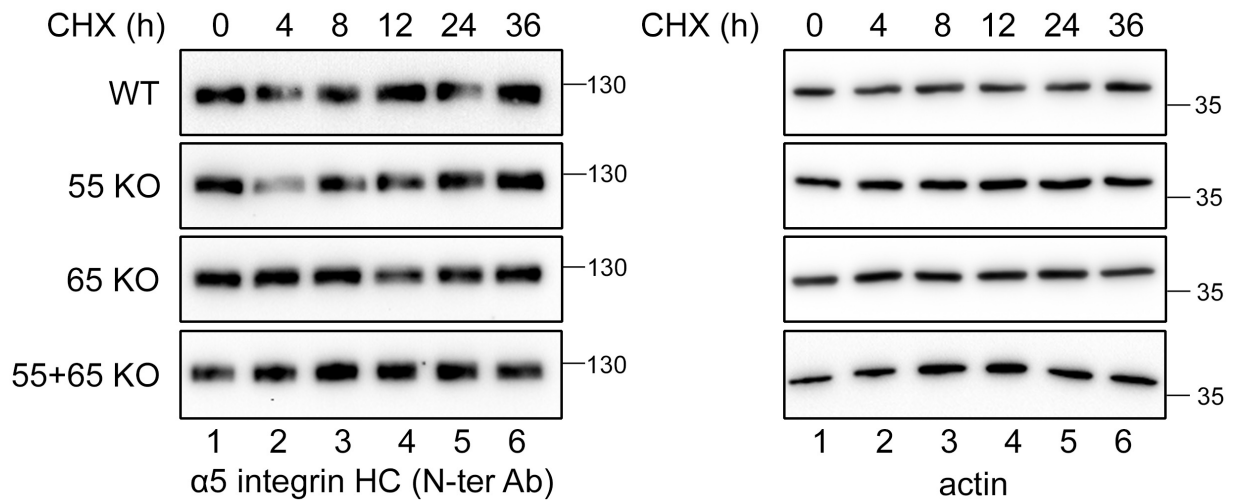
Supplemental Figure 2.4. Depletion of GRASP55 and/or GRASP65 reduces $\alpha 5$ and $\beta 1$ integrin levels.

(A) Western blots of HeLa cells transfected with indicated siRNAs. Note the reduced the expression of both $\alpha 5$ and $\beta 1$ integrin. (B) Quantitation of (A) normalized with α -tubulin. Statistics was assessed by comparing to control siRNA (ctrl) treated cells. **, $p < 0.01$. (C) Western blots of HeLa cells treated with Brefeldin A (BFA) or nocodazole (Noc) for 2 h. DMSO was used as a control. Note that $\alpha 5$ and $\beta 1$ integrin levels did not change in each treatment.



Supplemental Figure 2.5. Restoration of $\alpha 5\beta 1$ integrin level rescues the decreased cell migration in GRASP-knockout (KO) cells.

(A) $\alpha 5$ integrin expression rescues the decreased cell migration in GRASP KO HeLa cells. Cells transfected with indicated constructs were tested in a wound-healing assay and images were processed by Wimasis Image Analysis. Images were taken at 0 h and 20 h after scratching. Scale bar, 500 μm . (B) Quantitation of the migration rate in (A). Statistical analysis was assessed by comparing $\alpha 5$ -GFP to corresponding GFP expressing cells by student's *t*-test. *, $p < 0.05$; **, $p < 0.01$; ***, $p < 0.001$.



Supplemental Figure 2.6. GRASP knockout does not increase $\alpha 5$ integrin turnover.

Wild type (WT) and GRASP knockout (KO) HeLa cells were treated with 100 μ M cycloheximide (CHX) for 0, 4, 8, 12, 24 and 36 h, lysed and analyzed by Western blot for $\alpha 5$ integrin heavy chain ($\alpha 5$ integrin N-ter antibody) and actin. Note that $\alpha 5$ integrin level does not seem to change within 36 h CHX treatment in all cell lines.

Chapter 3 Golgi Structural Defect Impairs Glycosaminoglycan Synthesis, Sulfation, and Secretion

Abstract

Synthesis of glycosaminoglycans such as heparan sulfate (HS) and chondroitin sulfate (CS) occurs in the lumen of the Golgi but the relationship between Golgi structural integrity and glycosaminoglycan synthesis is not clear. In this study, we disrupted the Golgi structure by knocking out GRASP55 and GRASP65 and determined its effect on the synthesis, sulfation, and secretion of HS and CS. We found that GRASP depletion increased HS synthesis while decreasing CS synthesis in cells, altered HS and CS sulfation, and reduced both HS and CS secretion. Using proteomics, RNA-seq and biochemical approaches, we identified EXTL3, a key enzyme in the HS synthesis pathway, whose level is upregulated in GRASP knockout cells; while GalNacT1, an essential CS synthesis enzyme, is robustly reduced. In addition, we found that GRASP depletion decreased HS sulfation via the reduction of PAPSS2, a bifunctional enzyme in HS sulfation. Our study provides the first evidence that Golgi structural defect may significantly alter the synthesis and secretion of glycosaminoglycans.

Introduction

The Golgi apparatus is a central station in the intracellular trafficking pathway and serves as the principal hub for sorting and post-translational modifications of proteins and lipids (Li et al., 2019b). The basic structure of the Golgi is a stack of flattened cisternae. In mammalian cells, multiple Golgi stacks are latterly linked into a ribbon-like structure located in the perinuclear region of the cell. It has been previously demonstrated that two Golgi peripheral membrane proteins, GRASP55 and GRASP65, function as the “glue” that links Golgi membranes together and facilitates Golgi stacking and ribbon formation. Knocking down or knocking out either one of these two GRASP proteins decreases the number of cisternae per stack, whereas depleting both GRASPs disrupt the entire Golgi structure (Xiang and Wang, 2010, Bekier et al., 2017, Ahat et al., 2019a).

Functional studies revealed that destruction of the Golgi structure by GRASP-depletion accelerates protein trafficking in the Golgi, but impairs accurate N-glycosylation and protein sorting (Xiang et al., 2013). At the cellular level, GRASP depletion reduces cancer cell attachment and invasion mainly through the reduction of $\alpha 5\beta 1$ integrin synthesis (Ahat et al., 2019c), indicating a role of GRASPs and/or the Golgi structure in transcription regulation. In addition to Golgi structure formation, GRASPs are also involved in autophagy and unconventional secretion. Under starvation or stress conditions, GRASP55, but not GRASP65, translocates from the Golgi to other membrane structures such as autophagosomes and endoplasmic reticulum (ER) to regulate autophagy and unconventional secretion of certain cytosolic or transmembrane proteins (Zhang et al., 2018, Zhang and Wang, 2018b, Gee et al., 2011, Cruz-Garcia et al., 2017, Nüchel et al., 2021).

Glycosaminoglycans (GAGs) are main components of the cell surface glycome and extracellular matrix (Annaval et al., 2020). GAGs are long linear polysaccharides consisting of repeating disaccharide units. Based on the core disaccharide structures, GAGs are classified into three major forms, heparan sulfate (HS), chondroitin sulfate (CS), and hyaluronan (HA). While HA is synthesized at the plasma membrane and released, HS and CS are synthesized and attached to serine residues of cargo proteins in the Golgi, from where they are transported to the cell surface and secreted to the extracellular space. The biosynthesis of both HS and CS begins with the formation of a tetrasaccharide linker on a serine residue in a protein core, which is subsequently diversified to HS or CS depending on the subsequent enzymatic reactions (Figure 3.1A) (Annaval et al., 2020).

For HS, the initiation of HS biosynthesis occurs as the transferases Exostosin-like 2 (EXTL2) and 3 (EXTL3) transfer an *N*-Acetylglucosamine (GlcNAc) to the initial linker chain (Figure 3.1A) (Kim et al., 2001, Kitagawa et al., 1999). Next, Exostosin-1 (EXT1) and -2 (EXT2), and Exostosin-like 1 (EXTL1) and EXTL3, extend the chain by alternatively transferring GlcNAc and D-Glucuronic acid (GlcA) residues to the sugar chain (Kreuger and Kjellen, 2012). This HS chain is then modified by the enzymes bifunctional heparan sulfate *N*-deacetylase/*N*-sulfotransferase 1-4 (NDST1-4) that have both *N*-deacetylase and *N*-sulfotransferase activities (Carlsson et al., 2008). Other enzymes involved in HS sulfation include heparan sulfate 2-*O*-sulfotransferase (H2ST), 6-*O*-sulfotransferases (H6ST1-3), and 3-*O*-sulfotransferases (H3ST) 1, 2, 3A, 3B, 4, 5, and 6 (Maeda, 2015). These NDST enzymes and sulfotransferases rely on sulfur donor bifunctional 3'-phosphoadenosine 5'-phosphosulfate

synthase (PAPS) which are synthesized by 3'-phosphoadenosine 5'-phosphosulfate synthase-1 (PAPSS1) and -2 (PAPSS2) in the cytosol and transported by adenosine 3'-phospho 5'-phosphosulfate transporter 1 (PAPST1) and PAPST2 into the Golgi lumen (Fuda et al., 2002, Stelzer et al., 2007, Kamiyama et al., 2006, Dick et al., 2015). Most HS chains are sulfated, which significantly affects their activity and function. For example, it has been shown that 3-*O*-sulfation of HS increases its binding with Tau at the cell surface, which facilitates Tau internalization (Zhao et al., 2020).

For CS, chain formation initiates with *N*-acetylgalactosaminyltransferases, GalNAcT1-2, and is then elongated by chondroitin sulfate synthase 1-3 (CHSY1-3) and chondroitin sulfate glucuronyltransferase (CHPF) that alternatively transfer GalNAc and GlcA residues to the sugar chain (Figure 3.1A) (Maeda, 2015). CS is sulfated by sulfotransferases chondroitin 4-sulfotransferase 1-3 (C4ST1-3), chondroitin 6-sulfotransferase 1-2 (C6ST1-2) and *N*-acetylgalactosamine 4-sulfate 6-*O*-sulfotransferase (GalNAc4S-6ST), or by dermatan sulfate epimerases 1-2 (DS-epi 1-2) if the 2-*O*-sulfated D-glucuronic acid (GlcA) residues are C5-epimerized to L-iduronic acid (IdoA). Subsequently, when the chain is further sulfated by dermatan sulfotransferase D4ST, uronyl 2-*O*-sulfotransferase (UST), or GalNAc4S-6ST, it is referred to as dermatan sulfate (DS) (Maeda, 2015).

While the synthesis of the tetrasaccharide linker of HS and CS is initiated in the ER or ERGIC, the bulk parts of HS and CS are synthesized in the Golgi lumen (Prydz, 2015), similar to that of *N*-linked glycans. Consistently, most enzymes involved in HS and CS synthesis, such as EXT1 and EXT2 in HS synthesis and GalNAcT-1 in CS synthesis, reside in the Golgi

(Kobayashi et al., 2000, Uliana et al., 2006). Therefore, it is reasonable to speculate that Golgi structural defect may significantly impact the synthesis of HS and CS as *N*-glycans as we previously showed (Xiang et al., 2013). Consistently, depletion of certain subunits of the Conserved Oligomeric Golgi (COG) complex, which transports Golgi enzymes to their proper locations within the Golgi, reduces GAG modification (Adusumalli et al., 2021); while depletion of giantin, another membrane tether in the Golgi, reduces the mRNA level of polypeptide *N*-acetylgalactosaminyltransferase 3 (GALNT3) (Stevenson et al., 2017). However, the relationship between Golgi structural integrity and GAG synthesis has not been systematically explored.

In this study, we disrupted the Golgi structure by knocking out GRASP55 and GRASP65 and determined the effect on GAG synthesis, sulfation, and secretion. We also performed proteomic and RNA-seq analysis to identify the enzymes whose alternation is responsible for the defects in HS and CS synthesis in GRASP knockout (KO) cells.

Results

3.1 GRASP KO increases GAG synthesis but decreases their secretion.

Given that GRASP55 and GRASP65 are major regulators of Golgi stack formation, we knocked them out, single or in combination, in HeLa cells to disrupt the Golgi structure (Bekier et al., 2017), and thereby determined the effect on GAG synthesis. As shown in Figure 3.1B, we cultured wildtype (WT), GRASP55 knockout (55KO), GRASP65 knockout (65KO), and GRASP55 and GRASP65 double knockout (DKO) cells in serum-free medium for 8 h, collected cell lysate and conditioned media, and performed GAG analysis by liquid chromatography-mass spectrometry (LC-MS) (Supplemental Tables 1 and 2). The amount of GAGs, including (HS, CS

and HA) in the cell lysate was increased in GRASP KO cells, with its level in 65KO the highest (Figure 3.1C). In contrast to the cell lysate, the amount of GAGs in the conditioned media was reduced (Figure 3.1D). The total amount of GAGs (cells + media) was higher in GRASP KO cells compared to WT, again with 65KO to be the highest (Figure 3.1E). In summary, disruption of the Golgi structure by GRASP depletion increases GAG synthesis while reducing its secretion.

3.2 GRASP KO increases HS synthesis but decreases its sulfation and secretion.

Given that HS and CS but not HA are synthesized in the Golgi, we further characterized HS and CS synthesis and sulfation in GRASP KO cells. When the Golgi structure was disrupted by GRASP KO, HS synthesis was significantly increased compared to WT cells as analyzed by LC-MS (Figure 3.2A; Supplemental Table 3.1-3.2). The increase of HS in GRASP KO cells or at the cell surface was confirmed by immunostaining of HS with an anti-HS antibody 10E4 followed by immunofluorescence microscopy with or without permeabilization (Figure 3.2B; Supplemental Figure 3.1A). The HS signal by this antibody was specific as it was largely quenched by preincubation of the antibody with heparin (Supplemental Figure 3.1B). The increased level of HS in GRASP KO cells was further validated by flow cytometry (Figure 3.2C).

HS is covalently linked to core proteins that are secreted by cells, so we analyzed the level of HS in the conditioned media. GRASP KO largely reduced HS secretion compared to that of WT cells (Figure 3.2D). Although the absolute amount of HS in the media was not reduced by GRASP KO, the percentage of HS in the media was significantly lower in the KOs than WT due

to the increased HS synthesis (Supplemental Tables 3.1-3.2). Given the importance of HS sulfation, we also quantified the different sulfated forms of HS in cells and conditioned media by 2-aminoacridone (AMAC) labeling and LC-MS (Supplemental Tables 3.3 and 3.4). In contrast to the increased level of HS synthesis, the overall sulfation of HS was significantly reduced by GRASP KO in both the cells and conditioned media (Figure 3.2E-F). This indicates that Golgi destruction via GRASP depletion negatively regulates the sulfation pathway of HS. Taken together, disruption of the Golgi structure by GRASP KO increases HS synthesis but decreases its sulfation and secretion.

3.3 GRASP KO decreases CS synthesis and secretion.

Like HS, CS is synthesized in the Golgi and sulfated. HS and CS share the same tetrasaccharide precursor, which branches into either the HS pathway via the action of the EXTL enzymes, or the CS pathway via the reaction of the GalNAcT enzymes (Figure 3.1A). Therefore, it is reasonable to speculate that increased branching into the HS pathway may lead to reduced branching into the CS pathway. Indeed, GRASP KO reduced CS synthesis as analyzed by LC-MS, the opposite to HS (Figure 3.3A; Supplemental Tables 3.1 and 3.2). To confirm this result by an alternative approach, we stained WT and GRASP KO cells with an CS antibody (CS-56) and analyzed the levels of CS by fluorescence microscopy and flow cytometry. Consistent with the LC-MS results, GRASP KO reduced the level of CS in cells compared to WT (Figure 3.3B-C). Here, the degree of CS reduction examined by microscopy and flow cytometry was more dramatic than by LC-MS. The cause of this difference could be that LC-MS includes both CS and DS in the results, while the CS antibody only recognizes CS but not DS (Avnur and Geiger, 1984), which more accurately reflects the CS level in cells.

Next, we analyzed the secretion of CS in WT and GRASP KO cells. Both the amount and percentage of CS in the conditioned media were largely reduced by GRASP KO (Figure 3.3D; Supplemental Tables 3.1-2). Lastly, we analyzed the different subtypes of CS sulfation and found that GRASP KO increased 4-sulfation but decreased 6-sulfation in both the cell lysate and conditioned media (Figure 3.3E-F; Supplemental Tables 3.5 and 3.6). Taken together, disruption of the Golgi structure by GRASP KO decreases CS synthesis, alters its sulfation, and decreases its secretion.

3.4 GRASP KO regulates key enzymes in HS and CS synthesis and sulfation.

The regulation of HS and CS synthesis and sulfation is complex and involves numerous enzymes (Figure 3.1A). A majority of these enzymes are localized in the Golgi and thus their level and localization could be regulated by Golgi structural changes. Therefore, we performed systematic RNA-seq and proteomic analysis of WT and GRASP KO cells to identify genes related to the observed alterations in HS and CS synthesis and sulfation. As expected, many enzymes involved in HS and CS synthesis were affected by GRASP KO (Table 3.1). Consistent with the increased HS level in cells, the mRNA levels of several HS synthesis enzymes, such as EXTL2, EXTL3, EXT1, NDST1 and Adenosine 3'-phospho 5'-phosphosulfate transporter 3 (SLC35B3), were increased in GRASP KO compared to WT cells. Similar to the trend of CS reduction in GRASP KO cells, the mRNA levels of many CS synthesis enzymes, including GalNAcT1, CHSY1, C4ST2, GalNAc4S-6ST, C6ST1 and DS-epi1, were all decreased upon GRASP KO (Figure 3.4A). The altered expression of HS and CS synthesis enzymes in GRASP KO cells was further confirmed at the protein level by proteomic analysis (Table 3.1) and

Western blots (Figure 3.4B). GRASP KO increased the protein level of EXTL3, a key enzyme in HS synthesis, while decreased the level of GalNAcT1 in the CS synthesis pathway (Figure 3.4B-C). In addition to EXTL3, the protein levels of EXT1 and EXT2 were slightly higher in 65KO cells, which might explain why 65KO cells have the highest HS level in all cell lines.

To decipher the underlying mechanism of the reduced HS sulfation in GRASP KO cells, we analyzed the levels of multiple HS sulfation enzymes in the RNA-seq data and found that GRASP KO reduced the expression of the sulfur synthase PAPSS2 and the major PAPS transporter PAPST1 (SLC35B2) (Table 3.1). Consistently, the protein level of PAPSS2 was also significantly lower in GRASP KOs than WT cells as shown by proteomic analysis (Table 3.1) and Western blot (Figure 3.4D-E). Unlike a global reduction in HS sulfation, we only observed a significant shift from 6-sulfation (6S) to 4-sulfation (4S) in CS (Figure 3.3E-F). GRASP depletion largely increased the ratio of 4S/6S compared to WT. Repeating disaccharide units of CS are sulfated at C4 and C6 by C4ST-1 and C6ST-1, respectively. In our RNA-seq analysis, the mRNA levels of C6ST1 and C6ST2 were significantly decreased in GRASP KOs, especially 65KO and DKO (Table 3.1), which may explain the reduction of 6S in GRASP KO cells.

To confirm that the observed effects in HS and CS were caused by GRASP KO, we transfected 55KO and 65KO cells with GRASP55-GFP and GRASP65-GFP, respectively, which has previously been shown to rescue the Golgi structure and correct the defects in *N*-glycosylation and cell attachment (Xiang et al., 2013, Bekier et al., 2017, Ahat et al., 2019c). Indeed, re-expression of GRASP55 and GRASP65 in the corresponding KO cells not only restored the levels of major enzymes such as EXTL3 and GalNAcT1 (Figure 3.4F), but also

normalized the levels of HS (Figure 3.4G-I) and CS (Supplemental Figure 3.1C). Taken together, these results revealed that Golgi structure formation and defect regulate HS and CS synthesis and sulfation through modulating the expression of key enzymes.

Discussion

In this study we found that GRASP depletion and subsequent disruption of the Golgi structure increased overall GAG synthesis but decreased their secretion. As HS and CS are the two main types of GAGs synthesized in the Golgi, we further analyzed their levels and sulfation in WT and GRASP KO cells. Our results revealed that GRASP depletion increased HS synthesis but reduced its sulfation mainly through the upregulation of EXTL3 and downregulation of PAPSS2, respectively. GRASP depletion, however, reduced CS synthesis by decreasing GalNAcT1 expression; GRASP KO also altered the balance between 4-sulfation and 6-sulfation of CS. These effects were due to GRASP depletion as re-expression of GRASPs corrected the observed defects in HS and CS synthesis.

HS and CS levels and sulfation are tightly related to their functions in various biological processes including extracellular matrix (ECM) assembly, cell adhesion, coagulation and immune response (Aquino et al., 2010). It has been shown that abnormal sulfation of HS causes defects in FGF-2–induced proliferation and survival of multipotent progenitor cells via reducing FGF-2 and FGFR1 interaction, which contribute to Hurler syndrome (Pan et al., 2005). Similarly, in *Drosophila melanogaster* and *Caenorhabditis elegans*, reduced HS sulfation results in a delay in wound closure and defects in actin stress fiber formation (Götte et al., 2008). In another example, reduction of functional heparan sulfate proteoglycan (HSPG) has been shown

to increase pericyte number while reducing its adhesion to nascent sprouts via the regulation of transforming growth factor β signal transduction (Le Jan et al., 2012). Similar to HS, CS and its synthesis enzymes are also altered in multiple disease conditions. Deficiency of an essential chondroitin synthase CHSY1 causes Temtamy preaxial brachydactyly syndrome (TPBS) (Sasarman et al., 2016). GalNAcT deficient mice showed defects in heart valve development and cardiac function via the remodulation of ECM and mitogen-activated protein kinase (MAPK) signaling pathway (Tian et al., 2015). In developing mouse brain, the 6S level of CS is gradually decreased while 4S is gradually increased, resulting in a progressive increase of 4S/6S ratio during brain development. This change in CS sulfation was shown to reduce cortex plasticity (Miyata et al., 2012). Interestingly, in neurodegenerative diseases such as Alzheimer's, the Golgi is fragmented possibly due to the loss of function of the GRASP proteins (Joshi et al., 2014), indicating a potential link between Golgi fragmentation, increased 4S/6S ratio, and reduced cortex plasticity in aging and neurodegenerative diseases.

How does Golgi structural defect and/or GRASP depletion affect the expression of HS and CS synthesis and sulfation enzymes is an interesting but unanswered question. This not only includes EXTL3 and GalNAcT1 that reside in the Golgi, but also PAPSS2 that is localized in the cytosol. It has been shown that many signaling molecules including mammalian target of rapamycin (mTOR), KRAS and some transcription factors such HIF1 α are localized on the Golgi (Gosavi et al., 2018, Philips, 2004, Baumann et al., 2018). Golgi unstacking may affect these signaling pathways or the activity of the transcription factor, which in turn may regulate the expression of HS and CS enzymes. Similarly, it has been shown that GRASP depletion reduces the synthesis of $\alpha 5\beta 1$ integrins, major cell adhesion molecules at the cell surface, which

subsequently decreases cell adhesion but increases cell growth (Ahat et al., 2019c). This indicates an exciting possibility that cells may possess a sensing mechanism for Golgi structural changes, which when activated, may regulate the expression of multiple proteins to control different cellular activities.

It was surprising to see that the secretion of both HS and CS was reduced in GRASP KO cells compared to WT as it has previously been shown that GRASP depletion accelerated protein trafficking through the Golgi membranes (Wang et al., 2008, Xiang et al., 2013, Lee et al., 2014). This result can be explained in several ways. First, given that all marker proteins used in the previous studies, including the vesicular stomatitis virus G (VSV-G) protein, CD8, and $\alpha 5\beta 1$ integrins, are mainly modified by N-glycosylation, it is possible that GRASP depletion and/or Golgi structural disruption may affect the trafficking and secretion of different cargo molecules differently. Similarly, it has been shown that GRASP depletion alters the level of glycolipids by decreasing the level of globotriaosylceramide (Gb3) and increasing the level of monosialotetrahexosylganglioside (GM1) (Bekier et al., 2017). Second, our analysis only revealed the amount of disaccharides but did not determine whether the HS and CS sugar chains are properly attached to core proteins. Our previous studies demonstrated that GRASP depletion increased the amount of free polysaccharides in the N-glycosylation pathway (Xiang et al., 2013). It is so far unknown whether free polysaccharides travel through the Golgi at the same speed as those attached to core proteins. Third, altered sulfation of HS and CS may affect their conjugation to the core proteins as well as their secretion and stability. As sugar modifications affect protein stability and activity (Sola and Griebenow, 2009), reduced sulfation may lead to certain core proteins to be sent for degradation instead of secretion. Finally, there is a possibility

that more HS and CS are degraded in the conditioned media of GRASP KO cells. It has previously been shown that GRASP depletion causes missorting of lysosomal enzymes and results in their secretion (Xiang et al., 2013). It is possible that GRASP KO cells may secrete HS and CS degrading enzymes such as endoglycosidases and exohydrolases that normally reside in the lysosomes (Freeman and Hopwood, 1992). Nevertheless, the molecular mechanism that reduces HS and CS secretion in GRASP depleted cells requires further investigation.

Taken together, our results showed that disruption of the Golgi stacked structure via GRASP depletion led to the increase of total GAG synthesis, where HS level was increased due to the upregulation of EXTL3 expression and CS level was reduced because of GalNAcT1 down-regulation. In addition, Golgi defect also reduced HS sulfation via the reduction of PAPSS2. In summary, this study revealed that Golgi structural integrity and GAG synthesis are tightly linked.

Materials and Methods

Cell culture and transfection

Wild type, GRASP55 knockout (55KO), GRASP65 knockout (65KO), GRASP55 and GRASP65 double knockout (DKO) HeLa cells were maintained in Dulbecco's modified Eagle's medium (DMEM 4.5 g/l glucose) supplemented with 10% fetal bovine serum (ThermoFisher, Waltham, MA), 1% L-glutamine, 1% penicillin-streptomycin under 5% CO₂ at 37°C as previously described (Bekier et al., 2017).

To express exogenous GRASP proteins, HeLa cells of ~50% confluency were transfected with indicated GRASP constructs (Xiang and Wang, 2010, Tang et al., 2010). For a 6 cm plate, 6 µg of pEGFP-N1-GRASP65 or pEGFP-N1-GRASP55 (both wild type) construct was mixed with 18 µl polyethylenimine (PEI) and 0.5 ml serum-free medium for 15 min at room temperature and then added to the cells in 4 ml DMEM containing 10% super calf serum. For control transfection, 4 µg of pEGFP-N1 construct was mixed with 18 µl PEI and 0.5 ml serum-free medium for 15 min and then added to the cells in 4 ml DMEM containing 10% super calf serum.

Materials and sample preparation for LC-MS and PAGE analysis

Unsaturated disaccharide standards of HS (Δ UA-GlcNAc; Δ UA-GlcNS; Δ UA-GlcNAc6S; Δ UA2S-GlcNAc; Δ UA2S-GlcNS; Δ UA-GlcNS6S; Δ UA2S-GlcNAc6S; Δ UA2S-GlcNS6S), unsaturated disaccharide standards of CS (Δ UA-GalNAc; Δ UA-GalNAc4S; Δ UA-GalNAc6S; Δ UA2S-GalNAc; Δ UA2S-GalNAc4S; Δ UA2S-GalNAc6S; Δ UA-GalNAc4S6S; Δ UA2S-GalNAc4S6S), and unsaturated disaccharide standard of HA (Δ UA-GlcNAc), where

Δ UA is 4-deoxy- α -L-threo-hex-4-enopyranosyluronic acid, were purchased from Iduron (UK). Actinase E was obtained from Kaken Biochemicals (Japan). Chondroitin lyase ABC from *Proteus vulgaris* was expressed in Linhardt's laboratory. Recombinant Flavobacterial heparin lyases I, II, and III were expressed in Linhardt's laboratory using *Escherichia coli* strains provided by Jian Liu (College of Pharmacy, University of North Carolina). 2-Aminoacridone (AMAC), sodium cyanoborohydride were obtained from Sigma-Aldrich (St. Louis, MO, USA). All solvents used in LC-MS were HPLC grade.

GAG preparation for disaccharide analysis

Cells were proteolyzed at 55°C with 500 μ l of 10-mg/mL actinase E for 24 h and followed by actinase E deactivation at 100°C for 30 min. The volume of the above solution containing 2 million cells was transferred to a 3-kDa molecular weight cut off (MWCO) spin tube. The filter unit was washed three times with 400 μ l distilled water and then added with 300- μ l digestion buffer (50 mM ammonium acetate containing 2 mM calcium chloride adjusted to pH 7.0). Recombinant heparin lyase I, II, III (pH optima 7.0–7.5) and recombinant chondroitin lyase ABC (pH optimum 7.4, 10 mU each) were added to each filter unit containing sample and mixed well. The samples were all incubated at 37 °C for 24 h. The enzymatic digestion was terminated by ultrafiltration through the 3-kDa spin tube. The filtrate was collected, and the filter unit was washed twice with 200 μ l distilled water. All the filtrates containing the disaccharide products were combined and dried via freeze dry. For the medium samples, 400- μ l medium from each specimen was ultrafiltered through a 3-kDa molecular weight cut off (MWCO) spin tube to remove small molecular compounds, and then went through the same digestion procedure as mentioned above.

AMAC labeling of disaccharides

The dried samples were AMAC-labeled by adding 10 μ l of 0.1 M AMAC in DMSO/acetic acid (17/3, V/V) incubating at room temperature for 10 min, followed by adding 10 μ l of 1 M aqueous sodium cyanoborohydride and incubating for 1 h at 45°C. A mixture containing all 17-disaccharide standards prepared at 0.5ng/ μ l was similarly AMAC-labeled and used for each run as an external standard. After the AMAC-labeling reaction, the samples were centrifuged, and each supernatant was recovered.

LC-MS

LC was performed on an Agilent 1200 LC system at 45 °C using an Agilent Poroshell 120 ECC18 (2.7 μ m, 3.0 \times 50 mm) column. Mobile phase A (MPA) was 50 mM ammonium acetate aqueous solution, and the mobile phase B (MPB) was methanol. The mobile phase passed through the column at a flow rate of 300 μ l/min. The gradient was 0-10 min, 5-45% B; 10-10.2 min, 45-100%B; 10.2-14 min, 100%B; 14-22 min, 100-5%B. Injection volume is 5 μ l.

A triple quadrupole mass spectrometry system equipped with an ESI source (Thermo Fisher Scientific, San Jose, CA) was used as a detector. The online MS analysis was at the Multiple Reaction Monitoring (MRM) mode. MS parameters: negative ionization mode with a spray voltage of 3000 V, a vaporizer temperature of 300°C, and a capillary temperature of 270°C.

Western blot

Wild type and GRASP KO cells are lysed in 20 mM Tris-HCl, pH 8.0, 150 mM NaCl, 1% Triton X-100 and protease inhibitors for 30 min on ice. Lysates were cleared by centrifugation (20,000 g for 20 min at 4°C). After electrophoresis and transfer, nitrocellular membranes were incubated with antibodies to actin (Sigma, A2066), EXT1 (Santa Cruz, sc-515144), EXT2 (Santa Cruz, sc-514092), EXTL3 (Santa Cruz, sc-271986), GalNAcT1 (Novus, NBP1-81852), GFP (Proteintech, 66002-1-Ig), GRASP55 (Proteintech, 10598-1-AP), GRASP65 (Santa Cruz, sc-374423), or PAPSS2 (Santa Cruz, sc-271429) overnight at 4°C. The membranes were extensively washed and further incubated with HRP conjugated goat anti-Rabbit or goat anti-mouse secondary antibodies for 1 h at room temperature and exposed to a FluorChem M machine (Proteinsimple).

Immunofluorescence microscopy

Cells were grown on sterile glass coverslips and rinsed with phosphate buffered saline (PBS) before fixation. For total protein staining, cells were fixed in 4% paraformaldehyde for 10 min and permeabilized with 0.2% Triton X-100 in PBS for 10 min. For cell surface staining, cells were fixed in 1% paraformaldehyde for 10 min and not permeabilized. Cells were incubated with primary antibodies for HS (10E4, Amsbio 370255, 1:100) and CS (CS-56, Abcam ab11570, 1:50) overnight at 4°C, washed and probed with the appropriate secondary antibodies conjugated to TRITC for 45 min. To confirm that the detected 10E4 signal was specific to HS, the HS antibody (10E4 1:100) was incubated with or without 40 µg/ml heparin overnight at 4°C and then used for primary antibody staining of fixed cells. DNA was stained with Hoechst for 5 min. Coverslips were rinsed with PBS and mounted with Mowiol onto slides. Images were taken with

a 20x air objective or a 63x oil objective on a Nikon ECLIPSE Ti2 Confocal microscope and shown as max projections.

Flow cytometry

HeLa cells (WT and KO) were detached using 20 mM EDTA and resuspended in PBS with 0.5% BSA. The cells were fixed and permeabilized with 4% PFA for 10 min and 0.2% Triton X-100 for 10 min, respectively. After washing with PBS twice, the cells were incubated with the primary antibody for HS (10E4, 1:100) or CS (CS-56, 1:50) (or control without a primary antibody) with rotation for 1.5 h at room temperature. Both primary antibodies and the control group were incubated with goat anti mouse secondary antibodies (TRITC) for 1 h with rotation at room temperature. The cells were sorted with a Sony MA900 Multi-Application Cell Sorter, and the data was analyzed with FlowJo software.

Proteomics analysis

Sample Preparation: Three replicates of each WT, 55KO and 65KO cells were propagated as described above in 15 cm dishes. Upon achieving 80% confluency, the growth media were aspirated, and the cells were washed with PBS five times, then changed to 20 ml serum free medium and further incubated for 12 h. The media were first cleared by centrifugation at 500 g for 10 min at 4°C and then at 4000 g for 15 min at 4°C, and then filtered with a 0.45 µm filter. The cleaned media were concentrated with a 3 kDa cutoff ultrafilter (Millipore, UFC900324) to 200-300 µl, and the protein concentration was determined with Bradford assay (Bio-Rad, Cat # 5000006). For cell lysates collection, after removing the media, cells were washed with PBS twice, and collected in 10 ml PBS by scraping, lysed in Pierce™

RIPA buffer (Thermo, 89900) with a protein inhibitor cocktail (Thermo). The protein concentration was tested with Bradford assay and normalized, 75 µg of each sample was provided to the Mass Spectrometry-Based Proteomics Resource Facility at Department of Pathology, University of Michigan for TMT labeling, LC-MS/MS and bioinformatics analysis.

Protein Digestion and TMT labeling: Samples were proteolysed and labeled with TMT 10-plex essentially by following manufacturer's protocol (ThermoFisher, Cat # 90110, Lot # VJ306782). Briefly, upon reduction and alkylation of cysteines, the proteins were precipitated by adding 6 volumes of ice-cold acetone followed by overnight incubation at -20°C. The precipitate was spun down, and the pellet was allowed to air dry. The pellet was resuspended in 0.1 M TEAB and overnight digestion with trypsin (1:50; enzyme:protein) at 37°C was performed with constant mixing using a thermomixer. The TMT 10-plex reagents were dissolved in 41 µl of anhydrous acetonitrile and labeling was performed by transferring the entire digest to TMT reagent vial and incubating at room temperature for 1 h. Reaction was quenched by adding 8 µl of 5% hydroxyl amine and further 15 min incubation. Labeled samples were mixed, and dried using a vacufuge. An offline fractionation of the combined sample (~200 µg) into 8 fractions was performed using high pH reversed-phase peptide fractionation kit according to the manufacturer's protocol (Pierce; Cat # 84868). Fractions were dried and reconstituted in 9 µl of 0.1% formic acid/2% acetonitrile in preparation for LC-MS/MS analysis.

Liquid chromatography-mass spectrometry analysis (LC-multinotch MS3): In order to obtain superior quantitation accuracy, we employed multinotch-MS3 (McAlister GC) which minimizes the reporter ion ratio distortion resulting from fragmentation of co-isolated peptides

during MS analysis. Orbitrap Fusion (Thermo Fisher Scientific) and RSLC Ultimate 3000 nano-UPLC (Dionex) was used to acquire the data. 2 μ l of the sample was resolved on a PepMap RSLC C18 column (75 μ m i.d. x 50 cm; Thermo Scientific) at the flowrate of 300 nl/min using 0.1% formic acid/acetonitrile gradient system (2-22% acetonitrile in 150 min; 22-32% acetonitrile in 40 min; 20 min wash at 90% followed by 50 min re-equilibration) and directly spray onto the mass spectrometer using EasySpray source (Thermo Fisher Scientific). Mass spectrometer was set to collect one MS1 scan (Orbitrap; 120K resolution; AGC target 2x10⁵; max IT 100 ms) followed by data-dependent, “Top Speed” (3 seconds) MS2 scans (collision induced dissociation; ion trap; NCE 35; AGC 5x10³; max IT 100 ms). For multinotch-MS3, top 10 precursors from each MS2 were fragmented by HCD followed by Orbitrap analysis (NCE 55; 60K resolution; AGC 5x10⁴; max IT 120 ms, 100-500 m/z scan range).

Data analysis: Proteome Discoverer (v2.4; Thermo Fisher) was used for data analysis. MS2 spectra were searched against SwissProt human protein database (20353 entries; downloaded on 06/20/2019) using the following search parameters: MS1 and MS2 tolerance were set to 10 ppm and 0.6 Da, respectively; carbamidomethylation of cysteines (57.02146 Da) and TMT labeling of lysine and N-termini of peptides (229.16293 Da) were considered static modifications; oxidation of methionine (15.9949 Da) and deamidation of asparagine and glutamine (0.98401 Da) were considered variable. Identified proteins and peptides were filtered to retain only those that passed $\leq 1\%$ FDR threshold. Quantitation was performed using high-quality MS3 spectra (Average signal-to-noise ratio of 10 and $< 50\%$ isolation interference).

RNA-Seq analysis

RNA samples were collected from each of the four HeLa cell lines: WT, 55KO, 65KO, and DKO. Cells at an exponential growth phase (~ 80% confluency) in 6 well dishes were collected. Five replicates of each cell line were lysed using Trizol. RNA samples were prepared using the Direct-zol™ RNA Miniprep Plus kit and treated with DNase I provided in the same kit. The samples were sent to UMich Advanced Genomic Core for library creation and processing. At the core, after passing quality control for quantity and purity, RNA samples were used to create 3' mRNA libraries using the QuantSeq 3' mRNA-Seq Library Prep Kit FWD for Illumina kit with the UMI add-on kit (Lexogen, Cat # 081.96), which used oligoT priming to generate the first cDNA strand from RNAs with a poly-A tail. Single-read sequencing for the cDNA library was performed on Illumina NextSeq sequencer for 100 cycles. Sequencing results were trimmed using Trim Galore (v 0.5.0). Alignment of reads to human genome GRCh38 from ENSEMBL (<https://useast.ensembl.org/index.html>) was performed in house using STAR (v 2.6.0). Trim_Galore and STAR can be found on https://www.bioinformatics.babraham.ac.uk/projects/trim_galore/ and <https://www.ncbi.nlm.nih.gov/pmc/articles/PMC3530905/>, respectively.

Quantification and statistics

In all figures, the quantification results are expressed as the mean \pm SEM (standard error of the mean) from 3-5 independent experiments, unless otherwise stated. The statistical significance of the results was assessed using Student's *t*-test. *, $p < 0.05$, **, $p < 0.01$, ***, $p < 0.001$.

Supplemental Information

Supplemental Information includes one supplemental figure and six supplemental tables. Supplemental Figure 3.1 shows that GRASP depletion increases HS cell surface staining and re-expression of GRASPs in GRASP KO cells rescue CS levels. Supplemental Table 3.1 and 3.2 are the amount of three types of GAGs from cell lysate and medium samples, respectively. Supplemental Table 3.3 and 3.4 are the amount of HS from the cell lysate and medium samples, respectively. Supplemental Table 3.5 and 3.6 are the amount of CS from the cell lysate and medium samples, respectively.

Acknowledgments

We thank Ge Yu, Judith Meyers Opp and the University of Michigan Advanced Genomics Core for their contribution in the RNA-Seq experiment. We thank Drs. Venkatesha Basrur, Felipe da Veiga Leprevost, Alexey Nesvizhskii and the Mass Spectrometry-Based Proteomics Resource Facility in the Department of Pathology at the University of Michigan for their contribution in Proteomics analysis. We thank the members of the Wang lab and Linhardt lab for stimulating discussions and technical support. This work was supported by the National Institutes of Health (Grant R35GM130331), MCubed, and the Fast Forward Protein Folding Disease Initiative of the University of Michigan to Y. Wang, and a University of Michigan Rackham Predoctoral fellowship to E. Ahat.

Competing Interest

The authors declare that no competing interests exist.

Figures and Figure legends

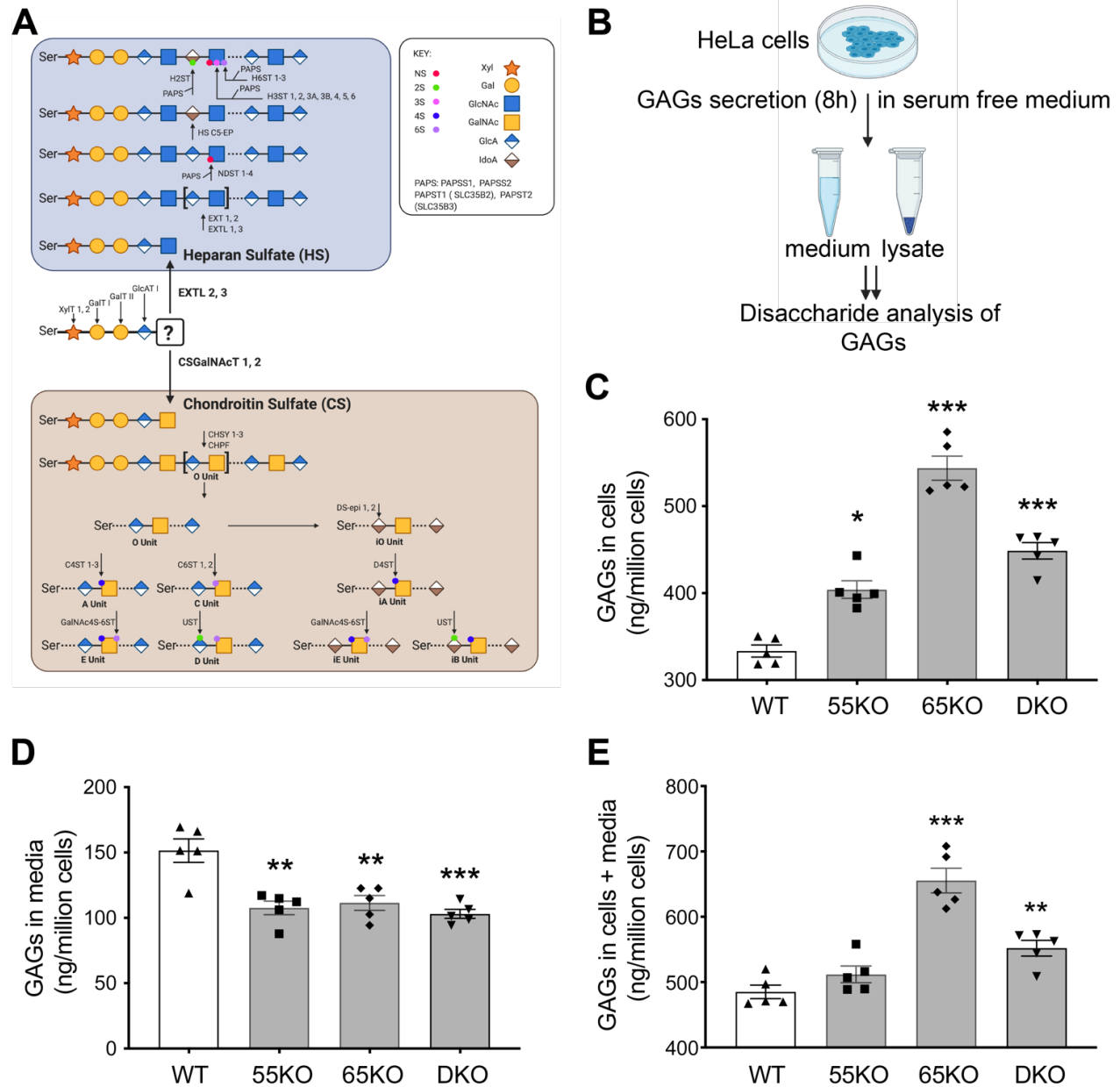


Figure 3.1. Golgi structure disruption by GRASP KO increases GAG synthesis but reduces its secretion.

(A) Schematic diagram illustrating the HS and CS synthesis pathways; major enzymes in each pathway are indicated at their designated steps of reactions. (B) Schematic workflow for cell lysate and medium sample preparation to analyze GAGs by LC-MS. (C) GRASP KO increases

the amount of GAGs in cells. Shown are the amounts of GAGs in the lysates of wildtype (WT), GRASP55 knockout (55KO), GRASP65 knockout (65KO), and GRASP55 and GRASP65 double knockout (DKO) HeLa cells. **(D)** GRASP KO decreases GAG secretion. WT and indicated GRASP KO cells were incubated in serum-free medium for 8 h and GAGs in the conditioned media were analyzed by LC-MS. **(E)** GRASP KO increases the total amount of GAGs in cells and media. Shown are the total amount of GAGs per million cells in both cell lysates and conditioned medium in each cell line. Results are presented as mean \pm SEM, statistical analysis was assessed by comparing KO cells to WT cells by student's t-test. *, $p < 0.05$; **, $p < 0.01$; ***, $p < 0.001$.

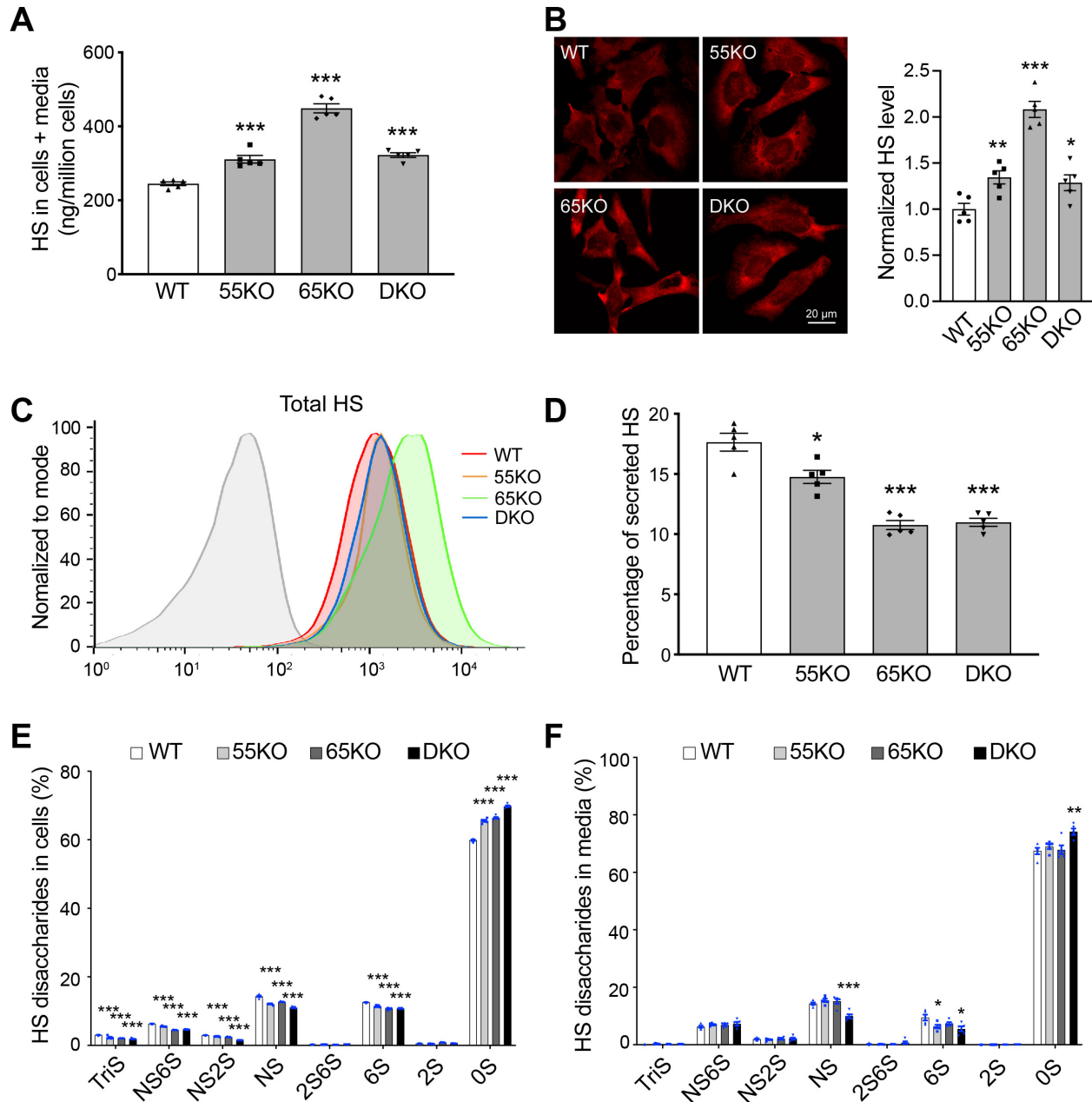


Figure 3.2. GRASP KO increases HS synthesis but reduces its sulfation and secretion.

(A) GRASP KO increases HS synthesis analyzed by LC-MS. Shown are the total amount of HS in both cells and medium of indicated cell lines. (B) GRASP KO increases HS synthesis analyzed by immunofluorescence microscopy. Indicated cells were permeabilized and stained for HS with an HS antibody 10E4. Shown are microscopic images (left) and quantitation (right). (C)

GRASP KO increases HS synthesis analyzed by flow cytometry. Indicated cells were permeabilized, stained for HS with an HS antibody and analyzed by flow cytometry. **(D)** GRASP KO decreases HS secretion. The percentage of secreted HS (HS in media/HS in cell lysate and conditioned media) was analyzed by LC-MS. **(E)** GRASP KO reduces HS sulfation in the cell lysate. Shown are the percentage of each sulfated form of HS in cells. **(F)** GRASP KO reduces HS sulfation in the conditioned media. Shown are the percentage of each sulfated form of HS in the conditioned media.

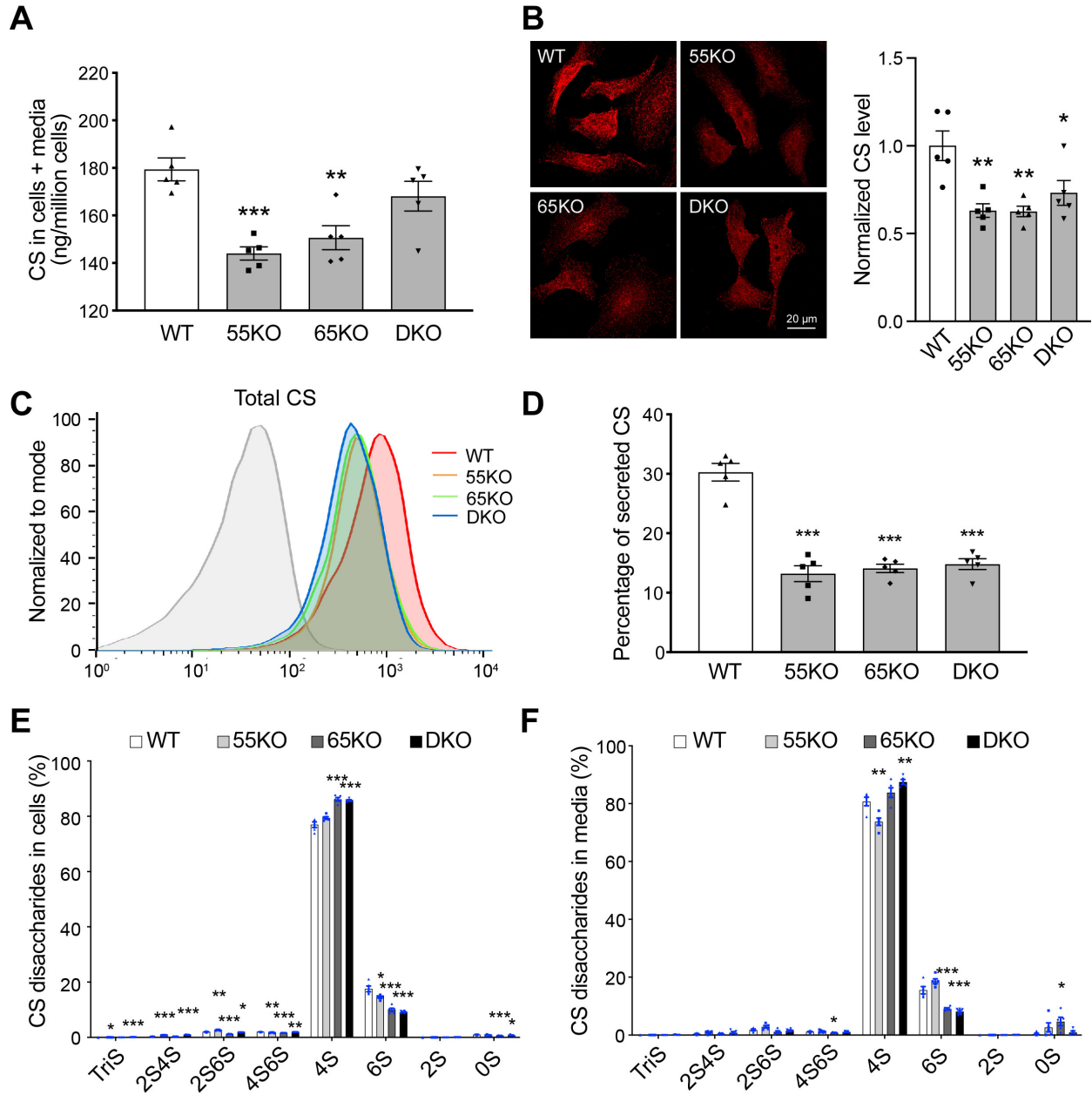


Figure 3.3. GRASP KO reduces CS synthesis and secretion.

(A) GRASP KO reduces CS synthesis analyzed by LC-MS. Shown are the total amount of CS in both cells and medium of indicated cell lines. **(B)** GRASP KO decreases CS synthesis analyzed by immunofluorescence microscopy. Indicated cells were permeabilized and stained for CS with a CS antibody (CS-56). Shown are microscopic images (left) and quantitation (right). **(C)** GRASP KO decreases CS synthesis shown by flow cytometry. Indicated cells were

permeabilized, stained for CS with a CS antibody and analyzed by flow cytometry. **(D)** GRASP KO decreases CS secretion. The percentage of secreted CS (CS in media/HS in cell lysate and conditioned media) was analyzed by LC-MS. **(E)** GRASP KO alters CS sulfation in the cell lysate. Shown are the percentage of each sulfated form of CS in cells. **(F)** GRASP KO alters CS sulfation in the conditioned media. Shown are the percentage of each sulfated form of CS in the conditioned media. Note that GRASP depletion increased 4-sulfation while decreases 6-sulfation in both the cell lysate (E) and conditioned media (F).

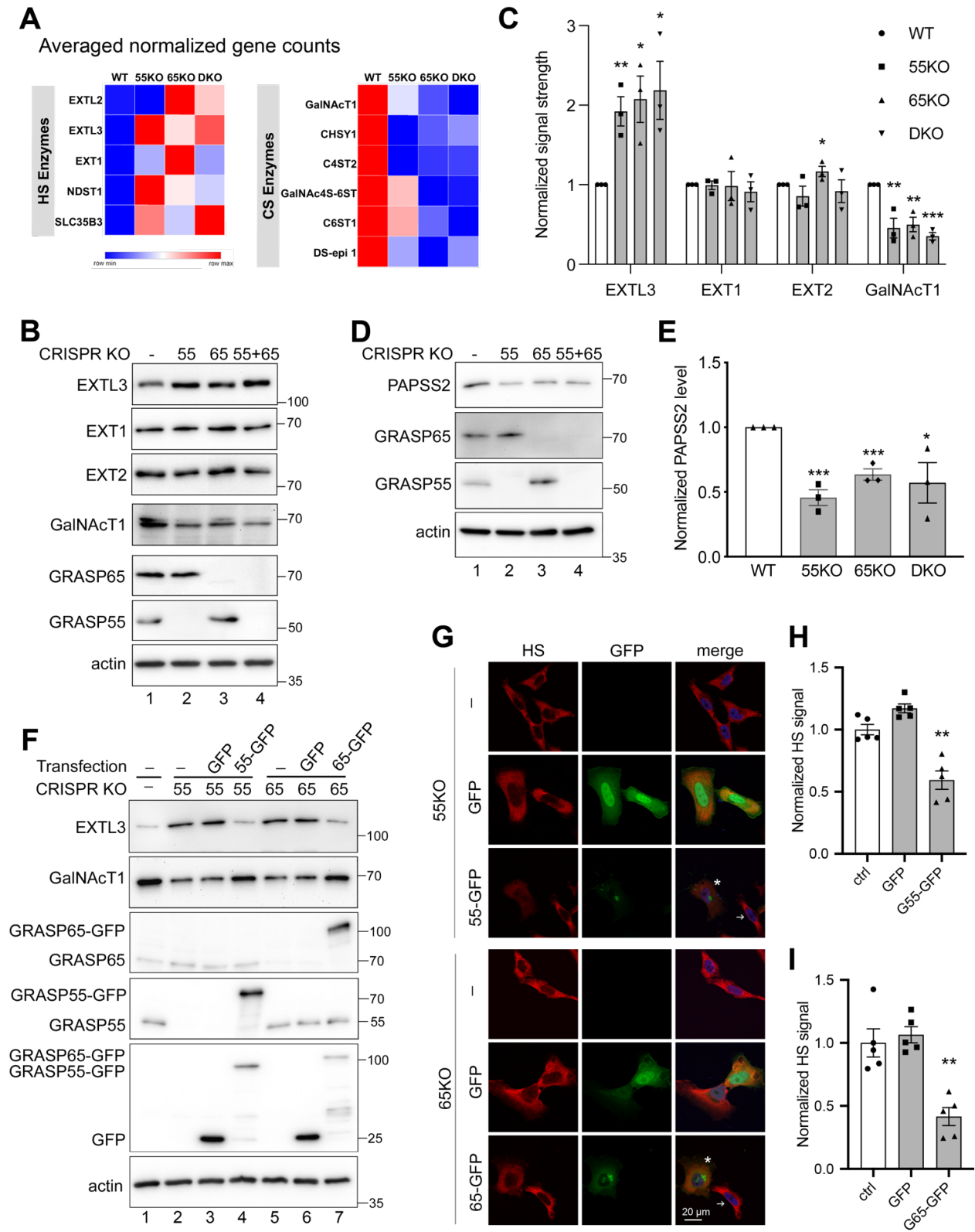


Figure 3.4. GRASP KO alters the expression level of GAG synthesis and sulfation enzymes.

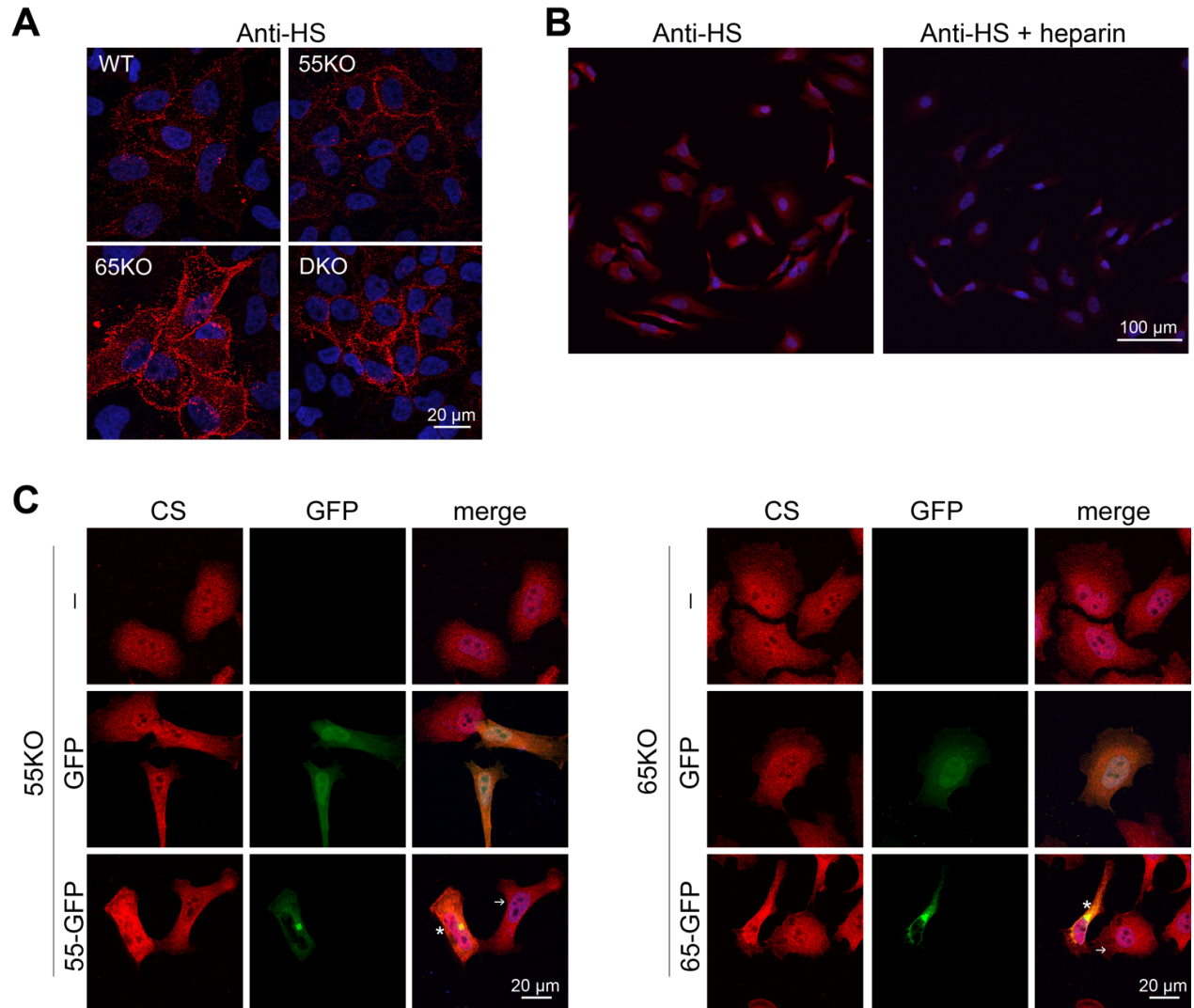
(A) GRASP KO increases the expression of HS synthesis enzymes while decreases CS synthesis enzymes. Results are based on RNA-Seq analysis of each cell line for indicated genes. **(B)** Quantification of C. **(C)** GRASP KO increases the protein level of HS synthesis enzymes while decreases that of CS synthesis enzymes. Cell lysate of indicated cells were analyzed for three HS synthesis enzymes EXTL3, EXT1 and EXT2, and a key CS synthesis enzyme GalNAcT1. Note the increased level of EXTL3 and decreased GalNAcT1 level in GRASP KO cells. Results are representative of three independent experiments. **(D)** GRASP KO decreases the protein level of the HS sulfation enzyme PAPSS2. Shown are representative western blots of indicated proteins in the four cell lines from three independent experiments. **(E)** Quantitation of D. **(F)** Re-expression of GRASP proteins in GRASP KO cells corrects the expression level of HS and CS synthesis enzymes. Indicated cell lines were transfected with GRASP constructs and probed for EXTL3, GalNAcT1, GRASP65, GRASP55, GFP, and actin. The major enzymes EXTL3 and GalNAcT1 in 55KO and 65KO cells were rescued by expressing GRASP55-GFP or GRASP65-GFP, respectively, but not by GFP alone (lanes 4 & 7 vs. 3 & 6). **(G)** Re-expression of GRASP proteins corrects the HS and CS defects in GRASP KO cells. Confocal images of HeLa cells transfected with indicated constructs followed by HS staining. The level of HS in 55KO and 65KO cells was decreased by the expression of GRASP55-GFP or GRASP65-GFP, respectively, but not by GFP alone. Note the different HS signals in cells expressing GRASP55- or GRASP65-GFP (asterisks) vs. non-transfected cells (arrows). **(H-I)** Quantification of G. Results are presented as mean \pm SEM, statistical analysis was assessed by comparing KO cells to WT cells by student's t-test. *, $p < 0.05$; **, $p < 0.01$; ***, $p < 0.001$.

Table 3.1. GRASP KO alters HS and CS synthesis enzymes at both the mRNA and protein levels.

WT and GRASP KO cells were analyzed by proteomic and RNA-seq analyses. Shown are the fold changes of the indicated GAG synthesis enzymes in GRASP KO cells compared to that in WT cells. Enzymes in bold were further tested by Western blot. NA, data not available; ND, not detected.

| Enzymes | Proteomics | | | | RNA-seq | | | | | |
|--------------------------------|------------|-----------|---------|-------------|----------------|-----------|----------------|-----------|---------------|-----------|
| | 55KO/WT | p-value | 65KO/WT | p-value | log2 (55KO/WT) | p-value | log2 (65KO/WT) | p-value | log2 (DKO/WT) | p-value |
| Common Enzymes | | | | | | | | | | |
| XylIT1 | ND | | ND | | -0.009 | NA | 6.511E-04 | NA | -0.007 | NA |
| XylIT2 | ND | | ND | | 0.100 | 0.770 | -0.250 | 0.290 | -0.100 | 0.740 |
| GalT1 (B4GALT7) | ND | | ND | | 0.210 | 0.440 | -0.170 | 0.500 | 0.140 | 0.590 |
| GalIT2 | ND | | ND | | -0.850 | 0.020 | -0.410 | 0.340 | -0.110 | 0.840 |
| GlcAT1 (B3GAT3) | ND | | ND | | -0.370 | 0.210 | -0.110 | 0.750 | 0.020 | 0.960 |
| Enzymes in HS synthesis | | | | | | | | | | |
| EXTL2 | ND | | ND | | -0.170 | 0.420 | 0.320 | 0.030 | 0.090 | 0.670 |
| EXTL3 | ND | | ND | | 0.330 | 0.120 | 0.130 | 0.620 | 0.290 | 0.160 |
| EXTL1 | ND | | ND | | -0.010 | NA | -0.010 | NA | -0.010 | NA |
| EXT1 | ND | | ND | | 0.200 | 0.420 | 0.660 | 3.090E-05 | 0.180 | 0.430 |
| EXT2 | ND | | ND | | -0.080 | 0.790 | -0.100 | 0.690 | -0.230 | 0.240 |
| NDST 1 | ND | | ND | | 0.230 | 0.260 | 0.120 | 0.600 | -0.170 | 0.400 |
| NDST 2 | ND | | ND | | 0.280 | 0.620 | -0.030 | 0.960 | -0.050 | 0.940 |
| NDST 3 | ND | | ND | | -0.210 | 0.700 | -0.460 | 0.200 | 0.100 | 0.850 |
| NDST 4 | ND | | ND | | ND | | ND | | ND | |
| PAPSS 1 | 0.047 | 0.411 | -0.093 | 0.082 | 3.733E-03 | 0.990 | -0.060 | 0.790 | -0.120 | 0.460 |
| PAPSS 2 | -0.825 | 1.854E-05 | -0.873 | 2.289E-06 | -0.910 | 7.920E-10 | -0.690 | 2.269E-06 | -0.690 | 3.599E-06 |
| PAPST 1 (SLC35B2) | -0.141 | 0.034 | -0.069 | 0.256 | -0.120 | 0.750 | 0.380 | 0.080 | 0.400 | 0.060 |
| PAPST 2 (SLC35B3) | ND | | ND | | 0.290 | 0.190 | 0.070 | 0.800 | 0.370 | 0.050 |
| HS C5-EP (HSGLCE) | ND | | ND | | ND | | ND | | ND | |
| H2ST | ND | | ND | | ND | | ND | | ND | |
| H3ST 1 | ND | | ND | | ND | | ND | | ND | |
| H3ST 2 | ND | | ND | | ND | | ND | | ND | |
| H3ST 3A | ND | | ND | | ND | | ND | | ND | |
| H3ST 3B | ND | | ND | | ND | | ND | | ND | |
| H3ST 4 | ND | | ND | | ND | | ND | | ND | |
| H3ST 5 | ND | | ND | | ND | | ND | | ND | |
| H3ST 6 | ND | | ND | | ND | | ND | | ND | |
| H6ST 1 | ND | | ND | | ND | | ND | | ND | |
| H6ST 2 | ND | | ND | | ND | | ND | | ND | |
| H6ST 3 | ND | | ND | | ND | | ND | | ND | |
| Enzymes in CS synthesis | | | | | | | | | | |
| GalNAcT1 (GALNT1) | -0.404 | 8.206E-05 | -0.521 | 1.34308E-05 | -0.521 | 2.856E-09 | -0.884 | 3.668E-26 | -1.135 | 7.254E-42 |
| GalNAcT2 (GALNT2) | -0.095 | 0.094 | 0.096 | 0.111 | -0.140 | 0.480 | 0.290 | 0.040 | -0.290 | 0.040 |
| CHPF2 | 0.159 | 0.368 | 0.197 | 0.227 | 0.040 | 0.950 | -0.050 | 0.910 | 0.200 | 0.540 |
| CHSY1 | ND | | ND | | -0.880 | 8.023E-07 | -0.693 | 9.417E-05 | -0.579 | 1.442E-03 |
| CHSY2 | ND | | ND | | NA | | NA | | NA | |
| CHSY3 | ND | | ND | | -0.110 | 0.790 | 0.050 | 0.900 | 0.110 | 0.740 |
| C4ST 1 (CHST11) | ND | | ND | | -0.184 | 0.472 | 0.163 | 0.461 | -0.177 | 0.424 |
| C4ST 2 (CHST12) | ND | | ND | | -0.092 | 0.732 | -0.022 | 0.935 | -0.026 | 0.925 |
| C4ST 3 (CHST13) | ND | | ND | | -0.270 | 0.635 | 0.480 | 0.240 | 0.903 | 0.008 |
| GalNAc4S-6ST (CHST15) | ND | | ND | | -0.083 | 0.866 | -0.734 | 0.003 | -0.678 | 0.007 |
| C6ST 1 (CHST3) | ND | | ND | | -0.242 | 0.471 | -0.641 | 0.005 | -0.839 | 1.600E-04 |
| C6ST 2 (CHST4) | ND | | ND | | 0 | NA | 0 | NA | 0.013 | NA |
| UST | ND | | ND | | ND | | ND | | ND | |
| DS-epi 1 (DSE) | ND | | ND | | -0.715 | 6.146E-10 | -1.274 | 3.265E-28 | -0.788 | 7.330E-12 |
| DS-epi 2 (DSEL) | ND | | ND | | 0.721 | 8.811E-05 | 0.505 | 8.939E-03 | -0.001 | 9.967E-01 |
| D4ST | ND | | ND | | ND | | ND | | ND | |
| Enzymes in HA synthesis | | | | | | | | | | |
| HAS1 | ND | | ND | | -0.009 | NA | -0.009 | NA | -0.007 | NA |
| HAS2 | ND | | ND | | 0.131 | 0.850 | 0.088 | 0.888 | 0.390 | 0.356 |
| HAS3 | ND | | ND | | 0.009 | 0.992 | -0.132 | 0.819 | 0.066 | 0.915 |

Supplemental information



Supplemental Figure 3.1. GRASP KO increases HS level at the cell surface and GRASP re-expression rescues CS defects in GRASP KO cells.

(A) GRASP KO increases HS level at the cell surface. Confocal images of indicated cell lines stained with an anti-HS antibody (10E4) without permeabilization. (B) The HS signal of the anti-HS antibody is specific. Permeabilized WT cells were stained with the anti-HS antibody (left panel) or with the anti-HS antibody preincubated with excess amount of heparin (right) before imaging. (C) Rescue of the Golgi structure by GRASP re-expression corrects the CS defects in

GRASP KO cells. Confocal images of 55KO or 65KO cells transfected with indicated constructs and stained for CS with the CS-56 antibody. Scale bars in all panels, 20 μm .

Supplemental Table 3.1. The amount of three kinds of GAG from cell samples.

Cell lysate from indicated cells were analyzed for total GAGs by LC-MS, results are normalized to one million cells. Five technical replicates are shown for each cell line.

| Sample | | Total cell number (million) | Amount of GAG (ng) per million cells | Amount of each kind of GAG (ng) per million cells | | |
|--------|---|-----------------------------|--------------------------------------|---|--------|-------|
| | | | | HS | CS | HA |
| WT | 1 | 7.8 | 319.21 | 194.28 | 118.17 | 6.76 |
| | 2 | 7.5 | 330.74 | 202.97 | 121.16 | 6.61 |
| | 3 | 8.0 | 350.40 | 208.69 | 134.50 | 7.21 |
| | 4 | 8.5 | 348.29 | 209.07 | 131.77 | 7.45 |
| | 5 | 7.8 | 318.55 | 192.44 | 119.37 | 6.74 |
| G55KO | 1 | 13.0 | 383.04 | 251.87 | 117.20 | 13.97 |
| | 2 | 12.5 | 400.88 | 260.51 | 126.35 | 14.02 |
| | 3 | 12.1 | 394.46 | 256.32 | 123.61 | 14.53 |
| | 4 | 11.9 | 443.26 | 292.82 | 135.39 | 15.06 |
| | 5 | 12.0 | 399.19 | 263.36 | 122.38 | 13.45 |
| G65KO | 1 | 12.2 | 524.01 | 388.18 | 122.26 | 13.57 |
| | 2 | 10.5 | 585.35 | 425.57 | 144.65 | 15.12 |
| | 3 | 11.7 | 522.45 | 381.23 | 127.40 | 13.81 |
| | 4 | 10.9 | 569.16 | 426.28 | 128.02 | 14.85 |
| | 5 | 11.7 | 517.92 | 379.43 | 124.36 | 14.13 |
| DKO | 1 | 12.5 | 464.67 | 295.77 | 149.16 | 19.74 |
| | 2 | 12.9 | 442.95 | 286.77 | 138.89 | 17.29 |
| | 3 | 12.6 | 458.21 | 293.83 | 146.51 | 17.87 |
| | 4 | 13.4 | 463.56 | 290.90 | 152.24 | 20.41 |
| | 5 | 14.0 | 414.50 | 267.46 | 128.44 | 18.59 |

Supplemental Table 3.2. The amount of three kinds of GAG from medium samples.

Conditioned media from indicated cells were analyzed for total GAGs by LC-MS. Five technical replicates are shown for each cell line. GAG amounts per million cells were calculated and shown in Figure 3.1D.

| Sample | | Total cell number (million) | Total amount of GAG in the medium (ng) | Amount of each kind of GAG (ng) | | |
|---------|---|-----------------------------|--|---------------------------------|--------|--------|
| | | | | HS | CS | HA |
| WT-M | 1 | 7.8 | 1182.12 | 267.40 | 436.71 | 478.01 |
| | 2 | 7.5 | 1246.76 | 362.17 | 448.02 | 436.57 |
| | 3 | 8.0 | 1356.15 | 368.26 | 502.05 | 485.84 |
| | 4 | 8.5 | 1011.04 | 370.29 | 369.62 | 271.13 |
| | 5 | 7.8 | 1179.66 | 345.07 | 390.76 | 443.83 |
| G55KO-M | 1 | 13.0 | 1381.84 | 540.55 | 256.11 | 585.18 |
| | 2 | 12.5 | 1098.50 | 493.11 | 157.56 | 447.83 |
| | 3 | 12.1 | 1358.76 | 545.61 | 262.69 | 550.46 |
| | 4 | 11.9 | 1366.89 | 684.66 | 203.67 | 478.55 |
| | 5 | 12.0 | 1405.03 | 561.53 | 288.87 | 554.62 |
| G65KO-M | 1 | 12.2 | 1251.66 | 537.08 | 235.84 | 478.73 |
| | 2 | 10.5 | 1288.60 | 584.23 | 253.50 | 450.86 |
| | 3 | 11.7 | 1345.90 | 597.45 | 276.86 | 471.59 |
| | 4 | 10.9 | 1337.10 | 532.68 | 250.96 | 553.46 |
| | 5 | 11.7 | 1104.74 | 491.10 | 190.63 | 423.01 |
| DKO-M | 1 | 12.5 | 1332.16 | 492.36 | 320.53 | 519.27 |
| | 2 | 12.9 | 1308.39 | 459.76 | 337.71 | 510.92 |
| | 3 | 12.6 | 1441.38 | 489.11 | 374.16 | 578.11 |
| | 4 | 13.4 | 1323.26 | 431.75 | 366.56 | 524.95 |
| | 5 | 14.0 | 1320.19 | 439.70 | 232.61 | 647.88 |

Supplemental Table 3.3. The percentage of each detected HS disaccharide from cell samples.

Cell lysate from indicated cells were analyzed for HS by LC-MS, results are normalized to one million cells. Five technical replicates are shown for each cell line.

| Sample | HS disaccharides (%) | | | | | | | | |
|--------|----------------------|------|------|------|-------|------|-------|------|-------|
| | TriS | NS6S | NS2S | NS | 2S6S | 6S | 2S | 0S | |
| WT | 1 | 3.06 | 6.37 | 3.02 | 14.31 | 0.28 | 12.72 | 0.66 | 59.57 |
| | 2 | 3.11 | 6.36 | 3.09 | 13.55 | 0.28 | 12.63 | 0.67 | 60.30 |
| | 3 | 3.13 | 6.30 | 2.89 | 14.33 | 0.29 | 12.39 | 0.39 | 60.28 |
| | 4 | 2.84 | 6.21 | 2.91 | 14.33 | 0.29 | 12.52 | 0.64 | 60.28 |
| | 5 | 3.04 | 6.36 | 3.03 | 15.03 | 0.30 | 12.61 | 0.43 | 59.20 |
| G55KO | 1 | 2.11 | 5.50 | 2.46 | 11.68 | 0.23 | 11.22 | 0.35 | 66.45 |
| | 2 | 2.39 | 5.82 | 2.70 | 12.09 | 0.26 | 11.67 | 0.46 | 64.62 |
| | 3 | 2.02 | 5.52 | 2.64 | 12.21 | 0.19 | 11.76 | 0.42 | 65.24 |
| | 4 | 2.03 | 5.51 | 2.57 | 12.16 | 0.25 | 11.26 | 0.53 | 65.69 |
| | 5 | 2.05 | 5.46 | 2.68 | 12.21 | 0.22 | 11.17 | 0.43 | 65.79 |
| G65KO | 1 | 2.14 | 4.64 | 2.61 | 12.77 | 0.23 | 10.83 | 0.83 | 65.97 |
| | 2 | 2.03 | 4.46 | 2.48 | 12.62 | 0.23 | 11.05 | 0.95 | 66.19 |
| | 3 | 2.18 | 4.50 | 2.44 | 12.61 | 0.23 | 10.86 | 0.76 | 66.41 |
| | 4 | 2.05 | 4.40 | 2.30 | 12.56 | 0.23 | 10.08 | 1.01 | 67.38 |
| | 5 | 2.16 | 4.55 | 2.41 | 12.94 | 0.25 | 10.65 | 0.80 | 66.24 |
| DKO | 1 | 1.72 | 4.50 | 1.51 | 11.15 | 0.24 | 10.71 | 0.51 | 69.65 |
| | 2 | 1.81 | 4.63 | 1.46 | 10.94 | 0.26 | 10.66 | 0.52 | 69.73 |
| | 3 | 1.72 | 4.68 | 1.42 | 11.31 | 0.24 | 10.84 | 0.63 | 69.16 |
| | 4 | 1.75 | 4.60 | 1.46 | 10.89 | 0.24 | 10.89 | 0.43 | 69.74 |
| | 5 | 1.50 | 4.51 | 1.41 | 10.65 | 0.24 | 10.49 | 0.51 | 70.69 |

Supplemental Table 3.4. The percentage of each detected HS disaccharide from medium samples.

Conditioned media from indicated cells were analyzed for HS by LC-MS. Five technical replicates are shown for each cell line.

| Sample | HS disaccharides (%) | | | | | | | | |
|---------|----------------------|------|------|------|-------|------|-------|------|-------|
| | TriS | NS6S | NS2S | NS | 2S6S | 6S | 2S | 0S | |
| WT-M | 1 | 0.17 | 5.91 | 2.62 | 14.48 | 0.66 | 7.68 | 0.14 | 68.35 |
| | 2 | 0.19 | 6.55 | 2.20 | 15.61 | 0.10 | 7.13 | 0.01 | 68.21 |
| | 3 | 0.19 | 6.22 | 1.52 | 13.04 | 0.20 | 11.53 | 0.01 | 67.30 |
| | 4 | 0.11 | 5.38 | 1.54 | 13.96 | 0.00 | 8.87 | 0.15 | 69.98 |
| | 5 | 0.25 | 7.51 | 1.97 | 14.62 | 0.12 | 12.16 | 0.01 | 63.36 |
| G55KO-M | 1 | 0.33 | 7.29 | 1.76 | 15.27 | 0.08 | 4.68 | 0.00 | 70.58 |
| | 2 | 0.17 | 6.97 | 1.17 | 17.13 | 0.17 | 6.02 | 0.00 | 68.37 |
| | 3 | 0.32 | 6.46 | 2.14 | 14.95 | 0.27 | 5.77 | 0.07 | 70.02 |
| | 4 | 0.51 | 6.80 | 1.93 | 16.23 | 0.17 | 8.39 | 0.00 | 65.98 |
| | 5 | 0.18 | 7.61 | 1.78 | 13.62 | 0.09 | 6.84 | 0.00 | 69.89 |
| G65KO-M | 1 | 0.37 | 7.50 | 2.50 | 15.82 | 0.19 | 6.45 | 0.00 | 67.15 |
| | 2 | 0.36 | 7.60 | 1.46 | 15.20 | 0.28 | 9.28 | 0.18 | 65.62 |
| | 3 | 0.30 | 7.47 | 2.84 | 16.26 | 0.33 | 7.28 | 0.11 | 65.40 |
| | 4 | 0.00 | 5.94 | 1.71 | 11.87 | 0.14 | 6.57 | 0.00 | 73.76 |
| | 5 | 0.17 | 6.33 | 2.15 | 16.54 | 0.19 | 7.23 | 0.00 | 67.39 |
| DKO-M | 1 | 0.19 | 6.42 | 3.39 | 10.37 | 0.60 | 3.21 | 0.01 | 75.82 |
| | 2 | 0.00 | 5.37 | 1.84 | 8.90 | 0.29 | 6.48 | 0.00 | 77.12 |
| | 3 | 0.17 | 9.08 | 2.17 | 8.40 | 2.42 | 3.77 | 0.01 | 73.98 |
| | 4 | 0.23 | 7.99 | 1.07 | 9.64 | 0.21 | 7.99 | 0.00 | 72.86 |
| | 5 | 0.27 | 7.70 | 2.00 | 12.44 | 0.30 | 6.26 | 0.00 | 71.02 |

Supplemental Table 3.5. The percentage of each detected CS disaccharide from cell samples.

Cell lysate from indicated cells were analyzed for CS by LC-MS, results are normalized to one million cells. Five technical replicates are shown for each cell line.

| Sample | CS disaccharides (%) | | | | | | | | |
|--------|----------------------|------|------|------|------|-------|-------|------|------|
| | TriS | 2S4S | 2S6S | 4S6S | 4S | 6S | 2S | 0S | |
| WT | 1 | 0.03 | 0.30 | 2.31 | 2.05 | 75.28 | 18.87 | 0.00 | 1.14 |
| | 2 | 0.01 | 0.38 | 2.09 | 1.97 | 78.45 | 16.10 | 0.00 | 1.00 |
| | 3 | 0.02 | 0.37 | 2.05 | 1.90 | 78.87 | 15.76 | 0.00 | 1.03 |
| | 4 | 0.02 | 0.38 | 1.73 | 2.12 | 78.49 | 16.13 | 0.00 | 1.13 |
| | 5 | 0.02 | 0.24 | 1.92 | 2.06 | 73.82 | 21.10 | 0.00 | 0.84 |
| G55KO | 1 | 0.13 | 0.76 | 2.38 | 1.65 | 81.11 | 13.32 | 0.00 | 0.66 |
| | 2 | 0.04 | 0.80 | 2.80 | 1.87 | 78.89 | 14.84 | 0.00 | 0.75 |
| | 3 | 0.05 | 0.77 | 2.75 | 1.78 | 78.35 | 15.44 | 0.00 | 0.86 |
| | 4 | 0.04 | 0.83 | 2.49 | 1.54 | 79.13 | 14.87 | 0.00 | 1.11 |
| | 5 | 0.07 | 0.81 | 2.68 | 1.87 | 79.58 | 14.22 | 0.00 | 0.77 |
| G65KO | 1 | 0.01 | 0.38 | 1.13 | 1.72 | 87.58 | 8.63 | 0.00 | 0.55 |
| | 2 | 0.01 | 0.23 | 1.25 | 1.70 | 85.73 | 10.32 | 0.00 | 0.76 |
| | 3 | 0.02 | 0.31 | 1.36 | 1.59 | 84.01 | 11.98 | 0.00 | 0.72 |
| | 4 | 0.01 | 0.38 | 1.29 | 1.63 | 87.37 | 8.71 | 0.00 | 0.60 |
| | 5 | 0.04 | 0.36 | 1.12 | 1.64 | 86.05 | 10.16 | 0.00 | 0.64 |
| DKO | 1 | 0.08 | 0.97 | 1.74 | 1.87 | 84.94 | 9.65 | 0.00 | 0.75 |
| | 2 | 0.05 | 0.73 | 1.73 | 1.76 | 86.61 | 8.71 | 0.00 | 0.40 |
| | 3 | 0.04 | 0.85 | 1.76 | 1.88 | 85.79 | 9.06 | 0.00 | 0.63 |
| | 4 | 0.07 | 0.79 | 1.70 | 1.87 | 85.39 | 9.53 | 0.00 | 0.66 |
| | 5 | 0.08 | 0.90 | 1.77 | 1.90 | 85.56 | 8.76 | 0.00 | 1.03 |

Supplemental Table 3.6. The percentage of each detected CS disaccharide from medium samples.

Conditioned media from indicated cells were analyzed for CS by LC-MS. Five technical replicates are shown for each cell line.

| Sample | CS disaccharides (%) | | | | | | | | |
|---------|----------------------|------|------|------|------|-------|-------|------|------|
| | TriS | 2S4S | 2S6S | 4S6S | 4S | 6S | 2S | 0S | |
| WT-M | 1 | 0.12 | 0.00 | 2.22 | 0.78 | 75.42 | 20.04 | 0.01 | 1.40 |
| | 2 | 0.00 | 0.78 | 0.94 | 1.28 | 83.32 | 13.68 | 0.01 | 0.00 |
| | 3 | 0.00 | 0.35 | 1.00 | 0.96 | 82.93 | 14.40 | 0.00 | 0.36 |
| | 4 | 0.00 | 0.71 | 2.56 | 1.29 | 82.27 | 13.16 | 0.01 | 0.00 |
| | 5 | 0.00 | 0.22 | 2.19 | 1.63 | 79.71 | 16.25 | 0.01 | 0.00 |
| G55KO-M | 1 | 0.00 | 1.09 | 2.64 | 1.90 | 77.56 | 16.53 | 0.01 | 0.27 |
| | 2 | 0.00 | 1.31 | 2.15 | 1.09 | 73.76 | 21.66 | 0.01 | 0.00 |
| | 3 | 0.00 | 1.27 | 1.85 | 0.90 | 69.86 | 17.63 | 0.01 | 8.49 |
| | 4 | 0.00 | 0.60 | 3.36 | 0.87 | 74.88 | 18.56 | 0.01 | 1.72 |
| | 5 | 0.00 | 0.00 | 4.22 | 1.62 | 72.77 | 18.60 | 0.01 | 2.79 |
| G65KO-M | 1 | 0.00 | 0.35 | 2.40 | 0.71 | 78.54 | 8.66 | 0.01 | 9.33 |
| | 2 | 0.00 | 0.41 | 1.01 | 0.67 | 86.18 | 9.38 | 0.01 | 2.34 |
| | 3 | 0.00 | 0.72 | 0.97 | 0.76 | 88.41 | 8.36 | 0.01 | 0.77 |
| | 4 | 0.00 | 0.25 | 0.86 | 1.03 | 83.47 | 8.69 | 0.01 | 5.69 |
| | 5 | 0.00 | 0.73 | 0.35 | 0.90 | 82.55 | 10.16 | 0.01 | 5.30 |
| DKO-M | 1 | 0.00 | 1.36 | 1.81 | 0.67 | 87.24 | 8.91 | 0.01 | 0.00 |
| | 2 | 0.17 | 0.10 | 0.94 | 1.44 | 90.08 | 6.72 | 0.01 | 0.54 |
| | 3 | 0.00 | 0.14 | 1.51 | 0.70 | 86.15 | 8.96 | 0.01 | 2.53 |
| | 4 | 0.00 | 0.77 | 1.10 | 1.31 | 88.57 | 6.86 | 0.01 | 1.38 |
| | 5 | 0.00 | 1.94 | 2.29 | 1.06 | 85.54 | 9.02 | 0.01 | 0.14 |

Chapter 4 GRASP55 Regulates Mutant Huntingtin Unconventional Secretion and Aggregation

Abstract

Recent studies demonstrated that the Golgi stacking proteins, GRASPs, especially GRASP55, regulate Golgi-independent unconventional secretion, but the underlying mechanism remains unknown. Here, we used mutant huntingtin (Htt-Q74) as a model system to address this question. Our results demonstrate that Htt secretion is GRASP55- and autophagy-dependent, and is enhanced under stress conditions such as starvation and ER stress. Mechanistically, GRASP55 facilitates Htt secretion by tethering autophagosomes to lysosomes to promote autophagosome maturation and by stabilizing p23/TMED10, a channel for translocation of cytoplasmic proteins into the ERGIC lumen. Moreover, GRASP55 level is upregulated by various stresses to facilitate unconventional secretion, while inhibition of Htt-Q74 secretion by GRASP55 knockout enhances Htt aggregation and toxicity. Lastly, comprehensive secretomic analysis identified novel cargoes secreted by the same unconventional pathway, such as TAGLN, PAICS and PRDX1. This study provides important information on the role of GRASP55 in unconventional protein secretion and Huntington's disease progression.

Introduction

Neurodegenerative diseases are characterized by increased neuronal cell death and decreased cognitive abilities of patients. Different diseases, such as Alzheimer's disease (AD), Parkinson's disease (PD), Huntington's disease (HD) and Amyotrophic lateral sclerosis (ALS), are caused by different protein-based aberrations that affect different pathways; yet all cause neuronal cell death by forming inclusion bodies (Lee et al., 2005, Umeda et al., 2014, Arrasate and Finkbeiner, 2012). These include protein aggregates formed by hyperphosphorylated tau in AD (Umeda et al., 2014), mutant superoxide dismutase 1 (SOD1) (Dangoumau et al., 2014) and TAR DNA binding protein TDP43 in ALS (Johnson et al., 2009), and mutant huntingtin (Htt) in HD (Bates et al., 2015, Saudou and Humbert, 2016). Many of these neurotoxic proteins have been detected in the cerebrospinal fluid (CSF) of disease patients, indicating that these proteins could be secreted from cells (Wild et al., 2015, Mecocci et al., 1998, Winer et al., 2013). How the secretion affects protein aggregation and toxicity in neurons, and whether secretion facilitates the spreading of toxic proteins to neighboring cells, remain elusive.

In the conventional secretory pathway, transmembrane and secretory proteins, such as the amyloid precursor protein (APP), are synthesized by the endoplasmic reticulum (ER) and transported to the Golgi, from where they are targeted to their final destinations. However, many neurotoxic proteins, such as Htt, SOD1, α -synuclein, tau, and TDP-43, are synthesized as cytosolic proteins. Secretion of these proteins is independent of the traditional secretory pathway in which the Golgi functions as a trafficking center. For example, mutant Htt exists in two forms,

an intracellular form in patient neurons, and an extracellular form in CSF (Wild et al., 2015) exported through a not well characterized secretory pathway (Trajkovic et al., 2017, Caron et al., 2021).

Little is known about the machinery that controls unconventional secretion, and the interplay between Golgi-dependent conventional trafficking and Golgi-independent unconventional secretion has not been explored. Although the unconventional pathway is independent of the Golgi, unconventional secretion of numerous cytosolic proteins reported so far requires the Golgi reassembly stacking protein of 55 kDa (GRASP55) (Lee et al., 2016, Rabouille and Linstedt, 2016, Villeneuve et al., 2018). GRASP55, and its homolog GRASP65, were first characterized as key Golgi stacking proteins (Barr et al., 1997, Wang et al., 2003). They both form *trans*-oligomers to link the Golgi cisternae into the unique stacked architecture (Xiang and Wang, 2010). Knockdown (KD) of GRASP55 and GRASP65 by RNAi, or knockout (KO) of both GRASPs by CRISPR/cas9, results in Golgi fragmentation (Xiang and Wang, 2010, Bekier et al., 2017). GRASPs were first linked to unconventional secretion of Acyl-CoA binding protein (AcbA/Acb1) in *Dictyostelium discoideum* and *Saccharomyces cerevisiae* (Duran et al., 2010, Kinseth et al., 2007). In *Drosophila*, the sole GRASP protein is involved in unconventional trafficking of α -integrin at specific stages of fly development (Schotman et al., 2008). In mammalian cells, GRASPs are required for unconventional trafficking of Cystic Fibrosis Transmembrane Conductance Regulator (CFTR) and the cytokine IL-1 β (Gee et al., 2011, Dupont et al., 2011). How GRASP55 regulates autophagosome-dependent unconventional

secretion, and whether GRASP55 is required for secretion of neurotoxic proteins such as Htt, are unknown.

In this study, we report that mutant Htt is unconventionally secreted in a GRASP55-dependent manner. Htt secretion is elevated under stress conditions, including energy deprivation and nutrient starvation, inhibition of proteasomal degradation, and induction of ER stress, which also upregulate GRASP55 expression. GRASP55 facilitates Htt secretion through two actions, one is to accelerate autophagic flux by facilitating autophagosome and lysosome fusion, the other is to stabilize p23/TMED10, a protein channel in the ER-Golgi-intermediate compartment (ERGIC) that translocates cytosolic proteins into the ERGIC lumen for unconventional secretion. Lastly, we performed systematic proteomic and secretomic analysis of wild-type (WT) and GRASP55 KO (55KO) cells and identified a list of cytoplasmic proteins whose secretion depends on GRASP55.

Results

4.1 GRASP55 is required for unconventional secretion of mutant Htt.

To determine if GRASP55 is required for the secretion of cytosolic proteins related to neurodegeneration, we expressed a number of neurotoxic proteins, including Htt exon 1 fragment with a long polyglutamine (Q74) stretch (GFP-Htt-Q74), WT SOD1 (GFP-SOD1), TDP43 (TDP43-GFP), and Tau (Flag-Tau), in WT and 55KO HeLa cells established earlier (Bekier et

al., 2017). For Htt, we chose the Htt exon 1 fragment because it has been shown that this fragment is harder to degrade, more toxic than full-length Htt, and detected in the CSF with an elevated concentration in HD (Sathasivam et al., 2013, Chen and Wolynes, 2017, Fodale et al., 2017, Gerson et al., 2020). At 48 h post transfection, we cultured the cells in a serum-free medium for 4 h and determined the level of the corresponding cargo in the conditioned media by western blot. A conventional secretory pathway cargo, clusterin, was used as a control. All these proteins were found in the conditioned media (Supplemental Figure 4.1A-D), but Htt-Q74 secretion was the most robust and GRASP55 dependent (Supplemental Figure 4.1A). Therefore, we used GFP-Htt-Q74 as a main marker to study the mechanism of GRASP55-dependent unconventional secretion.

Since both GRASP55 and GRASP65 have been shown to be involved in unconventional secretion (Kim et al., 2016), we expressed GFP-Htt-Q74 in WT, 55KO, 65KO or DKO (double KO of both GRASP55 and GRASP65) HeLa cells. In this experiment GFP-Htt-Q74 expression did not cause cell death. At 48 h post transfection, about 90-95% cells contained soluble Htt in the cytosol, as indicated by the diffused GFP signal. Another 5-10% of cells contained Htt aggregates that appeared as bright dots in the cytoplasm (Figure 4.1A). Interestingly, these Htt aggregates were often found in the perinuclear region where the Golgi was localized. This prompted us to look at the effect of Htt expression on the Golgi morphology. While soluble Htt did not seem to affect Golgi morphology, Htt aggregates induced Golgi defects as previously reported (Sbodio et al., 2018, Brandstaetter et al., 2014), and the effect was more robust in 55KO

cells (Figure 4.1A). For comparison, we also tested GFP-Htt-Q23 in parallel, which did not form aggregates or significantly affect the Golgi morphology (Supplemental Figure 4.1E). Similarly, expression of SOD1, TDP43 or Tau in WT cells had no significant impact on the Golgi structure (Supplemental Figure 4.1F).

Next, we tested whether Htt secretion is GRASP dependent. After transfection of GFP-Htt-Q74 in WT, 55KO, 65KO and DKO cells for 24 h, we cultured the cells in a serum-free medium for 4 h and determined the level of Htt in the conditioned media by western blot. Htt was readily detectable in the conditioned media, and the level was significantly reduced in 55KO but not 65KO cells (Figure 4.1B-C), indicating that Htt secretion depends on GRASP55 but not GRASP65. In this assay, actin was not detected in the conditioned media, indicating that Htt was secreted rather than non-selectively released from dead cells, while the secretion and processing of clusterin, a cargo molecule secreted by the conventional secretory pathway, were not affected by GRASP KO. Taken together, GFP-Htt-Q74 expression causes Golgi defects especially in 55KO cells, while 55KO reduces GFP-Htt-Q74 secretion.

4.2 Mutant Htt is selectively secreted through a Golgi-independent pathway.

To confirm that Htt is secreted through an unconventional Golgi-independent pathway, we blocked ER-to-Golgi trafficking by brefeldin A (BFA) treatment. As shown in Figure 4.1D-E, BFA treatment diminished clusterin in the conditioned media, indicating a block of

conventional secretion. Htt secretion was unaffected by BFA treatment, confirming that it is secreted via a Golgi-independent unconventional secretory pathway.

The toxicity of Htt is associated with the length of the polyQ track within the exon 1 fragment; Htt with more than ~35 glutamines in the stretch is regarded as a disease mutant (Bates et al., 2015, Saudou and Humbert, 2016). To determine whether the length of the polyQ track affects Htt secretion, we co-expressed GFP-Htt-Q74 and GFP-Htt-Q23 in the same cells and compared their secretion. As shown in Figure 4.1F, when GFP-Htt-Q74 and GFP-Htt-Q23 were co-expressed, the level of GFP-Htt-Q74 in the conditioned media was higher than that of GFP-Htt-Q23.

Interestingly, Htt exhibited two bands, and only the lower band was detected in the conditioned media; we were curious about the difference between the two bands. Htt is highly modified by post-translational modifications such as phosphorylation, acetylation, and cleavage (Arbez et al., 2017). Among these, phosphorylation at S13 and S16 by TANK-Binding Kinase 1 (TBK1) or I κ B kinase (IKK) has been shown to reduce Htt aggregation and toxicity (Thompson et al., 2009, Hegde et al., 2020). To determine whether the two bands represent different phosphorylation forms of Htt, we treated cells with a general serine/threonine kinase inhibitor, staurosporine (STS), or a general phosphatase inhibitor, okadaic acid (OA). STS treatment increased the intensity of the lower band, while OA treatment accumulated the upper band, suggesting that the upper band represents a phosphorylated form while the lower band is

dephosphorylated. This conclusion was confirmed using a phospho-specific antibody pS13 for Htt (Hegde et al., 2020), which recognized only the upper band (Figure 4.1H-I). More importantly, STS treatment increased Htt secretion, whereas OA treatment reduced its secretion (Figure 4.1J-K), indicating that the dephosphorylated, aggregate-prone form of Htt is preferentially secreted compared to the phosphorylated, soluble form of Htt. Taken together, these results demonstrate that unconventional secretion is selective, at least to a certain degree, and may serve as a clearing mechanism for cells to expel toxic proteins.

4.3 GFP-Htt-Q74 secretion is enhanced by cellular stress.

It has been demonstrated that unconventional secretion is elevated under different stress conditions when the autophagy level is high (Giuliani et al., 2011), and that unconventional secretion of CFTR and Acb1 depends on autophagy or autophagy genes (Noh et al., 2018, Bruns et al., 2011). In addition, we discovered that GRASP55 functions as an energy sensor through O-GlcNAcylation to regulate autophagosome maturation. Under growth conditions, GRASP55 is O-GlcNAcylated and concentrated on the Golgi. Upon glucose starvation, GRASP55 is de-O-GlcNAcylated and relocated from the Golgi to the interface between autophagosomes and lysosomes, where it interacts with LC3 on autophagosomes and LAMP2 on lysosomes and functions as a membrane tether to facilitate autophagosome-lysosome fusion (Zhang et al., 2018). Similar responses of GRASP55 occur under amino acid starvation (Zhang et al., 2019c). In addition, GRASP55 also interacts with Beclin-1 to facilitate the assembly and membrane

association of the UVRAG phosphatidylinositol 3-kinase (PtdIns3K) complex, and thereby facilitates autophagosome maturation (Zhang et al., 2019c).

These observations prompted us to test the effect of energy deprivation and nutrient starvation on Htt secretion. As expected, both glucose starvation (GS) and amino acid deprivation [E, by incubating cells in Earle's Balanced Salt Solution (EBSS)] increased the level of Htt in the conditioned media compared to DMEM (D) (Figure 4.2A-B). A similar effect was observed in 55KO cells, although the overall secretion was significantly lower than WT cells. In addition to starvation, inhibiting proteasomal degradation with MG132, or inducing ER stress with tunicamycin (Tu), both enhanced Htt secretion (Figure 4.2C-F). These results confirm that Htt secretion is elevated under stress conditions.

4.4 GRASP55 level is upregulated by cellular stress and by Htt expression.

The fact that GRASP55 localization and function are regulated by cellular stressors suggests that GRASP55 may serve as both a stress sensor and effector (Zhang and Wang, 2020). In addition to its relocalization from the Golgi to autophagosomes under starvation conditions (Zhang et al., 2018), we wondered whether GRASP55 level might also be upregulated to meet the high demand for its roles in Golgi structure formation, autophagy, and unconventional secretion in response to stress. To test this hypothesis, we incubated WT HeLa cells in EBSS for 0, 2, 4 and 8 h and measured GRASP55 level by western blot. Indeed, EBSS treatment increased

GRASP55 expression, but had no effect on other Golgi proteins we tested, including GRASP65, Golgin-160, Golgin-97, and GCC88 (Figure 4.3A-B). The elevation of GRASP55 expression was not limited to amino acid starvation, as it also applied to ER stress. When cells were treated with ER stress inducers, including Tu, thapsigargin (Tg) and DTT, the level of GRASP55 but not that of other Golgi proteins increased (Figure 4.3C-D).

Since mutant Htt forms aggregates that could induce proteostasis stress, we tested the effect of Htt-Q23 and Htt-Q74 on GRASP55 expression. Both Htt-Q23 and Htt-Q74 expression increased the GRASP55 level in cells, although Htt-Q74 exhibited a stronger effect (Supplemental Figure 4.1G-H). To validate this observation in mice, we took advantage of a previously established knock-in mouse model that expresses full-length Htt-Q200 in the brain (Heng et al., 2010, Gerson et al., 2020). These studies have shown that expression of Htt-Q200 upregulated both LC3-II and p62 levels compared to control, indicating an enhanced autophagosome formation but reduced lysosomal degradation. This conclusion was validated in our Htt mice and cell samples, as indicated by p62 accumulation (Figure 4.3E-F; Supplemental Figure 4.1G-H) (Heng et al., 2010). In response to the proteostasis stress, GRASP55 level was also elevated in the brain tissues, while other proteins such as GRASP65 and GM130 did not change (Figure 4.3E-F). Taken together, GRASP55 level is upregulated by cellular stress and Htt expression, possibly to meet the high demand of unconventional secretion.

4.5 GFP-Htt-Q74 secretion is autophagy dependent.

The fact that GRASP55 expression, autophagy and unconventional secretion are all elevated under stress conditions implies that these events are related. To test if Htt secretion depends on autophagy, we expressed GFP-Htt-Q74 in the Atg7 knockout mouse embryonic fibroblast (MEF) cell line established by Dr. Masaaki Komatsu (Komatsu et al., 2005) in which autophagosome formation was abolished, as indicated by the lack of LC3-II (Figure 4.4A). Htt secretion was reduced in Atg7 KO cells to an almost undetectable level (Figure 4.4A-B). In addition, inhibition of autophagosome-lysosome fusion by bafilomycin A1 (BafA1) treatment also decreased Htt secretion in WT but not 55KO cells (Figure 4.4C-D).

The results described above are consistent with the role of GRASP55 in autophagosome-lysosome fusion, suggesting that GRASP55 regulates Htt unconventional secretion via controlling autophagosome maturation. If this conclusion is correct, we would expect to see more colocalization of Htt with the autophagosome marker LC3 in 55KO and BafA1-treated cells. Consistent with this idea, Htt partially colocalized with LC3 in WT cells, while 55KO and BafA1 treatment enhanced the colocalization (Figure 4.4E-F). It has been indicated that unconventional secretion could occur through lysosomal secretion (Villeneuve et al., 2018). Indeed, GFP-Htt-Q74 expression, but not GFP expression, enhanced the signal of the lysosome protein LAMP1 at the cell surface (Figure 4.4F), while this effect was highly reduced in 55KO cells (Figure 4.4G-H). These results indicate that Htt is probably taken up by autophagosomes, and once autophagosomes are fused with lysosomes, Htt can be released by lysosome exocytosis.

It has previously been shown that Htt is secreted in exosomes (Trajkovic et al., 2017), which is in conflict with our conclusion that Htt secretion is autophagy dependent. Therefore, we performed differential centrifugation to pellet exosomes in the conditioned media and determined the level of Htt in different fractions. As shown in Figure 4.4I, exosomes were highly enriched in the pellet of the 100,000 g spin as indicated by the exosome marker TSG101 (lane 3), while Htt was only found in the supernatant (lane 4). To confirm that Htt was not secreted in membrane-bound structures such as exosomes, we treated the conditioned media of Htt expressing cells with proteinase K with or without Triton X-100 (TX-100). The results showed that Htt was degraded by proteinase K regardless of whether TX-100 was included (Figure 4.4J). Taken together, these results demonstrate that Htt secretion depends on autophagy but not exosome secretion.

4.6 GRASP55 facilitates GFP-Htt-Q74 secretion through promoting autophagosome maturation and stabilizing p23/TMED10.

GRASP55 facilitates autophagosome maturation by tethering autophagosomes and lysosomes through the interactions with LC3-II on autophagosomes and LAMP2B on lysosomes (Zhang et al., 2018). To confirm that GRASP55 promotes Htt secretion through regulating autophagosome maturation, we re-expressed GRASP55 and its autophagy mutants in 55KO cells and tested their effect on Htt secretion. Expression of WT GRASP55 restored GFP-Htt-Q74

secretion, showing that the reduced Htt secretion in 55KO cells was specific for GRASP55 depletion (Figure 4.5A). In contrast, expression of the F37A mutant of GRASP55, which abolishes GRASP55-LC3 interaction (Zhang et al., 2018), failed to rescue the secretion defect of Htt in 55KO cells (Figure 4.5B-C). The 5A mutant of GRASP55, whose O-GlcNAcylation is disabled and thus its role in autophagy is constitutively active, also rescued Htt secretion similar to WT GRASP55. In this experiment, GRASP55 itself is not secreted with Htt; and we did not detect an interaction between Htt and GRASP55 by co-immunoprecipitation. These results demonstrate that GRASP55 facilitates Htt secretion by promoting autophagosome maturation.

Recently it has been reported that an ERGIC protein p23, also known as TMED10, functions as a protein channel for cytosolic proteins to be translocated into the ERGIC lumen before they are transported to autophagosomes and secreted to the extracellular space (Zhang et al., 2020). Indeed, p23 depletion largely reduced GFP-Htt-Q74 secretion (Supplemental Figure 4.2A). Considering that some members of the p24 family proteins interact with GRASP65 (Barr et al., 2001) and that GRASP55 is partially relocated to the ER under stress conditions for CFTR trafficking (Kim et al., 2016), inhibition of Htt secretion by p23 depletion and 55KO suggested that GRASP55 may function together with p23 in Htt secretion. This speculation was first supported by the observation that the p23 level was reduced in 55KO but not 65KO cells (Supplemental Figure 4.2B-C). In addition, p23 co-immunoprecipitated with GRASP55 but not GRASP65, while known interactions between GRASP65 and GM130 and between GRASP55 and Golgin-45 were readily detectable in the same experiment (Supplemental Figure 4.2D).

These results support the idea that GRASP55 interacts with p23 to facilitate Htt unconventional secretion.

4.7 Inhibition of Htt secretion by 55KO enhances Htt aggregation and toxicity in the cell.

It is generally believed that HD is caused by the accumulation of toxic mutant Htt protein in the cell. To determine the functional significance of Htt secretion, we assessed Htt aggregation in WT and 55KO cells. We lysed GFP-Htt-Q74 expressing cells in detergent and separated Htt aggregates from its soluble form by centrifugation. Western blot analysis of the two fractions showed that Htt formed more aggregates in 55KO than WT cells (Figure 4.5D). Expression of WT GRASP55 and its 5A mutant, but not the autophagy inactive F37A mutant, reduced Htt aggregation in 55KO cells (Figure 4.5E), consistent with their roles in Htt secretion. In this experiment, a significant amount of GRASP55 and GM130 were found in the pellet (Figure 4.5E), consistent with the idea that they form a detergent-insoluble Golgi matrix (Xiang and Wang, 2011, Wang and Seemann, 2011). We also confirmed the effect of GRASP55 KO on Htt aggregation by microscopy. At both 48 h and 72 h post-transfection, 55KO cells showed more and larger aggregates compared to WT (Figure 4.5F-H). These results demonstrate that GRASP55 dependent Htt secretion reduces its aggregation and toxicity in the cell.

4.8 Secretome analysis of WT and 55KO cells identifies new proteins secreted by GRASP55-dependent unconventional secretion.

To identify native proteins that are secreted in a GRASP55-dependent mechanism, we analyzed the conditioned media of WT and 55KO cells by Tandem Mass Tag (TMT) labeling and liquid-chromatography mass spectrometry (LC-MS). With a 1% false discovery rate (FDR), we identified 1696 proteins in the media (Supplemental Table 4.1). We plotted all 1696 secreted proteins on a volcano plot to display their changes in the 55KO vs. WT secretome (Figure 4.6A). Significantly changed cargoes [$|\text{Log}_2\text{FC (55KO/WT)}| > 0.5$, $p < 0.05$] without predicted signal peptides are shown in black. On this plot, majority of the unconventional targets were reduced in 55KO.

Next, we systematically analyzed the impact of GRASP55 depletion on the secretion of both conventional and unconventional pathway cargoes. Among the 1696 proteins, we identified a total of 445 proteins whose secretion is highly affected by 55KO [$|\text{Log}_2\text{FC (55KO/WT)}| > 0.5$, $p < 0.05$] (Supplemental Table 4.1). Within these 445 significantly changed proteins, 169 contained an ER signal sequence predicted by the SignalP-5.0 Server (<http://www.cbs.dtu.dk/services/SignalP>), while 276 proteins did not appear to have ER signal peptides (Supplemental Table 4.1). Within the 169 proteins with ER signal sequences, 134 (79%) of them were increased in 55KO secretion (Figure 4.6B), consistent with our previous findings that GRASP depletion accelerates protein trafficking (Xiang et al., 2013). In contrast to the proteins with ER signal sequence, 196 (71%) of the 276 proteins without ER signal sequences

were reduced in 55KO secretion (Figure 4.6C). These results support our conclusion that GRASP55 plays essential roles in unconventional protein secretion.

To identify the pathways affected by 55KO, we performed Gene Ontology (GO) analysis of the significantly changed proteins. GO term pathway analysis of the 169 proteins with predicted ER signal peptides identified the following pathways as significantly changed in 55KO: lysosomal enzymes and structural proteins, extracellular matrix organization, glycosaminoglycan metabolism, cell adhesion and proliferation, cellular response to growth factor stimuli, immune response and tissue remodeling, and response to amyloid-beta, unfolded protein response and aging (Figure 4.6D; Supplemental Table 4.2). The most affected pathway is related to lysosomal biogenesis, consistent with our previous finding that Golgi unstacking by GRASP depletion causes missorting and increased secretion of lysosomal enzymes (Xiang et al., 2013). Given the central role of the Golgi in protein trafficking, glycosylation, and secretion, it is also reasonable to see that GRASP55 depletion significantly alters extracellular matrix organization and glycosaminoglycan metabolism. In addition, our secretome analysis also validated our previous findings that 55KO affects cell adhesion, migration, and growth (Ahat et al., 2019c).

GO term analysis of the 276 significantly changed proteins without signal sequences identified pathways such as cellular response to stimuli, oxidative stress, nutrient levels, heat, wounding, protein folding, macroautophagy, programmed cell death and cell-cell communication

(Figure 4.6E; Supplemental Table 4.2), which are consistent with the role of GRASP55 in stress response (Zhang and Wang, 2020). These findings further suggest a link between GRASP55, autophagy dependent-unconventional secretion and stress response. Consistent with this notion, previously identified unconventional secretion cargoes such as SOD1 and IL- β 1 are related to oxidative stress and inflammation, and their secretion is increased under certain stress conditions such as nutrient starvation (Cruz-Garcia et al., 2017, Dupont et al., 2011).

To confirm that the identified proteins without ER signal sequences are indeed secreted through a GRASP55-dependent mechanism, we tested a few top candidates (Figure 4.6A), including transgelin 1 (TAGLN), multifunctional protein ADE2 (PAICS) and peroxiredoxin-1 (PRDX1), using the secretion assay we established for Htt. These proteins were selected because they are predicted to be highly secreted by the SecretomeP 2.0 server (<http://www.cbs.dtu.dk/services/SecretomeP>), an online tool to predict the probability of unconventional protein secretion, although their secretion and the GRASP55-dependence in the secretion have not been experimentally confirmed. Indeed, these proteins were all detected in the conditioned media, and their secretion was all reduced in GRASP55 KO cells (Figure 4.6F-K). In summary, the unbiased secretomic analysis provided new evidence that GRASP55 depletion accelerates conventional protein trafficking and secretion but inhibits unconventional secretion. It also identified a list of bona fide candidates that are secreted by GRASP55-dependent unconventional secretion (Figure 4.6L).

Discussion

In this study, we used GFP-Htt-Q74 as a model protein to study the role of GRASP55 in unconventional secretion and cytosolic aggregation of neurotoxic proteins. We discovered that mutant Htt is secreted through a GRASP55- and autophagy-dependent but Golgi-independent pathway. Our results also revealed a link between enhanced Htt secretion, elevated autophagy, and increased GRASP55 expression under various stress conditions, and confirmed a novel role of GRASP55 in stress response (Zhang and Wang, 2020). Htt may enter autophagosomes through p23-mediated translocation or by direct engulfment by phagophores. Due to lysosomal dysfunction, undegraded proteins in autophagosomes and lysosomes could be released by autophagosome or lysosome exocytosis (Figure 4.6L). GRASP55 enhances Htt secretion through two actions, one is to facilitate autophagosome-lysosome fusion by interacting with LC3 and LAMP2, and another is to stabilize p23, the translocon that allows cytosolic proteins enter the lumen of the ERGIC, from where they are transported to autophagosomes. Lastly, using systematic secretomic analysis, we identified and catalogued new proteins in GRASP55-dependent unconventional secretion.

It is interesting to see that GRASP55-dependent unconventional secretion is selective, at least to some degree. First, among all marker proteins tested, Htt and SOD1 are preferably secreted than TDP-43 and Tau. Consistently, the secretion of Htt and SOD1, but not TDP-43 and Tau, depends on GRASP55. It has been previously shown that Tau is secreted via direct translocation across the plasma membrane, which is regulated by heparan sulfate and

PtdIns(4,5)P₂ (Merezhko et al., 2018). So far there is no indication that GRASP55 is involved in this pathway. TDP43, on the other hand, has been shown to be secreted in a prion-like manner via exosomes (McAlary et al., 2020). While it is not clear whether GRASP55 directly regulates exosome secretion, our data indicates that it plays no role in TDP43 secretion. Second, Htt-Q74 is preferentially secreted than Htt-Q23. Given that Htt-Q74 forms more aggregates than Htt-Q23, one possible explanation is that aggregated proteins are selectively secreted. This speculation is supported by the third observation that of the two bands of Htt-Q74, only the aggregation-prone, dephosphorylated form is secreted. Whether Htt-Q74 aggregates are preferably enclosed by autophagosomes or selectively translocated into the ERGIC lumen requires further investigation.

In HD, mutant Htt with a long polyQ stretch tends to form toxic protein aggregates that cause cellular toxicity and neurodegeneration (Bates et al., 2015, Leitman et al., 2014, Arrasate and Finkbeiner, 2012). In this study we used the N-terminal fragment of Htt as a cargo due to its relevance to the disease. The exon 1 fragment of Htt contains the polyQ stretch which is the source of the toxicity of mutant Htt. This fragment is harder to degrade, more toxic than full-length Htt, and detected in the CSF with an elevated concentration in HD (Sathasivam et al., 2013, Chen and Wolynes, 2017). Like full-length Htt, the aggregation and toxicity of the exon 1 fragment are regulated by phosphorylation of S13 and S16, which indicates similar regulation. For these reasons we believe that the N-terminal fragment of Htt serves as an excellent reporter in our study.

Autophagy is an energy and nutrient deprivation-induced, lysosome-mediated degradation pathway essential for organelle turnover and degradation of aggregated proteins. Compared to non-neuronal cells, neurons need to maintain high basal autophagy for survival (Mizuno et al., 2001, Fujita et al., 2002). Autophagy and autophagy defects have been linked to neurodegenerative diseases (Hegde et al., 2020, Levine and Kroemer, 2008). While wildtype Htt is required for selective autophagy (Rui et al., 2015), mutant huntingtin has been shown to hinder autophagy flux, and certain population of toxic Htt is immune to autophagy-dependent degradation (Fu et al., 2017). It is possible that defects in lysosomal function and impairment of protein degradation may activate GRASP55-dependent unconventional secretion to clear out the toxic, autophagy-resistant Htt aggregates. Indeed, our data demonstrates that inhibition of proteasomal degradation pathway also significantly increase unconventional secretion of mutant Htt.

Htt secretion could be a double-edged sword to the neuronal cells and the disease. On the one hand, the aggregation-prone, dephosphorylated Htt with a long polyQ stretch is selectively secreted, which reduces the amount of Htt aggregates in the cells and subsequently ameliorates its toxicity in the cell. In this sense Htt secretion is beneficial to the cell. Our results support this hypothesis as GRASP55 depletion increases overall Htt aggregation in the cell (Figure 4.5D-H). On the other hand, secreted Htt aggregates may serve as seeds for internalization into the neighboring cells to trigger more Htt aggregation. Here Htt secretion may facilitate the spreading and propagation of Htt aggregates from disease to healthy neurons, which may contribute to the

development of the disease. This hypothesis, however, is unlikely since we observed overall significantly more and larger Htt aggregates in GRASP55 KO cells compared to WT. Future studies will test the biological significance of Htt secretion through the intervention of GRASP55 in HD animal models. New information provided in this study may shed light on novel therapeutic approaches for the treatment of this devastating disease.

Materials and Method

Reagents, plasmids, and antibodies

All reagents were purchased from Sigma-Aldrich, Roche, Calbiochem, and Fisher unless otherwise stated. The following cDNA constructs have been described previously: pEGFP-N1-GRASP55 (WT, 37A, 5A) and pEGFP-N1-GRASP65 (WT) (Zhang et al., 2018). Others cDNAs include GFP-Htt-Q74 (Addgene, Cat# 40262), GFP-Htt-Q23 (Addgene, Cat # 40261), TAGLN-Myc (OriGene, Cat # RC215789), PAICS-EGFP (Addgene, Cat #99108), pFRT/TO/HIS/FLAG/HA-PRDX1 (Addgene, Cat # 38086).

Antibodies used in this study include monoclonal antibodies against β -actin (Proteintech, Cat# 66009-1-Ig), Clusterin (Santa Cruz, Cat# SC-5289), Flag (Sigma, Cat# M1804), GFP (Proteintech, Cat# 66002-1-Ig), Myc (9E10, Dr. David Sheff) and PolyQ (Sigma, Cat# MAB1574); polyclonal antibodies against Atg7 (Cell Signaling, Cat# 2631S), Bip (Santa Cruz, Cat# sc-13968), GCC88 (Proteintech, Cat# 16271), Golgin-97 (Proteintech, Cat# 12640-1-AP), Golgin-160 (Proteintech, Cat#2 1193), GRASP55 (Proteintech, Cat# 10598-1-AP), human GRASP65 (Dr. Joachim Seemann, University of Texas Southwestern Medical Center), $\alpha 5$ integrin (Cell Signaling, Cat# 4705), LC3 (Cell Signaling, Cat#2755), and p62 (Proteintech, Cat# 18420-1-AP).

Cell culture, transfection, and treatment

For cell culture, HeLa and MEF cells were grown in DMEM (Invitrogen) containing 10% super calf serum (Gemini, Cat# 100-510) and glutamax at 37°C in a 5% CO₂ incubator. For Htt expression, GFP-Htt-Q74 was transfected into WT or GRASP KO HeLa cells in 3.5 cm dishes when the cells reached the confluency of 50-60%. For drug treatment, 5 µg/ml BFA, 500 ng/ml nocodazole, 100 µg/ml CHX, 50 µM MG132, 1 µM staurosporine, 1 µM okadaic acid or 5 µg/ml tunicamycin was directly applied to the medium for the indicated times.

Protein secretion assay and TCA precipitation

WT or GRASP KO HeLa cells grown in 3.5 cm dishes were transfected with GFP-Htt-Q74 (4 µg DNA for a 3.5 cm dish) when the cells reached the confluency of 50-60% and incubated in full growth medium for 24 h. Cells were washed with phosphate buffered saline (PBS) five times and further incubated in 1 ml DMEM without serum for 4 h. Conditioned media were collected, cleared by centrifugation at 500 g for 10 min at 4°C and 2000 g for 20 min at 4°C. 0.9 ml of precleared conditioned medium was then mixed with 0.11 volumes of ice-cold 100% TCA (2.2 g/ml) and placed on ice. After 10 min, 500 µl of ice-cold 10% TCA were added to the sample-TCA mix. After 20 min samples were centrifuged at 20,000 g for 30 min at 4°C. Pellet was washed with cold acetone (-20°C), dried, and dissolved in 1x SDS loading buffer for western blot analysis. The cells were washed with cold PBS twice, scraped and lysed in 20 mM Tris-HCl, pH 8.0, 150 mM NaCl, 1% Triton X-100 and protease inhibitor cocktail for 30 min on ice. Lysates were cleared by centrifugation (20,000 g for 20 min at 4°C). The cell lysate and medium precipitate were loaded at 1:8 ratio. After electrophoresis and transfer, nitrocellulose

membranes were incubated with corresponding primary antibodies overnight at 4°C. The membranes were extensively washed and further incubated with HRP conjugated goat anti-rabbit or goat anti-mouse secondary antibodies for 1 h at room temperature and exposed to a FluorChem M machine (Proteinsimple). To quantify the efficiency of protein secretion, the intensity of the bands of the cargo protein in the conditioned media and lysate on the same gels were quantified using ImageJ (Schindelin et al., 2012), and then the amount of the secreted protein was normalized to that in the cell lysate. For Htt, because the two bands in the cell lysate are exchangeable (Figure 4.1H) and in many cases are too close to separately quantify, we used the total Htt amount in the cell lysate for normalization. To maintain the consistency of the quantitation results, we normalized the secretion in WT cells (or other controls) to one and so a clear comparison between control and experimental groups can be easily visualized in the same and different experiments.

Immunofluorescence microscopy

Cells were grown on sterile glass coverslips and rinsed with PBS before fixation. To stain total cellular proteins, cells were fixed in 4% paraformaldehyde (PFA) for 10 min and permeabilized with 0.2% Triton X-100 in PBS for 10 min. Cells were incubated with primary antibodies overnight at 4°C, washed and probed with the appropriate secondary antibodies conjugated to TRITC for 45 min. To stain cell surface LAMP1, cells were fixed with 1% PFA for 10 min without permeabilization. Cells were incubated with an anti-LAMP1 antibody (H4A3, DSHB, 1:100) overnight at 4°C, washed and probed with the appropriate secondary antibodies

conjugated to TRITC for 45 min at room temperature. To analyze LC3 and Htt colocalization, cells were pre-permeabilized in KHM buffer (125 mM potassium acetate, 25 mM Hepes, pH 7.2, and 2.5 mM magnesium acetate) containing 0.1% saponin (prefiltered) for 2 min on ice to release the cytosol and washed by KHM buffer for 5 min at room temperature. Cells were then fixed with 4% PFA, permeabilized in 0.2% Triton X-100 and incubated with primary and secondary antibodies as described above. DNA was stained with Hoechst in PBS for 5 min. Coverslips were rinsed with PBS and mounted with Mowiol onto slides. Images were taken with a 20x air objective or a 63x oil objective on a Nikon ECLIPSE Ti2 Confocal microscope and shown as max projections.

Protease K protection assay

Protease K protection assay of the conditioned media was performed as previously described (Zhang et al., 2019c). Briefly, conditioned medium from HeLa cells expressing GFP-Htt-Q74 was collected as described above and was equally divided into three tubes, one was left untreated on ice, the second was incubated with 2.5 µg/ml Protease K (Thermo Fisher Scientific, Cat # AM2542) on ice, and the third was treated with both protease K and 1% Triton X-100 (from 20% stock) for 10 min on ice. Protease K was then inhibited by adding 1 mM PMSF (from 100 mM stock in isopropanol) and further incubated on ice for 10 min. Proteins in each sample were pelleted by TCA precipitation as above. The pellets were dissolved in 1x SDS sample buffer (50 mM Tris-HCl, pH 6.8, and 2% SDS) and analyzed by western blotting.

Separation of insoluble Htt aggregates from its soluble forms

WT or GRASP KO cells were transfected with GFP-HttQ74 for indicated times. Cells were washed three times with cold PBS, scraped in cold PBS, centrifuged at 1000 g for 3 min at 4°C, and lysed in lysis buffer (20 mM Tris 8.0, 150 mM NaCl, 0.5% NP40, protease inhibitors) for 20 min on ice. The supernatant and pellet were collected after spinning down at 55,000 rpm for 1 h. The supernatants concentration was adjusted to 1.5 mg/ml (the volumes of the samples are different) and supplemented with 1/5 volume of 6x SDS loading buffer with DTT (final 1x SDS in the sample). The pellet was dissolved in the same amount of 2x SDS loading buffer with DTT. Both samples were boiled, and the pellet and supernatant were loaded onto the gel at a 6:1 ratio.

Proteomics analysis

WT and 55KO cells were cultured in full growth medium in 15 cm dishes in triplicates till they reach 80% confluency. The medium was exchanged to 20 ml DMEM only (without serum) for 12 h, cells and conditioned media were collected. The media were cleaned by centrifugation at 500 g for 10 min at 4°C followed by 4000 g for 15 min at 4°C, and filtered with a 0.45 µm filter. The media then were concentrated with a 3kDa cutoff ultrafilter (Millipore, UFC900324), and the protein concentration was determined with Bradford assay (Bio-Rad, Cat # 5000006). Cells were lysed in Pierce™ RIPA buffer (Thermo, Cat # 89900) with a protease inhibitor cocktail (Thermo) and the protein concentration was tested with Bradford assay. 75 µg of each sample was provided to the Mass Spectrometry-Based Proteomics Resource Facility at

Department of Pathology, University of Michigan for TMT labeling, LC-MS/MS and bioinformatics analysis.

For TMT labeling, cell and medium samples were proteolysed and labeled with TMT 10-plex essentially by following manufacturer's protocol (ThermoFisher, Cat # 90110, Lot # VJ306782). For liquid chromatography-mass spectrometry (LC-MS) analysis, as previously described (Tank et al., 2018). An Orbitrap Fusion (Thermo Fisher Scientific) and RSLC Ultimate 3000 nano-UPLC (Dionex) was used to acquire the data. 2 μ l of the sample was resolved on a PepMap RSLC C18 column (75 μ m i.d. x 50 cm; Thermo Scientific) at the flowrate of 300 nl/min using 0.1% formic acid/acetonitrile gradient system (2-22% acetonitrile in 150 min; 22-32% acetonitrile in 40 min; 20 min wash at 90% followed by 50 min re-equilibration) and directly spray onto the mass spectrometer using EasySpray source (Thermo Fisher Scientific). Mass spectrometer was set to collect one MS1 scan (Orbitrap; 120K resolution; AGC target 2x10⁵; max IT 100 ms) followed by data-dependent, "Top Speed" (3 seconds) MS2 scans (collision induced dissociation; ion trap; NCE 35; AGC 5x10³; max IT 100 ms). For multistage MS3, top 10 precursors from each MS2 were fragmented by HCD followed by Orbitrap analysis (NCE 55; 60K resolution; AGC 5x10⁴; max IT 120 ms, 100-500 m/z scan range).

Data analysis was performed using Proteome Discoverer (v2.4; Thermo Fisher). In data analysis, MS2 spectra were searched against SwissProt human protein database (20353 entries; downloaded on 06/20/2019) with the search parameters: MS1 and MS2 tolerance were set to 10

ppm and 0.6 Da, respectively; carbamidomethylation of cysteines (57.02146 Da) and TMT labeling of lysine and N-termini of peptides (229.16293 Da) were considered static modifications; oxidation of methionine (15.9949 Da) and deamidation of asparagine and glutamine (0.98401 Da) were considered variable. Identified proteins and peptides were filtered to retain only those that passed $\leq 1\%$ FDR threshold. Quantitation was performed using high-quality MS3 spectra (Average signal-to-noise ratio of 10 and $< 50\%$ isolation interference).

Quantification and statistics

In all figures, the quantification results are expressed as the mean \pm SEM (standard error of the mean) from three independent experiments, unless otherwise stated. The statistical significance of the results was assessed using a two-tailed Student's *t*-test. *, $p < 0.05$, **, $p < 0.01$, ***, $p < 0.001$.

Figure assembly

All figures were assembled using Adobe Illustrator; Figure 6L was drawn with Biorender.

Supplemental Information

Supplemental Information includes 2 supplemental figures and 2 supplemental tables. Supplemental Figure 4.1 demonstrates that GRASP55 is required for the secretion of a subset of neurotoxic proteins in addition to Htt. Supplemental Figure 4.2 provides evidence that GRASP55

facilitates Htt secretion by stabilizing p23. Supplemental Table 4.1 lists the proteins whose secretion is altered by 55KO in the secretome study. Supplemental Table 4.2 lists the selected GO term analysis for the secretome of WT and 55KO cells.

Acknowledgments

We thank Dr. Masaaki Komatsu and Dr. Lois Weisman for Atg7 KO MEF cell lines. We thank Dr. Venkatesha Basrur and the Mass Spectrometry-Based Proteomics Resource Facility in the Department of Pathology at the University of Michigan for their contribution to the Proteomics analysis. We thank the current and former members of the Wang lab for stimulating discussions and technical support. We also thank Dr. Prabhodh Abbineni and Vi Tang from David Ginsburg lab at the University of Michigan for their valuable input in secretome experiment design. This work was supported by the National Institutes of Health (Grant R35GM130331) and the Fast Forward Protein Folding Disease Initiative of the University of Michigan to Y. Wang, and a University of Michigan Rackham Predoctoral Fellowship to E. Ahat.

Competing Interest

The authors declare that no competing interests exist.

Figures and Figure legends

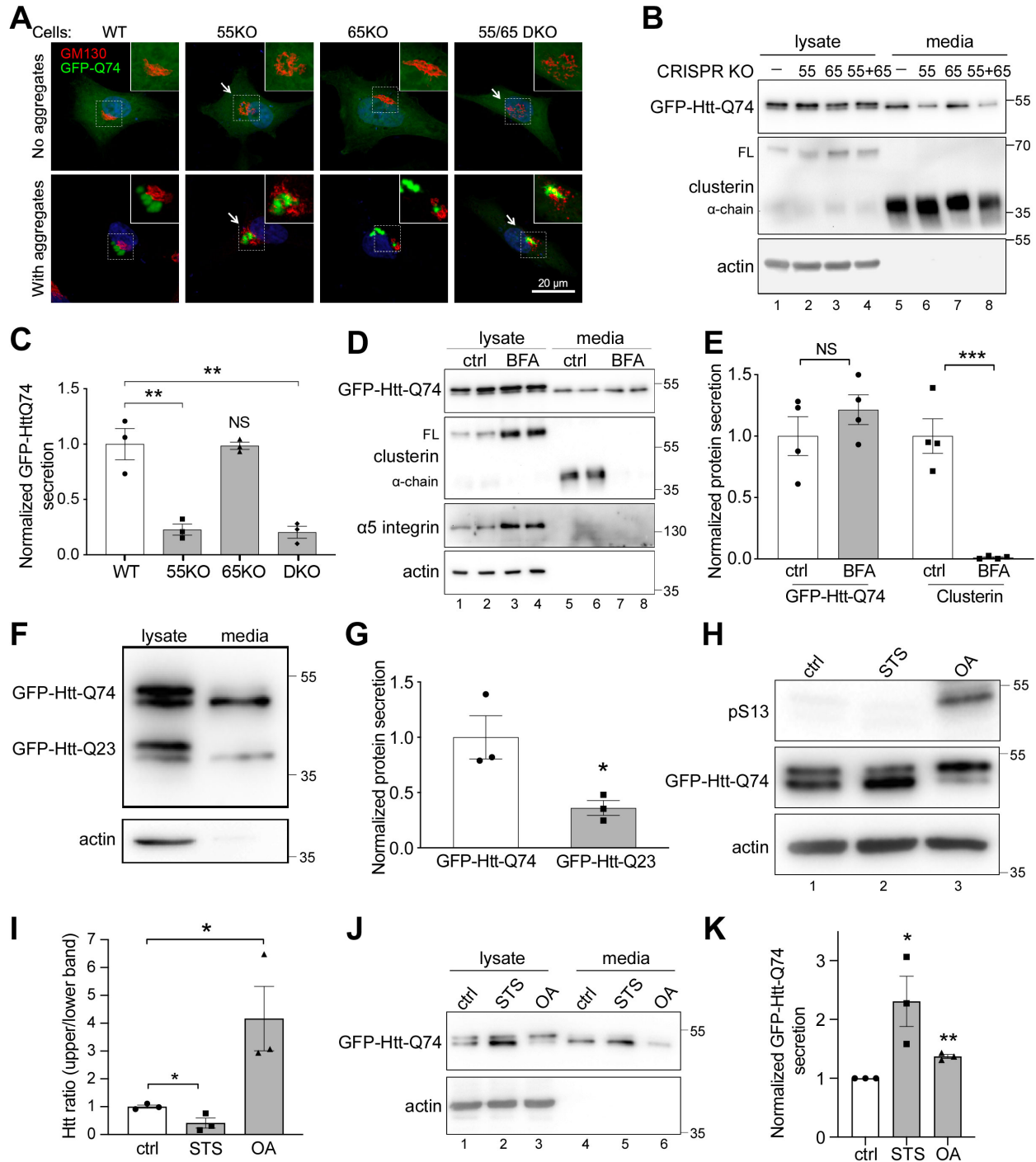


Figure 4.1. GRASP55 is required for unconventional secretion of mutant huntingtin.

(A) GFP-Htt-Q74 aggregation induces Golgi fragmentation in GRASP55 KO (55KO) cells. WT and indicated GRASP KO HeLa cells expressing GFP-Htt-Q74 were stained for GM130 (red) and DNA (blue). Shown are example cells without (upper panels) or with (lower panels) Htt aggregates (arrows). **(B)** Htt secretion requires GRASP55 but not GRASP65. Cell lysates and conditioned media of GFP-Htt-Q74 expressing WT and GRASP KO cells were analyzed by western blot for Htt. Clusterin was used as a marker for conventional secretion. FL, full length clusterin; α -chain, mature clusterin. **(C)** Quantitation of Htt secretion in B. Htt in the medium was normalized to the corresponding total Htt in the cell lysate. Htt secretion in WT is set to 1. **(D)** Htt secretion is unaffected by the block of ER-to-Golgi trafficking. GFP-Htt-Q74 expressing WT cells were treated with or without 5 μ g/ml BFA for 4 h and Htt in the cell lysates and conditioned media were analyzed by western blot. Note that BFA treatment reduced the level of clusterin but not Htt in the conditioned media. **(E)** Quantitation of Htt and clusterin secretion in D, with their normalized levels in control (ctrl) set to 1. **(F)** Htt-Q74 is preferably secreted than Htt-Q23. WT cells were cotransfected by GFP-Htt-Q23 and GFP-Htt-Q74 for 24 h. Cells were then incubated in serum-free medium for 4 h followed by western blot of Htt in the cell lysate and conditioned media. **(G)** Quantification of Htt-Q74 and -Q23 in the conditioned media normalized to corresponding protein amount in the lysate, with Htt-Q74 secretion normalized to 1. **(H)** Htt is phosphorylated. GFP-Htt-Q74 expressing cells were treated with 1 μ M staurosporine (STS) or 1 μ M okadaic acid (OA) for 4 h and analyzed by western blotting for GFP and pS13-Htt. The pS13 antibody recognizes Htt phosphorylated at serine-13. **(I)** Quantification of Htt in H based on the GFP blot. **(J)** Dephosphorylated Htt is preferably

secreted. Cells treated as in H were analyzed for GFP-Htt-Q74 secretion. **(K)** Quantification of J. Quantitation results are presented as mean \pm SEM, with secreted Htt normalized to that in the cell lysate; statistical analysis was performed using Student's t-test. *, $p < 0.05$; **, $p < 0.01$; ***, $p < 0.001$.

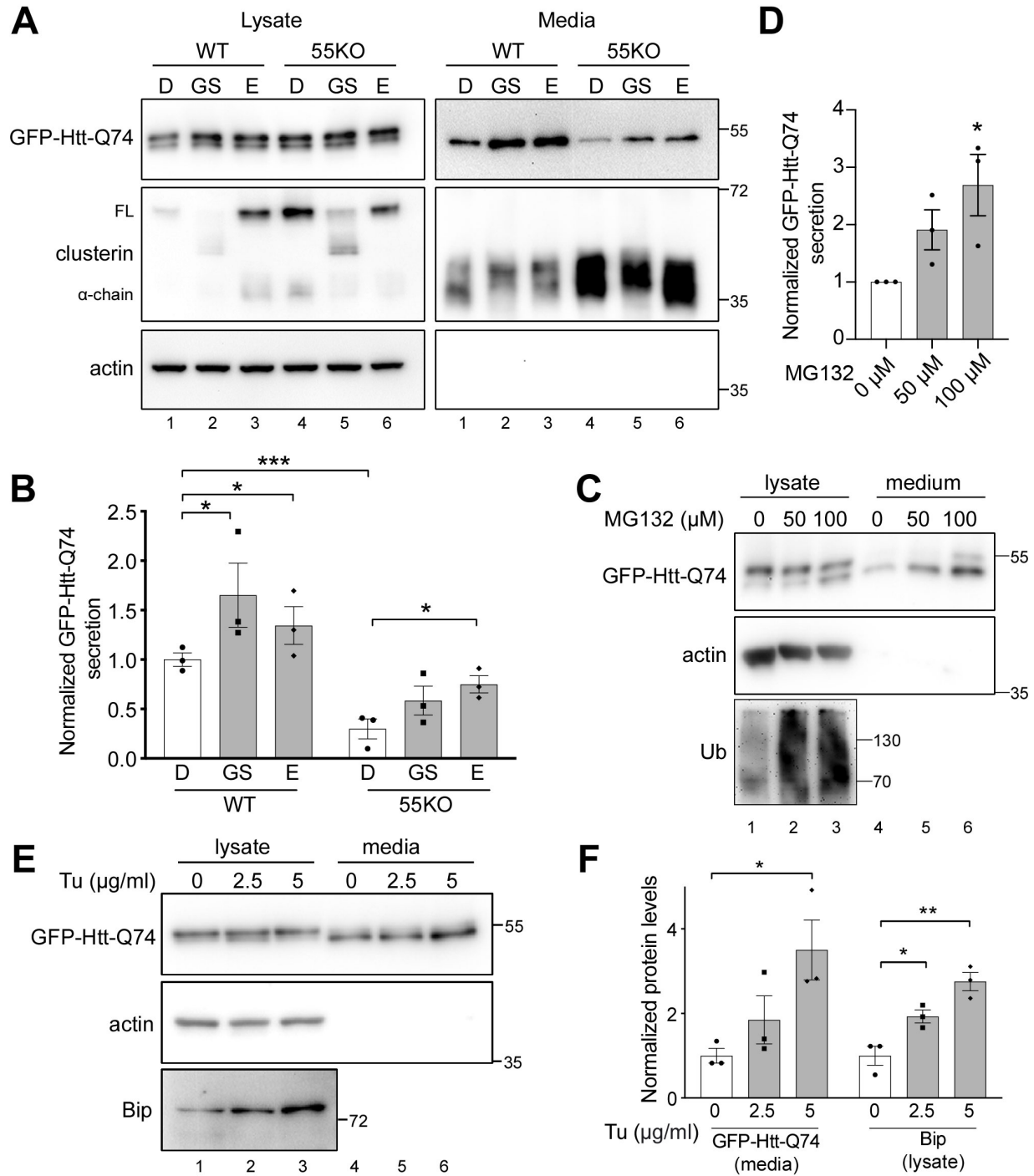


Figure 4.2. Htt secretion is enhanced by various stress stimuli.

(A) Htt secretion is elevated by energy deprivation and nutrient starvation. WT and 55KO HeLa cells transfected with GFP-Htt-Q74 were incubated in serum-free DMEM (D), glucose free medium (GS) or EBSS (E) for 4 h followed by western blot of Htt and clusterin in the cell lysates and conditioned media. **(B)** Quantification of Htt secretion in A. **(C)** Htt secretion is enhanced by proteostasis stress. WT HeLa cells expressing GFP-Htt-Q74 were treated with indicated concentration of MG132 for 4 h followed by western blot of Htt in the cell lysates and conditioned media. Ubiquitin (Ub) was used as a control for MG132 treatment. **(D)** Quantification of Htt secretion in C. **(E)** Htt secretion is enhanced by ER stress. WT HeLa cells expressing GFP-Htt-Q74 were treated with indicated concentration of tunicamycin (Tu) for 4 h and analyzed by western blot for Htt. Bip was used as a marker for ER stress response. **(F)** Quantification of E. Results are presented as mean \pm SEM, with secreted Htt normalized to that in the cell lysate; statistical analysis was performed using Student's *t*-test. *, $p < 0.05$; **, $p < 0.01$.

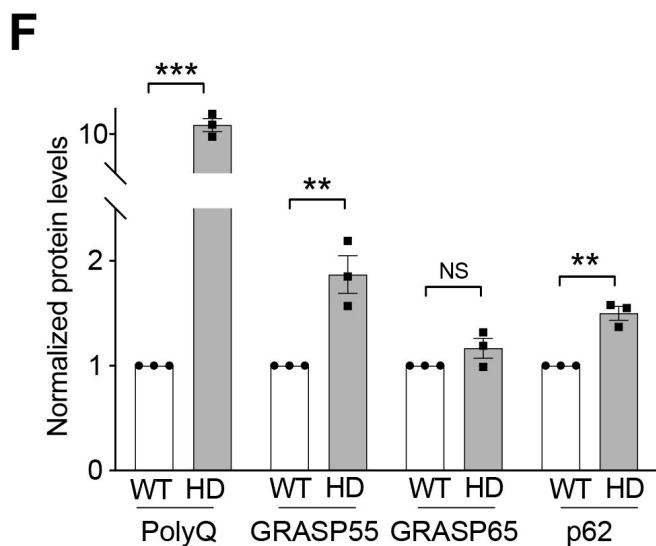
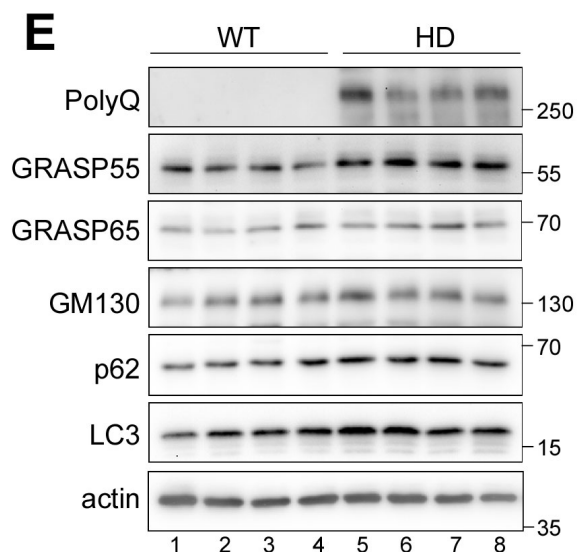
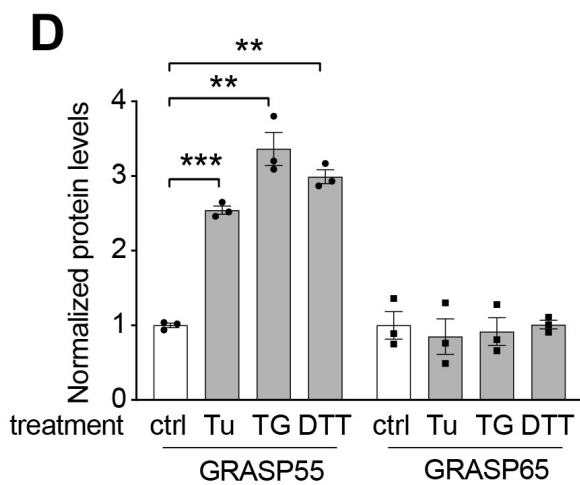
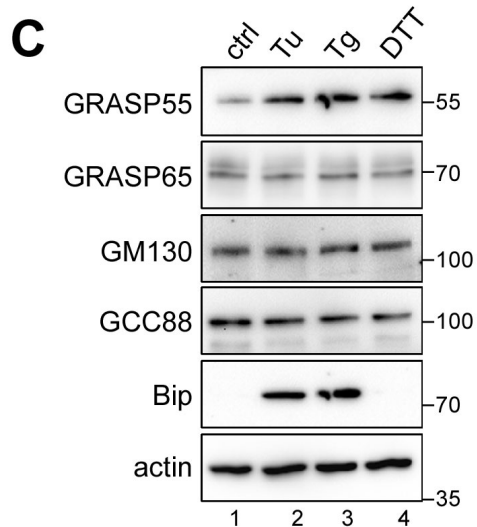
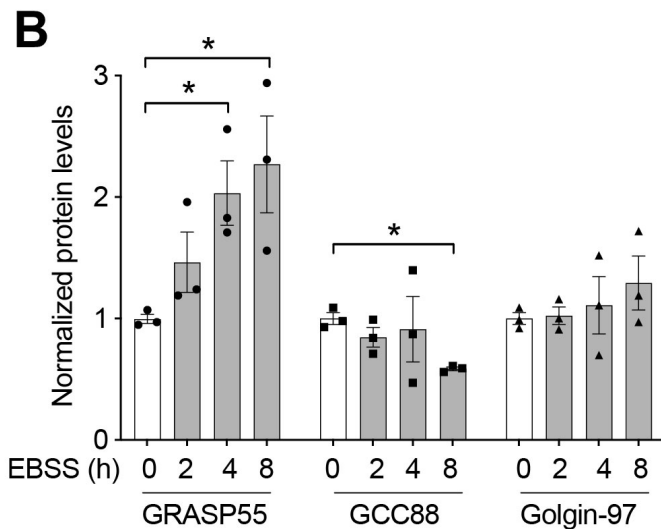
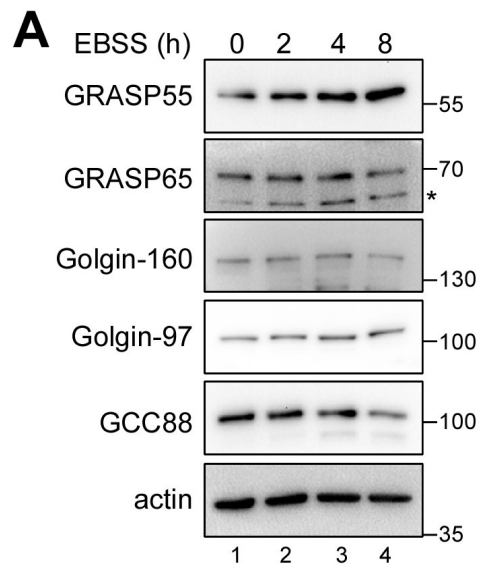


Figure 4.3. GRASP55 expression is upregulated under different stress conditions.

(A) GRASP55 level is increased after amino acid starvation. WT HeLa cells were treated with EBSS for 0, 2, 4 or 8 h and analyzed for indicated Golgi proteins. Note that only GRASP55 is upregulated over time. *, nonspecific band. **(B)** Quantitation of indicated proteins in A. **(C)** GRASP55 expression is upregulated by ER stress. Cells were treated with 1 $\mu\text{g}/\mu\text{l}$ tunicamycin (Tu), 1 μM thapsigargin (Tg) or 0.5 mM DTT for 24 h and probed for indicated Golgi proteins and an ER stress marker Bip. **(D)** Quantitation of GRASP55 and GRASP65 in C. **(E)** GRASP55 expression is elevated in Htt transgenic mice. Brain samples of 8-10 months old Htt transgenic mice (HD, Htt-Q200 expressed under the Htt promoter in knock-in mice) and WT littermates were analyzed by western blot of indicated proteins. Only GRASP55 increased its level in HD mice compared to WT. **(F)** Quantitation of indicated proteins in E. Results are presented as mean \pm SEM; statistical analysis was performed using Student's *t*-test. *, $p < 0.05$; **, $p < 0.01$; ***, $p < 0.001$.

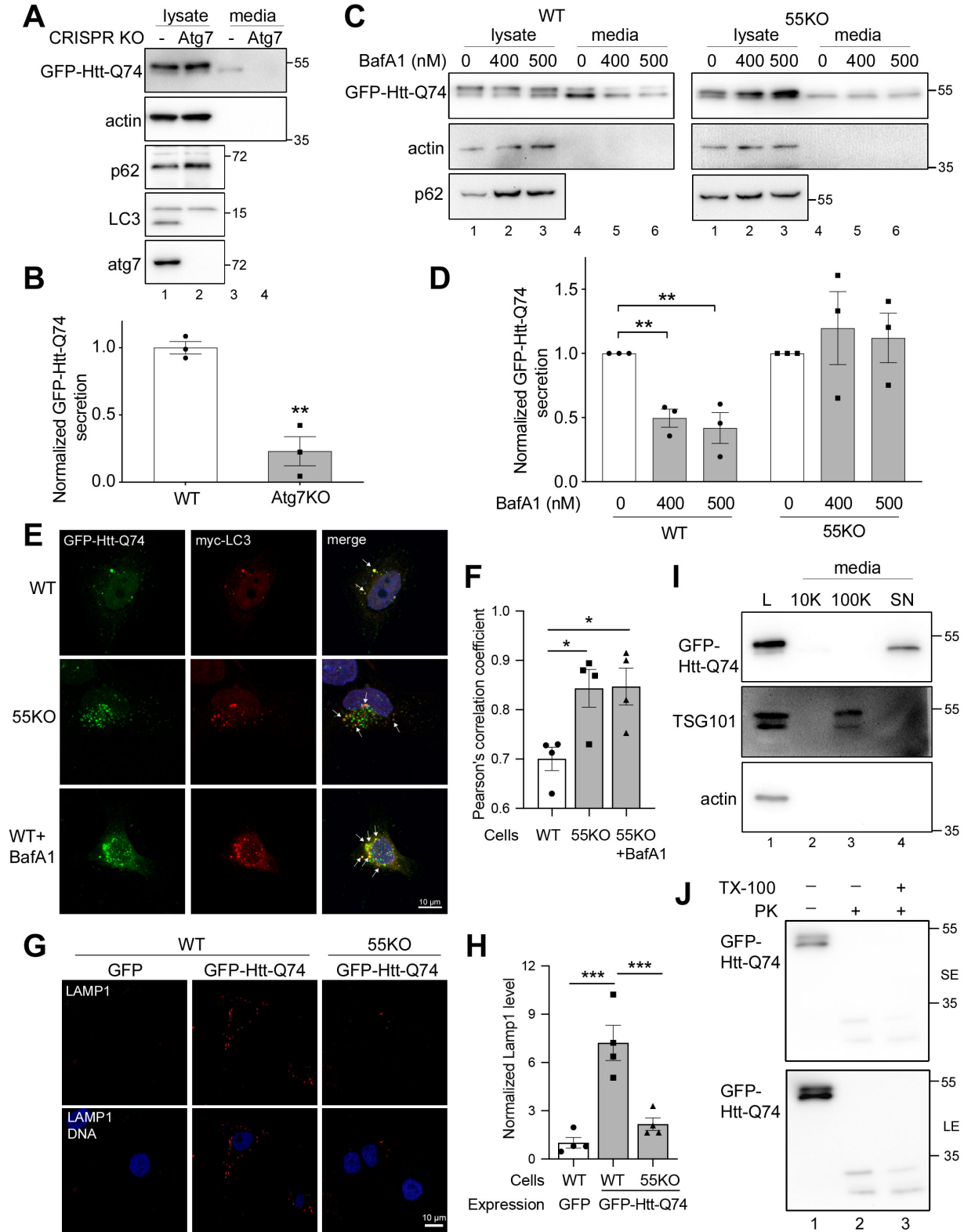


Figure 4.4. Htt secretion is autophagy dependent.

(A) Htt secretion is inhibited by ATG7 KO. WT and ATG7 KO MEF cells were transfected with GFP-Htt-Q74 and analyzed for Htt secretion by western blot. **(B)** Quantitation of Htt secretion in A. **(C)** Htt secretion is reduced by autophagy inhibition. WT and 55KO HeLa cells expressing GFP-Htt-Q74 were treated with 0, 400, or 500 nM BafA1 for 4 h and analyzed for Htt secretion by western blot. Note that BafA1 reduced Htt secretion in WT but not 55KO cells. **(D)** Quantitation of Htt secretion in C. Results are presented as mean \pm SEM, with secreted Htt normalized to that in the cell lysate; statistical analysis was performed using Student's *t*-test. *, $p < 0.05$; **, $p < 0.01$; ***, $p < 0.001$. **(E)** Htt colocalizes with autophagosomes. Htt expressing cells were pre-permeabilized with 0.1% saponin for 2 min, fixed and immunostained with a myc antibody. **(F)** Quantitation of Htt and LC3 colocalization in C. **(G)** Htt is likely released by lysosome exocytosis. WT HeLa cells expressing GFP or GFP-Htt-Q74 were stained for LAMP1 without permeabilization. **(H)** Quantitation of cell surface Lamp1. The level of Lamp1 per cell in WT GFP is normalized to 1. **(I)** Htt secretion is exosome independent. Conditioned medium from GFP-Htt-Q74 expressing cells was harvested and subjected to differential centrifugation. Equal proportions of each pellet and soluble fraction were analyzed by western blot for actin, TSG101, and GFP. L, whole cell lysate; 10K, 10,000 g 30 min pellet; 100K, 100,000 g 60 min pellet; SN, 100,000 g 60 min supernatant. **(J)** Secreted Htt is not enclosed in membrane structures. Conditioned media from GFP-Htt-Q74 expressing cells was treated with 2.5 μ g/ml proteinase K (PK) for 10 min in the presence or absence of Triton X-100 followed by western blot of GFP. SE, short exposure; LE, long exposure.

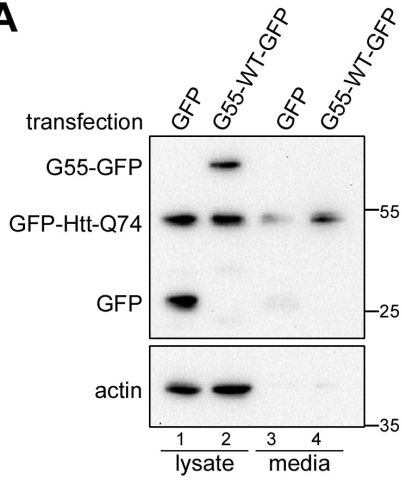
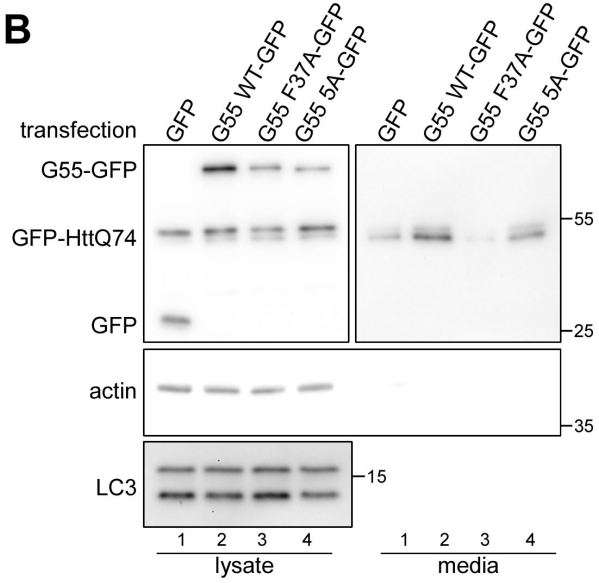
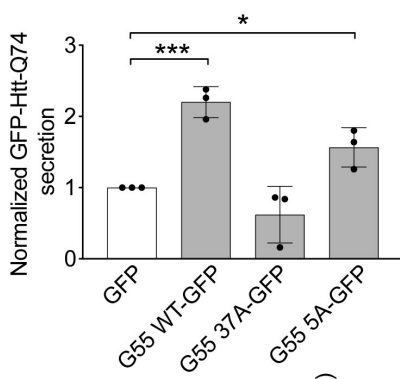
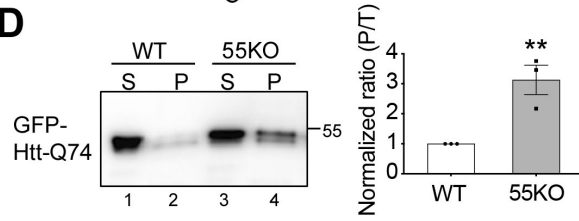
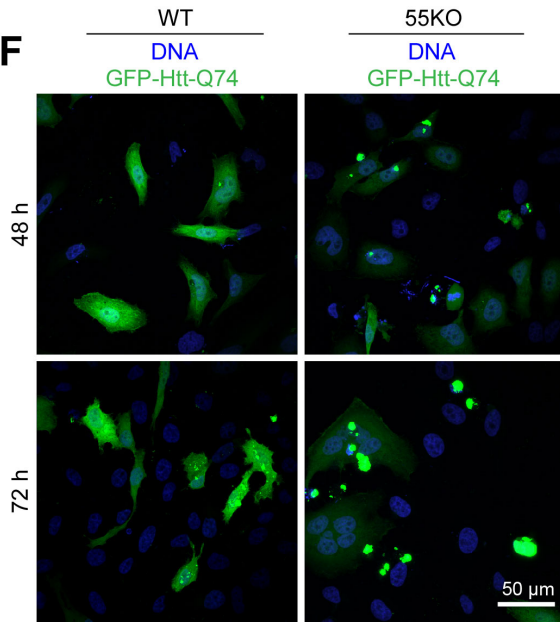
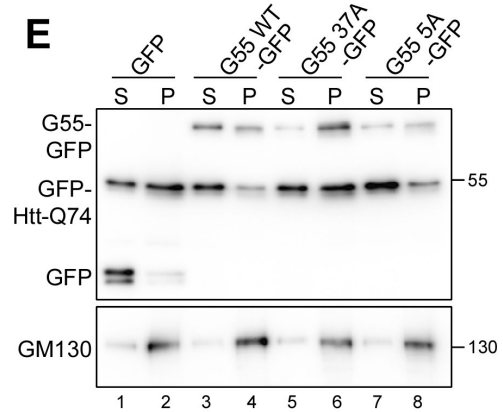
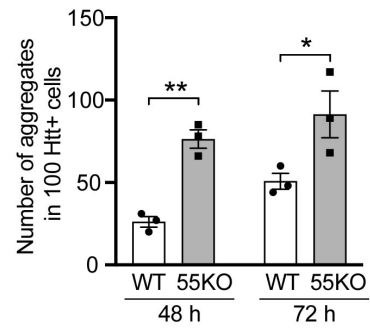
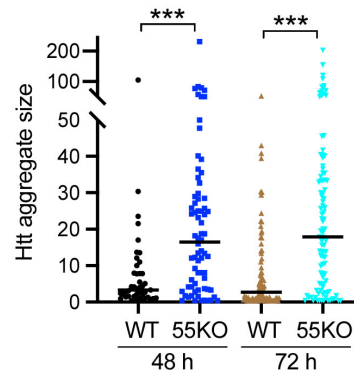
A**B****C****D****F****E****G****H**

Figure 4.5. GRASP55 regulates Htt secretion via autophagy and p23.

(A) GRASP55 expression rescues the defect of Htt secretion in 55KO cells. 55KO cells were first transfected with GFP-Htt-Q74 for 24 h, and then with either GFP or WT GRASP55-GFP for another 24 h. Htt secretion was analyzed by western blot. **(B)** Expression of WT GRASP55 but not its autophagy inactive F37A mutant rescues the defect of Htt secretion in 55KO cells. GFP-Htt-Q74 expressing 55KO cells were transfected with GFP, WT GRASP55-GFP or its F37A or 5A mutant for 24 h. Htt secretion was analyzed by western blot. **(C)** Quantitation of Htt secretion in B. The Htt amount in each conditioned media was normalized to the total Htt amount in the cell lysate in each corresponding condition. **(D)** Htt aggregation is enhanced by 55KO. WT and 55KO cells were transfected by GFP-Htt-Q74 for 48 h and lysed by 0.5% NP-40 followed by centrifugation at 136,000 g at 4°C for 1 h. Supernatant (S) and pellet (P) were loaded at a 1:6 ratio and blotted for GFP. T, total. **(E)** Expression of WT GRASP55 but not F37A reduces Htt aggregation in 55KO cells. 55KO cells transfected as in B were analyzed for Htt aggregation as in D. **(F)** Htt forms more aggregates in 55KO than WT cells. WT and 55KO cells were transfected with GFP-Htt-Q74 for 48 h (upper panels) or 72 h (lower panels), stained for DNA, and imaged. **(G)** Quantification of the number of Htt aggregates in F. **(H)** Quantification of the size of Htt aggregates in F. Htt aggregate size quantification is performed using NIS-Elements software simple ROI editor function. Results are presented as mean \pm SEM; statistical analysis was performed using Student's *t*-test. *, $p < 0.05$; **, $p < 0.01$; ***, $p < 0.001$.

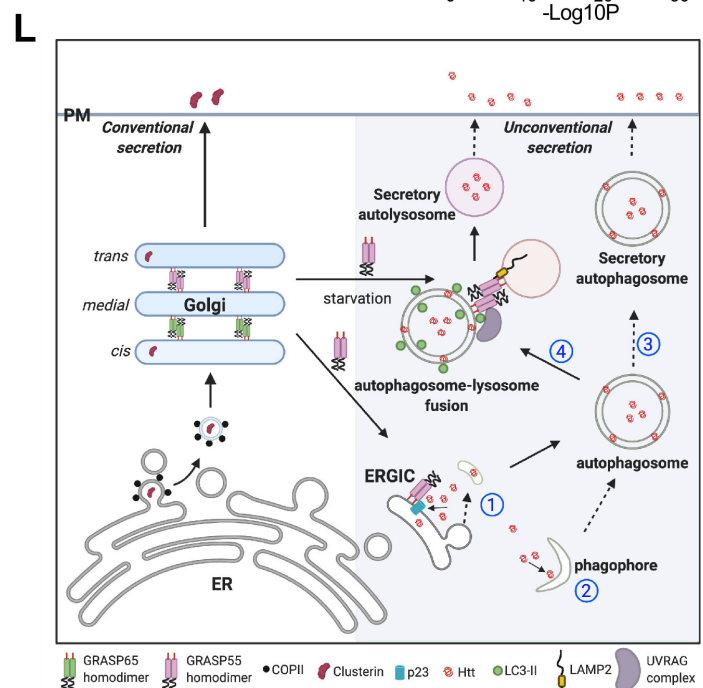
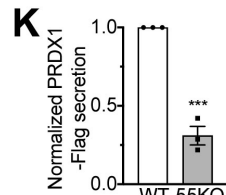
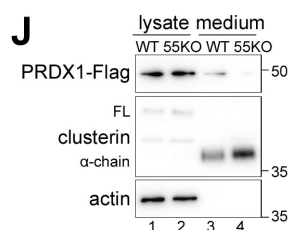
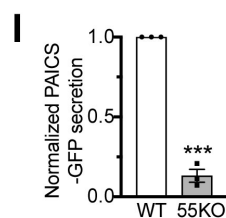
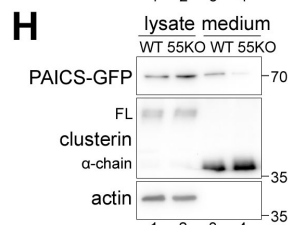
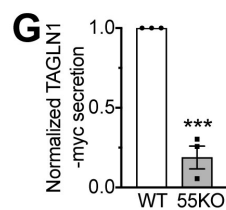
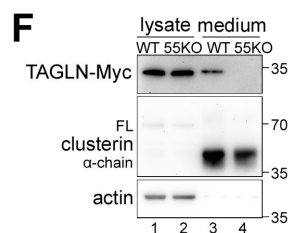
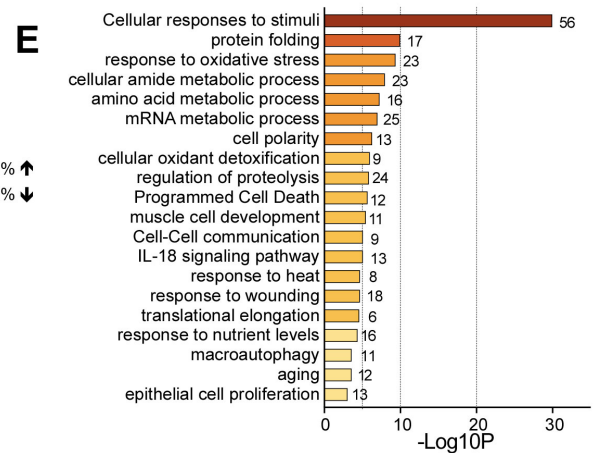
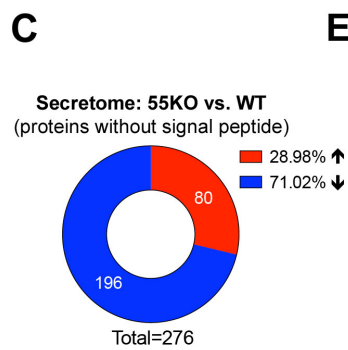
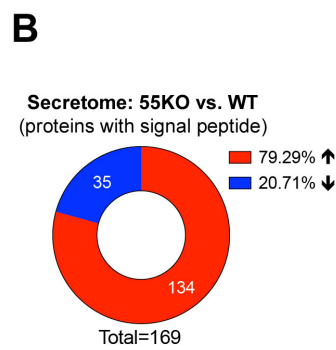
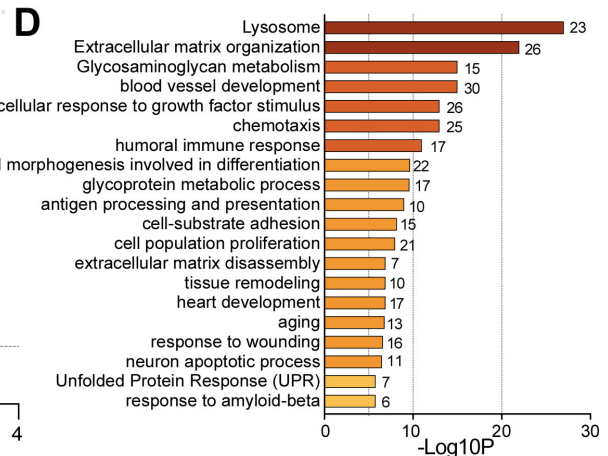
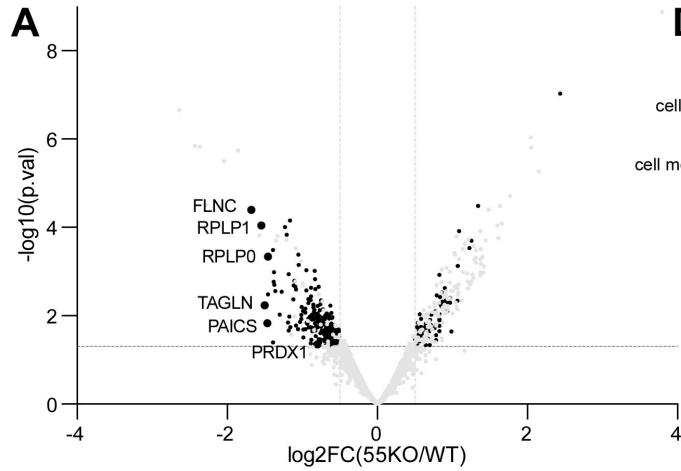
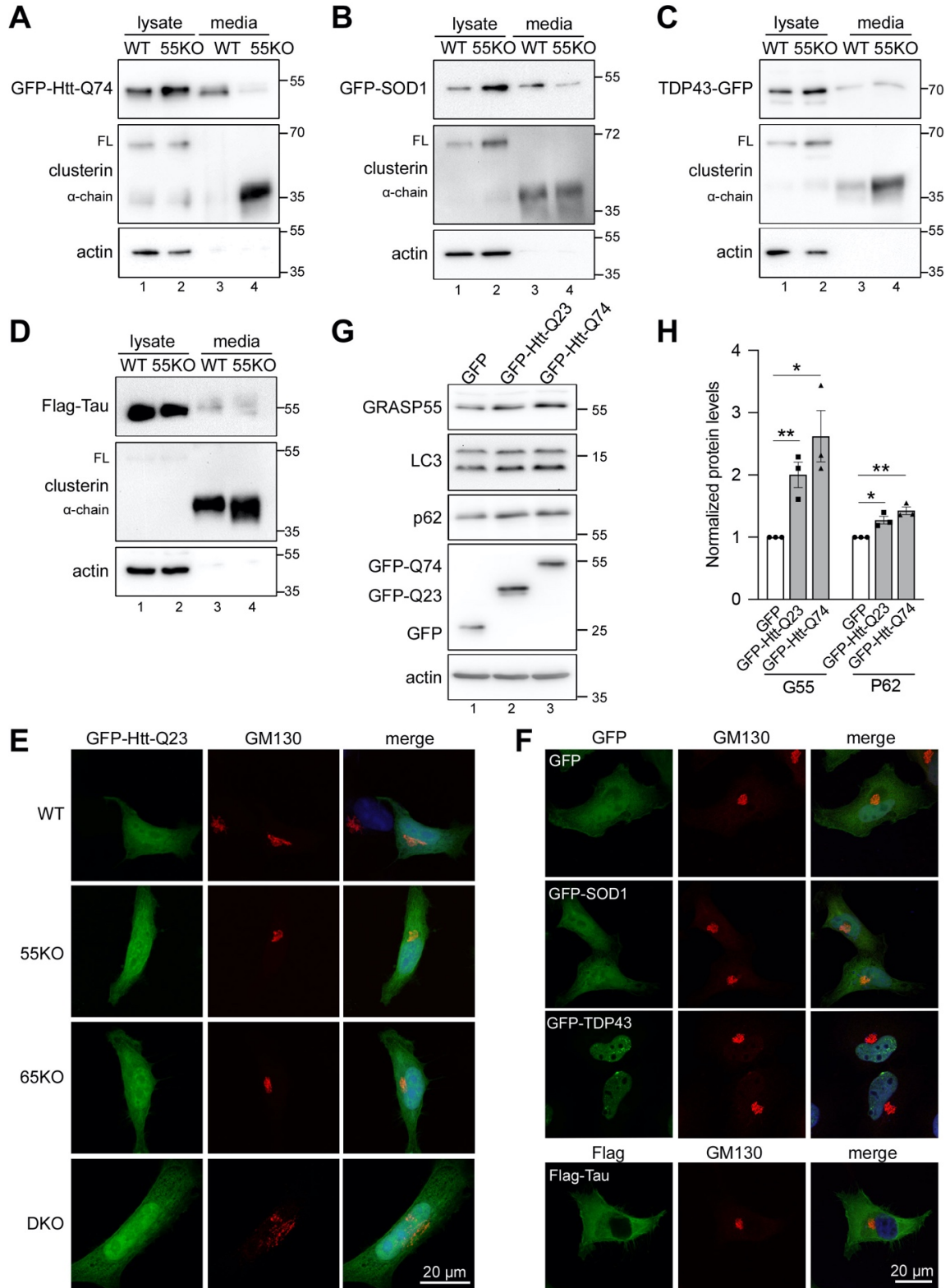


Figure 4.6. Secretome analysis identifies candidate proteins secreted by GRASP55-dependent unconventional secretion.

(A) Volcano plot of candidate proteins in 55KO vs. WT secretome. Black dots represent significantly altered cargoes without signal peptide. All other cargoes are shown in gray. A few top candidates (large black dots) in the unconventional pathway are labeled. (B) GRASP55 KO increases overall conventional secretion. Indicated are the numbers of candidate proteins with ER signal sequences whose secretion was significantly increased or decreased in 55KO compared to WT cells ($|\text{Log}_2\text{FC} (55\text{KO}/\text{WT})| > 0.5$; $p < 0.05$). (C) GRASP55 KO decreases overall unconventional secretion. Number and percentage of candidates with no signal sequence that are increased or reduced in GRASP55 KO secretome compared to WT. (D) Metascape Gene Ontology (GO) enrichment analysis of identified candidate proteins with predicted ER signal sequences whose secretion was significantly altered in 55KO compared to WT ($|\text{Log}_2\text{FC} (55\text{KO}/\text{WT})| > 0.5$; $p < 0.05$). The number of proteins in each pathway is indicated on the right of the graph. (E) GO enrichment analysis of candidate proteins without predicted ER signal sequences whose secretion was significantly altered ($|\text{Log}_2\text{FC} (55\text{KO}/\text{WT})| > 0.5$; $p < 0.05$). (F-K) TAGLN, PAICS and PRDX1 are secreted in a GRASP55 dependent manner. Western blot and quantitation of each protein are shown. Results are presented as mean \pm SEM, with secreted protein normalized to that in the cell lysate; statistical analysis was performed using Student's t test. ***, $p < 0.001$. (L) GRASP55 functions in conventional and unconventional protein secretion. In the conventional secretory pathway (left), secretory proteins such as clusterin are transported from the ER to the Golgi and then to the plasma membrane (PM). GRASP55

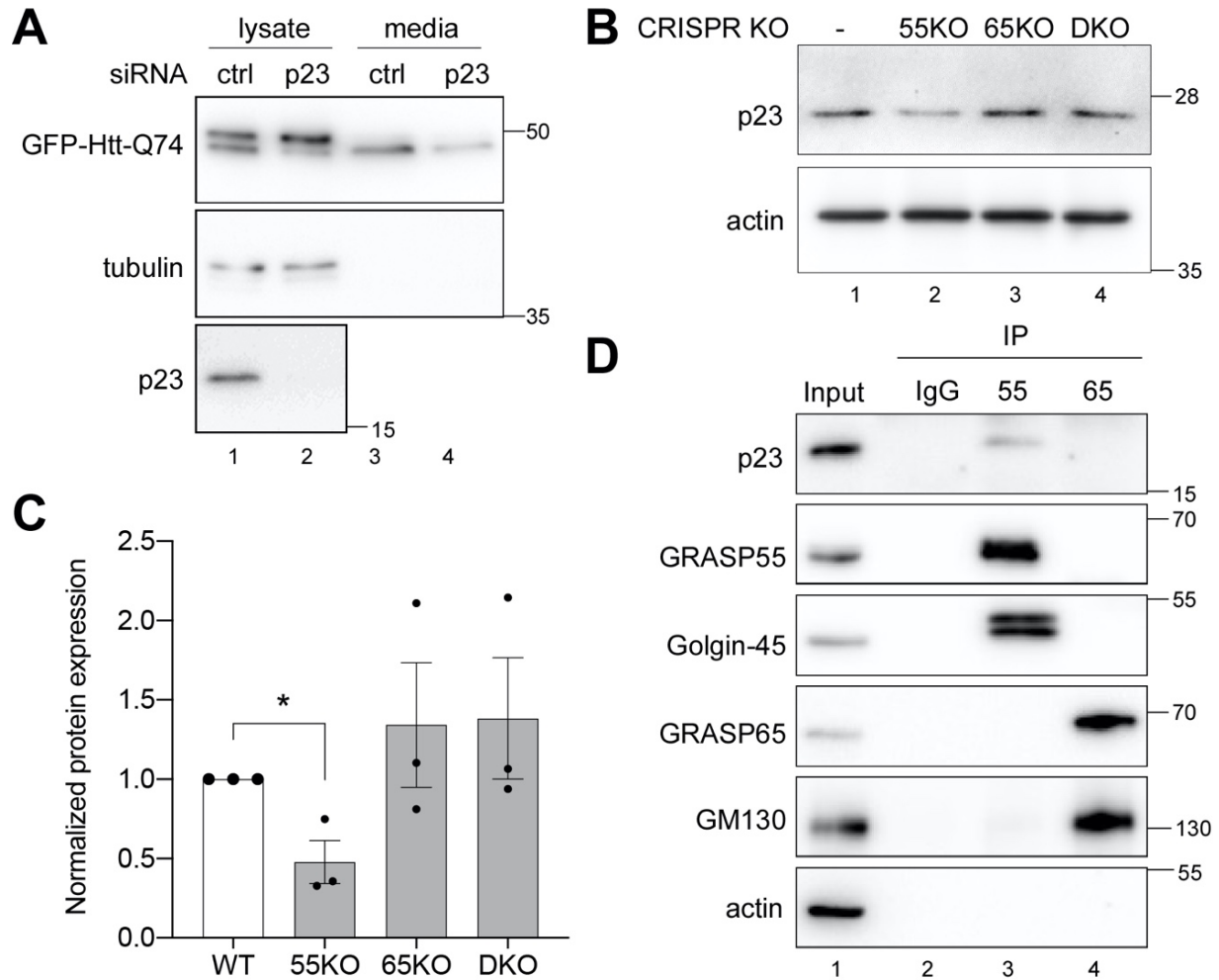
depletion-mediated Golgi unstacking enhances the overall secretion of cargoes in the conventional pathway, as shown in Fig. 4.6C. In the unconventional pathway induced by stress (right), cytosolic proteins such as Htt may enter autophagosomes either via p23/TMED10-mediated translocation into the ERGIC lumen (1), from where it is incorporated into autophagosomes, or by direct sequestration into phagophores from cytosol (2). Htt in autophagosomes can be secreted directly by autophagosome exocytosis (3), or first transferred to lysosomes by membrane fusion (4) and released by lysosome exocytosis. Upon starvation, GRASP55 is relocated from the Golgi to 1) the autophagosome and lysosome interface to facilitate their fusion; 2) ERGIC to interact with p23/TMED10 and regulate cytosolic protein translocation into the lumen. Our results that depletion of TMED10 and GRASP55 both reduce Htt secretion indicate that the dominant pathway for Htt translocation and secretion is 1 and 4.

Supplemental Figures and Figure Legend



Supplemental Figure 4.1. GRASP55 is required for the secretion of a subset of neurotoxic proteins.

(A-B) Htt and SOD1 secretion is reduced by 55KO. WT and 55KO cells were transfected with GFP-Htt-Q74 (A) or GFP-SOD1 (B) and analyzed for secretion by western blot. Note that 55KO reduced the secretion of both Htt and SOD1. **(C-D)** TDP43 and Tau secretion is GRASP55 independent. WT and 55KO cells were transfected with TDP43-GFP (C) or Flag-Tau (D) followed by the analysis of TDP43 and Tau in the cell lysate and conditioned media. **(E)** GFP-Htt-Q23 expression does not disrupt the Golgi structure. GFP-Htt-Q23 was transfected to WT and GRASP KO cells and stained for GM130. The GM130 signal in DKO was increased to better visualize the Golgi morphology. **(F)** Expression of SOD1, TDP43 or Tau does not impact the Golgi structure. WT cells were transfected with indicated constructs and stained for GM130. **(G)** GRASP55 level is upregulated by GFP-Htt-Q74 expression. WT cells expressing GFP, GFP-Htt-Q23 or GFP-Htt-Q74 were analyzed by western blot for indicated proteins. **(H)** Quantification of GRASP55 and p62 levels in G. Results are presented as mean \pm SEM; statistical analysis was performed using Student's *t*-test. *, $p < 0.05$; **, $p < 0.01$.



Supplemental Figure 4.2. GRASP55 facilitates Htt secretion by stabilizing p23.

(A) p23 KD reduces Htt secretion. WT HeLa cells were first transfected with control (ctrl) or p23 siRNA for 36 h and then transfected with GFP-Htt-Q74 for 24 h. Htt secretion was analyzed by western blot. (B) p23 level is reduced in 55KO cells. Western blot analysis of p23 in WT and GRASP KO cells. (C) Quantitation of p23 in B. Results are presented as mean \pm SEM; statistical analysis was performed using Student's *t*-test. *, $p < 0.05$. (D) p23 interacts with GRASP55 but not GRASP65. Endogenous GRASP55 or GRASP65 was immunoprecipitated and their

interaction with p23 was analyzed by western blot. Golgin-45 and GM130 were used as positive controls for GRASP55 and GRASP65, respectively.

Supplemental Table

Supplemental Table 4.1. List of differentially secreted proteins in 55KO vs. WT.

Gene names, fold changes [\log_2FC (55KO/WT media)], p value, and ER signal sequence (SS) are shown. Genes with significant change in 55KO compared to WT ($p < 0.05$) are manually selected and indicated whether they contain ER signal sequences.

| Gene | log ₂ FC (55KO/WT) | p value | SS | Gene | log ₂ FC (55KO/WT) | p value | SS | Gene | log ₂ FC (55KO/WT) | p value | SS | Gene | log ₂ FC (55KO/WT) | p value | SS |
|-----------|-------------------------------|----------|-----|----------|-------------------------------|----------|-----|-----------|-------------------------------|----------|-----|---------|-------------------------------|----------|-----|
| PCOLCE | -2.8400 | 2.25E-07 | yes | RAC1 | -0.8827 | 3.70E-03 | no | EIF3M | -0.8967 | 1.59E-02 | no | DYNC1H1 | -0.5687 | 3.80E-02 | no |
| EPHA7 | -2.4303 | 1.45E-06 | yes | NACA2 | -0.8800 | 3.54E-02 | no | TWF2 | -0.6843 | 1.98E-02 | no | PACSIN2 | -0.5680 | 1.89E-02 | no |
| BGN | -2.3617 | 1.51E-06 | yes | RPS28 | -0.8730 | 1.32E-01 | no | ARHGDI1A | -0.6830 | 3.12E-02 | no | CHMP5 | -0.5673 | 1.07E-01 | no |
| CXCL1 | -2.3307 | 4.04E-03 | yes | EIF1AX | -0.8687 | 9.53E-03 | no | MTRXC | -0.6830 | 3.76E-02 | no | GBP5 | -0.5673 | 1.80E-02 | no |
| SRGN | -2.2757 | 3.13E-05 | yes | NSFL1C | -0.8667 | 1.23E-02 | no | GBP2 | -0.6810 | 9.80E-03 | no | CLTB | -0.5670 | 5.19E-02 | no |
| RARRS2 | -2.1750 | 4.30E-05 | yes | TXLNA | -0.8663 | 2.28E-02 | no | BTF3L4 | -0.6807 | 9.42E-02 | no | SMC3 | -0.5663 | 4.48E-02 | no |
| MAN1A1 | -2.0443 | 3.18E-06 | yes | PRDX5 | -0.8633 | 1.89E-02 | no | ILF3 | -0.6790 | 1.06E-02 | no | FARSA | -0.5660 | 5.65E-02 | no |
| CXCL3 | -1.9083 | 1.49E-02 | yes | RTRAF | -0.8617 | 5.14E-02 | no | RPL11 | -0.6747 | 4.01E-02 | no | PRDX2 | -0.5640 | 1.03E-01 | no |
| CCL2 | -1.8555 | 0.84E-06 | yes | STIP1 | -0.8613 | 2.13E-02 | no | CDKN2A | -0.6737 | 2.12E-02 | no | CAPRN1 | -0.5637 | 7.70E-02 | no |
| TNFAIP6 | -1.8083 | 8.52E-05 | yes | AHSA1 | -0.8513 | 1.12E-02 | no | DDX39B | -0.6723 | 9.11E-03 | no | TRIM28 | -0.5623 | 1.14E-01 | no |
| FLNC | -1.6797 | 4.05E-05 | no | NAP1L1 | -0.8507 | 6.52E-03 | no | PLEC | -0.6713 | 1.65E-02 | no | EPPK1 | -0.5590 | 3.08E-02 | no |
| DCN | -1.5717 | 1.53E-04 | yes | NIBAN2 | -0.8490 | 5.64E-03 | no | ARPC1A | -0.6703 | 9.08E-03 | no | PPA1 | -0.5567 | 3.10E-02 | no |
| RPLP1 | -1.5423 | 9.14E-05 | no | RGS16 | -0.8483 | 1.21E-02 | no | SERPINH1 | -0.6667 | 1.58E-02 | yes | GSN | -0.5563 | 1.63E-02 | yes |
| TAGLN | -1.5010 | 5.84E-03 | no | NCKAP1 | -0.8437 | 8.21E-03 | no | TK1 | -0.6660 | 9.09E-02 | no | TPM2 | -0.5543 | 4.83E-02 | no |
| FAI3C | -1.4683 | 1.49E-02 | no | PCOLCE2 | -0.8417 | 2.15E-02 | yes | USP5 | -0.6623 | 3.08E-02 | no | CAPNS1 | -0.5540 | 3.96E-02 | no |
| CIAPIN1 | -1.4567 | 3.31E-03 | no | NAP1L4 | -0.8383 | 7.34E-03 | no | PDCC8IP | -0.6610 | 2.43E-02 | no | ADAMTS3 | -0.5537 | 1.74E-02 | yes |
| RPLP0 | -1.4550 | 4.61E-04 | no | PDLIM5 | -0.8333 | 9.82E-04 | no | SNRPE | -0.6590 | 4.08E-02 | no | COPB1 | -0.5533 | 4.07E-02 | no |
| RPLP2 | -1.3907 | 3.31E-04 | no | SMU1 | -0.8327 | 4.46E-02 | no | SEPTIN9 | -0.6583 | 1.69E-02 | no | EIF3H | -0.5510 | 2.90E-02 | no |
| SNRPA | -1.3873 | 4.08E-02 | no | HMOX1 | -0.8300 | 1.49E-02 | no | RAB1A | -0.6570 | 2.64E-02 | no | CANT1 | -0.5503 | 5.99E-02 | no |
| TLN1 | -1.3780 | 1.73E-03 | no | ISG15 | -0.8273 | 1.51E-03 | no | SBDS | -0.6567 | 6.68E-02 | no | SPAG9 | -0.5500 | 6.43E-02 | no |
| EIF3J | -1.3760 | 1.05E-03 | no | HNRNP1 | -0.8263 | 2.19E-02 | no | FSTL3 | -0.6563 | 4.42E-02 | yes | IGFBP3 | -0.5493 | 3.58E-01 | no |
| CAP1 | -1.3700 | 2.02E-03 | no | B4GALT1 | -0.8237 | 2.52E-03 | no | PCMT1 | -0.6560 | 2.08E-02 | no | FN1 | -0.5463 | 6.99E-02 | no |
| TFM1 | -1.3590 | 2.79E-03 | no | STIP1 | -0.8217 | 2.95E-02 | no | SERP1 | -0.6553 | 2.12E-02 | no | AKR1C2 | -0.5460 | 2.13E-02 | no |
| TGFBI | -1.3490 | 2.03E-04 | yes | RAP1GDS1 | -0.8190 | 9.19E-03 | no | ACT1 | -0.6540 | 5.06E-02 | no | RTN4 | -0.5453 | 2.71E-02 | no |
| TGFBI | -1.3257 | 1.58E-04 | yes | RPS2 | -0.8173 | 1.70E-02 | no | FBN1 | -0.6540 | 3.86E-02 | yes | CSE1L | -0.5450 | 3.30E-02 | no |
| ST13 | -1.3013 | 9.51E-03 | no | CDC37 | -0.8123 | 9.67E-03 | no | PSME3 | -0.6517 | 2.23E-02 | no | SEPTIN7 | -0.5403 | 9.02E-02 | no |
| EEF1A1 | -1.2753 | 2.87E-03 | no | LGALS1 | -0.8120 | 1.19E-02 | no | RP2A | -0.6503 | 1.00E-01 | no | SNX12 | -0.5393 | 1.21E-01 | no |
| HNRNPA2B1 | -1.2307 | 9.91E-05 | no | NAA50 | -0.8103 | 8.97E-02 | no | LASP1 | -0.6457 | 5.53E-02 | no | FERMT2 | -0.5380 | 5.63E-02 | no |
| B4GALT5 | -1.2100 | 1.92E-04 | yes | EDF1 | -0.8070 | 8.85E-02 | no | GABARAPL2 | -0.6407 | 9.95E-03 | no | SNRPD2 | -0.5363 | 7.58E-02 | no |
| NAMPT | -1.2053 | 1.48E-04 | no | HSP90AB1 | -0.8010 | 1.11E-02 | no | SFN1 | -0.6403 | 1.17E-02 | no | PRDC2 | -0.5360 | 3.70E-02 | no |
| RPSA | -1.1910 | 1.44E-02 | no | EIF2S1 | -0.7993 | 1.34E-02 | no | MAP4 | -0.6397 | 7.47E-02 | no | DCTN2 | -0.5337 | 2.92E-02 | no |
| PRDX6 | -1.1820 | 1.16E-03 | no | NIP7 | -0.7983 | 1.28E-02 | no | ABCE1 | -0.6387 | 6.39E-02 | no | PCNA | -0.5333 | 2.50E-02 | no |
| VIM | -1.1783 | 2.18E-02 | no | PRDX1 | -0.7960 | 4.49E-02 | no | LUC7L2 | -0.6387 | 4.13E-02 | no | UBE2K | -0.5317 | 3.93E-02 | no |
| PABPC1 | -1.1700 | 1.06E-02 | no | DENR | -0.7953 | 6.12E-03 | no | DYNC1L11 | -0.6380 | 2.02E-02 | no | CSDE1 | -0.5297 | 5.14E-02 | no |
| PKM | -1.1630 | 7.12E-05 | no | PTGES3 | -0.7943 | 9.11E-03 | no | SRP9 | -0.6350 | 2.08E-02 | no | PPP6R3 | -0.5290 | 3.97E-02 | no |
| TAGLN2 | -1.1587 | 1.83E-02 | no | G3BP1 | -0.7933 | 1.83E-02 | no | RANBP3 | -0.6330 | 2.87E-02 | no | CITPS2 | -0.5280 | 3.69E-02 | no |
| COL4A2 | -1.1480 | 2.74E-02 | yes | I57B1 | -0.7853 | 3.28E-03 | yes | TFM1 | -0.6323 | 3.52E-02 | no | CSNK1A1 | -0.5253 | 3.70E-02 | no |
| GFR1 | -1.1400 | 4.32E-03 | no | APP | -0.7817 | 3.40E-03 | yes | RRM1 | -0.6307 | 4.87E-02 | no | EIF4A1 | -0.5193 | 5.64E-02 | no |
| MAP2K1 | -1.1120 | 2.10E-03 | no | SEPTIN11 | -0.7797 | 3.39E-02 | no | RPS3 | -0.6267 | 5.82E-02 | no | MESD | -0.5190 | 6.37E-02 | no |
| EIF2A | -1.1043 | 1.63E-03 | no | PTGR1 | -0.7780 | 2.24E-03 | no | CTNNA1 | -0.6263 | 1.76E-02 | no | CLF2 | -0.5187 | 2.46E-02 | no |
| TPST1 | -1.1020 | 1.05E-02 | yes | SPTAN1 | -0.7733 | 1.32E-02 | no | EIF3E | -0.6247 | 2.40E-02 | no | PDIA6 | -0.5187 | 3.14E-02 | yes |
| LCN2 | -1.0927 | 1.71E-03 | yes | NUDT5 | -0.7713 | 1.50E-02 | no | HMGCS1 | -0.6227 | 1.59E-02 | no | CAPZB | -0.5153 | 2.24E-02 | no |
| CDC42 | -1.0900 | 2.25E-03 | no | UFM1 | -0.7657 | 7.54E-03 | no | TARS1 | -0.6223 | 5.97E-03 | no | STAT1 | -0.5153 | 2.42E-02 | no |
| MMIP2 | -1.0853 | 3.03E-04 | yes | SYNCRIP | -0.7653 | 1.05E-02 | no | UBE2N | -0.6223 | 3.94E-02 | no | CAPN1 | -0.5150 | 2.18E-02 | no |
| CACYBP | -1.0830 | 2.57E-03 | no | CHORDC1 | -0.7613 | 3.84E-03 | no | SRP11 | -0.6213 | 2.65E-02 | no | EIF3L | -0.5147 | 7.14E-02 | no |
| AHNAK | -1.0803 | 1.67E-02 | no | FEN1 | -0.7607 | 4.14E-02 | no | CKAP5 | -0.6197 | 4.73E-02 | no | ACTN1 | -0.5133 | 2.07E-02 | no |
| PITPNB | -1.0557 | 2.04E-02 | no | UBE2H | -0.7590 | 5.56E-03 | no | F5 | -0.6187 | 7.97E-02 | no | EZR | -0.5127 | 5.72E-02 | no |
| MAP1B | -1.0500 | 4.17E-04 | no | STAG2 | -0.7587 | 2.51E-02 | no | DDX6 | -0.6147 | 7.50E-02 | no | EIF4A2 | -0.5123 | 5.95E-02 | no |
| GBP1 | -1.0473 | 7.09E-04 | no | GSPT1 | -0.7560 | 3.46E-02 | no | ILF2 | -0.6130 | 1.82E-02 | no | TLL12 | -0.5097 | 5.19E-02 | no |
| CSRP1 | -1.0310 | 1.40E-02 | no | MTAP | -0.7537 | 1.19E-02 | no | KCTD12 | -0.6110 | 1.51E-02 | no | EIF3F | -0.5080 | 6.21E-02 | no |
| HTRA1 | -1.0167 | 5.90E-04 | yes | SEMA4B | -0.7530 | 1.59E-02 | yes | TPM4 | -0.6107 | 7.02E-02 | no | CORO1C | -0.5053 | 4.94E-02 | no |
| HSPBP1 | -1.0123 | 1.20E-02 | no | HSPBP1 | -0.7483 | 1.82E-02 | no | SEB7A | -0.6100 | 8.75E-03 | no | KPNA4 | -0.5040 | 2.85E-02 | no |
| ETF1 | -1.0103 | 9.74E-03 | no | EIF2S2 | -0.7473 | 4.51E-03 | no | EIF2B1 | -0.6090 | 3.02E-02 | no | PSMD4 | -0.5033 | 6.40E-02 | no |
| NUDT21 | -1.0053 | 6.39E-03 | no | LMNA | -0.7413 | 1.49E-02 | no | ATP6V1C1 | -0.6083 | 4.85E-02 | no | TWF1 | -0.5027 | 4.98E-02 | no |
| CXCL8 | -0.9947 | 2.07E-03 | yes | SPTBN1 | -0.7397 | 2.22E-02 | no | ACBD3 | -0.6073 | 3.93E-02 | no | LIF | -0.5010 | 5.05E-02 | no |
| SPOCK1 | -0.9930 | 1.83E-03 | yes | RHOA | -0.7363 | 1.64E-02 | no | MTA2 | -0.6050 | 8.11E-02 | no | EIF4G1 | -0.4993 | 2.72E-02 | no |
| MAPK1 | -0.9873 | 7.81E-03 | no | DCTN3 | -0.7320 | 1.20E-02 | no | EIF5 | -0.6047 | 1.14E-02 | no | UBLCP1 | -0.4983 | 1.10E-01 | no |
| NUDC | -0.9837 | 2.07E-02 | no | GALNT2 | -0.7313 | 4.78E-03 | yes | ATP6V1A | -0.6023 | 4.14E-02 | no | STRAP | -0.4957 | 4.88E-02 | no |
| HSPB1 | -0.9833 | 3.13E-02 | no | ITTM2B | -0.7253 | 1.09E-01 | no | TNPO1 | -0.6020 | 1.12E-02 | no | IGFBP5 | -0.4957 | 1.57E-01 | no |
| SEPTIN2 | -0.9587 | 8.57E-03 | no | TULIN | -0.7233 | 1.43E-02 | no | RP43 | -0.6017 | 7.32E-02 | no | RPS16 | -0.4907 | 1.07E-01 | no |
| PFKFB | -0.9570 | 6.98E-03 | no | RPL12 | -0.7213 | 7.22E-03 | no | MARCOL | -0.6010 | 7.53E-02 | no | AARS1 | -0.4900 | 1.10E-01 | no |
| HNRNPK | -0.9567 | 2.03E-02 | no | MYH9 | -0.7207 | 1.12E-02 | no | BZV1 | -0.6007 | 3.20E-02 | no | PSME1 | -0.4897 | 1.07E-01 | no |
| GCLM | -0.9457 | 2.69E-03 | no | NACA | -0.7143 | 2.48E-02 | no | RAB14 | -0.5977 | 1.10E-02 | no | SNRPB | -0.4890 | 5.64E-02 | no |
| IQGAP1 | -0.9433 | 9.38E-04 | no | APLP2 | -0.7140 | 7.61E-03 | yes | ADAM9 | -0.5933 | 5.37E-02 | no | CDK2 | -0.4883 | 4.81E-02 | no |
| NSUN2 | -0.9410 | 1.45E-02 | no | EIF2S3 | -0.7127 | 5.09E-02 | no | IGSF10 | -0.5900 | 7.39E-02 | no | LARS1 | -0.4880 | 4.83E-02 | no |
| DSTN | -0.9333 | 1.55E-02 | no | RPL23 | -0.7093 | 8.80E-02 | no | MARS1 | -0.5897 | 2.70E-02 | yes | SFB3 | -0.4860 | 7.71E-02 | no |
| BIN1 | -0.9290 | 1.41E-02 | no | XRCC5 | -0.7080 | 3.49E-02 | no | CANX | -0.5883 | 4.27E-02 | no | RPS12 | -0.4857 | 4.19E-01 | no |
| MAP2 | -0.9247 | 1.32E-02 | yes | ENSA | -0.7073 | 1.24E-01 | no | ARPC5L | -0.5877 | 2.11E-02 | no | PSME2 | -0.4857 | 1.30E-01 | no |
| PDC3L3 | -0.9187 | 5.24E-03 | no | TPM3 | -0.7063 | 3.78E-02 | no | DIEXF | -0.5853 | 3.17E-02 | no | ABCF1 | -0.4830 | 3.79E-02 | no |
| MAPRE1 | -0.9183 | 4.19E-03 | no | XRCC6 | -0.7053 | 2.71E-02 | no | CDV3 | -0.5843 | 6.21E-02 | no | NME2P1 | -0.4810 | 3.07E-01 | no |
| DNAJA1 | -0.9180 | 1.17E-02 | no | XPO5 | -0.7033 | 2.15E-02 | no | RP1A | -0.5843 | 6.80E-02 | no | TMOD3 | -0.4810 | 7.33E-02 | no |
| RPS20 | -0.9137 | 1.87E-02 | no | COL4A1 | -0.7010 | 7.59E-02 | no | EEF1G | -0.5837 | 1.63E-02 | no | RPS11 | -0.4793 | 6.41E-02 | no |
| FLN3 | -0.9087 | 5.12E-02 | no | PFND4 | -0.6993 | 1.21E-02 | no | TAX1BP3 | -0.5817 | 1.49E-01 | no | HARS1 | -0.4780 | 7.94E-02 | no |
| FLNA | -0.8943 | 1.05E-02 | no | TUBB4B | -0.6957 | 8.59E-02 | no | SEPHS1 | -0.5777 | 6.99E-02 | no | FKBP4 | -0.4767 | 6.96E-02 | no |
| TUBA4A | -0.8933 | 7.63E-02 | no | OGA | -0.6947 | 1.64E-02 | no | SEC23IP | -0.5773 | 2.15E-01 | no | PABPC4 | -0.4763 | 1.15E-01 | no |
| BTF3 | -0.8927 | 1.85E-02 | no | DNAJC8 | -0.6890 | 4.82E-02 | no | ARHGAP2 | -0.5763 | 8.24E-02 | no | ANXA2 | -0.4750 | 7.35E-02 | no |

| | | | | | | | | | | | |
|----------|---------|----------|---------|---------|----------|----------|---------|----------|----------|---------|----------|
| GCLC | -0.4683 | 7.26E-02 | CCT2 | -0.3790 | 1.03E-01 | CLTC | -0.3223 | 1.18E-01 | CMBL | -0.2497 | 2.71E-01 |
| HAT1 | -0.4683 | 8.17E-02 | FASN | -0.3787 | 7.85E-02 | UBE2D3 | -0.3213 | 1.16E-01 | MSN | -0.2497 | 2.18E-01 |
| HK1 | -0.4630 | 5.10E-02 | FRAS1 | -0.3780 | 1.17E-01 | RDX | -0.3200 | 1.70E-01 | SNRNP200 | -0.2460 | 2.50E-01 |
| ULBP2 | -0.4630 | 8.65E-02 | MCM6 | -0.3780 | 1.98E-01 | RPL8 | -0.3193 | 1.99E-01 | CDK1 | -0.2457 | 2.56E-01 |
| UBE2E1 | -0.4607 | 1.07E-01 | AKAP12 | -0.3747 | 6.43E-02 | CBFB | -0.3187 | 1.86E-01 | PSMC6 | -0.2450 | 3.20E-01 |
| NARS1 | -0.4603 | 5.70E-02 | WARS1 | -0.3747 | 8.76E-02 | GTF2F1 | -0.3187 | 1.89E-01 | NCBP1 | -0.2447 | 3.13E-01 |
| EIF3K | -0.4590 | 1.01E-01 | TCP1 | -0.3730 | 9.33E-02 | RPS24 | -0.3183 | 1.46E-01 | NAA20 | -0.2440 | 2.29E-01 |
| MTHFD1 | -0.4567 | 1.05E-01 | CAPZA2 | -0.3720 | 6.88E-02 | PSMD11 | -0.3143 | 2.01E-01 | PODXL | -0.2417 | 2.84E-01 |
| RANBP1 | -0.4563 | 6.10E-02 | KPNA2 | -0.3703 | 7.75E-02 | HSPB1 | -0.3130 | 1.14E-01 | RPS15A | -0.2417 | 2.59E-01 |
| SF3A3 | -0.4557 | 7.36E-02 | MRC2 | -0.3703 | 1.86E-01 | EEF1E1 | -0.3107 | 2.02E-01 | ARPC1B | -0.2413 | 2.52E-01 |
| SF3A1 | -0.4510 | 1.43E-01 | DPYSL2 | -0.3687 | 2.96E-01 | PLS3 | -0.3107 | 1.36E-01 | CTTN | -0.2410 | 2.21E-01 |
| JPT2 | -0.4507 | 1.08E-01 | EIF4G2 | -0.3680 | 1.21E-01 | CASF8 | -0.3087 | 1.90E-01 | STAT3 | -0.2410 | 2.30E-01 |
| MGAT5 | -0.4497 | 4.53E-02 | EPRS1 | -0.3683 | 1.06E-01 | CDC73 | -0.3093 | 1.48E-01 | APOH | -0.2407 | 4.24E-01 |
| GBA | -0.4460 | 1.38E-01 | AP2B1 | -0.3680 | 1.48E-01 | PNF4 | -0.3093 | 1.42E-01 | VAPB | -0.2367 | 3.35E-01 |
| DYNC1I2 | -0.4457 | 1.58E-01 | EMG1 | -0.3677 | 2.21E-01 | SDF4 | -0.3087 | 2.36E-01 | PTBP1 | -0.2363 | 2.65E-01 |
| PFDN5 | -0.4423 | 4.56E-02 | HSPA4L | -0.3673 | 1.18E-01 | C9orf64 | -0.3080 | 2.16E-01 | LMNB1 | -0.2353 | 3.32E-01 |
| PRKAR2A | -0.4407 | 9.10E-02 | UBFD1 | -0.3673 | 1.98E-01 | GALNT1 | -0.3077 | 1.75E-01 | COPE | -0.2350 | 3.05E-01 |
| LRRFIP1 | -0.4387 | 3.73E-02 | RAD23A | -0.3657 | 1.66E-01 | HDFGL2 | -0.3077 | 1.38E-01 | PRPF | -0.2347 | 2.44E-01 |
| TUBA1C | -0.4367 | 5.21E-02 | DARS1 | -0.3653 | 1.25E-01 | CCT4 | -0.3070 | 1.59E-01 | UBE2V2 | -0.2343 | 4.09E-01 |
| EDL3 | -0.4353 | 1.03E-01 | PSMD6 | -0.3650 | 1.07E-01 | IP09 | -0.3070 | 1.64E-01 | GSTM1 | -0.2320 | 3.55E-01 |
| CCT7 | -0.4347 | 4.97E-02 | SNX2 | -0.3637 | 1.51E-01 | PPP6C | -0.3063 | 1.39E-01 | ASF1A | -0.2310 | 2.25E-01 |
| SERPINE2 | -0.4343 | 9.00E-02 | CAPG | -0.3627 | 2.39E-01 | SMC2 | -0.3060 | 1.48E-01 | VAC14 | -0.2303 | 3.92E-01 |
| CPE | -0.4310 | 7.43E-02 | DNAJA2 | -0.3607 | 1.95E-01 | AP2M1 | -0.3057 | 1.69E-01 | COP59 | -0.2300 | 3.24E-01 |
| ADRM1 | -0.4300 | 1.53E-01 | MSRA | -0.3607 | 1.10E-01 | PPP3R1 | -0.3053 | 1.71E-01 | ANP32A | -0.2287 | 3.84E-01 |
| CTB8 | -0.4283 | 7.19E-02 | EIF3I | -0.3593 | 2.71E-01 | SNRP1 | -0.3030 | 1.64E-01 | AKR1B1 | -0.2263 | 3.13E-01 |
| RANAP1 | -0.4280 | 6.63E-02 | IRTG1 | -0.3583 | 1.36E-01 | PSMD7 | -0.3030 | 1.32E-01 | EXOSC9 | -0.2233 | 3.96E-01 |
| DCAF8 | -0.4267 | 7.00E-02 | NQO1 | -0.3570 | 1.47E-01 | KIF5B | -0.3000 | 2.37E-01 | BCAP31 | -0.2227 | 3.05E-01 |
| NAA15 | -0.4267 | 6.43E-02 | COPS6 | -0.3563 | 1.08E-01 | GFFT1 | -0.2997 | 2.06E-01 | COPS4 | -0.2223 | 2.99E-01 |
| PRPF19 | -0.4263 | 7.76E-02 | BLVRB | -0.3560 | 1.57E-01 | AP2A1 | -0.2957 | 1.80E-01 | PQB1P | -0.2210 | 5.49E-01 |
| METAF2 | -0.4223 | 1.02E-01 | HNRNP1U | -0.3553 | 9.08E-02 | ERO1A | -0.2957 | 1.34E-01 | CSTB | -0.2200 | 3.26E-01 |
| PUF60 | -0.4220 | 4.99E-02 | PCNP | -0.3550 | 9.19E-02 | S100A2 | -0.2953 | 2.00E-01 | UBE2R2 | -0.2197 | 2.50E-01 |
| HNRNPA1 | -0.4207 | 9.28E-02 | RPL35A | -0.3543 | 1.86E-01 | ZPR1 | -0.2897 | 1.67E-01 | XPO1 | -0.2197 | 2.74E-01 |
| CT5 | -0.4160 | 5.16E-02 | MCM5 | -0.3510 | 1.14E-01 | NUM2 | -0.2880 | 2.70E-01 | PRPF7 | -0.2187 | 4.39E-01 |
| CRK | -0.4183 | 1.09E-01 | METRNL | -0.3540 | 2.48E-01 | DCTN1 | -0.2877 | 1.61E-01 | EXOSC7 | -0.2180 | 2.61E-01 |
| TIPRL | -0.4177 | 9.51E-02 | CCT3 | -0.3530 | 1.12E-01 | CKB | -0.2873 | 1.59E-01 | PRMT5 | -0.2160 | 2.68E-01 |
| SGTA | -0.4170 | 1.70E-01 | CALD1 | -0.3527 | 1.04E-01 | EFTUD2 | -0.2873 | 2.22E-01 | XPNPPE1 | -0.2147 | 3.53E-01 |
| BAG2 | -0.4167 | 4.62E-02 | IMPDH2 | -0.3527 | 1.97E-01 | COPB2 | -0.2870 | 1.89E-01 | ECPAS | -0.2137 | 3.02E-01 |
| FABP5 | -0.4167 | 1.18E-01 | SMS | -0.3523 | 8.80E-02 | PSMD2 | -0.2870 | 2.10E-01 | PIN1 | -0.2130 | 3.10E-01 |
| SND1 | -0.4163 | 5.63E-02 | RPS27 | -0.3520 | 2.49E-01 | RUVBL2 | -0.2860 | 2.54E-01 | ARPC2 | -0.2107 | 3.22E-01 |
| CAPZA1 | -0.4157 | 5.96E-02 | SORD | -0.3510 | 1.62E-01 | NUMA2 | -0.2847 | 1.62E-01 | PAM | -0.2090 | 3.99E-01 |
| IFOC | -0.4157 | 8.81E-02 | CCDC96 | -0.3507 | 2.25E-01 | DHK15 | -0.2830 | 2.42E-01 | SUB1 | -0.2087 | 3.71E-01 |
| EIF3A | -0.4140 | 8.92E-02 | DIS3 | -0.3503 | 1.54E-01 | ARNX1 | -0.2820 | 1.51E-01 | SHMT1 | -0.2073 | 4.73E-01 |
| SEC22B | -0.4140 | 1.05E-01 | ARPC4 | -0.3500 | 1.09E-01 | IP07 | -0.2817 | 1.74E-01 | EIF3D | -0.2067 | 3.27E-01 |
| SLC9A3R1 | -0.4133 | 1.87E-01 | CA12 | -0.3500 | 1.48E-01 | SERPINB8 | -0.2810 | 1.91E-01 | FTO | -0.2043 | 3.83E-01 |
| GLRX3 | -0.4120 | 9.49E-02 | B4GAT1 | -0.3497 | 1.90E-01 | EIF4A3 | -0.2807 | 2.96E-01 | COPS8 | -0.2033 | 3.71E-01 |
| NID1 | -0.4117 | 1.00E-01 | L3HYPDH | -0.3487 | 7.68E-02 | TRAP1 | -0.2803 | 1.92E-01 | SERPINE1 | -0.2030 | 3.89E-01 |
| AP2S1 | -0.4100 | 5.23E-02 | VBP1 | -0.3447 | 1.05E-01 | IDE | -0.2797 | 1.98E-01 | MAD2L1 | -0.2027 | 3.88E-01 |
| CNO22 | -0.4100 | 9.12E-02 | MRTG4 | -0.3440 | 1.05E-01 | ANP32E | -0.2793 | 2.89E-01 | COP2 | -0.2013 | 3.16E-01 |
| PM1G | -0.4100 | 9.12E-02 | CUL3 | -0.3440 | 1.40E-01 | MCM4 | -0.2793 | 2.89E-01 | ELP1 | -0.2013 | 3.16E-01 |
| PSMD1 | -0.4097 | 7.76E-02 | SMC4 | -0.3440 | 1.06E-01 | URM1 | -0.2793 | 1.82E-01 | GSTP1 | -0.2010 | 3.18E-01 |
| COL1A1 | -0.4093 | 1.14E-01 | FKBP3 | -0.3437 | 1.56E-01 | ADAM10 | -0.2773 | 3.08E-01 | PSMC2 | -0.2003 | 3.73E-01 |
| BMP6 | -0.4090 | 7.29E-02 | TRIP10 | -0.3413 | 1.17E-01 | COPG1 | -0.2767 | 1.89E-01 | SUMF1 | -0.1997 | 4.51E-01 |
| BZV2 | -0.4090 | 8.63E-02 | ARPC5 | -0.3407 | 1.03E-01 | CHCHD2 | -0.2763 | 3.82E-01 | AGL | -0.1993 | 2.94E-01 |
| PPP3CA | -0.4090 | 1.49E-01 | CUL2 | -0.3400 | 1.32E-01 | TRAPP3 | -0.2757 | 2.26E-01 | RPL29 | -0.1993 | 3.29E-01 |
| CAS2 | -0.4087 | 6.70E-02 | UBA1 | -0.3400 | 1.10E-01 | RPP1R7 | -0.2750 | 1.95E-01 | RPL23A | -0.1973 | 3.66E-01 |
| CLTA | -0.4060 | 7.65E-02 | HDFGL3 | -0.3397 | 1.47E-01 | RPL37 | -0.2743 | 2.02E-01 | NUDCD1 | -0.1973 | 3.40E-01 |
| HMG15 | -0.4047 | 8.15E-02 | CORO1B | -0.3390 | 1.42E-01 | CDH13 | -0.2740 | 2.25E-01 | SETD7 | -0.1967 | 4.10E-01 |
| ACOT7 | -0.4037 | 1.18E-01 | PDLIM7 | -0.3387 | 9.91E-02 | CUL4B | -0.2703 | 2.32E-01 | TXNL4A | -0.1953 | 3.69E-01 |
| ARPC3 | -0.4023 | 8.03E-02 | PSMD3 | -0.3387 | 1.30E-01 | CTPS1 | -0.2690 | 2.27E-01 | DEK | -0.1950 | 3.65E-01 |
| HNRNPD | -0.4013 | 1.36E-01 | PRKAR1A | -0.3383 | 9.73E-02 | ACTR3 | -0.2687 | 2.05E-01 | ANPEP | -0.1937 | 4.52E-01 |
| EEF1D | -0.4000 | 7.02E-02 | RAD23B | -0.3383 | 1.20E-01 | SKP1 | -0.2687 | 2.26E-01 | DCUN1D1 | -0.1937 | 3.69E-01 |
| RAN | -0.3987 | 1.06E-01 | CCL2 | -0.3377 | 1.26E-01 | IP05 | -0.2686 | 1.84E-01 | LRRC47 | -0.1913 | 3.97E-01 |
| HMG13 | -0.3987 | 1.33E-01 | SYAP1 | -0.3377 | 1.16E-01 | EEF1B2 | -0.2680 | 1.84E-01 | KYNU | -0.1903 | 4.25E-01 |
| VARS1 | -0.3990 | 1.14E-01 | SUPT16H | -0.3373 | 1.19E-01 | AKR1C3 | -0.2657 | 1.75E-01 | RCN2 | -0.1900 | 3.22E-01 |
| UBE2L3 | -0.3987 | 7.92E-02 | CLIC4 | -0.3367 | 1.03E-01 | PIR | -0.2650 | 1.71E-01 | CLSTN3 | -0.1893 | 3.72E-01 |
| BCCIP | -0.3977 | 6.50E-02 | ACAT2 | -0.3363 | 1.08E-01 | PRDX3 | -0.2637 | 2.94E-01 | DYNLL1 | -0.1890 | 3.33E-01 |
| ACLY | -0.3970 | 5.53E-02 | AIMP2 | -0.3363 | 1.23E-01 | FLNB | -0.2630 | 2.19E-01 | JPT1 | -0.1877 | 3.91E-01 |
| RSU1 | -0.3957 | 6.04E-02 | ITH4 | -0.3360 | 1.43E-01 | ATIC | -0.2627 | 1.81E-01 | UBE2M | -0.1853 | 4.62E-01 |
| TP53BP1 | -0.3940 | 7.38E-02 | RANBP6 | -0.3360 | 1.23E-01 | ATC | -0.2627 | 3.75E-01 | CAND1 | -0.1850 | 3.39E-01 |
| PR | -0.3937 | 1.23E-01 | GRB2 | -0.3357 | 1.77E-02 | GFS1 | -0.2603 | 2.47E-02 | PAPSS2 | -0.1850 | 4.75E-01 |
| GCN1 | -0.3930 | 3.41E-01 | FARS5 | -0.3347 | 1.29E-01 | PDCD6 | -0.2597 | 2.04E-01 | PWP1 | -0.1843 | 4.41E-01 |
| LYPLA1 | -0.3917 | 1.15E-01 | HMG13 | -0.3340 | 1.37E-01 | PFN1 | -0.2590 | 2.00E-01 | AIDA | -0.1837 | 3.51E-01 |
| UQCQRH | -0.3917 | 1.24E-01 | NMT1 | -0.3333 | 1.20E-01 | USP4 | -0.2580 | 2.27E-01 | RPS6 | -0.1837 | 3.37E-01 |
| RUVBL1 | -0.3903 | 9.78E-02 | ZC3H15 | -0.3330 | 1.34E-01 | VCL7 | -0.2577 | 2.33E-01 | SIRPA | -0.1833 | 5.48E-01 |
| ACTR1A | -0.3900 | 9.51E-02 | ZRANB2 | -0.3327 | 1.91E-01 | NCAPG | -0.2573 | 1.89E-01 | TNC | -0.1833 | 4.69E-01 |
| LIPR1 | -0.3893 | 3.35E-01 | KTN1 | -0.3327 | 1.63E-01 | HUWE1 | -0.2570 | 2.19E-01 | PSMD12 | -0.1820 | 4.25E-01 |
| MYH14 | -0.3887 | 1.15E-01 | ATXN10 | -0.3313 | 2.24E-01 | USP14 | -0.2563 | 2.41E-01 | FDP5 | -0.1817 | 3.86E-01 |
| QARS1 | -0.3883 | 7.24E-02 | TIMP2 | -0.3310 | 2.11E-01 | ARL6IP5 | -0.2560 | 2.12E-01 | CBX5 | -0.1803 | 4.38E-01 |
| TP53I3 | -0.3880 | 9.42E-02 | INPP1 | -0.3307 | 1.09E-01 | LAP3 | -0.2553 | 2.35E-01 | GDA | -0.1803 | 4.36E-01 |
| FAM50A | -0.3873 | 1.40E-01 | CHD4 | -0.3293 | 1.45E-01 | MCAM | -0.2540 | 3.56E-01 | PSMC4 | -0.1803 | 5.11E-01 |
| MAPK14 | -0.3857 | 1.20E-01 | PFN2 | -0.3287 | 1.01E-01 | ASNS | -0.2530 | 2.73E-01 | C3 | -0.1797 | 4.62E-01 |
| CTG6A | -0.3850 | 7.78E-02 | PRCQL | -0.3277 | 1.01E-01 | BAG3 | -0.2527 | 2.38E-01 | SMC1A | -0.1790 | 4.04E-01 |
| ASS1 | -0.3847 | 1.59E-01 | CARS1 | -0.3250 | 1.18E-01 | ATPBV1E1 | -0.2513 | 2.37E-01 | TGFB1 | -0.1783 | 6.11E-01 |
| PDE3A | -0.1777 | 3.70E-01 | HMG13 | -0.1087 | 5.71E-01 | SRM | -0.0380 | 8.79E-01 | ECAM | 0.0203 | 9.25E-01 |
| PLS1 | -0.1773 | 3.96E-01 | RABGGTB | -0.1070 | 5.91E-01 | CD44 | -0.0357 | 9.02E-01 | PCBD1 | 0.0203 | 9.28E-01 |
| COP3 | -0.1767 | 3.93E-01 | PM2 | -0.1050 | 6.15E-01 | PFND2 | -0.0357 | 8.58E-01 | YWHAG | 0.0207 | 9.33E-01 |
| LRRC59 | -0.1767 | 5.44E-01 | LRBA | -0.1027 | 6.40E-01 | GMFB | -0.0343 | 8.64E-01 | NBDY | 0.0217 | 9.32E-01 |
| ACTR2 | -0.1763 | 4.27E-01 | DDX1 | -0.1020 | 6.15E-01 | VAMP8 | -0.0343 | 8.92E-01 | TKFC | 0.0217 | 9.10E-01 |
| PRSS23 | -0.1753 | 4.07E-01 | ITPA | -0.1017 | 6.24E-01 | SEC23B | -0.0343 | 8.52E-01 | PCSK9 | 0.0237 | 9.10E-01 |
| KARS1 | -0.1747 | 3.80E-01 | GARS1 | -0.0993 | 6.09E-01 | LSM 8.00 | -0.0337 | 8.70E-01 | BSGAT3 | 0.0240 | 9.18E-01 |
| GMPT7 | -0.1731 | 3.65E-01 | SCY1 | -0.0983 | 6.02E-01 | NUMA1 | -0.0317 | 8.95E-01 | FKBP1A | 0.0243 | 8.96E-01 |
| CLUH | -0.1717 | 4.35E-01 | VAPA | -0.0983 | 6.50E-01 | TBCD | -0.0310 | 8.70E-01 | TNPO3 | 0.0243 | 9.00E-01 |
| RPS9 | -0.1707 | 4.18E-01 | HSPH1 | -0.0973 | 6.39E-01 | USP7 | -0.0307 | 8.68E-01 | RBP6 | 0.0250 | 9.07E-01 |
| SCRN3 | | | | | | | | | | | |

| | | | | | | | | | | | |
|---------|---------|----------|----------|---------|----------|----------|---------|----------|----------|--------|----------|
| RPL19 | -0.1573 | 5.16E-01 | FBN2 | -0.0873 | 7.90E-01 | ANP32B | -0.0190 | 9.44E-01 | PGAM1 | 0.0393 | 8.55E-01 |
| STC2 | -0.1573 | 4.71E-01 | PAFAH1B1 | -0.0870 | 6.43E-01 | CHAC2 | -0.0177 | 9.41E-01 | GSR | 0.0397 | 8.73E-01 |
| GALNT10 | -0.1570 | 4.77E-01 | TOP2A | -0.0850 | 6.74E-01 | ANKFY1 | -0.0173 | 9.32E-01 | DUT | 0.0403 | 8.50E-01 |
| RPL34 | -0.1563 | 4.59E-01 | COPPS | -0.0847 | 6.48E-01 | RRBP1 | -0.0167 | 9.41E-01 | PAF1 | 0.0407 | 8.37E-01 |
| UBE2E3 | -0.1557 | 4.92E-01 | IPO11 | -0.0840 | 7.04E-01 | ROCK2 | -0.0153 | 9.34E-01 | PRPF8 | 0.0407 | 8.30E-01 |
| NELL2 | -0.1553 | 5.36E-01 | TDPI | -0.0837 | 6.74E-01 | HMBS | -0.0147 | 9.40E-01 | NAA10 | 0.0413 | 8.42E-01 |
| USP39 | -0.1553 | 5.54E-01 | PPP2R5D | -0.0820 | 6.89E-01 | PSMC1 | -0.0143 | 9.53E-01 | UAP1 | 0.0420 | 8.28E-01 |
| HEBP2 | -0.1550 | 4.65E-01 | LGALS3 | -0.0810 | 6.71E-01 | PRRC2C | -0.0140 | 9.44E-01 | RPS3A | 0.0423 | 8.43E-01 |
| HSPA1B | -0.1537 | 4.18E-01 | SERPINC1 | -0.0797 | 7.10E-01 | VPS29 | -0.0140 | 9.43E-01 | ACTN4 | 0.0427 | 8.25E-01 |
| MCM3 | -0.1520 | 4.22E-01 | ALDOC | -0.0787 | 7.42E-01 | GD11 | -0.0127 | 9.54E-01 | PCID2 | 0.0433 | 8.26E-01 |
| BMS1 | -0.1517 | 5.16E-01 | RAD50 | -0.0787 | 6.85E-01 | GNPTG | -0.0127 | 9.59E-01 | RPL31 | 0.0440 | 8.29E-01 |
| AARS01 | -0.1510 | 4.88E-01 | SLC7A5 | -0.0783 | 7.34E-01 | SERPINB9 | -0.0120 | 9.55E-01 | GART | 0.0453 | 8.25E-01 |
| COPA | -0.1510 | 4.22E-01 | SNRNP70 | -0.0783 | 7.26E-01 | HYOU1 | -0.0107 | 9.56E-01 | NPC2 | 0.0460 | 8.42E-01 |
| CD46 | -0.1500 | 5.35E-01 | BPNT1 | -0.0770 | 7.18E-01 | OLA1 | -0.0107 | 9.56E-01 | UBE2I | 0.0467 | 8.15E-01 |
| BOLA2 | -0.1493 | 5.37E-01 | EPHB2 | -0.0770 | 7.33E-01 | BLVRA | -0.0090 | 9.64E-01 | TXNRD1 | 0.0477 | 8.32E-01 |
| PSMD14 | -0.1490 | 5.09E-01 | MARCKS | -0.0743 | 7.05E-01 | SMARCC2 | -0.0077 | 9.67E-01 | VPS26A | 0.0500 | 7.88E-01 |
| CKD6 | -0.1483 | 5.32E-01 | SDCBP | -0.0740 | 7.38E-01 | DHX9 | -0.0077 | 9.74E-01 | PDGFRL | 0.0503 | 8.50E-01 |
| TXN | -0.1473 | 5.47E-01 | PCPN | -0.0740 | 7.95E-01 | TXNDC5 | -0.0070 | 9.74E-01 | DKC | 0.0527 | 8.18E-01 |
| OGFR | -0.1470 | 5.05E-01 | MATR3 | -0.0730 | 6.97E-01 | MCM7 | -0.0070 | 9.75E-01 | PAFAH1B3 | 0.0530 | 8.38E-01 |
| ACHY | -0.1467 | 4.44E-01 | SRP14 | -0.0723 | 6.94E-01 | SERF2 | -0.0067 | 9.72E-01 | ESYT1 | 0.0530 | 7.96E-01 |
| WDR31B | -0.1463 | 4.66E-01 | SLTM | -0.0720 | 7.13E-01 | COLGALT1 | -0.0053 | 9.79E-01 | WDR61 | 0.0537 | 7.79E-01 |
| PRIM1 | -0.1460 | 4.93E-01 | OLR1 | -0.0713 | 7.96E-01 | IRGQ | -0.0050 | 9.81E-01 | CCDC25 | 0.0540 | 7.98E-01 |
| RAD1 | -0.1457 | 4.48E-01 | UBE2T | -0.0690 | 7.68E-01 | DBB2 | -0.0030 | 9.87E-01 | CSOX2 | 0.0540 | 7.97E-01 |
| FBXO3 | -0.1453 | 5.17E-01 | HSP90AA1 | -0.0673 | 7.31E-01 | ALYREF | -0.0010 | 9.97E-01 | CKAP4 | 0.0543 | 8.02E-01 |
| CREDL2 | -0.1450 | 5.86E-01 | DBN1 | -0.0670 | 7.44E-01 | PPP5C | -0.0007 | 9.98E-01 | SRSF4 | 0.0547 | 7.75E-01 |
| CLIF1 | -0.1447 | 6.43E-01 | AKP1 | -0.0673 | 7.80E-01 | PKC | 0.0000 | 1.00E+00 | GNPDS | 0.0553 | 7.29E-01 |
| UFC1 | -0.1417 | 4.80E-01 | CCN1 | -0.0657 | 7.43E-01 | FKBP5 | 0.0007 | 9.97E-01 | GNPDA2 | 0.0553 | 7.86E-01 |
| CCDC86 | -0.1410 | 4.59E-01 | DYNLL2 | -0.0657 | 7.34E-01 | IAH1 | 0.0017 | 9.94E-01 | TTC1 | 0.0570 | 8.02E-01 |
| ALDH9A1 | -0.1407 | 4.60E-01 | LMNB2 | -0.0657 | 7.70E-01 | DDAH1 | 0.0023 | 9.92E-01 | ITGB1 | 0.0580 | 8.48E-01 |
| TIGAR | -0.1397 | 4.88E-01 | EEF1A2 | -0.0647 | 8.06E-01 | RPL30 | 0.0027 | 9.91E-01 | RSL1D1 | 0.0587 | 7.73E-01 |
| JUP | -0.1390 | 5.28E-01 | PPIC | -0.0630 | 7.99E-01 | MTDH | 0.0037 | 9.85E-01 | CYRIB | 0.0597 | 7.52E-01 |
| PTRHD1 | -0.1377 | 4.81E-01 | UBE2A | -0.0620 | 7.51E-01 | RPL22 | 0.0040 | 9.83E-01 | CREG1 | 0.0600 | 8.49E-01 |
| NAK25 | -0.1367 | 5.08E-01 | DXR3 | -0.0627 | 7.73E-01 | TXNL1 | 0.0043 | 9.89E-01 | TBCA | 0.0600 | 7.88E-01 |
| ELOC | -0.1363 | 4.99E-01 | PSMD5 | -0.0593 | 7.75E-01 | HNRNPUL2 | 0.0047 | 9.80E-01 | COL12A1 | 0.0607 | 7.71E-01 |
| CHSY3 | -0.1353 | 5.96E-01 | SHPK | -0.0590 | 7.71E-01 | PSMD8 | 0.0060 | 9.75E-01 | PDIA3 | 0.0610 | 8.09E-01 |
| RPL4 | -0.1353 | 6.03E-01 | LRP1B | -0.0587 | 7.84E-01 | MET | 0.0070 | 9.75E-01 | ZFYV91 | 0.0610 | 8.90E-01 |
| SEC13 | -0.1343 | 5.11E-01 | VPS35 | -0.0583 | 7.56E-01 | LTBP1 | 0.0077 | 9.81E-01 | PPP4C | 0.0610 | 7.77E-01 |
| HINT1 | -0.1337 | 5.97E-01 | PRMT1 | -0.0577 | 7.97E-01 | ETP1 | 0.0077 | 9.70E-01 | C1S | 0.0623 | 8.21E-01 |
| RARS1 | -0.1337 | 5.19E-01 | CRIM1 | -0.0573 | 7.70E-01 | PARP1 | 0.0080 | 9.62E-01 | PSMG3 | 0.0627 | 7.47E-01 |
| FPAT | -0.1333 | 5.32E-01 | RPL10B | -0.0563 | 7.83E-01 | LRNPAP1 | 0.0087 | 9.69E-01 | GYL1 | 0.0630 | 7.51E-01 |
| ARL6IP1 | -0.1297 | 5.01E-01 | ADPRS | -0.0543 | 8.19E-01 | CTSD | 0.0100 | 9.66E-01 | RECK | 0.0630 | 7.85E-01 |
| ARH2 | -0.1267 | 5.37E-01 | PIIB | -0.0533 | 8.40E-01 | EEA1 | 0.0100 | 9.58E-01 | TOP1100 | 0.0657 | 7.46E-01 |
| FAF1 | -0.1250 | 5.51E-01 | CNTNAP4 | -0.0523 | 8.12E-01 | LAMA5 | 0.0103 | 9.69E-01 | MCTS1 | 0.0677 | 7.32E-01 |
| SSNA1 | -0.1247 | 6.70E-01 | ID1 | -0.0523 | 8.00E-01 | AIMP1 | 0.0107 | 9.58E-01 | ATOX1 | 0.0687 | 7.43E-01 |
| EIFS5 | -0.1223 | 5.29E-01 | NEDD8 | -0.0520 | 8.16E-01 | GSTO1 | 0.0107 | 9.65E-01 | XPO7 | 0.0693 | 7.55E-01 |
| NAGPA | -0.1210 | 6.03E-01 | GLG1 | -0.0483 | 8.35E-01 | PROCR | 0.0110 | 9.70E-01 | ADSS2 | 0.0700 | 7.19E-01 |
| RPL38 | -0.1207 | 6.42E-01 | TBCB | -0.0483 | 8.35E-01 | MK167 | 0.0113 | 9.58E-01 | SRR1 | 0.0710 | 7.54E-01 |
| HSRST2 | -0.1187 | 6.42E-01 | ACTN2 | -0.0480 | 8.20E-01 | BRX1 | 0.0113 | 9.58E-01 | MTFN | 0.0717 | 7.68E-01 |
| CBX1 | -0.1183 | 5.60E-01 | ALDOA | -0.0470 | 8.21E-01 | DNPH1 | 0.0143 | 9.52E-01 | NTSDC1 | 0.0720 | 7.44E-01 |
| DDX39A | -0.1173 | 6.66E-01 | OTUB1 | -0.0467 | 8.28E-01 | PPP2R2A | 0.0147 | 9.40E-01 | COL5A1 | 0.0730 | 7.37E-01 |
| PSMC5 | -0.1163 | 6.33E-01 | RTF2 | -0.0460 | 8.87E-01 | NANS | 0.0163 | 9.31E-01 | VASN | 0.0737 | 7.53E-01 |
| UNC45A | -0.1157 | 6.05E-01 | OVCA2 | -0.0457 | 8.32E-01 | PIN4 | 0.0190 | 9.21E-01 | ADSL | 0.0747 | 7.07E-01 |
| HNRNPC | -0.1147 | 5.40E-01 | EML4 | -0.0453 | 8.33E-01 | INH3 | 0.0193 | 9.25E-01 | SH3BGR3 | 0.0750 | 7.68E-01 |
| EIF4B | -0.1143 | 5.70E-01 | PSPH | -0.0447 | 8.32E-01 | SYCP2 | 0.0193 | 9.44E-01 | ASL | 0.0763 | 7.39E-01 |
| YARS1 | -0.1137 | 6.16E-01 | NCL | -0.0427 | 8.27E-01 | CDK2 | 0.0207 | 9.25E-01 | SERPINC1 | 0.0767 | 7.68E-01 |
| CLF1 | -0.1120 | 5.58E-01 | RNMT | -0.0407 | 8.50E-01 | TCOF1 | 0.0197 | 9.20E-01 | RBM8A | 0.0797 | 6.85E-01 |
| PSMC3 | -0.1090 | 6.48E-01 | CLIC1 | -0.0380 | 8.60E-01 | KIF6P | 0.0200 | 9.22E-01 | NAXD | 0.0807 | 7.33E-01 |
| RPS14 | 0.0820 | 7.11E-01 | RPL21 | 0.1410 | 5.20E-01 | H3-3A | 0.2123 | 2.99E-01 | NOTCH2 | 0.2747 | 1.80E-01 |
| RBMX | 0.0820 | 6.95E-01 | TFG | 0.1420 | 5.72E-01 | TFRF | 0.2147 | 4.37E-01 | TBL1XR1 | 0.2747 | 2.27E-01 |
| FAT4 | 0.0840 | 7.01E-01 | NUDT2 | 0.1440 | 5.64E-01 | GYG1 | 0.2150 | 3.31E-01 | SDHA | 0.2750 | 2.24E-01 |
| SAE1 | 0.0840 | 6.74E-01 | NUFUFAB1 | 0.1443 | 5.83E-01 | VTN | 0.2153 | 3.06E-01 | GL01 | 0.2757 | 2.25E-01 |
| OLFML2A | 0.0843 | 7.53E-01 | IGFBP1 | 0.1447 | 5.44E-01 | MT2A | 0.2160 | 5.24E-01 | NIF3L1 | 0.2761 | 2.53E-01 |
| YWHA8 | 0.0843 | 6.92E-01 | ECTE1 | 0.1460 | 5.18E-01 | MYG1 | 0.2160 | 3.16E-01 | TOR1B | 0.2757 | 2.53E-01 |
| RAB1F | 0.0843 | 6.89E-01 | PPT1 | 0.1477 | 5.64E-01 | SUMF2 | 0.2163 | 3.67E-01 | NUDT1 | 0.2760 | 2.31E-01 |
| CUL1 | 0.0847 | 6.49E-01 | THRAP3 | 0.1487 | 4.69E-01 | CTH | 0.2167 | 3.48E-01 | SEMA3F | 0.2770 | 2.32E-01 |
| WDR1 | 0.0850 | 7.20E-01 | NME1 | 0.1497 | 4.84E-01 | VEGFA | 0.2177 | 2.61E-01 | GNPNAT1 | 0.2773 | 1.58E-01 |
| CARHSP1 | 0.0873 | 6.68E-01 | PLXDC2 | 0.1500 | 5.34E-01 | COCH | 0.2180 | 3.88E-01 | NPEPPS | 0.2773 | 2.49E-01 |
| DTD1 | 0.0897 | 6.63E-01 | YWHAE | 0.1507 | 5.04E-01 | KYAT1 | 0.2183 | 4.21E-01 | CTSS | 0.2787 | 2.07E-01 |
| COA4 | 0.0907 | 6.58E-01 | RACK1 | 0.1517 | 4.78E-01 | CRYZ1 | 0.2193 | 3.44E-01 | RPL13 | 0.2790 | 2.79E-01 |
| H11-10 | 0.0907 | 6.45E-01 | SMPP1 | 0.1517 | 4.97E-01 | RPL26 | 0.2203 | 2.95E-01 | SERPINB6 | 0.2790 | 2.42E-01 |
| ACO1 | 0.0910 | 7.21E-01 | GM2A | 0.1527 | 5.86E-01 | CNDP2 | 0.2227 | 3.51E-01 | FAT1 | 0.2797 | 2.09E-01 |
| DDR1 | 0.0927 | 6.79E-01 | PGM2 | 0.1530 | 4.73E-01 | PDXP | 0.2227 | 2.98E-01 | IHH | 0.2810 | 3.01E-01 |
| MANF | 0.0933 | 6.14E-01 | PRKDC | 0.1533 | 4.92E-01 | PSAT1 | 0.2237 | 3.74E-01 | PSMB7 | 0.2833 | 2.65E-01 |
| UBA2 | 0.0933 | 6.23E-01 | NOP2 | 0.1537 | 4.88E-01 | CAVIN3 | 0.2240 | 2.64E-01 | DDX21 | 0.2850 | 2.30E-01 |
| SOD2 | 0.0937 | 7.52E-01 | OTL1 | 0.1540 | 4.66E-01 | YWHAZ | 0.2240 | 3.53E-01 | EED | 0.2860 | 2.59E-01 |
| DKK3.00 | 0.0943 | 6.79E-01 | UCHL3 | 0.1543 | 4.16E-01 | PUDP | 0.2243 | 3.49E-01 | PURA | 0.2867 | 1.68E-01 |
| AAMP | 0.0950 | 6.89E-01 | RPS9 | 0.1550 | 5.15E-01 | DCD | 0.2247 | 4.65E-01 | F2 | 0.2870 | 2.53E-01 |
| SDC4 | 0.0950 | 7.94E-01 | UPF3B | 0.1553 | 4.67E-01 | PSMB3 | 0.2247 | 3.77E-01 | LDHB | 0.2883 | 2.11E-01 |
| IGF2R | 0.0957 | 6.94E-01 | NUCKS1 | 0.1563 | 5.00E-01 | RCC2 | 0.2257 | 2.75E-01 | HTATSF1 | 0.2887 | 1.70E-01 |
| CRLF1 | 0.0973 | 6.93E-01 | KYAT3 | 0.1567 | 5.33E-01 | PRDX4 | 0.2277 | 3.52E-01 | MDH1 | 0.2893 | 2.36E-01 |
| CBX3 | 0.1000 | 6.00E-01 | RRP9 | 0.1573 | 3.99E-01 | PSMB8 | 0.2277 | 2.89E-01 | REXO2 | 0.2903 | 1.86E-01 |
| CSTF1 | 0.1000 | 6.07E-01 | RPL7A | 0.1617 | 5.76E-01 | SRSF5 | 0.2277 | 3.07E-01 | RARRRES1 | 0.2910 | 3.06E-01 |
| PAPPA | 0.1003 | 6.82E-01 | DSC2 | 0.1630 | 5.48E-01 | CRKL | 0.2280 | 3.18E-01 | ENOPH1 | 0.2927 | 2.00E-01 |
| SRP19 | 0.1010 | 7.24E-01 | PNP | 0.1640 | 4.80E-01 | SGCE | 0.2280 | 3.25E-01 | CHD1 | 0.2933 | 1.79E-01 |
| PTGFRN | 0.1013 | 6.83E-01 | LZTS1 | 0.1660 | 5.08E-01 | DNPEP | 0.2283 | 3.09E-01 | IL18 | 0.2940 | 1.78E-01 |
| UBR4 | 0.1017 | 5.80E-01 | NIT2 | 0.1663 | 3.93E-01 | GNPDA1 | 0.2283 | 3.54E-01 | PGM3 | 0.2943 | 1.52E-01 |
| HSP90B1 | 0.1020 | 6.57E-01 | ADH5 | 0.1670 | 4.51E-01 | FAM20C | 0.2327 | 2.36E-01 | ADI1 | 0.2947 | 1.89E-01 |
| TTC37 | 0.1030 | 5.94E-01 | AGRN | 0.1680 | 5.41E-01 | MEMO1 | 0.2327 | 2.36E-01 | GOLM1 | 0.2953 | 2.14E-01 |
| HFP1 | 0.1037 | 6.56E-01 | SLC16A3 | 0.1680 | 4.54E-01 | CENPV | 0.2330 | 3.45E-01 | IGFBP6 | 0.2977 | 2.42E-01 |
| MBD10 | 0.1043 | 6.53E-01 | MAN1B1 | 0.1687 | 4.22E-01 | EFNA5 | 0.2340 | 2.73E-01 | APIP | 0.2990 | 1.50E-01 |
| PSMD10 | 0.1057 | 6.27E-01 | RALLY | 0.1690 | 4.72E-01 | DDAH2 | 0.2343 | 3.72E-01 | DDAH2 | 0.2993 | 1.62E-01 |
| RP2 | 0.1080 | 6.14E-01 | PLOD2 | 0.1717 | 4.80E-01 | FAHD2A | 0.2347 | 2.65E-01 | PSMA5 | 0.2993 | 2.08E-01 |
| ZNF594 | 0.1073 | 5.93E-01 | GNS | 0.1723 | 5.81E-01 | GOT1 | 0.2367 | 3.48E-01 | PSMB1 | 0.2993 | 2.32E-01 |
| F | | | | | | | | | | | |

| | | | | | | | | | | | |
|----------|--------|----------|----------|--------|----------|------------|----------|----------|-------------|----------|----------|
| SEC23A | 0.1173 | 5.47E-01 | CAD | 0.1913 | 3.11E-01 | SEMA3C | 0.2470 | 2.50E-01 | CALU | 0.3177 | 1.79E-01 |
| NME2 | 0.1177 | 5.92E-01 | TSNAX | 0.1913 | 3.54E-01 | TMA7 | 0.2477 | 2.11E-01 | SCRN1 | 0.3177 | 1.91E-01 |
| CLIC3 | 0.1200 | 5.83E-01 | PYCR3 | 0.1920 | 3.91E-01 | P3H1 | 0.2480 | 2.59E-01 | SRSF2 | 0.3200 | 1.40E-01 |
| DST1P1 | 0.1200 | 5.77E-01 | NBL1 | 0.1937 | 3.39E-01 | ROBO1 | 0.2480 | 2.63E-01 | PSMA4 | 0.3217 | 1.90E-01 |
| PPR4R3A | 0.1200 | 5.30E-01 | MDK | 0.1943 | 4.75E-01 | POU1F1 | 0.2510 | 2.41E-01 | PSMA3 | 0.3220 | 2.19E-01 |
| H1-2 | 0.1213 | 5.85E-01 | SAP18 | 0.1947 | 3.50E-01 | ME1 | 0.2513 | 2.90E-01 | TMSB10 | 0.3233 | 2.33E-01 |
| DBI | 0.1220 | 5.20E-01 | PI3 | 0.1953 | 3.68E-01 | PTMA | 0.2513 | 3.18E-01 | MRI1 | 0.3253 | 1.58E-01 |
| C19orf53 | 0.1223 | 6.51E-01 | CRYZ | 0.1970 | 3.63E-01 | IL6ST | 0.2523 | 2.39E-01 | PSMA7 | 0.3253 | 1.91E-01 |
| ACOT13 | 0.1243 | 5.40E-01 | NPM1 | 0.1970 | 3.49E-01 | LDHA | 0.2527 | 2.87E-01 | ARHGAP17 | 0.3270 | 1.40E-01 |
| RPL10A | 0.1273 | 5.31E-01 | TYRO3 | 0.1973 | 4.61E-01 | BPNT2 | 0.2540 | 2.23E-01 | WDR12 | 0.3273 | 1.47E-01 |
| ACAT1 | 0.1280 | 5.44E-01 | ACP1 | 0.1977 | 3.03E-01 | CGFOD1 | 0.2553 | 2.09E-01 | PPA2 | 0.3310 | 1.39E-01 |
| PDS5A | 0.1280 | 6.45E-01 | S100A13 | 0.1977 | 3.07E-01 | AFEH | 0.2557 | 2.98E-01 | PSMA1 | 0.3310 | 1.97E-01 |
| GAPDH | 0.1310 | 6.19E-01 | STMN1 | 0.2007 | 4.32E-01 | FDX1 | 0.2580 | 5.61E-01 | ACTL6A | 0.3337 | 1.17E-01 |
| PABPN1 | 0.1313 | 5.65E-01 | ANXA3 | 0.2013 | 4.16E-01 | IMPA1 | 0.2587 | 2.24E-01 | ENO1 | 0.3363 | 1.74E-01 |
| ACACA | 0.1323 | 6.12E-01 | CP | 0.2020 | 5.73E-01 | DPYD | 0.2603 | 3.31E-01 | NOP58 | 0.3383 | 1.49E-01 |
| POLR2H | 0.1337 | 5.03E-01 | CRIP1 | 0.2020 | 3.41E-01 | TNFRSF1A | 0.2603 | 2.42E-01 | PSMB5 | 0.3393 | 1.75E-01 |
| CBSL | 0.1340 | 5.30E-01 | ERP44 | 0.2027 | 3.11E-01 | CZIB | 0.2620 | 2.66E-01 | MAT2A | 0.3407 | 9.95E-02 |
| PYGB | 0.1340 | 4.80E-01 | SMOC1 | 0.2033 | 4.79E-01 | GOLIM4 | 0.2637 | 2.82E-01 | WDR48 | 0.3410 | 1.09E-01 |
| RNPEP | 0.1340 | 5.69E-01 | CAT1 | 0.2040 | 3.70E-01 | CNPY2 | 0.2653 | 1.91E-01 | ACYP2 | 0.3423 | 1.36E-01 |
| CHST3 | 0.1343 | 6.04E-01 | NRDC | 0.2047 | 3.63E-01 | NEPEL1 | 0.2657 | 2.06E-01 | SLC3A2 | 0.3433 | 2.02E-01 |
| ERP29 | 0.1350 | 4.75E-01 | FURIN | 0.2053 | 3.99E-01 | ACY1 | 0.2677 | 2.82E-01 | H1-4 | 0.3470 | 1.12E-01 |
| PFND6 | 0.1350 | 4.89E-01 | PLOD3 | 0.2060 | 3.76E-01 | AK2 | 0.2680 | 1.90E-01 | PFAS | 0.3480 | 1.17E-01 |
| PREPL | 0.1353 | 5.24E-01 | PIPE | 0.2060 | 3.64E-01 | SUMO4 | 0.2683 | 2.44E-01 | LUM | 0.3483 | 1.95E-01 |
| HCC5 | 0.1360 | 5.26E-01 | EML2 | 0.2080 | 3.59E-01 | NUDT9 | 0.2690 | 1.92E-01 | COL6A1 | 0.3490 | 1.42E-01 |
| ECM1 | 0.1363 | 5.58E-01 | LYPAL1 | 0.2083 | 3.12E-01 | GANAB | 0.2693 | 1.92E-01 | FBLN1 | 0.3500 | 3.21E-01 |
| C9orf18 | 0.1370 | 5.97E-01 | WINK1 | 0.2090 | 3.40E-01 | CD38 | 0.2697 | 2.09E-01 | FKBP9 | 0.3510 | 1.95E-01 |
| CRTPA | 0.1370 | 5.14E-01 | PYGL | 0.2110 | 3.30E-01 | MIF | 0.2703 | 2.04E-01 | PGGT1B | 0.3517 | 1.34E-01 |
| PPII3 | 0.1380 | 5.49E-01 | YBX1 | 0.2110 | 3.25E-01 | MT1E | 0.2703 | 3.53E-01 | ENO3 | 0.3530 | 1.57E-01 |
| TSN | 0.1380 | 5.13E-01 | CALM3 | 0.2117 | 3.10E-01 | NEGR1 | 0.2707 | 2.27E-01 | TP1 | 0.3530 | 1.65E-01 |
| WDR82 | 0.1380 | 5.12E-01 | QDPR | 0.2117 | 2.80E-01 | LAMB2 | 0.2710 | 2.94E-01 | TMEM132A | 0.3537 | 1.40E-01 |
| PCDH9 | 0.1410 | 5.19E-01 | BMPR2 | 0.2123 | 3.06E-01 | UBA6 | 0.2743 | 2.79E-01 | PSIP1 | 0.3543 | 1.05E-01 |
| PSMB4 | 0.1547 | 1.83E-01 | NUTF2 | 0.4520 | 5.35E-02 | GPI | 0.5863 | 3.41E-02 | ASAH1 | 0.8230 | 5.15E-03 |
| PTT2 | 0.1740 | 1.48E-01 | RNPPO | 0.4520 | 4.93E-02 | EPHA5 | 0.5880 | 3.29E-02 | PITRM1 | 0.8270 | 9.36E-03 |
| CMPK1 | 0.3573 | 1.18E-01 | CSA | 0.4523 | 4.73E-02 | SLC39A10 | 0.5883 | 3.50E-02 | NHLRC2 | 0.8277 | 2.26E-02 |
| LRP8 | 0.3580 | 1.87E-01 | TATDN1 | 0.4527 | 5.43E-02 | MAGED2 | 0.5887 | 2.03E-02 | ACAA2 | 0.8283 | 1.22E-02 |
| PSMA2 | 0.3597 | 1.54E-01 | GLB1 | 0.4530 | 1.29E-01 | ATP7B | 0.5897 | 2.03E-01 | S100A4 | 0.8283 | 1.20E-03 |
| PLPBP | 0.3607 | 9.39E-02 | DKC1 | 0.4543 | 1.55E-01 | TXNDC17 | 0.5917 | 2.50E-02 | H2AX | 0.8290 | 1.73E-02 |
| CJMTA | 0.3610 | 1.73E-01 | HLA-A | 0.4550 | 4.59E-02 | BANF1 | 0.5940 | 2.99E-02 | DLG | 0.8303 | 1.27E-02 |
| HMGGA1 | 0.3610 | 1.12E-01 | HSPA13 | 0.4577 | 5.41E-02 | HSPA5 | 0.5943 | 3.61E-02 | PLD3 | 0.8313 | 5.30E-03 |
| PPII1 | 0.3620 | 1.28E-01 | NCR3L1G1 | 0.4580 | 5.23E-02 | 0.5960 | 6.02E-02 | TLL | 0.8377 | 3.33E-03 | |
| B2M | 0.3630 | 1.25E-01 | GRN | 0.4587 | 5.76E-02 | MEGF9 | 0.6030 | 2.06E-02 | SLLTRKS | 0.8453 | 5.71E-03 |
| NUCB2 | 0.3633 | 9.98E-02 | PDIA4 | 0.4593 | 7.14E-02 | FAHD1 | 0.6057 | 2.91E-02 | ANG | 0.8520 | 3.03E-03 |
| LAMB1 | 0.3650 | 1.93E-01 | OXC1T | 0.4607 | 1.31E-01 | IMPA2 | 0.6093 | 2.01E-02 | RNA5E4 | 0.8567 | 1.77E-03 |
| NAGK | 0.3663 | 1.13E-01 | BLMH | 0.4630 | 7.78E-02 | MEGF8 | 0.6137 | 9.89E-03 | HSPD1 | 0.8577 | 6.21E-03 |
| PLXNB2 | 0.3673 | 9.96E-02 | PRG4 | 0.4647 | 1.57E-01 | PGLS | 0.6160 | 2.16E-02 | CPS1 | 0.8583 | 3.00E-03 |
| EPDR1 | 0.3680 | 1.88E-01 | PGK 2.00 | 0.4677 | 1.49E-01 | PTPRU | 0.6187 | 7.51E-03 | ARSK | 0.8600 | 9.08E-04 |
| FIM1 | 0.3690 | 1.17E-01 | NECTIN2 | 0.4680 | 5.14E-02 | HMG2N | 0.6210 | 1.98E-02 | no LTF | 0.8603 | 3.28E-02 |
| FAM120A | 0.3700 | 1.79E-01 | H1-1 | 0.4690 | 3.25E-01 | SP117 | 0.6217 | 3.62E-02 | SLC12G2 | 0.8613 | 9.05E-03 |
| TIMP1 | 0.3707 | 1.84E-01 | PGK 1.00 | 0.4707 | 8.05E-02 | CLSTN1 | 0.6220 | 4.07E-02 | SDC1 | 0.8660 | 3.58E-02 |
| MAN2A1 | 0.3710 | 1.21E-01 | APOA1 | 0.4710 | 4.33E-01 | ENOSF1 | 0.6260 | 1.97E-02 | EC1 | 0.8670 | 4.87E-03 |
| MUC1 | 0.3720 | 2.29E-01 | MARCKSL1 | 0.4730 | 2.94E-02 | PTPRK | 0.6283 | 3.03E-02 | CDCP1 | 0.8720 | 6.65E-03 |
| SLC16A1 | 0.3730 | 1.41E-01 | WDR11 | 0.4730 | 2.19E-01 | SMDY5 | 0.6347 | 5.97E-02 | FUCA1 | 0.8787 | 1.44E-02 |
| PPARD | 0.3737 | 1.55E-01 | CS | 0.4737 | 5.06E-02 | PARK7 | 0.6360 | 1.79E-02 | no GCSH | 0.8807 | 7.35E-03 |
| PTMS | 0.3747 | 9.70E-02 | H3HBGRL | 0.4740 | 6.51E-02 | NLN | 0.6367 | 1.12E-02 | C10BP | 0.8857 | 5.76E-03 |
| FKBP10 | 0.3753 | 8.40E-02 | IKL5 | 0.4763 | 1.97E-01 | no FH | 0.6393 | 1.98E-02 | ANGLU | 0.8893 | 9.05E-03 |
| NEFN | 0.3753 | 7.25E-02 | DOB1 | 0.4787 | 4.99E-02 | HDHD2 | 0.6430 | 7.82E-02 | NEO1 | 0.9017 | 3.70E-03 |
| CPA4 | 0.3757 | 1.33E-01 | SPINK4 | 0.4790 | 5.01E-02 | TMSB15B | 0.6460 | 4.70E-02 | no ECH1 | 0.9020 | 2.40E-03 |
| SCRN2 | 0.3763 | 1.78E-01 | PRNP | 0.4797 | 5.12E-02 | COL25A1 | 0.6473 | 1.51E-02 | AIFM1 | 0.9097 | 4.62E-03 |
| ABHD14B | 0.3767 | 8.84E-02 | NAPRT | 0.4807 | 4.36E-02 | MYRIP | 0.6473 | 1.09E-01 | CTSF | 0.9113 | 3.48E-03 |
| DSC3 | 0.3770 | 1.35E-01 | TXNDC12 | 0.4817 | 4.99E-02 | IDUA | 0.6527 | 3.27E-02 | CD59 | 0.9197 | 2.83E-03 |
| RABEPK | 0.3773 | 1.12E-01 | AZM | 0.4820 | 1.66E-01 | JMJD8 | 0.6543 | 2.32E-02 | HSPG2 | 0.9197 | 6.35E-03 |
| NEFH | 0.3780 | 1.21E-01 | GPC1 | 0.4840 | 1.33E-01 | GALNT7 | 0.6587 | 3.29E-02 | yes CALR | 0.9203 | 8.30E-03 |
| PSG | 0.3783 | 1.23E-01 | SDC2 | 0.4907 | 1.25E-01 | MSLN | 0.6610 | 1.38E-02 | yes SPARCL1 | 0.9243 | 8.38E-02 |
| LAMA1 | 0.3793 | 1.27E-01 | SOD1 | 0.4907 | 6.83E-02 | HIBCH | 0.6633 | 9.50E-03 | no CT5B | 0.9350 | 4.92E-03 |
| ENO3 | 0.3797 | 1.27E-01 | GLA | 0.4927 | 4.43E-02 | LRP1 | 0.6673 | 2.70E-02 | yes HIBADH | 0.9373 | 7.90E-03 |
| PPIA | 0.3827 | 1.09E-01 | IDS | 0.4930 | 1.56E-01 | NUCB1 | 0.6717 | 1.78E-02 | yes ANTXR1 | 0.9390 | 4.26E-03 |
| RBBP7 | 0.3843 | 5.91E-02 | GOT2 | 0.4987 | 8.56E-02 | PLBD2 | 0.6720 | 3.61E-02 | yes MANBA | 0.9397 | 6.16E-03 |
| GSTM3 | 0.3847 | 7.81E-02 | SLC39A6 | 0.4993 | 2.86E-02 | HEXA | 0.6767 | 3.56E-02 | yes FAM3C | 0.9470 | 7.20E-03 |
| ROB0 | 0.3847 | 1.10E-01 | SPAG7 | 0.4997 | 3.97E-02 | MUC16 | 0.6773 | 3.35E-02 | SLP1 | 0.9653 | 1.03E-03 |
| DAG1 | 0.3857 | 1.10E-01 | LINPEP7 | 0.5017 | 4.40E-02 | no MUC13 | 0.6773 | 8.54E-02 | yes ERAP1 | 0.9680 | 3.88E-02 |
| HAGH | 0.3887 | 1.15E-01 | EFNB1 | 0.5047 | 5.23E-02 | TNFRSF21 | 0.6787 | 1.78E-02 | yes SKIV2L | 0.9693 | 4.02E-03 |
| BCL7B | 0.3910 | 8.00E-02 | SRSF1 | 0.5050 | 3.91E-02 | no SLCUG1 | 0.6797 | 3.44E-02 | no BCAT2 | 0.9713 | 5.10E-03 |
| NEU1 | 0.3937 | 1.28E-01 | COL28A1 | 0.5057 | 7.65E-02 | HLC-C | 0.6810 | 1.85E-02 | yes SPINK6 | 0.9717 | 1.80E-03 |
| PSMB6 | 0.3950 | 1.38E-01 | HSPA9 | 0.5057 | 3.55E-02 | no GALM | 0.6853 | 1.43E-02 | no L1CAM | 0.9843 | 2.74E-03 |
| LSM 6.00 | 0.3957 | 6.02E-02 | CSPG4 | 0.5120 | 3.26E-02 | yes MDH2 | 0.6853 | 1.92E-02 | no HBA1 | 0.9907 | 2.30E-02 |
| WDR5 | 0.3957 | 1.13E-01 | PSAP | 0.5127 | 5.16E-02 | CD58 | 0.6883 | 1.74E-02 | yes TF | 1.0043 | 9.03E-03 |
| GLOD4 | 0.3960 | 1.17E-01 | LAMP2 | 0.5133 | 4.08E-02 | yes MBTPS1 | 0.6890 | 1.34E-02 | yes CTSC | 1.0063 | 2.77E-03 |
| HLA-B | 0.3990 | 7.94E-02 | PEBP1 | 0.5167 | 4.60E-02 | no SSBP1 | 0.6947 | 2.24E-02 | no CCN3 | 1.0267 | 3.86E-04 |
| SUMO3 | 0.3993 | 7.85E-02 | GRPEL1 | 0.5187 | 3.28E-02 | yes SHISA5 | 0.6957 | 1.59E-02 | yes PVR | 1.0317 | 2.20E-03 |
| SNX27 | 0.4020 | 5.46E-02 | BAZ2B | 0.5213 | 6.94E-02 | CPQ | 0.6963 | 6.55E-02 | yes EFNA1 | 1.0367 | 4.17E-04 |
| WDR92 | 0.4023 | 5.44E-02 | EXT1 | 0.5213 | 3.39E-02 | yes CST3 | 0.6963 | 6.41E-03 | yes AGA | 1.0473 | 5.11E-03 |
| MYCBP | 0.4027 | 5.16E-02 | GPC5 | 0.5223 | 3.49E-02 | yes SYNM | 0.7007 | 4.69E-02 | no AKL | 1.0567 | 6.38E-03 |
| POLR1G | 0.4027 | 6.75E-02 | TRAF2B | 0.5237 | 8.03E-02 | yes ECHS1 | 0.7020 | 1.99E-02 | no HTRA3 | 1.0567 | 1.52E-04 |
| C11orf54 | 0.4040 | 1.21E-01 | PPIH | 0.5267 | 4.74E-02 | no NQO2 | 0.7027 | 1.26E-02 | no GAA | 1.0637 | 2.45E-03 |
| LAMP1 | 0.4040 | 1.69E-01 | TRIP12 | 0.5287 | 1.69E-01 | MDN1 | 0.7117 | 1.62E-02 | no NAGA | 1.0667 | 7.18E-03 |
| SUMO2 | 0.4053 | 8.44E-02 | C1R | 0.5307 | 9.68E-02 | EFNB2 | 0.7140 | 1.78E-02 | yes ATRN | 1.0697 | 4.60E-03 |
| GON7 | 0.4057 | 1.05E-01 | HSPE1 | 0.5310 | 1.85E-02 | no BTG2 | 0.7217 | 9.46E-03 | no HMGN3 | 1.0723 | 7.57E-04 |
| TMOD2 | 0.4057 | 9.62E-02 | PIPF | 0.5357 | 4.77E-02 | no IARS2 | 0.7220 | 9.37E-03 | no COL15A1 | 1.0727 | 2.06E-03 |
| FRMPD1 | 0.4080 | 2.63E-01 | DSG2 | 0.5370 | 6.27E-02 | JCHAIN | 0.7267 | 3.81E-02 | yes LOXL2 | 1.0737 | 3.40E-03 |
| SASPN1 | 0.4080 | 9.83E-02 | CDGFRB | 0.5400 | 3.53E-02 | yes HNTL2 | 0.7307 | 8.57E-03 | yes CTSZ | 1.0747 | 3.03E-03 |
| MYDGF | 0.4107 | 1.08E-01 | CAB39 | 0.5407 | 1.46E-02 | no EXT1 | 0.7320 | 2.15E-02 | yes ARSA | 1.0813 | 3.03E-03 |
| CLU | 0.4107 | 1.58E-01 | FBLN7 | 0.5463 | 3.16E-02 | yes MANEAL | 0.7353 | 2.06E-02 | yes MAN2B2 | 1.0883 | 1.98E-03 |
| GGCT | 0.4117 | 9.17E-02 | HADH | 0.5477 | 2.95E-02 | no ERBB4 | 0.7360 | | | | |

| | | | | | | | | | | | | | | | |
|---------|--------|----------|-----|-----------|--------|----------|-----|--------|--------|----------|-----|--------|--------|----------|-----|
| IMUP | 0.4403 | 5.46E-02 | | ADGRG6 | 0.5817 | 2.13E-02 | yes | TCN1 | 0.7917 | 8.27E-03 | yes | ARSB | 1.2963 | 5.35E-04 | yes |
| NECTIN1 | 0.4413 | 1.54E-01 | | HMG1 | 0.5820 | 2.17E-02 | no | H4C1 | 0.7920 | 3.47E-03 | no | CD55 | 1.3123 | 6.31E-04 | yes |
| CTSA | 0.4423 | 1.10E-01 | | TNFRSF19 | 0.5827 | 6.65E-02 | | GLUD1 | 0.7923 | 1.57E-02 | no | PTX3 | 1.3150 | 4.86E-04 | yes |
| MAN2B1 | 0.4447 | 8.58E-02 | | MACROH2A1 | 0.5930 | 1.20E-02 | no | PTK7 | 0.7930 | 8.68E-03 | yes | PTPRJ | 1.3193 | 3.34E-04 | yes |
| SMPDL3A | 0.4457 | 1.68E-01 | | PRKCSH | 0.5850 | 2.19E-02 | yes | ICAM1 | 0.8090 | 8.79E-03 | yes | GLUL | 1.3437 | 3.29E-05 | no |
| CDA | 0.4460 | 6.23E-02 | | DHFR | 0.5863 | 1.81E-02 | no | PODXL2 | 0.8223 | 1.04E-02 | yes | LYPD3 | 1.3740 | 5.31E-04 | yes |
| GGH | 1.3750 | 1.23E-03 | yes | CFB | 1.4017 | 4.73E-04 | yes | NRCAM | 1.6023 | 9.17E-05 | yes | OLFM1 | 2.0450 | 9.21E-07 | yes |
| COL3A1 | 1.3757 | 1.22E-04 | yes | LGALS3BP | 1.4137 | 1.06E-03 | yes | NRCAM | 1.6143 | 1.75E-04 | yes | CFD | 2.0493 | 1.59E-06 | yes |
| FUCA2 | 1.3780 | 1.06E-03 | yes | ADM | 1.4207 | 7.81E-04 | yes | PTPRM | 1.6393 | 3.29E-05 | yes | LMAN2 | 2.1553 | 5.44E-06 | yes |
| HEXB | 1.3787 | 6.82E-04 | yes | GUSB | 1.4460 | 1.99E-04 | yes | AGT | 1.6620 | 8.31E-05 | yes | BOD1L1 | 2.4360 | 9.51E-08 | no |
| PRCP | 1.3803 | 3.10E-04 | yes | CGREF1 | 1.4830 | 4.01E-05 | yes | CPM | 1.7697 | 1.98E-05 | yes | NPNT | 3.7973 | 1.35E-09 | yes |

Supplemental Table 4.2. List of selected GO term analysis of WT and 55KO secretome.

Secreted proteins with significant change in 55KO compared to WT ($|\log_2FC(55KO/WT)| > 0.5$; $p < 0.05$) are selected. Protein with or without ER signal sequence are separately processed in Metascape (<https://metascape.org/gp/index.html#/main/step1>) using the default setting. Top20 significant and relevant GO terms are selected out of Top100 GO terms.

| Category | Term | Description | LogP | minus LogP | InTerm_InList |
|-------------------------|---|--|------|------------|---------------|
| | Signal peptide containing cargos GO terms | | | | |
| KEGG Pathway | hsa04142 | Lysosome | -27 | 27 | 23 |
| Reactome Gene Sets | R-HSA-1474244 | Extracellular matrix organization | -22 | 22 | 26 |
| GO Biological Processes | GO:0001568 | blood vessel development | -15 | 15 | 30 |
| Reactome Gene Sets | R-HSA-1630316 | Glycosaminoglycan metabolism | -15 | 15 | 15 |
| GO Biological Processes | GO:0071363 | cellular response to growth factor stimulus | -13 | 13 | 26 |
| GO Biological Processes | GO:0006935 | chemotaxis | -13 | 13 | 25 |
| GO Biological Processes | GO:0006959 | humoral immune response | -11 | 11 | 17 |
| GO Biological Processes | GO:0000904 | cell morphogenesis involved in differentiation | -9.7 | 9.7 | 22 |
| GO Biological Processes | GO:0009100 | glycoprotein metabolic process | -9.6 | 9.6 | 17 |
| GO Biological Processes | GO:0019882 | antigen processing and presentation | -9 | 9 | 10 |
| GO Biological Processes | GO:0031589 | cell-substrate adhesion | -8.2 | 8.2 | 15 |
| GO Biological Processes | GO:0008285 | negative regulation of cell population proliferation | -8 | 8 | 21 |
| GO Biological Processes | GO:0007507 | heart development | -6.9 | 6.9 | 17 |
| GO Biological Processes | GO:0048771 | tissue remodeling | -6.9 | 6.9 | 10 |
| GO Biological Processes | GO:0022617 | extracellular matrix disassembly | -6.9 | 6.9 | 7 |
| GO Biological Processes | GO:0007568 | aging | -6.8 | 6.8 | 13 |
| GO Biological Processes | GO:0009611 | response to wounding | -6.6 | 6.6 | 16 |
| GO Biological Processes | GO:0051402 | neuron apoptotic process | -6.5 | 6.5 | 11 |
| Reactome Gene Sets | R-HSA-381119 | Unfolded Protein Response (UPR) | -5.8 | 5.8 | 7 |
| GO Biological Processes | GO:1904645 | response to amyloid-beta | -5.8 | 5.8 | 6 |
| | No Signal peptide containing cargos GO terms | | | | |
| Reactome Gene Sets | R-HSA-8953897 | Cellular responses to stimuli | -30 | 30 | 56 |
| GO Biological Processes | GO:0006457 | protein folding | -10 | 10 | 17 |
| GO Biological Processes | GO:0006979 | response to oxidative stress | -9.4 | 9.4 | 23 |
| GO Biological Processes | GO:0034248 | regulation of cellular amide metabolic process | -8 | 8 | 23 |
| GO Biological Processes | GO:0006520 | cellular amino acid metabolic process | -7.3 | 7.3 | 16 |
| GO Biological Processes | GO:0016071 | mRNA metabolic process | -7 | 7 | 25 |
| GO Biological Processes | GO:0007163 | establishment or maintenance of cell polarity | -6.3 | 6.3 | 13 |
| GO Biological Processes | GO:0098869 | cellular oxidant detoxification | -6 | 6 | 9 |
| GO Biological Processes | GO:0030162 | regulation of proteolysis | -5.9 | 5.9 | 24 |
| Reactome Gene Sets | R-HSA-5357801 | Programmed Cell Death | -5.7 | 5.7 | 12 |
| GO Biological Processes | GO:0055001 | muscle cell development | -5.5 | 5.5 | 11 |
| WikiPathways | WP4754 | IL-18 signaling pathway | -5.1 | 5.1 | 13 |
| Reactome Gene Sets | R-HSA-1500931 | Cell-Cell communication | -5.1 | 5.1 | 9 |
| GO Biological Processes | GO:0009611 | response to wounding | -4.7 | 4.7 | 18 |
| GO Biological Processes | GO:0009408 | response to heat | -4.7 | 4.7 | 8 |
| GO Biological Processes | GO:0006414 | translational elongation | -4.6 | 4.6 | 6 |
| GO Biological Processes | GO:0031667 | response to nutrient levels | -4.4 | 4.4 | 16 |
| GO Biological Processes | GO:0007568 | aging | -3.6 | 3.6 | 12 |
| GO Biological Processes | GO:0016236 | macroautophagy | -3.6 | 3.6 | 11 |
| GO Biological Processes | GO:0050673 | epithelial cell proliferation | -3.1 | 3.1 | 13 |

Chapter 5 Summary and Future Directions

The Golgi apparatus is the central organelle in the intracellular trafficking system that serves as a hub for post-translational modifications and sorting of proteins and lipids. Golgi structural and functional defects, which have been observed in many diseases, cause global defects in protein trafficking, glycosylation, and sorting that impact essential cell activities in many cell types including cancer cells and neurons. Discovering the factors that drive these changes may help us understand and treat protein trafficking disorders such as cancer and Huntington's disease.

The approach we took is to disrupt the Golgi structure without blocking the protein trafficking via the depletion of GRASP55 and/or GRASP65, and study the downstream effect of the Golgi structural disruption in a few cellular processes: 1) cellular activities including cell adhesion, migration, and cell growth (Chapter 2); 2) HS and CS synthesis, secretion, and sulfation (Chapter 3); 3) unconventional protein secretion which is Golgi independent (Chapter 4). Using biochemical and imaging assays in combination with omics analysis, we identified the underlying mechanism that drives these changes upon GRASP depletion-mediated Golgi unstacking.

5.1 Effects of Golgi destruction on cell attachment, migration, and growth

In Chapter 2, we studied the global effect of Golgi unstacking and ribbon unlinking on cellular activities such as cell attachment, migration, and growth. GRASP KD or KO reduces cell adhesion to fibronectin-coated dishes and reduces the migration, invasion of HeLa and MDA-MB-231 cells. While single GRASP depletion displays significant phenotypes on cell adhesion and migration, double depletion further reduces these cellular activities. Considering that cell adhesion proteins on the cell surface, such as integrins, regulate cell attachment and migration, we assessed the levels of numerous integrin complexes expressed in the cell lines we studied. We tested 10 integrin α and β subunits, which can form 8 different heterodimers. Among these, $\alpha 5 \beta 1$ integrin, the best-characterized integrin complex in HeLa and MDA-MB-231 cells, showed the most dramatic reduction (Mierke et al., 2011).

Using cell surface biotinylation experiments, we showed that GRASP depletion reduces $\alpha 5 \beta 1$ integrin levels in the whole cell lysate and at the cell surface. Consistently, exogenous expression of either $\alpha 5 \beta 1$ integrins or GRASPs rescues the cell migration and cell attachment defects in GRASP KO cells, further confirming that it is indeed $\alpha 5 \beta 1$ integrin specific phenotype. Correspondingly, we found that $\alpha 5 \beta 1$ integrin reduction is specific to Golgi unstacking since Golgi ribbon unlinking via the depletion of Golgin-84 or by nocodazole treatment does not reduce integrin levels in cells (Xiang et al., 2013). There are three different possibilities for the reduction of $\alpha 5 \beta 1$ integrin post GRASP depletion: reduced synthesis, increased degradation, or both. Our radioactive labeling pulse-chase and cycloheximide pulse-

chase experiments showed that GRASP depletion does not affect the half-life of $\alpha 5\beta 1$ integrin. Interestingly, we found that GRASP depletion reduces the synthesis of $\alpha 5\beta 1$ integrin even though total protein synthesis is increased in the cell.

Recently, we confirmed that GRASP depletion reduces not only the protein levels but also the mRNA levels of $\alpha 5\beta 1$ integrin, which indicates transcriptional regulation of integrins by Golgi unstacking. There are a few possibilities for the relationship between Golgi stacks and integrin gene transcription. First, considering that the Golgi periphery is a hub for numerous signaling pathways including mTORC1, N-RAS, and H-RAS, it is possible that GRASP-depletion-mediated Golgi unstacking affects one or more of these signaling pathways through which regulates gene transcription (Nüchel et al., 2021, Perez de Castro et al., 2004). Indeed, some preliminary results have shown that GRASP55 depletion inhibits the reactivation of mTORC1, and it also regulates the activities of AKT and ERK.

Second, in our secretome analysis (Chapter 4), one of the top pathways that are affected in 55KO secretome vs. WT secretome is Extracellular Matrix Organization. Considering that integrins are connected to the extracellular matrix proteins such as fibronectin which has been shown to regulate integrin levels and activity (Katz et al., 2000), it is possible that Golgi-fragmentation-induced extracellular matrix re-organization indirectly regulates integrin synthesis. To test this possibility, in the future, one can analyze the levels and secretion of the known extracellular matrix proteins, mainly fibronectin, that interact with $\alpha 5\beta 1$ integrin. Next,

manipulation of fibronectin levels or its secretion can be used to analyze $\alpha 5\beta 1$ integrin synthesis for the confirmation of the potential link between Golgi unstacking, fibronectin, and integrin levels.

Third, a few transcription factors such as ATF6 and SERBP are processed in the Golgi by its residing enzymes including S1P and S2P. Golgi structural defects may affect the functions of Golgi residing enzymes which causes defects in the transcription factor processing in the Golgi. However, there is no evidence if ATF6 or SERBP regulates integrin transcription. To pursue this possibility of Golgi stack disruption changing gene transcription via affecting transcription factors, we recently did RNA-seq analysis in WT, GRASP55 KO, GRASP65 KO, and DKO cells to systematically study the effect of Golgi fragmentation on gene transcription. GRASP depletion changed the levels of numerous transcription factors such as SP1, RUNX2 and JUN which have been previously reported to regulate the synthesis of integrins (Tan et al., 2016, Gingras et al., 2009). Future studies of screening these and other potential transcription factors for the regulation of GRASP-dependent integrin synthesis are necessary.

5.2 Heparan sulfate (HS) and Chondroitin sulfate (CS) synthesis, sulfation and secretion are regulated by GRASPs

Glycosaminoglycans (GAGs) such as HS and CS synthesis mainly takes place in the lumen of the Golgi where numerous regulatory enzymes reside (Sasarman et al., 2016). Accurate

localization and function of those synthase and transferases controls the fine tuning of HS and CS synthesis, modification, secretion, and function. However, the relationship between Golgi structural integrity and GAG synthesis was not well understood. In Chapter 3 of my thesis, we studied the mechanistic regulation of GAG synthesis, secretion, and sulfation by Golgi structural integrity.

We disrupted the Golgi structure by knocking out two Golgi stacking proteins, GRASP55 and GRASP65, and studied its effect on GAGs synthesis, secretion, and sulfation using the combination of LC-MS/MS, immunofluorescence microscopy, flow cytometry, and biochemical studies. We discovered that Golgi destruction increases the total level of HS but decreases its overall sulfation mainly via increasing the level of HS synthesis enzyme EXTL3 and reducing the level of sulfation enzyme PAPSS2, respectively. CS synthesis, however, is largely reduced in GRASP depleted cells largely due to the downregulation of CS synthesis enzyme GalNacT1. Lastly, Golgi unstacking increases the secretion of both HS and CS with an unknown mechanism.

Previously, it has been shown that disruption of Golgi structure by BFA treatment affects HS/CS biosynthesis. BFA treatment, however, blocks ER-to-Golgi trafficking and causes a merge of the Golgi stack but not the TGN to the ER. Because HS synthesis enzymes are localized in early Golgi while CS enzymes are more in the *trans*-Golgi area, BFA treatment affects HS and CS synthesis differently than depletion of GRASPs. Unlike BFA treatment, in our

study GRASP depletion disrupts the Golgi stack structure (Xiang and Wang, 2010) but does not block membrane trafficking (Xiang et al., 2013, Ahat et al., 2019b).

We observed some dramatic changes in HS and CS levels and sulfation after GRASP depletion. However, the exact mechanism of how GRASPs regulate the synthesis of GAG regulating enzymes levels is still unknown. Identifying the potential transcription factors and/or signaling pathways that link the GRASPs and GAG enzymes is a potential direction for future studies. In the literature, by analyzing the promoter regions of HS synthesis enzymes, a few transcription factors have been reported to potentially regulate the synthesis of numerous HS enzymes (Weiss et al., 2020). Among them, transcription factor NFIL3 (nuclear factor, interleukin 3 regulated) has been predicted to bind to the promoter regions of EXT1, EXT2, and EXTL3, the major enzymes in HS synthesis pathway that are changed upon GRASP depletion. Interestingly, in our RNA-seq analysis, we identified that NFIL3 is ubiquitously downregulated in GRASP KO cells compared to that of WT. It is possible that GRASP depletion causes the reduction of NFIL3 which regulates the synthesis of EXT1, EXT2, and EXTL3. Future studies are needed to explore this possibility which will enrich our understanding of the GRASP-dependent transcriptional regulation of HS and CS synthesis enzymes.

5.3 GRASP55 and autophagy regulates mutant huntingtin unconventional secretion and aggregation.

In Chapter 4 of my thesis, we studied the mechanism of how GRASP55 facilitates the secretion of mutant huntingtin (Htt) and its significance in Huntington's disease progression. Protein aggregation and the formation of insoluble inclusion bodies are the common hallmarks of neurodegenerative diseases (Ross and Poirier, 2004). These include Tau in Alzheimer's disease, α -synuclein in Parkinson's disease, and Htt in Huntington's disease. Neurotoxic proteins such as Htt polyQ mutants have been found both in neurons and cerebral spinal fluid of disease patients, indicating that these proteins may be secreted (Wild et al., 2015). New advances in the field showed that GRASP55 has Golgi independent functions. Our lab discovered that under certain stress conditions, GRASP55 regulates the "self-eating" process called autophagy (Zhang et al., 2019a, Zhang et al., 2018). Most recent reports also showed that GRASPs, especially GRASP55, regulate the unconventional secretion of some cytoplasmic proteins that lack obvious ER signal sequences (Villeneuve et al., 2018, Rabouille and Linstedt, 2016). However, it was not clear how a Golgi protein such as GRASP55 controls unconventional secretion, which bypasses Golgi.

In this study, we used Htt-Q74 as a model system to study the mechanism of GRASP55-dependent unconventional secretion. Our results demonstrate that Htt-Q74 secretion is GRASP55 and autophagy-dependent and enhanced under stress conditions such as energy and nutrient starvation, ER stress, and proteostatic stress. Mechanistically, GRASP55 facilitates Htt secretion by tethering autophagosomes to lysosomes to promote autophagosome maturation and

by stabilizing p23/TMED10, an ERGIC protein that functions as a channel for the translocation of cytoplasmic proteins into the lumen. Moreover, the GRASP55 level is upregulated in various stresses, and inhibition of Htt-Q74 secretion by GRASP55 knockout enhances Htt aggregation and toxicity in the cell. Lastly, we performed a comprehensive secretome analysis to study the role of GRASP55 in the regulation of both conventional and unconventional protein secretion. Strikingly, we identified that the secretion of the majority of the conventional pathway cargoes is enhanced upon GRASP55 depletion while the secretion of the majority of the unconventional cargoes is reduced. This further confirms that Golgi unstacking via GRASP depletion accelerates protein trafficking through the Golgi.

GRASP55 is the master regulator of unconventional protein secretion. Our observations that GRASP55 is upregulated and translocated to other membrane structures (puncta outside of the Golgi) upon various stresses imply that it plays essential roles in certain processes outside of the Golgi. Indeed, GRASP55 interacts with p23/TMED10 on ERGIC to regulate cargo translocation into the lumen of ERGIC, which is the first step of unconventional secretion of cytosolic cargoes. In addition, GRASP55 also functions as a tether to regulate membrane fusion events of autophagosomes and lysosomes that are essential for the late steps of unconventional secretion and autophagic degradation of cargoes.

In this study, we also identified that GRASP55 is upregulated upon various stresses. It is highly likely that this is a transcriptional upregulation. Considering that GRASP55 plays

complex roles in autophagy and unconventional secretion upon stress, it is reasonable that its level is upregulated. Upon stress, many autophagy genes including Atg1, Atg13 are upregulated by transcription factor ATF4 (B'Chir et al., 2013). It is possible that ATF4 also plays a role in GRASP55 upregulation since GRASP55 is an “autophagy gene”. In addition to transcriptional upregulation, increased protein stability may also contribute to its higher levels. Preliminary results from a former undergraduate student, Shun Enomoto, showed that GRASP55 O-GlcNAcylation deficient mutant GRASP55-5A has a higher half-life than GRASP55-F37A mutant, which is an autophagy defective mutant. This implies that the non-Golgi-localized GRASP55 mutant is more stable than the Golgi-localized GRASP55. More future dedication is needed to identify the factors that regulate the selective upregulation of GRASP55 but not GRASP65 upon stress conditions, and its significance in Golgi-dependent and -independent functions of GRASP55.

GRASP55-mediated Htt unconventional secretion reduces its aggregation in the cell. However, HeLa and MEF cells are not well-suited model systems to best reflect the phenotype of Htt secretion in HD. Therefore, as a continuation of this study, in the future, we will test the secretion of Htt exon1 fragment and full-length Htt in neuronal cells as well as primary neurons. In addition, endogenous polyQ Htt expressing striatal neurons (ST Q111/111) can be used to confirm our observations in Htt overexpressing systems. The effect of Htt secretion on its cellular toxicity will be evaluated using cell toxicity assays.

It has been previously shown that the internalization of numerous neurotoxic proteins such as Tau is regulated by cell surface HSPG (Zhao et al., 2020). It has not been reported, however, if Htt internalization also requires HSPG. Considering that HS levels in the cell lysate and on the cell surface are increased by GRASP depletion, GRASP55 and GRASP65 possibly also indirectly regulate the internalization and uptake of GRASP55-dependent secreted neurotoxic proteins. The possibility of HSPG-dependent internalization of Htt would be pursued in our lab.

References

- ADUSUMALLI, R., ÅSHEIM, H. C., LUPASHIN, V., BLACKBURN, J. B. & PRYDZ, K. 2021. Proteoglycan synthesis in conserved oligomeric Golgi subunit deficient HEK293T cells is affected differently, depending on the lacking subunit. *Traffic*, 22, 230-239.
- AHAT, E., LI, J. & WANG, Y. 2019a. New Insights Into the Golgi Stacking Proteins. *Front Cell Dev Biol*, 7, 131.
- AHAT, E., XIANG, Y., ZHANG, X., BEKIER, M. E. & WANG, Y. 2019b. GRASP depletion-mediated Golgi destruction decreases cell adhesion and migration via the reduction of alpha5beta1 integrin. *Mol Biol Cell*, mbcE18070462.
- AHAT, E., XIANG, Y., ZHANG, X., BEKIER, M. E. & WANG, Y. 2019c. GRASP depletion-mediated Golgi destruction decreases cell adhesion and migration via the reduction of alpha5beta1 integrin. *Mol Biol Cell*, 30, 766-777.
- ANNAVAL, T., WILD, R., CRETINON, Y., SADIR, R., VIVES, R. R. & LORTAT-JACOB, H. 2020. Heparan Sulfate Proteoglycans Biosynthesis and Post Synthesis Mechanisms Combine Few Enzymes and Few Core Proteins to Generate Extensive Structural and Functional Diversity. *Molecules*, 25.
- AQUINO, R. S., LEE, E. S. & PARK, P. W. 2010. Diverse functions of glycosaminoglycans in infectious diseases. *Prog Mol Biol Transl Sci*, 93, 373-94.
- ARBEZ, N., RATOVITSKI, T., ROBY, E., CHIGHLADZE, E., STEWART, J. C., REN, M., WANG, X., LAVERY, D. J. & ROSS, C. A. 2017. Post-translational modifications clustering within proteolytic domains decrease mutant huntingtin toxicity. *J Biol Chem*, 292, 19238-19249.
- ARIDOR, M. & BALCH, W. E. 1999. Integration of endoplasmic reticulum signaling in health and disease. *Nat Med*, 5, 745-51.
- ARRASATE, M. & FINKBEINER, S. 2012. Protein aggregates in Huntington's disease. *Exp Neurol*, 238, 1-11.
- AVNUR, Z. & GEIGER, B. 1984. Immunocytochemical localization of native chondroitin-sulfate in tissues and cultured cells using specific monoclonal antibody. *Cell*, 38, 811-22.
- B'CHIR, W., MAURIN, A. C., CARRARO, V., AVEROUS, J., JOUSSE, C., MURANISHI, Y., PARRY, L., STEPIEN, G., FAFOURNOUX, P. & BRUHAT, A. 2013. The eIF2alpha/ATF4 pathway is essential for stress-induced autophagy gene expression. *Nucleic Acids Res*, 41, 7683-99.
- BARR, F. A., NAKAMURA, N. & WARREN, G. 1998. Mapping the interaction between GRASP65 and GM130, components of a protein complex involved in the stacking of Golgi cisternae. *Embo J*, 17, 3258-68.
- BARR, F. A., PREISINGER, C., KOPAJTICH, R. & KORNER, R. 2001. Golgi matrix proteins interact with p24 cargo receptors and aid their efficient retention in the Golgi apparatus. *J Cell Biol*, 155, 885-91.

- BARR, F. A., PUYPE, M., VANDEKERCKHOVE, J. & WARREN, G. 1997. GRASP65, a protein involved in the stacking of Golgi cisternae. *Cell*, 91, 253-62.
- BATES, G. P., DORSEY, R., GUSELLA, J. F., HAYDEN, M. R., KAY, C., LEAVITT, B. R., NANCE, M., ROSS, C. A., SCAHILL, R. I., WETZEL, R., WILD, E. J. & TABRIZI, S. J. 2015. Huntington disease. *Nat Rev Dis Primers*, 1, 15005.
- BAUMANN, J., IGNASHKOVA, T. I., CHIRASANI, S. R., RAMIREZ-PEINADO, S., ALBORZINIA, H., GENDARME, M., KUHNIGK, K., KRAMER, V., LINDEMANN, R. K. & REILING, J. H. 2018. Golgi stress-induced transcriptional changes mediated by MAPK signaling and three ETS transcription factors regulate MCL1 splicing. *Mol Biol Cell*, 29, 42-52.
- BEKIER, M. E., 2ND, WANG, L., LI, J., HUANG, H., TANG, D., ZHANG, X. & WANG, Y. 2017. Knockout of the Golgi stacking proteins GRASP55 and GRASP65 impairs Golgi structure and function. *Mol Biol Cell*, 28, 2833-2842.
- BERGMAN, M., JOUKOV, V., VIRTANEN, I. & ALITALO, K. 1995. Overexpressed Csk tyrosine kinase is localized in focal adhesions, causes reorganization of alpha v beta 5 integrin, and interferes with HeLa cell spreading. *Mol Cell Biol*, 15, 711-22.
- BIZZARO, N., PASINI, P., GHIRARDELLO, A. & FINCO, B. 1999. High anti-golgi autoantibody levels: an early sign of autoimmune disease? *Clin Rheumatol*, 18, 346-8.
- BOTTCHER, R. T., STREMMEL, C., MEVES, A., MEYER, H., WIDMAIER, M., TSENG, H. Y. & FASSLER, R. 2012. Sorting nexin 17 prevents lysosomal degradation of beta1 integrins by binding to the beta1-integrin tail. *Nat Cell Biol*, 14, 584-92.
- BRANDIZZI, F. & BARLOWE, C. 2013. Organization of the ER-Golgi interface for membrane traffic control. *Nat Rev Mol Cell Biol*, 14, 382-92.
- BRANDSTAETTER, H., KRUPPA, A. J. & BUSS, F. 2014. Huntingtin is required for ER-to-Golgi transport and for secretory vesicle fusion at the plasma membrane. *Dis Model Mech*, 7, 1335-40.
- BREUKSCH, I., PROSINGER, F., BAEHR, F., ENGELHARDT, F. P., BAUER, H. K., THUROFF, J. W., HEIMES, A. S., HASENBURG, A., PRAWITT, D. & BRENNER, W. 2017. Integrin alpha5 triggers the metastatic potential in renal cell carcinoma. *Oncotarget*, 8, 107530-107542.
- BRUNS, C., MCCAFFERY, J. M., CURWIN, A. J., DURAN, J. M. & MALHOTRA, V. 2011. Biogenesis of a novel compartment for autophagosome-mediated unconventional protein secretion. *J Cell Biol*, 195, 979-92.
- CARLSSON, P., PRESTO, J., SPILLMANN, D., LINDAHL, U. & KJELLÉN, L. 2008. Heparin/heparan sulfate biosynthesis: processive formation of N-sulfated domains. *J Biol Chem*, 283, 20008-14.
- CARON, N. S., BANOS, R., YANICK, C., ALY, A. E., BYRNE, L. M., SMITH, E. D., XIE, Y., SMITH, S. E. P., POTLURI, N., FINDLAY BLACK, H., CASAL, L., KO, S., CHEUNG, D., KIM, H., SEONG, I. S., WILD, E. J., SONG, J. J., HAYDEN, M. R. & SOUTHWELL, A. L. 2021. Mutant Huntingtin Is Cleared from the Brain via Active Mechanisms in Huntington Disease. *J Neurosci*, 41, 780-796.
- CARTIER-MICHAUD, A., BAILLY, A. L., BETZI, S., SHI, X., LISSITZKY, J. C., ZARUBICA, A., SERGE, A., ROCHE, P., LUGARI, A., HAMON, V., BARDIN, F., DERVIAUX, C., LEMBO, F., AUDEBERT, S., MARCHETTO, S., DURAND, B., BORG, J. P., SHI, N., MORELLI, X. & AURRAND-LIONS, M. 2017. Genetic, structural, and chemical insights into the dual function of GRASP55 in germ cell Golgi

- remodeling and JAM-C polarized localization during spermatogenesis. *PLoS Genet*, 13, e1006803.
- CHEN, M. & WOLYNES, P. G. 2017. Aggregation landscapes of Huntingtin exon 1 protein fragments and the critical repeat length for the onset of Huntington's disease. *Proc Natl Acad Sci U S A*, 114, 4406-4411.
- CHENG, J. P., BETIN, V. M., WEIR, H., SHELMANI, G. M., MOSS, D. K. & LANE, J. D. 2010. Caspase cleavage of the Golgi stacking factor GRASP65 is required for Fas/CD95-mediated apoptosis. *Cell Death Dis*, 1, e82.
- CHIRITOIU, M., BROUWERS, N., TURACCHIO, G., PIROZZI, M. & MALHOTRA, V. 2019. GRASP55 and UPR Control Interleukin-1beta Aggregation and Secretion. *Dev Cell*, 49, 145-155 e4.
- CRUZ-GARCIA, D., BROUWERS, N., DURAN, J. M., MORA, G., CURWIN, A. J. & MALHOTRA, V. 2017. A diacidic motif determines unconventional secretion of wild-type and ALS-linked mutant SOD1. *J Cell Biol*.
- CURWIN, A. J., BROUWERS, N., ALONSO, Y. A. M., TEIS, D., TURACCHIO, G., PARASHURAMAN, S., RONCHI, P. & MALHOTRA, V. 2016. ESCRT-III drives the final stages of CUPS maturation for unconventional protein secretion. *Elife*, 5.
- D'ANGELO, G., PRENCIPE, L., IODICE, L., BEZNOUSSENKO, G., SAVARESE, M., MARRA, P., DI TULLIO, G., MARTIRE, G., DE MATTEIS, M. A. & BONATTI, S. 2009. GRASP65 and GRASP55 sequentially promote the transport of C-terminal valine-bearing cargos to and through the Golgi complex. *J Biol Chem*, 284, 34849-60.
- DANGOUMAU, A., VERSCHUEREN, A., HAMMOUCHE, E., PAPON, M. A., BLASCO, H., CHERPI-ANTAR, C., POUGET, J., CORCIA, P., ANDRES, C. R. & VOURC'H, P. 2014. Novel SOD1 mutation p.V31A identified with a slowly progressive form of amyotrophic lateral sclerosis. *Neurobiol Aging*, 35, 266 e1-4.
- DENNIS, J. W., GRANOVSKY, M. & WARREN, C. E. 1999. Glycoprotein glycosylation and cancer progression. *Biochim Biophys Acta*, 1473, 21-34.
- DIAZ-CORRALES, F. J., ASANUMA, M., MIYAZAKI, I. & OGAWA, N. 2004. Rotenone induces disassembly of the Golgi apparatus in the rat dopaminergic neuroblastoma B65 cell line. *Neurosci Lett*, 354, 59-63.
- DICK, G., AKSLEN-HOEL, L. K., GRONDAHL, F., KJOS, I., MACCARANA, M. & PRYDZ, K. 2015. PAPST1 regulates sulfation of heparan sulfate proteoglycans in epithelial MDCK II cells. *Glycobiology*, 25, 30-41.
- DUPONT, N., JIANG, S., PILLI, M., ORNATOWSKI, W., BHATTACHARYA, D. & DERETIC, V. 2011. Autophagy-based unconventional secretory pathway for extracellular delivery of IL-1beta. *EMBO J*, 30, 4701-11.
- DURAN, J. M., ANJARD, C., STEFAN, C., LOOMIS, W. F. & MALHOTRA, V. 2010. Unconventional secretion of Acb1 is mediated by autophagosomes. *J Cell Biol*, 188, 527-36.
- DURAN, J. M., KINSETH, M., BOSSARD, C., ROSE, D. W., POLISHCHUK, R., WU, C. C., YATES, J., ZIMMERMAN, T. & MALHOTRA, V. 2008. The Role of GRASP55 in Golgi Fragmentation and Entry of Cells into Mitosis. *Mol Biol Cell*, 19, 2579-87.
- DURAND, G. & SETA, N. 2000. Protein glycosylation and diseases: blood and urinary oligosaccharides as markers for diagnosis and therapeutic monitoring. *Clin Chem*, 46, 795-805.

- EVIN, G. 2015. How accelerated Golgi trafficking may drive Alzheimer's disease (comment on DOI 10.1002/bies.201400116). *Bioessays*, 37, 232-3.
- FEINSTEIN, T. N. & LINSTEDT, A. D. 2007. Mitogen-activated protein kinase kinase 1-dependent Golgi unlinking occurs in G2 phase and promotes the G2/M cell cycle transition. *Mol Biol Cell*, 18, 594-604.
- FEINSTEIN, T. N. & LINSTEDT, A. D. 2008. GRASP55 Regulates Golgi Ribbon Formation. *Mol Biol Cell*, 19, 2696-707.
- FENG JIA, M. A. H., CHRISTOPHER W. CAIRO 2016. Integrin-mediated cell migration is blocked by inhibitors of human neuraminidase. *Biochimica et Biophysica Acta*
- FODALE, V., BOGGIO, R., DALDIN, M., CARIULO, C., SPIEZIA, M. C., BYRNE, L. M., LEAVITT, B. R., WILD, E. J., MACDONALD, D., WEISS, A. & BRESCIANI, A. 2017. Validation of Ultrasensitive Mutant Huntingtin Detection in Human Cerebrospinal Fluid by Single Molecule Counting Immunoassay. *J Huntingtons Dis*, 6, 349-361.
- FREEMAN, C. & HOPWOOD, J. 1992. Lysosomal degradation of heparin and heparan sulphate. *Adv Exp Med Biol*, 313, 121-34.
- FREEZE, H. H. & NG, B. G. 2011. Golgi glycosylation and human inherited diseases. *Cold Spring Harb Perspect Biol*, 3, a005371.
- FRITZLER, M. J., ETHERINGTON, J., SOKOLUK, C., KINSELLA, T. D. & VALENCIA, D. W. 1984. Antibodies from patients with autoimmune disease react with a cytoplasmic antigen in the Golgi apparatus. *J Immunol*, 132, 2904-8.
- FU, Y., WU, P., PAN, Y., SUN, X., YANG, H., DIFIGLIA, M. & LU, B. 2017. A toxic mutant huntingtin species is resistant to selective autophagy. *Nat Chem Biol*, 13, 1152-1154.
- FUDA, H., SHIMIZU, C., LEE, Y. C., AKITA, H. & STROTT, C. A. 2002. Characterization and expression of human bifunctional 3'-phosphoadenosine 5'-phosphosulphate synthase isoforms. *Biochem J*, 365, 497-504.
- FUJITA, Y., OKAMOTO, K., SAKURAI, A., KUSAKA, H., AIZAWA, H., MIHARA, B. & GONATAS, N. K. 2002. The Golgi apparatus is fragmented in spinal cord motor neurons of amyotrophic lateral sclerosis with basophilic inclusions. *Acta Neuropathol*, 103, 243-7.
- GEE, H. Y., KIM, J. & LEE, M. G. 2018. Unconventional secretion of transmembrane proteins. *Semin Cell Dev Biol*, 83, 59-66.
- GEE, H. Y., NOH, S. H., TANG, B. L., KIM, K. H. & LEE, M. G. 2011. Rescue of DeltaF508-CFTR Trafficking via a GRASP-Dependent Unconventional Secretion Pathway. *Cell*, 146, 746-60.
- GERSON, J. E., SAFREN, N., FISCHER, S., PATEL, R., CROWLEY, E. V., WELDAY, J. P., WINDLE, A. K., BARMADA, S., PAULSON, H. L. & SHARKEY, L. M. 2020. Ubiquilin-2 differentially regulates polyglutamine disease proteins. *Hum Mol Genet*, 29, 2596-2610.
- GINGRAS, M. E., MASSON-GADAIS, B., ZANIOLO, K., LECLERC, S., DROUIN, R., GERMAIN, L. & GUERIN, S. L. 2009. Differential binding of the transcription factors Sp1, AP-1, and NFI to the promoter of the human alpha5 integrin gene dictates its transcriptional activity. *Invest Ophthalmol Vis Sci*, 50, 57-67.
- GIULIANI, F., GRIEVE, A. & RABOUILLE, C. 2011. Unconventional secretion: a stress on GRASP. *Curr Opin Cell Biol*, 23, 498-504.
- GOLDFISCHER, S. 1982. The internal reticular apparatus of Camillo Golgi: a complex, heterogeneous organelle, enriched in acid, neutral, and alkaline phosphatases, and

- involved in glycosylation, secretion, membrane flow, lysosome formation, and intracellular digestion. *J Histochem Cytochem*, 30, 717-33.
- GOSAVI, P., HOUGHTON, F. J., MCMILLAN, P. J., HANSEN, E. & GLEESON, P. A. 2018. The Golgi ribbon in mammalian cells negatively regulates autophagy by modulating mTOR activity. *J Cell Sci*, 131.
- GÖTTE, M., SPILLMANN, D., YIP, G. W., VERSTEEG, E., ECHTERMEYER, F. G., VAN KUPPEVELT, T. H. & KIESEL, L. 2008. Changes in heparan sulfate are associated with delayed wound repair, altered cell migration, adhesion and contractility in the galactosyltransferase I (beta4GalT-7) deficient form of Ehlers-Danlos syndrome. *Hum Mol Genet*, 17, 996-1009.
- GU, J. & TANIGUCHI, N. 2004. Regulation of integrin functions by N-glycans. *Glycoconj J*, 21, 9-15.
- GUIZZUNTI, G. & SEEMANN, J. 2016. Mitotic Golgi disassembly is required for bipolar spindle formation and mitotic progression. *Proc Natl Acad Sci U S A*, 113, E6590-E6599.
- GUO, H. B., LEE, I., KAMAR, M., AKIYAMA, S. K. & PIERCE, M. 2002. Aberrant N-glycosylation of beta1 integrin causes reduced alpha5beta1 integrin clustering and stimulates cell migration. *Cancer Res*, 62, 6837-45.
- HANG, Q., ISAJI, T., HOU, S., WANG, Y., FUKUDA, T. & GU, J. 2017. A Key Regulator of Cell Adhesion: Identification and Characterization of Important N-Glycosylation Sites on Integrin alpha5 for Cell Migration. *Mol Cell Biol*, 37.
- HEBERT, D. N. & MOLINARI, M. 2007. In and out of the ER: protein folding, quality control, degradation, and related human diseases. *Physiol Rev*, 87, 1377-408.
- HEGDE, R. N., CHIKI, A., PETRICCA, L., MARTUFI, P., ARBEZ, N., MOUCHIROUD, L., AUWERX, J., LANGLES, C., BATES, G. P., SINGH-BAINS, M. K., DRAGUNOW, M., CURTIS, M. A., FAULL, R. L., ROSS, C. A., CARICASOLE, A. & LASHUEL, H. A. 2020. TBK1 phosphorylates mutant Huntingtin and suppresses its aggregation and toxicity in Huntington's disease models. *EMBO J*, 39, e104671.
- HEINRICH, F., NANDA, H., GOH, H. Z., BACHERT, C., LOSCHE, M. & LINSTEDT, A. D. 2014. Myristoylation restricts orientation of the GRASP domain on membranes and promotes membrane tethering. *J Biol Chem*, 289, 9683-91.
- HELENIUS, A. & AEBI, M. 2001. Intracellular functions of N-linked glycans. *Science*, 291, 2364-9.
- HENG, M. Y., DUONG, D. K., ALBIN, R. L., TALLAKSEN-GREENE, S. J., HUNTER, J. M., LESORT, M. J., OSMAND, A., PAULSON, H. L. & DETLOFF, P. J. 2010. Early autophagic response in a novel knock-in model of Huntington disease. *Hum Mol Genet*, 19, 3702-20.
- HILDITCH-MAGUIRE, P., TRETTEL, F., PASSANI, L. A., AUERBACH, A., PERSICHETTI, F. & MACDONALD, M. E. 2000. Huntingtin: an iron-regulated protein essential for normal nuclear and perinuclear organelles. *Hum Mol Genet*, 9, 2789-97.
- HU, F., SHI, X., LI, B., HUANG, X., MORELLI, X. & SHI, N. 2015. Structural Basis for the Interaction between the Golgi Reassembly-Stacking Protein GRASP65 and the Golgi Matrix Protein GM130. *J Biol Chem*.
- HUANG, S. & WANG, Y. 2017. Golgi structure formation, function, and post-translational modifications in mammalian cells. *F1000Res*, 6, 2050.
- ISAJI, T., SATO, Y., FUKUDA, T. & GU, J. 2009. N-glycosylation of the I-like domain of beta1 integrin is essential for beta1 integrin expression and biological function:

- identification of the minimal N-glycosylation requirement for alpha5beta1. *J Biol Chem*, 284, 12207-16.
- ISAJI, T., SATO, Y., ZHAO, Y., MIYOSHI, E., WADA, Y., TANIGUCHI, N. & GU, J. 2006. N-glycosylation of the beta-propeller domain of the integrin alpha5 subunit is essential for alpha5beta1 heterodimerization, expression on the cell surface, and its biological function. *J Biol Chem*, 281, 33258-67.
- ITAKURA, E., KISHI-ITAKURA, C. & MIZUSHIMA, N. 2012. The hairpin-type tail-anchored SNARE syntaxin 17 targets to autophagosomes for fusion with endosomes/lysosomes. *Cell*, 151, 1256-69.
- JAGER, S., BUCCI, C., TANIDA, I., UENO, T., KOMINAMI, E., SAFTIG, P. & ESKELINEN, E. L. 2004. Role for Rab7 in maturation of late autophagic vacuoles. *J Cell Sci*, 117, 4837-48.
- JAMESON, K. L., MAZUR, P. K., ZEHNDER, A. M., ZHANG, J., ZARNEGAR, B., SAGE, J. & KHAVARI, P. A. 2013. IQGAP1 scaffold-kinase interaction blockade selectively targets RAS-MAP kinase-driven tumors. *Nat Med*, 19, 626-630.
- JANIK, M. E., LITYNSKA, A. & VEREECKEN, P. 2010. Cell migration-the role of integrin glycosylation. *Biochim Biophys Acta*, 1800, 545-55.
- JESCH, S. A., LEWIS, T. S., AHN, N. G. & LINSTEDT, A. D. 2001. Mitotic phosphorylation of Golgi reassembly stacking protein 55 by mitogen-activated protein kinase ERK2. *Mol Biol Cell*, 12, 1811-7.
- JIANG, P., NISHIMURA, T., SAKAMAKI, Y., ITAKURA, E., HATTA, T., NATSUME, T. & MIZUSHIMA, N. 2014. The HOPS complex mediates autophagosome-lysosome fusion through interaction with syntaxin 17. *Mol Biol Cell*, 25, 1327-37.
- JOHNSON, B. S., SNEAD, D., LEE, J. J., MCCAFFERY, J. M., SHORTER, J. & GITLER, A. D. 2009. TDP-43 is intrinsically aggregation-prone, and amyotrophic lateral sclerosis-linked mutations accelerate aggregation and increase toxicity. *J Biol Chem*, 284, 20329-39.
- JOSHI, G., BEKIER, M. E., 2ND & WANG, Y. 2015. Golgi fragmentation in Alzheimer's disease. *Front Neurosci*, 9, 340.
- JOSHI, G., CHI, Y., HUANG, Z. & WANG, Y. 2014. Abeta-induced Golgi fragmentation in Alzheimer's disease enhances Abeta production. *Proc Natl Acad Sci U S A*, 111, E1230-9.
- JOSHI, G. & WANG, Y. 2015. Golgi defects enhance APP amyloidogenic processing in Alzheimer's disease. *Bioessays*, 37, 240-7.
- JUDWARE, R. & CULP, L. A. 1997. Concomitant down-regulation of expression of integrin subunits by N-myc in human neuroblastoma cells: differential regulation of alpha2, alpha3 and beta1. *Oncogene*, 14, 1341-50.
- KAMIYAMA, S., SASAKI, N., GODA, E., UI-TEI, K., SAIGO, K., NARIMATSU, H., JIGAMI, Y., KANNAGI, R., IRIMURA, T. & NISHIHARA, S. 2006. Molecular cloning and characterization of a novel 3'-phosphoadenosine 5'-phosphosulfate transporter, PAPST2. *J Biol Chem*, 281, 10945-53.
- KATZ, B. Z., ZAMIR, E., BERSHADSKY, A., KAM, Z., YAMADA, K. M. & GEIGER, B. 2000. Physical state of the extracellular matrix regulates the structure and molecular composition of cell-matrix adhesions. *Mol Biol Cell*, 11, 1047-60.
- KAYAGAKI, N., STOWE, I. B., LEE, B. L., O'ROURKE, K., ANDERSON, K., WARMING, S., CUELLAR, T., HALEY, B., ROOSE-GIRMA, M., PHUNG, Q. T., LIU, P. S., LILL,

- J. R., LI, H., WU, J., KUMMERFELD, S., ZHANG, J., LEE, W. P., SNIPAS, S. J., SALVESEN, G. S., MORRIS, L. X., FITZGERALD, L., ZHANG, Y., BERTRAM, E. M., GOODNOW, C. C. & DIXIT, V. M. 2015. Caspase-11 cleaves gasdermin D for non-canonical inflammasome signalling. *Nature*, 526, 666-71.
- KIM, B. T., KITAGAWA, H., TAMURA, J., SAITO, T., KUSCHE-GULLBERG, M., LINDAHL, U. & SUGAHARA, K. 2001. Human tumor suppressor EXT gene family members EXTL1 and EXTL3 encode alpha 1,4- N-acetylglucosaminyltransferases that likely are involved in heparan sulfate/ heparin biosynthesis. *Proc Natl Acad Sci U S A*, 98, 7176-81.
- KIM, J., NOH, S. H., PIAO, H., KIM, D. H., KIM, K., CHA, J. S., CHUNG, W. Y., CHO, H. S., KIM, J. Y. & LEE, M. G. 2016. Monomerization and ER Relocalization of GRASP Is a Requisite for Unconventional Secretion of CFTR. *Traffic*, 17, 733-53.
- KIMURA, T., JIA, J., KUMAR, S., CHOI, S. W., GU, Y., MUDD, M., DUPONT, N., JIANG, S., PETERS, R., FARZAM, F., JAIN, A., LIDKE, K. A., ADAMS, C. M., JOHANSEN, T. & DERETIC, V. 2017. Dedicated SNAREs and specialized TRIM cargo receptors mediate secretory autophagy. *EMBO J*, 36, 42-60.
- KINSETH, M. A., ANJARD, C., FULLER, D., GUIZZUNTI, G., LOOMIS, W. F. & MALHOTRA, V. 2007. The Golgi-associated protein GRASP is required for unconventional protein secretion during development. *Cell*, 130, 524-34.
- KITAGAWA, H., SHIMAKAWA, H. & SUGAHARA, K. 1999. The tumor suppressor EXT-like gene EXTL2 encodes an alpha1, 4-N-acetylhexosaminyltransferase that transfers N-acetylgalactosamine and N-acetylglucosamine to the common glycosaminoglycan-protein linkage region. The key enzyme for the chain initiation of heparan sulfate. *J Biol Chem*, 274, 13933-7.
- KLUMPERMAN, J. 2011. Architecture of the mammalian Golgi. *Cold Spring Harb Perspect Biol*, 3, 1-19.
- KLUTE, M. J., MELANCON, P. & DACKS, J. B. 2011. Evolution and diversity of the Golgi. *Cold Spring Harb Perspect Biol*, 3, a007849.
- KOBAYASHI, S., MORIMOTO, K., SHIMIZU, T., TAKAHASHI, M., KUROSAWA, H. & SHIRASAWA, T. 2000. Association of EXT1 and EXT2, hereditary multiple exostoses gene products, in Golgi apparatus. *Biochem Biophys Res Commun*, 268, 860-7.
- KOMATSU, M., WAGURI, S., UENO, T., IWATA, J., MURATA, S., TANIDA, I., EZAKI, J., MIZUSHIMA, N., OHSUMI, Y., UCHIYAMA, Y., KOMINAMI, E., TANAKA, K. & CHIBA, T. 2005. Impairment of starvation-induced and constitutive autophagy in Atg7-deficient mice. *J Cell Biol*, 169, 425-34.
- KREUGER, J. & KJELLEN, L. 2012. Heparan sulfate biosynthesis: regulation and variability. *J Histochem Cytochem*, 60, 898-907.
- KRISHNAN, V., BANE, S. M., KAWLE, P. D., NARESH, K. N. & KALRAIYA, R. D. 2005. Altered melanoma cell surface glycosylation mediates organ specific adhesion and metastasis via lectin receptors on the lung vascular endothelium. *Clin Exp Metastasis*, 22, 11-24.
- KUO, A., ZHONG, C., LANE, W. S. & DERYNCK, R. 2000. Transmembrane transforming growth factor-alpha tethers to the PDZ domain-containing, Golgi membrane-associated protein p59/GRASP55. *Embo J*, 19, 6427-6439.

- LANE, J. D., LUCOCQ, J., PRYDE, J., BARR, F. A., WOODMAN, P. G., ALLAN, V. J. & LOWE, M. 2002. Caspase-mediated cleavage of the stacking protein GRASP65 is required for Golgi fragmentation during apoptosis. *J Cell Biol*, 156, 495-509.
- LE JAN, S., HAYASHI, M., KASZA, Z., ERIKSSON, I., BISHOP, J. R., WEIBRECHT, I., HELDIN, J., HOLMBORN, K., JAKOBSSON, L., SÖDERBERG, O., SPILLMANN, D., ESKO, J. D., CLAEISSON-WELSH, L., KJELLÉN, L. & KREUGER, J. 2012. Functional overlap between chondroitin and heparan sulfate proteoglycans during VEGF-induced sprouting angiogenesis. *Arterioscler Thromb Vasc Biol*, 32, 1255-63.
- LEE, H. J., PATEL, S. & LEE, S. J. 2005. Intravesicular localization and exocytosis of alpha-synuclein and its aggregates. *J Neurosci*, 25, 6016-24.
- LEE, H. S., QI, Y. & IM, W. 2015. Effects of N-glycosylation on protein conformation and dynamics: Protein Data Bank analysis and molecular dynamics simulation study. *Sci Rep*, 5, 8926.
- LEE, I., TIWARI, N., DUNLOP, M. H., GRAHAM, M., LIU, X. & ROTHMAN, J. E. 2014. Membrane adhesion dictates Golgi stacking and cisternal morphology. *Proc Natl Acad Sci U S A*, 111, 1849-54.
- LEE, J. G., TAKAHAMA, S., ZHANG, G., TOMAREV, S. I. & YE, Y. 2016. Unconventional secretion of misfolded proteins promotes adaptation to proteasome dysfunction in mammalian cells. *Nat Cell Biol*, 18, 765-76.
- LEITMAN, J., BARAK, B., BENYAIR, R., SHENKMAN, M., ASHERY, U., HARTL, F. U. & LEDERKREMER, G. Z. 2014. ER stress-induced eIF2-alpha phosphorylation underlies sensitivity of striatal neurons to pathogenic huntingtin. *PLoS One*, 9, e90803.
- LEVI, S. K. & GLICK, B. S. 2007. GRASPing unconventional secretion. *Cell*, 130, 407-9.
- LEVINE, B. & KROEMER, G. 2008. Autophagy in the pathogenesis of disease. *Cell*, 132, 27-42.
- LI, J., AHAT, E. & WANG, Y. 2019a. Golgi structure and function in health, stress and diseases. *Springer Nature*, Accepted.
- LI, J., AHAT, E. & WANG, Y. 2019b. Golgi Structure and Function in Health, Stress, and Diseases. *Results Probl Cell Differ*, 67, 441-485.
- LI, J., TANG, D., IRELAND, S. C. & WANG, Y. 2019c. DjA1 maintains Golgi integrity via interaction with GRASP65. *Mol Biol Cell*, 30, 478-490.
- LIANG, C. C., PARK, A. Y. & GUAN, J. L. 2007. In vitro scratch assay: a convenient and inexpensive method for analysis of cell migration in vitro. *Nat Protoc*, 2, 329-33.
- LIU, Y., ZHAO, F., GU, W., YANG, H., MENG, Q., ZHANG, Y., YANG, H. & DUAN, Q. 2009. The roles of platelet GPIIb/IIIa and alphavbeta3 integrins during HeLa cells adhesion, migration, and invasion to monolayer endothelium under static and dynamic shear flow. *J Biomed Biotechnol*, 2009, 829243.
- LIVE, D. H., KUMAR, R. A., BEEBE, X. & DANISHEFSKY, S. J. 1996. Conformational influences of glycosylation of a peptide: a possible model for the effect of glycosylation on the rate of protein folding. *Proc Natl Acad Sci U S A*, 93, 12759-61.
- LOBERT, V. H., BRECH, A., PEDERSEN, N. M., WESCHE, J., OPPELT, A., MALEROD, L. & STENMARK, H. 2010. Ubiquitination of alpha 5 beta 1 integrin controls fibroblast migration through lysosomal degradation of fibronectin-integrin complexes. *Dev Cell*, 19, 148-59.
- MAEDA, N. 2015. Proteoglycans and neuronal migration in the cerebral cortex during development and disease. *Front Neurosci*, 9, 98.

- MANJITHAYA, R., ANJARD, C., LOOMIS, W. F. & SUBRAMANI, S. 2010. Unconventional secretion of *Pichia pastoris* Acb1 is dependent on GRASP protein, peroxisomal functions, and autophagosome formation. *J Cell Biol*, 188, 537-46.
- MARSH, B. J. & HOWELL, K. E. 2002. The mammalian Golgi--complex debates. *Nat Rev Mol Cell Biol*, 3, 789-95.
- MCALARY, L., YERBURY, J. J. & CASHMAN, N. R. 2020. The prion-like nature of amyotrophic lateral sclerosis. *Prog Mol Biol Transl Sci*, 175, 261-296.
- MECOCCI, P., CHERUBINI, A., BREGNOCCHI, M., CHIONNE, F., CECCHETTI, R., LOWENTHAL, D. T. & SENIN, U. 1998. Tau protein in cerebrospinal fluid: a new diagnostic and prognostic marker in Alzheimer disease? *Alzheimer Dis Assoc Disord*, 12, 211-4.
- MEREZHKO, M., BRUNELLO, C. A., YAN, X., VIHINEN, H., JOKITALO, E., URONEN, R. L. & HUTTUNEN, H. J. 2018. Secretion of Tau via an Unconventional Non-vesicular Mechanism. *Cell Rep*, 25, 2027-2035 e4.
- MIERKE, C. T., FREY, B., FELLNER, M., HERRMANN, M. & FABRY, B. 2011. Integrin alpha5beta1 facilitates cancer cell invasion through enhanced contractile forces. *J Cell Sci*, 124, 369-83.
- MIYATA, S., KOMATSU, Y., YOSHIMURA, Y., TAYA, C. & KITAGAWA, H. 2012. Persistent cortical plasticity by upregulation of chondroitin 6-sulfation. *Nat Neurosci*, 15, 414-22, S1-2.
- MIZUNO, Y., HATTORI, N., KITADA, T., MATSUMINE, H., MORI, H., SHIMURA, H., KUBO, S., KOBAYASHI, H., ASAKAWA, S., MINOSHIMA, S. & SHIMIZU, N. 2001. Familial Parkinson's disease. Alpha-synuclein and parkin. *Adv Neurol*, 86, 13-21.
- MUESCH, A., HARTMANN, E., ROHDE, K., RUBARTELLI, A., SITIA, R. & RAPOPORT, T. A. 1990. A novel pathway for secretory proteins? *Trends Biochem Sci*, 15, 86-8.
- NG, M. L., TAN, S. H., SEE, E. E., OOI, E. E. & LING, A. E. 2003. Proliferative growth of SARS coronavirus in Vero E6 cells. *J Gen Virol*, 84, 3291-3303.
- NOH, S. H., GEE, H. Y., KIM, Y., PIAO, H., KIM, J., KANG, C. M., LEE, G., MOOK-JUNG, I., LEE, Y., CHO, J. W. & LEE, M. G. 2018. Specific autophagy and ESCRT components participate in the unconventional secretion of CFTR. *Autophagy*, 14, 1761-1778.
- NÜCHEL, J., GHATAK, S., ZUK, A. V., ILLERHAUS, A., MÖRGELIN, M., SCHÖNBORN, K., BLUMBACH, K., WICKSTRÖM, S. A., KRIEG, T., SENGLER, G., PLOMANN, M. & ECKES, B. 2018. TGFB1 is secreted through an unconventional pathway dependent on the autophagic machinery and cytoskeletal regulators. *Autophagy*, 14, 465-486.
- NÜCHEL, J., TAUBER, M., NOLTE, J. L., MÖRGELIN, M., TÜRK, C., ECKES, B., DEMETRIADES, C. & PLOMANN, M. 2021. An mTORC1-GRASP55 signaling axis controls unconventional secretion to reshape the extracellular proteome upon stress. *Mol Cell*.
- ONO, M. & HAKOMORI, S. 2004. Glycosylation defining cancer cell motility and invasiveness. *Glycoconj J*, 20, 71-8.
- PALOMINO, W. A., FUENTES, A., GONZALEZ, R. R., GABLER, F., BORIC, M. A., VEGA, M. & DEVOTO, L. 2005. Differential expression of endometrial integrins and progesterone receptor during the window of implantation in normo-ovulatory women treated with clomiphene citrate. *Fertil Steril*, 83, 587-93.

- PAN, C., NELSON, M. S., REYES, M., KOODIE, L., BRAZIL, J. J., STEPHENSON, E. J., ZHAO, R. C., PETERS, C., SELLECK, S. B., STRINGER, S. E. & GUPTA, P. 2005. Functional abnormalities of heparan sulfate in mucopolysaccharidosis-I are associated with defective biologic activity of FGF-2 on human multipotent progenitor cells. *Blood*, 106, 1956-64.
- PAULE, S., ALJOFAN, M., SIMON, C., ROMBAUTS, L. J. & NIE, G. 2012. Cleavage of endometrial alpha-integrins into their functional forms is mediated by proprotein convertase 5/6. *Hum Reprod*, 27, 2766-74.
- PEARSE, B. R. & HEBERT, D. N. 2010. Lectin chaperones help direct the maturation of glycoproteins in the endoplasmic reticulum. *Biochim Biophys Acta*, 1803, 684-93.
- PEREZ DE CASTRO, I., BIVONA, T. G., PHILIPS, M. R. & PELLICER, A. 2004. Ras activation in Jurkat T cells following low-grade stimulation of the T-cell receptor is specific to N-Ras and occurs only on the Golgi apparatus. *Mol Cell Biol*, 24, 3485-96.
- PFEFFER, S. R. 2013. A prize for membrane magic. *Cell*, 155, 1203-6.
- PHILIPS, M. R. 2004. Sef: a MEK/ERK catcher on the Golgi. *Mol Cell*, 15, 168-9.
- PRYDZ, K. 2015. Determinants of Glycosaminoglycan (GAG) Structure. *Biomolecules*, 5, 2003-22.
- PUTHENVEEDU, M. A., BACHERT, C., PURI, S., LANNI, F. & LINSTEDT, A. D. 2006. GM130 and GRASP65-dependent lateral cisternal fusion allows uniform Golgi-enzyme distribution. *Nat Cell Biol*, 8, 238-48.
- RABOUILLE, C. 2017. Pathways of Unconventional Protein Secretion. *Trends Cell Biol*, 27, 230-240.
- RABOUILLE, C. & LINSTEDT, A. D. 2016. GRASP: A Multitasking Tether. *Front Cell Dev Biol*, 4, 1.
- RAMBOURG, A., CLERMONT, Y., HERMO, L. & SEGRETAIN, D. 1987. Tridimensional structure of the Golgi apparatus of nonciliated epithelial cells of the ductuli efferentes in rat: an electron microscope stereoscopic study. *Biol Cell*, 60, 103-15.
- RATCLIFFE, C. D., SAHGAL, P., PARACHONIAK, C. A., IVASKA, J. & PARK, M. 2016. Regulation of Cell Migration and beta1 Integrin Trafficking by the Endosomal Adaptor GGA3. *Traffic*, 17, 670-88.
- REDDY, A., CALER, E. V. & ANDREWS, N. W. 2001. Plasma membrane repair is mediated by Ca(2+)-regulated exocytosis of lysosomes. *Cell*, 106, 157-69.
- ROBERTS, J. D., KLEIN, J. L., PALMANTIER, R., DHUME, S. T., GEORGE, M. D. & OLDEN, K. 1998. The role of protein glycosylation inhibitors in the prevention of metastasis and therapy of cancer. *Cancer Detect Prev*, 22, 455-62.
- ROSS, C. A. & POIRIER, M. A. 2004. Protein aggregation and neurodegenerative disease. *Nat Med*, 10 Suppl, S10-7.
- RUI, Y. N., XU, Z., PATEL, B., CHEN, Z., CHEN, D., TITO, A., DAVID, G., SUN, Y., STIMMING, E. F., BELLEN, H. J., CUERVO, A. M. & ZHANG, S. 2015. Huntingtin functions as a scaffold for selective macroautophagy. *Nat Cell Biol*, 17, 262-75.
- SAMIE, M. A. & XU, H. 2014. Lysosomal exocytosis and lipid storage disorders. *J Lipid Res*, 55, 995-1009.
- SASARMAN, F., MAFTEI, C., CAMPEAU, P. M., BRUNEL-GUITTON, C., MITCHELL, G. A. & ALLARD, P. 2016. Biosynthesis of glycosaminoglycans: associated disorders and biochemical tests. *J Inherit Metab Dis*, 39, 173-88.

- SATHASIVAM, K., NEUEDER, A., GIPSON, T. A., LANDLES, C., BENJAMIN, A. C., BONDULICH, M. K., SMITH, D. L., FAULL, R. L., ROOS, R. A., HOWLAND, D., DETLOFF, P. J., HOUSMAN, D. E. & BATES, G. P. 2013. Aberrant splicing of HTT generates the pathogenic exon 1 protein in Huntington disease. *Proc Natl Acad Sci U S A*, 110, 2366-70.
- SAUDOU, F. & HUMBERT, S. 2016. The Biology of Huntingtin. *Neuron*, 89, 910-26.
- SBODIO, J. I., SNYDER, S. H. & PAUL, B. D. 2018. Golgi stress response reprograms cysteine metabolism to confer cytoprotection in Huntington's disease. *Proc Natl Acad Sci U S A*, 115, 780-785.
- SCHEFFER, K. D., GAWLITZA, A., SPODEN, G. A., ZHANG, X. A., LAMBERT, C., BERDITCHEVSKI, F. & FLORIN, L. 2013. Tetraspanin CD151 mediates papillomavirus type 16 endocytosis. *J Virol*, 87, 3435-46.
- SCHINDELIN, J., ARGANDA-CARRERAS, I., FRISE, E., KAYNIG, V., LONGAIR, M., PIETZSCH, T., PREIBISCH, S., RUEDEN, C., SAALFELD, S. & SCHMID, B. 2012. Fiji: an open-source platform for biological-image analysis. *Nature methods*, 9, 676-682.
- SCHOTMAN, H., KARHINEN, L. & RABOUILLE, C. 2008. dGRASP-mediated noncanonical integrin secretion is required for Drosophila epithelial remodeling. *Dev Cell*, 14, 171-82.
- SHENTAL-BECHOR, D. & LEVY, Y. 2008. Effect of glycosylation on protein folding: a close look at thermodynamic stabilization. *Proc Natl Acad Sci U S A*, 105, 8256-61.
- SHORT, B., PREISINGER, C., KORNER, R., KOPAJTICH, R., BYRON, O. & BARR, F. A. 2001. A GRASP55-rab2 effector complex linking Golgi structure to membrane traffic. *J Cell Biol*, 155, 877-83.
- SHORTER, J., WATSON, R., GIANNAKOU, M. E., CLARKE, M., WARREN, G. & BARR, F. A. 1999. GRASP55, a second mammalian GRASP protein involved in the stacking of Golgi cisternae in a cell-free system. *Embo J*, 18, 4949-4960.
- SOLA, R. J. & GRIEBENOW, K. 2009. Effects of glycosylation on the stability of protein pharmaceuticals. *J Pharm Sci*, 98, 1223-45.
- STELZER, C., BRIMMER, A., HERMANN, P., ZABEL, B. & DIETZ, U. H. 2007. Expression profile of Papss2 (3'-phosphoadenosine 5'-phosphosulfate synthase 2) during cartilage formation and skeletal development in the mouse embryo. *Dev Dyn*, 236, 1313-8.
- STEVENSON, N. L., BERGEN, D. J. M., SKINNER, R. E. H., KAGUE, E., MARTIN-SILVERSTONE, E., ROBSON BROWN, K. A., HAMMOND, C. L. & STEPHENS, D. J. 2017. Giantin-knockout models reveal a feedback loop between Golgi function and glycosyltransferase expression. *J Cell Sci*, 130, 4132-4143.
- SUTTERLIN, C., HSU, P., MALLABIABARRENA, A. & MALHOTRA, V. 2002. Fragmentation and dispersal of the pericentriolar Golgi complex is required for entry into mitosis in mammalian cells. *Cell*, 109, 359-69.
- TAN, C. C., LI, G. X., TAN, L. D., DU, X., LI, X. Q., HE, R., WANG, Q. S. & FENG, Y. M. 2016. Breast cancer cells obtain an osteomimetic feature via epithelial-mesenchymal transition that have undergone BMP2/RUNX2 signaling pathway induction. *Oncotarget*, 7, 79688-79705.
- TANG, D., YUAN, H., VIELEMEYER, O., PEREZ, F. & WANG, Y. 2012. Sequential phosphorylation of GRASP65 during mitotic Golgi disassembly. *Biol Open*, 1, 1204-14.
- TANG, D., YUAN, H. & WANG, Y. 2010. The Role of GRASP65 in Golgi Cisternal Stacking and Cell Cycle Progression. *Traffic*, 11, 827-42.

- TANG, D., ZHANG, X., HUANG, S., YUAN, H., LI, J. & WANG, Y. 2016. Mena-GRASP65 interaction couples actin polymerization to Golgi ribbon linking. *Mol Biol Cell*, 27, 137-52.
- TANK, E. M., FIGUEROA-ROMERO, C., HINDER, L. M., BEDI, K., ARCHBOLD, H. C., LI, X., WESKAMP, K., SAFREN, N., PAEZ-COLASANTE, X., PACUT, C., THUMMA, S., PAULSEN, M. T., GUO, K., HUR, J., LJUNGMAN, M., FELDMAN, E. L. & BARMADA, S. J. 2018. Abnormal RNA stability in amyotrophic lateral sclerosis. *Nat Commun*, 9, 2845.
- THOMPSON, L. M., AIKEN, C. T., KALTENBACH, L. S., AGRAWAL, N., ILLES, K., KHOSHANAN, A., MARTINEZ-VINCENTE, M., ARRASATE, M., O'ROURKE, J. G., KHASHWJI, H., LUKACSOVICH, T., ZHU, Y. Z., LAU, A. L., MASSEY, A., HAYDEN, M. R., ZEITLIN, S. O., FINKBEINER, S., GREEN, K. N., LAFERLA, F. M., BATES, G., HUANG, L., PATTERSON, P. H., LO, D. C., CUERVO, A. M., MARSH, J. L. & STEFFAN, J. S. 2009. IKK phosphorylates Huntingtin and targets it for degradation by the proteasome and lysosome. *J Cell Biol*, 187, 1083-99.
- TIAN, E., STEVENS, S. R., GUAN, Y., SPRINGER, D. A., ANDERSON, S. A., STAROST, M. F., PATEL, V., TEN HAGEN, K. G. & TABAK, L. A. 2015. Galnt1 is required for normal heart valve development and cardiac function. *PLoS One*, 10, e0115861.
- TIAN, G., ROPELEWSKI, P., NEMET, I., LEE, R., LODOWSKI, K. H. & IMANISHI, Y. 2014. An unconventional secretory pathway mediates the cilia targeting of peripherin/rds. *J Neurosci*, 34, 992-1006.
- TRAJKOVIC, K., JEONG, H. & KRAINIC, D. 2017. Mutant Huntingtin Is Secreted via a Late Endosomal/Lysosomal Unconventional Secretory Pathway. *J Neurosci*, 37, 9000-9012.
- ULIANA, A. S., GIRAUDO, C. G. & MACCIONI, H. J. 2006. Cytoplasmic tails of SialT2 and GalNAcT impose their respective proximal and distal Golgi localization. *Traffic*, 7, 604-12.
- UMEDA, T., MAEKAWA, S., KIMURA, T., TAKASHIMA, A., TOMIYAMA, T. & MORI, H. 2014. Neurofibrillary tangle formation by introducing wild-type human tau into APP transgenic mice. *Acta Neuropathol*, 127, 685-98.
- VAN ZIEL, A. M., LARGO-BARRIENTOS, P., WOLZAK, K., VERHAGE, M. & SCHEPER, W. 2019. Unconventional secretion factor GRASP55 is increased by pharmacological unfolded protein response inducers in neurons. *Sci Rep*, 9, 1567.
- VEENENDAAL, T., JARVELA, T., GRIEVE, A. G., VAN ES, J. H., LINSTEDT, A. D. & RABOUILLE, C. 2014. GRASP65 controls the cis Golgi integrity in vivo. *Biol Open*, 3, 431-43.
- VIELEMEYER, O., YUAN, H., MOUTEL, S., SAINT-FORT, R., TANG, D., NIZAK, C., GOUD, B., WANG, Y. & PEREZ, F. 2009. Direct Selection of Monoclonal Phosphospecific Antibodies without Prior Phosphoamino Acid Mapping. *J Biol Chem*, 284, 20791-5.
- VILLENEUVE, J., BASSAGANYAS, L., LEPREUX, S., CHIRITOIU, M., COSTET, P., RIPOCHE, J., MALHOTRA, V. & SCHEKMAN, R. 2018. Unconventional secretion of FABP4 by endosomes and secretory lysosomes. *J Cell Biol*, 217, 649-665.
- WAN, J., ZHU, F., ZASADIL, L. M., YU, J., WANG, L., JOHNSON, A., BERTHIER, E., BEEBE, D. J., AUDHYA, A. & WEAVER, B. A. 2014. A Golgi-localized pool of the mitotic checkpoint component Mad1 controls integrin secretion and cell migration. *Curr Biol*, 24, 2687-92.

- WANG, Y., SATOH, A. & WARREN, G. 2005. Mapping the functional domains of the Golgi stacking factor GRASP65. *J Biol Chem*, 280, 4921-8.
- WANG, Y. & SEEMANN, J. 2011. Golgi biogenesis. *Cold Spring Harb Perspect Biol*, 3, a005330.
- WANG, Y., SEEMANN, J., PYPAERT, M., SHORTER, J. & WARREN, G. 2003. A direct role for GRASP65 as a mitotically regulated Golgi stacking factor. *Embo J*, 22, 3279-90.
- WANG, Y., WEI, J. H., BISEL, B., TANG, D. & SEEMANN, J. 2008. Golgi Cisternal Unstacking Stimulates COPI Vesicle Budding and Protein Transport. *PLoS ONE*, 3, e1647.
- WEISS, R. J., SPAHN, P. N., TOLEDO, A. G., CHIANG, A. W., KELLMAN, B. P., LI, J., BENNER, C., GLASS, C. K., GORDTS, P. L. & LEWIS, N. E. 2020. ZNF263 is a transcriptional regulator of heparin and heparan sulfate biosynthesis. *Proceedings of the National Academy of Sciences*, 117, 9311-9317.
- WILD, E. J., BOGGIO, R., LANGBEHN, D., ROBERTSON, N., HAIDER, S., MILLER, J. R., ZETTERBERG, H., LEAVITT, B. R., KUHN, R., TABRIZI, S. J., MACDONALD, D. & WEISS, A. 2015. Quantification of mutant huntingtin protein in cerebrospinal fluid from Huntington's disease patients. *J Clin Invest*, 125, 1979-86.
- WINER, L., SRINIVASAN, D., CHUN, S., LACOMIS, D., JAFFA, M., FAGAN, A., HOLTZMAN, D. M., WANCEWICZ, E., BENNETT, C. F., BOWSER, R., CUDKOWICZ, M. & MILLER, T. M. 2013. SOD1 in cerebral spinal fluid as a pharmacodynamic marker for antisense oligonucleotide therapy. *JAMA Neurol*, 70, 201-7.
- XIANG, Y. & WANG, Y. 2010. GRASP55 and GRASP65 play complementary and essential roles in Golgi cisternal stacking. *J Cell Biol*, 188, 237-51.
- XIANG, Y. & WANG, Y. 2011. New components of the Golgi matrix. *Cell Tissue Res*, 344, 365-79.
- XIANG, Y., ZHANG, X., NIX, D. B., KATOH, T., AOKI, K., TIEMEYER, M. & WANG, Y. 2013. Regulation of protein glycosylation and sorting by the Golgi matrix proteins GRASP55/65. *Nat Commun*, 4, 1659.
- YE, Y. 2018. Regulation of protein homeostasis by unconventional protein secretion in mammalian cells. *Semin Cell Dev Biol*, 83, 29-35.
- YOSHIMURA, M., IHARA, Y., MATSUZAWA, Y. & TANIGUCHI, N. 1996. Aberrant glycosylation of E-cadherin enhances cell-cell binding to suppress metastasis. *J Biol Chem*, 271, 13811-5.
- YU, X., WANG, F., LIU, H., ADAMS, G., AIKHIONBARE, F., LIU, D., CAO, X., FAN, L., HU, G., CHEN, Y., FROST, A., PARTRIDGE, E., DING, X. & YAO, X. 2011. ACAP4 protein cooperates with Grb2 protein to orchestrate epidermal growth factor-stimulated integrin beta1 recycling in cell migration. *J Biol Chem*, 286, 43735-47.
- ZHANG, M., KENNY, S. J., GE, L., XU, K. & SCHEKMAN, R. 2015. Translocation of interleukin-1beta into a vesicle intermediate in autophagy-mediated secretion. *Elife*, 4.
- ZHANG, M., LIU, L., LIN, X., WANG, Y., LI, Y., GUO, Q., LI, S., SUN, Y., TAO, X., ZHANG, D., LV, X., ZHENG, L. & GE, L. 2020. A Translocation Pathway for Vesicle-Mediated Unconventional Protein Secretion. *Cell*, 181, 637-652.e15.
- ZHANG, X., WANG, L., IRELAND, S. C., AHAT, E., LI, J., BEKIER II, M. E., ZHANG, Z. & WANG, Y. 2019a. GORASP2/GRASP55 collaborates with the PtdIns3K UVRAG complex to facilitate autophagosome-lysosome fusion. *Autophagy*.

- ZHANG, X., WANG, L., IRELAND, S. C., AHAT, E., LI, J., BEKIER II, M. E., ZHANG, Z. & WANG, Y. 2019b. GORASP2/GRASP55 collaborates with the PtdIns3K UVRAG complex to facilitate autophagosome-lysosome fusion. *Autophagy*, 1-14.
- ZHANG, X., WANG, L., IRELAND, S. C., AHAT, E., LI, J., BEKIER, M. E., 2ND, ZHANG, Z. & WANG, Y. 2019c. GORASP2/GRASP55 collaborates with the PtdIns3K UVRAG complex to facilitate autophagosome-lysosome fusion. *Autophagy*, 15, 1787-1800.
- ZHANG, X., WANG, L., LAK, B., LI, J., JOKITALO, E. & WANG, Y. 2018. GRASP55 Senses Glucose Deprivation through O-GlcNAcylation to Promote Autophagosome-Lysosome Fusion. *Dev Cell*, 45, 245-261 e6.
- ZHANG, X. & WANG, Y. 2015a. GRASPs in Golgi Structure and Function. *Frontiers in Cell and Developmental Biology*, 3, 84.
- ZHANG, X. & WANG, Y. 2015b. GRASPs in Golgi Structure and Function. *Frontiers in Cell and Developmental Biology*, 3, 84.
- ZHANG, X. & WANG, Y. 2016. Glycosylation Quality Control by the Golgi Structure. *J Mol Biol*, 428, 3183-93.
- ZHANG, X. & WANG, Y. 2018a. The Golgi stacking protein GORASP2/GRASP55 serves as an energy sensor to promote autophagosome maturation under glucose starvation. *Autophagy*, 14, 1649-1651.
- ZHANG, X. & WANG, Y. 2018b. GRASP55 facilitates autophagosome maturation under glucose deprivation. *Mol Cell Oncol*, 5, e1494948.
- ZHANG, X. & WANG, Y. 2020. Nonredundant Roles of GRASP55 and GRASP65 in the Golgi Apparatus and Beyond. *Trends Biochem Sci*, 45, 1065-1079.
- ZHAO, J., LI, B., HUANG, X., MORELLI, X. & SHI, N. 2017. Structural Basis for the Interaction between Golgi Reassembly-stacking Protein GRASP55 and Golgin45. *J Biol Chem*, 292, 2956-2965.
- ZHAO, J., ZHU, Y., SONG, X., XIAO, Y., SU, G., LIU, X., WANG, Z., XU, Y., LIU, J., ELIEZER, D., RAMLALL, T. F., LIPPENS, G., GIBSON, J., ZHANG, F., LINHARDT, R. J., WANG, L. & WANG, C. 2020. 3-O-Sulfation of Heparan Sulfate Enhances Tau Interaction and Cellular Uptake. *Angew Chem Int Ed Engl*, 59, 1818-1827.
- ZHENG, M., FANG, H. & HAKOMORI, S. 1994. Functional role of N-glycosylation in alpha 5 beta 1 integrin receptor. De-N-glycosylation induces dissociation or altered association of alpha 5 and beta 1 subunits and concomitant loss of fibronectin binding activity. *J Biol Chem*, 269, 12325-31.